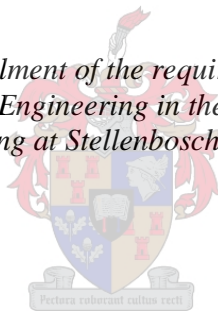# Experimental and Numerical Investigation on the Fire Behaviour of South African Passenger Trains with an Emphasis on Arson

by

Michelle Danille Gous

Thesis presented in fulfilment of the requirements for the degree of
Master of Engineering in the Faculty of
Engineering at Stellenbosch University

Supervisor: Prof. Richard Shaun Walls
Co-supervisor: Dr Antonio Cicione

March 2022

Declaration

By submitting this thesis electronically, I declare that the entirety of the work contained therein is my own, original work, that I am the sole author thereof (save to the extent explicitly otherwise stated), that reproduction and publication thereof by Stellenbosch University will not infringe any third party rights and that I have not previously in its entirety or in part submitted it for obtaining any qualification.

March 2022

i

Abstract

Internationally, passenger train fires have become a rare occurrence as trains are tested to strict standards in order to ensure passenger safety. At the same time, arson attacks have become a frequent occurrence on Metrorail trains in South Africa in recent years, resulting in severe damage, huge financial losses, and in some cases, even the injury and death of passengers. Intra-urban passenger trains form a crucial part of the economy as many people rely on this form of public transport to travel to work. Metrorail trains offer a low-cost alternative to other forms of public transport. Arson attacks threaten the existence of passenger trains as a form of public transport as these lead to damage to infrastructure, trains being destroyed and affect business continuity. Little is known about the fire behaviour in the carriages which is causing these very dangerous fires. This study aims to investigate this fire behaviour by using small-scale material tests, large-scale experiments, and full-scale numerical simulations to gain insight into this problem.

The small-scale material tests include the determination of material density, bomb calorimeter tests to determine the heat of combustion, and radiant panel tests in order to determine the ignition temperature and critical heat flux, as well as to observe how these materials react to heat. Further material properties are obtained from literature once all material types are identified.

The large-scale experiments involve the burning of full seat assemblies on a scale in an open-air environment, while taking heat flux and temperature readings. This is used to determine the mass loss rate of the seats, and are replicated in Fire Dynamics Simulator (FDS) version 6.7.6 numerical simulations to observe the accuracy of the simulation using the parameters determined through small-scale testing, large-scale experiments and literature values where required.

To study the approximate fire behaviour in a full-scale passenger train carriage, the carriages are replicated, and the seat models are used in numerical simulations involving various fire scenarios. These include a variation on the ventilation conditions, minimum and maximum, as well as varying the ignition position between the front and middle of the carriage to study the effect these variables have on fire behaviour. The results are used to analyse the tenability conditions and determine the time passengers have to evacuate before experiencing injury or death.

Passengers were found to have minimal time to evacuate the carriages, with a high risk of mortalities in the case of a full carriage. Some materials were found to be an extreme fire hazard which contributed to the high heat release rate and all fire scenarios leading to flashover before 300 seconds. The fires were found to be ventilation controlled, even in the maximum ventilation scenarios. All seats were found to be non-compliant when compared to EN 45545-2 requirements, by exceeding the limit of 350 kW on the peak heat release rate, and also exceeding limitations placed on fire spread and flame length.

Opsomming

Brande in passesiertreine het internasionaal 'n skaars verskynsel geword omdat treine volgens streng standaarde getoets word om die veiligheid van passasiers te verseker. Terselfdertyd, het brandstigting onlangs algemeen geword op Metrorail se treine in Suid-Afrika, wat lei tot ernstige skade, groot finansiële verliese, en in sommige gevalle selfs beserings en die dood van passasiers. Binnestedelike passesierstreine vorm 'n kritiese deel van die ekonomie aangesien talle mense op hierdie vorm van publieke vervoer staatmaak om werk toe te pendel. Metrorail treine bied 'n laekoste alternatief tot ander vorms van publieke vervoer. Brandstigtingsaanvalle bedreig die bestaan van passesierstreine as 'n vorm van publieke vervoer omdat hierdie aanvalle lei tot skade aan infrastruktuur, treine wat vernietig word en beïnvloed ook besigheidskontinuïteit. Min is bekend oor die brandgedrag wat hierdie gevaarlike brande veroorsaak in die waens. Hierdie studie mik om hierdie brandgedrag te ondersoek deur kleinskaalse materiaaltoetse, grootskaalse eksperimente en volskaalse numeriese simulasies om insig te kry rakende hierdie probleem.

Die kleinskaalse materiaaltoetse sluit in die bepaling van materiaal digtheid, *bomb calorimeter* toetse om die verbrandingshitte te bepaal, en uitstralingspaneel-toetse om die aansteektemperatuur en kritiese hittevloei te bepaal, asook om waar te neem hoe hierdie materiale reageer wanneer hulle blootgestel word aan hitte. Verdere materiaaleienskappe is verkry vanuit literatuur nadat alle materiaal tipes geïdentifiseer is.

Die grootskaalse eksperimente behels te verbranding van vol-sitplek samestellings op 'n skaal in 'n opelug omgewing, terwyl hittevloei en temperatuur lesings geneem word. Dit word dan gebruik om die massaverliestempo van die sitplekke te bepaal. Die eksperimente word nageboots in Fire Dynamics Simulator (FDS) weergawe 6.7.6 numeriese simulasies om die akkuraatheid van die simulasies waar te neem wanneer die eienskappe gebruik word wat bepaal is deur die kleinskaalse toetse, grootskaalse eksperimente en waardes verkry uit literatuur waar benodig.

Om die benaderde brandgedrag in 'n volskaalse passasiertreinwa te bestudeer, word die waens nageboots en die sitplek numeriese modelle gebruik vir die numeriese simulasies van verskeie brandgevalle. Hierdie brandgevalle sluit in 'n variasie van ventilasieomstandighede, minimum en maksimum, en die verskuiwing van die plek waar die brand gestig word in die wa, tussen voor en die middel van die wa, om die effek van hierdie veranderlikes op die brandgedrag te bestudeer. Die resultate word gebruik om die houdbaarheidsomstandighede te analiseer en die tyd wat passasiers het om te ontruim voor hulle beseer word of beswyk te bepaal.

Dit is bepaal dat die tyd wat passasiers het om te ontruim minimaal is, en dat daar 'n hoe risiko is van sterftes wanneer die wa volgelaai is. Dit is bevind dat sommige materiale 'n eksteme brandgevaar is, wat bydra tot die hoe hittevrylatingstempo en al die brandgevalle het gelei tot *flashover* binne 300 sekondes. Daar is bevind dat die brande ventilasiebeheerd is, selfs met die maksimum ventilasie brandgevalle. Al die sitplekke het nie aan vereistes voldoen wanneer hulle vergelyk is met die spesifikasies in EN 45545-2 nie, deurdat hulle die limiet van 350 kW oorskry het en ook die limiete op brandverspreiding en vlamlengte oorskry het.

Acknowledgements

I would like to express my gratitude to the following people and organisations for their contribution towards this work:

- My supervisors, Prof Richard Walls and Dr Antonio, for their guidance, assistance and patience in the completion of this thesis. I knew I could not let the opportunity slip by when I heard Richard had started FireSUN, and without him always ensuring I had the means financially, I would not have been able to grab the opportunity with both hands.

- PRASA for funding my studies.

- The FireSUN team for their support and readiness to help where possible.

- Ignis Testing for the use of their facilities.

- Julian Thompson from the Structures Lab for his assistance in sample preparation and expert hand in welding whenever any component needed fixing.

- Ruggero Poletto from CFD FEA Service for the assistance with setting up simulations to run with the highest efficiency, and running simulations on the cloud even late at night.

- Gerhard van Wageningen for his patience and assisting with troubleshooting on the HPC and supplying numerous scripts to ensure the simulations run without problems.

- The PRASA chair for their support and assisting with getting information and pulling strings to get things done.

- The workshop staff at the Salt River Depot for their assistance in getting the samples I needed and showing me the ropes regarding trains.

- Eugenie Pienaar for her assistance with small tasks when deadlines were looming.

- Richard Voges for assisting with sample preparation until the early morning hours, driving up and down with me to collect seats and samples, listening to all my ramblings about my research, enduring the late nights and busy days, and keeping things running at home when I was not able to. Without his patience, support and significant amounts of encouragement this thesis would not have been possible.

- My parent for always believing in me even when I did not and helping financially along the way, especially when times got tough. Their support over the years has allowed me to be where I am today.

- To God for providing me with the abilities I have and leading me along this path.

<u>PRASA Position Paper on Thesis</u>

In the following pages a Position Paper on the thesis has been included as provided by the Passenger Rail Agency of SA (PRASA). The research was conducted under the PRASA Chair at Stellenbosch University, with PRASA being involved in the work and the results being communicated directly to the organisation.

This page and the Position Paper on the following pages do not reflect the work of the author of this thesis. However, they have been included as the work has public safety implications and it has been important that Stellenbosch University engage with PRASA on the matter to enhance fire safety. PRASA has acknowledged the results and are putting in place measures to improve the safety of their trains based on the findings of this research. To this end the response and details, as documented on the following pages, have been included.

By: Prof Richard Walls – Thesis supervisor

prasa

PASSENGER RAIL AGENCY
OF SOUTH AFRICA

Umjantshi House
30 Wolmarans Str.
BRAAMFONTEIN
2001

Private Bag X101
Braamfontein, 2107
T +27 11 013 1667

www.prasa.com

PRASA POSITION PAPER IN SUPPORT OF THE UNIVERSITY OF STELLENBOSCH STUDENT RESEARCH.

PRASA position paper subsequent to the completion of the research paper on the *Experimental and Numerical Investigation on the Fire Behaviour of South African Passenger Trains with an Emphasis on Arson* by Michelle Danille Gous.The Thesis was presented in fulfilment of the requirements for the degree of the Master of Engineering in the Faculty of Engineering at Stellenbosch University.

PRASA values the role of Institutions of Higher learning collaborating with organizations like PRASA to inculcate the culture of critical thinking and development of new knowledge for progress and continuous improvement.

This research paper has been received with enthusiasm at the time when PRASA is in the process of recovering operations after the countrywide lockdown due to COVID-19 pandemic and severe theft and vadanlism of the rail network infrastructure.

PRASA is of the view that the research paper will be an excellent point of reference in the future as we strive to ensure safe operations of trains for our employees,passengers and the communities around PRASA network

As a point of departure, PRASA would like to acknowledge the research findings.

PRASA would want to put it on record that it is not all trains that have seats that are said to be prone to fire. The seats that are prone to fire are seats that are on a specific coaches (the MetroPlus) and only if the seats are tempered with. The MetroPlus coaches are specifically on the yellow trains.

PRASA has adopted the following resolutions to ensure the safety of employees,passenges and the communities around our network:

| Directors | L. Ramatlakane (Chairman), Adv. S. Sethene, N. Makaepea, M. Mukhuba, DK. Mohuba, N. Nokwe-Macamo, TN. Mpye, T. Zulu | Acting Group CEO Hishaam Emeran |

Acting Group Company Secretary

1. PRASA takes note of the findings of the research with interest.
2. PRASA has risk management initiatives.
3. PRASA has developed a national retirement strategy of phasing out the yellow (old) trains and phasing in and /ramping up with the blue (new) trains.

PRASA would like the reader of the research paper to take note of this position paper as a way of appreciation of research.

PRASA is a caring organization and the safety of our employees, passengers and the communities around the PRASA Network is of concern and remains our primary responsibility.

Where there are emerging risks, danger or threats, immediate and appropriate actions are taken.

PRASA continues to improve its processes and the safety performance of its assets as part of continuos improvement.

Yours sincerely

.:...................:...   ....:.....

Nelson Malefane   Fana Marutla

Acting Chief Executive Officer,   Acting Chief Executive Officer,

PRASA Rail   PRASA TECH

Date: 07 September 2022   Date: 07 September 2022

Table of Contents

List of Figures

List of Tables

List of Equations

List of Symbols

a	Absorptivity
A_v	Window area
c	Specific heat
c_p	Specific heat at constant pressure
Bi	Biot number
D*	Characteristic fire diameter
Fo	Fourier number
g	Gravitational acceleration
k	Thermal conductivity
h	Convective heat transfer coefficient
H_c, Δh_c	Heat of combustion
H_v	Height of window opening
m	Mass
$\dot{m}$, $\dot{m}_F$	Fuel mass loss rate
$\dot{Q}$	Heat release rate
$\dot{Q}"_R$	Radiative heat flux
Q_{vent}	Heat release rate for ventilation controlled fire
$Q"_{cr}$	Critical heat flux
t	Time
t_0	Initial time
t_{exp}	Time of exposure without incapacitation
t_{Iconv}	Time of exposure for convective heat
t_{ig}	Time to ignition
t_{Irad}	Time to burning of skin due to radiant heat
T_{ig}	Ignition temperature
T_0	Initial temperature
T_∞	Temperature of air
β	Cooling modulus
ε	Emissivity
ρ	Density
$ρ_\infty$	Density of air
τ	Thickness

List of Abbreviations

ASTM	American Society for Testing and Materials
BS	British Standard
CFD	Computational Fluid Dynamics
CHF	Critical Heat Flux
CSIRO	Commonwealth Scientific and Industrial Research Organisation
DFS	Design Fire Scenario
EN	Europäische Norm
FDS	Fire Dynamics Simulator
HF	Heat Flux
HRR	Heat Release Rate
HRRPUA	Heat Release Rate per Unit Area
H-TRIS	Heat-transfer Rating Inducing System
ISO	International Organization for Standardization
LES	Large-eddy Simulation
LPG	Liquid Petroleum Gas
MARHE	Maximum Average Rate of Heat Emission
MLR	Mass Loss Rate
NFPA	National Fire Protection Association
NIST	National Institute of Standards and Technology
PMMA	Polymethylmethacrylate
PRASA	Passenger Rail Association of South Africa
PU	Polyurethane
PVC	Polyvinylchloride

1   Introduction

1.1   Background

Trains have been transporting South African commuters since 26 June 1860 when the railway line between Market Square and Customs Point in Durban was used to transport over 800 passengers on a single day (Metrorail, 2007). The Cape Town to Wellington line was in service three years later, in 1863 (Metrorail, 2007). With urbanisation, especially in the 1970s, intra-urban trains have become popular along business lines (Metrorail, 2007). Trains around the world have had problems with fire since steam-powered trains became widely used. The fires were generally accidental and caused by sources of ignition normally found within the trains leading to fire spread or components overheating and leading to fire.

In South Africa, a problem has started to emerge over the last several years where trains are burnt down, not due to accidental causes but due to deliberate attacks in the form of arson. Between 2014 and the end of 2019, it was reported that R643 million worth of damage had been done to 213 Metrorail coaches in arson attacks (Hyman, 2019). Only 10 of the 24 platforms in Cape Town Station were in use at the end of 2019 due to various arson attacks on trains in the station causing severe damage (Hyman, 2019). On 21 November 2019, the Presidency signed the Critical Infrastructure Protection Act into law, in an effort to take decisive action against perpetrators who perform deliberate acts of destruction to critical infrastructure, such as the arsonists who damage trains and busses around the country.

Not only do the arson attacks damage the trains and put the commuters who use them in danger, but this also affects the service that can be provided by the Passenger Rail Association of South Africa (PRASA) to commuters, and thus the effect is felt by commuters who cannot get to work on time and no longer have access to affordable public transport services. This affects the community at large and can even be detrimental to the economy.

1.2   Problem Statement

Arson attacks on Metrorail trains usually lead to severe damage, unless a fire can be reached quickly and extinguished. In many cases, however, the passenger trains are set alight in such a way that the arsonists can safely exit the train, and the fire is not detected until they have escaped without being identified or noticed. The preferred time to start a fire is as the train pulls into a station, allowing perpetrators to get off the train.

As passenger-train fires should normally not spread and cause the entire carriage to become involved, the question arises as to the reasons for the fires spreading so quickly and involving the entire carriage, as observed in the case of the Metrorail carriages. EN 45545-2 (CEN, 2015), a European code specifying the fire performance for passenger train materials, places restrictions on the fire risk of various components in a passenger train carriage. In theory, if all the components of a train comply with this (or similar standards used such as NFPA 130 or BS 6853), the fires being observed in the Metrorail trains, would not be possible. An investigation is thus required into the fire behaviour in Metrorail trains and to identify the potential causes of the severe damage that results from arson attacks. An understanding of the performance of current materials used in trains is required. Various fire scenarios should also be considered, such as the position of ignition within the carriage and varying ventilation conditions involving open and closed doors and windows. This will give an indication of how much time passengers currently have to escape a burning carriage in each situation and what could be done to improve the safety of Metrorail trains.

1.3   Objectives

The main goal of this research is to investigate the fire performance of materials currently found in PRASA trains to understand why the trains are so susceptible to arson attacks. In order to do so, there are two main objectives:

- to experimentally determine material properties and their behaviour in fire,

- and to use these properties to model various scenarios that will show the fire behaviour of the full-scale carriage on fire.

A thorough literature review is required in order to understand fire behaviour in an enclosed space with various ventilation conditions, as well as the presence of many synthetic, oil-based materials, which may have an effect on the size and rate of spread of the fire. Testing of material samples is necessary to determine the properties thereof required for modelling. To this end, the following specific tasks will be undertaken in this thesis:

- small-scale tests of individual materials, such as bomb calorimeter tests (to determine the energy potential) and radiant panel tests (to quantify the ignition behaviour); and

- large-scale experiments which will allow the fire behaviour and properties of composite chair samples to be studied.

- The models are validated by comparing results with experimental data from single-seat experiments. The models are then extended to be applied to full carriages.

1.4   Scope and Limitations of Work

This research includes the testing of individual materials as well as seats used in the Metrorail passenger train carriages. The carriage containing the driver's compartment, also known as the motor coach, was not considered in this research, and only the plain trailers were studied. The individual materials that were focussed on include the materials that make up the seats, the inner lining of the wall and ceiling, as well as the windows. Materials found externally, as well as wiring, were not considered, as the development of the fire leading up to flashover, is the focus of this research. The data obtained during testing was used for modelling purposes. The modelling focussed on the inside of the carriage as well as the ventilation thereof but did not include fire spread from one carriage to the next. Only fires caused by the ignition of seats were considered, and thus electrical fires were not included. Smoke toxicity was not included in this research, and the behaviour of passengers and evacuation was also not considered. The effect of potential fire suppression systems was also not considered. The work is based on materials obtained from actual trains, which does result in variability in the samples obtained. Also, if new material specifications are adopted in the future, the applicability of these results will be influenced.

1.5   Outline of Thesis

1.5.1   Chapter 2 – Literature Review

In this chapter, important aspects of fire behaviour will be discussed, which are particularly relevant to the growth of fire leading up to flashover.

1.5.2   Chapter 3 – Background Information on Passenger Trains and Arson

This chapter provides information regarding the arson attacks on Metrorail trains. The components of the carriages and the materials found within the carriages, and their properties will also be covered.

1.5.3   Chapter 4 – Test and Experimental Setup

This chapter will focus on the various properties that are required and the tests and experiments that were conducted in order to obtain these values. The material properties that will be discussed include the density, heat of combustion, specific heat, thermal conductivity, critical heat flux, ignition temperature, mass loss rate (MLR), and heat release rate (HRR). The tests performed include bomb calorimeter tests and radiant panel tests. Experimental work was conducted to determine the mass loss rate of the seats.

1.5.4   Chapter 5 – Small-scale Test Results

In this chapter, the results obtained from the small-scale tests covered in Chapter 4 will be presented and discussed. Results will be compared to values found in literature.

1.5.5   Chapter 6 – Large-scale Experimental Results

In this chapter, the results obtained from the full-scale experiments also covered in Chapter 4 will be presented and discussed. Results from the different single-seat experiments are also contrasted.

1.5.6   Chapter 7 – Development and Results of Numerical Simulations

This chapter will include the identification of material properties that will be used for each component of the models. The various scenarios that were modelled will also be discussed, as the results obtained from these models will be presented, and compared to the experimental results where appropriate.

1.5.7   Chapter 8 – Conclusions and Recommendations

In this chapter, the research findings will be discussed, and recommendations will be made for the improvement of the passenger carriages, as well as recommendations for future work.

2   Literature Review

2.1   Introduction

In this chapter, an overview is given of basic fire principles and fire behaviour within compartments which provides an understanding of the discussions in the chapters which follow. Standards applicable to passenger trains in terms of fire safety is also covered as well experimental research and testing of passenger trains in fire. Finally, numerical simulations, particularly Fire Dynamics Simulator (FDS), is discussed.

2.2   Basic Fire Principles

For a fire to ignite and maintain combustion, three components are required; fuel, oxygen and heat, in sufficient amounts (Quintiere, 1998). Initially, heat is provided by the flame, which is applied to the seat or accelerant, but as the fire grows, the heat is supplied by the combustion process, which is exothermic.

Fuels, in this case, are the seats, interior lining, windows and window frames found within the train carriage, and in the case where an accelerant is used, it is also included as a fuel. Fuels, which are not considered in this work, include all the components between the inner wall panels and outer wall panels, as well as light fixtures and other small components which should not add a significant amount of fuel.

2.2.1   Combustion

Combustion can occur as smouldering or flaming combustion. When atmospheric oxygen reacts with a porous combustible solid matrix, such as foam, smouldering may occur, while flaming combustion, a much more rapid reaction, requires a fuel already in the gas phase. For a solid or liquid fuel to be available for combustion, such as in the case of polymers, thermal decomposition or pyrolysis must first occur in order to break them down into volatiles. (Hurley *et al.*, 1997, p. 172)

2.2.2   Heat Transfer

Heat transfer, which is the flow of energy through a system, takes place in three forms; conduction, convection and radiation.

2.2.2.1   Conduction

Conduction is the flow of heat through a solid. This takes place via free electrons, which also allows materials to conduct electricity. For this reason, good electrical conductors are usually also good thermal conductors. Heat is transferred from an area of high temperature within a solid, to an area with a lower temperature, and the rate of transfer is determined by the thermal conductivity. (Quintiere, 1998)

2.2.2.2   Convection

Convection is the flow of heat between a fluid, typically air, and a solid. Heat typically flows upwards due to the buoyant flow of gases, and in the process, heat is transferred to solids. The rate at which the temperature is transferred from the fluid to the solid is determined by the convective heat transfer coefficient, which is governed by the speed the fluid is moving at. Convection causes the upward movement of hot gases and smoke, and when a fire occurs within a compartment, convection is also responsible for allowing heat to escape through openings. (Quintiere, 1998; Karlsson and Quintiere, 1999)

2.2.2.3   Radiation

Radiation occurs when heat is emitted and transferred through electromagnetic waves from a body possessing thermal energy. This is the main mechanism for the transfer of heat from flames and the hot gas layer, onto material surfaces. These surfaces will then either absorb, transmit or reflect this heat, depending on the absorption coefficient and emissivity of the material. (Quintiere, 1998; Karlsson and Quintiere, 1999)

Turbulent flames, as would be seen in a train, have a lower temperature than laminar flames. Thick flames are turbulent and are governed by radiant heat flux, while laminar flames are governed by convection. (Quintiere, 1998)

2.3   Compartment Fires

Compartment fires occur when burning takes place within an enclosure. Various factors distinguish this type of fire from an open-air fire, including the geometry of the compartment and the ventilation conditions in the compartment.

2.3.1   Fire Development

Fire development occurs in four phases; the incipient phase, growth phase, fully-developed (burning) phase and decay phase, as can be seen in Figure 2.1. The incipient phase is the time leading up to ignition, during which heating of the potential fuel occurs. After ignition, the fire transitions into the growth phase. (Buchanan and Abu, 2017)
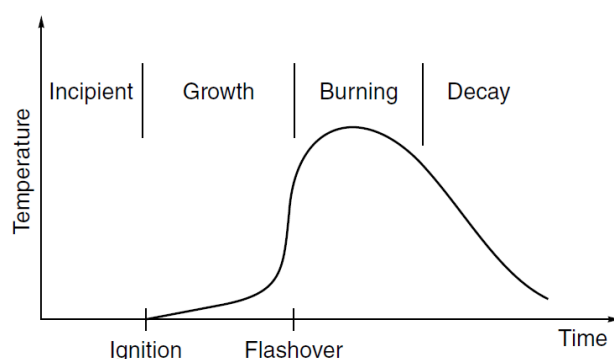
Figure 2.1: Time-temperature curve for fire development (Buchanan and Abu, 2017)

2.3.1.1   Ignition and Growth

Ignition can occur as spontaneous (auto-ignition) or piloted ignition, when a spark or flame is present. In the early stages of fire development, the enclosure does not affect the fire behaviour, and the combustible materials and their properties will govern the characteristics of the fire. Fire growth is influenced by three factors; ignition, flame spread and burning rate, all stimulated by heat fluxes (Quintiere, 2006). Typically, heat fluxes as low as 10 kW/m^2 can cause piloted ignition for thin materials, while for thick materials, this rises to 20 kW/m^2 (Quintiere, 2006). As the fire grows, these heat fluxes, particularly the radiant heat fluxes, are caused not only by the flames themselves, but by radiant feedback from the hot gases (Buchanan and Abu, 2017).

At the beginning of the growth phase, the fire behaviour is similar to a fire burning in the open, with the heat release rate (HRR) being determined by the fuel as oxygen concentrations remain normal (Quintiere, 1998). During the growth phase, a layer of smoke and hot gases, which are by-products of

combustion, starts to form in the enclosure just below the ceiling, as can be seen in Figure 2.2, and continues extending downward as it builds up.
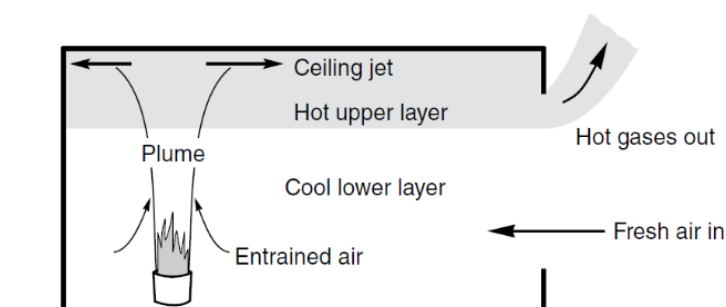
Figure 2.2: Hot layer formation in early stages of fire development (Buchanan and Abu, 2017)

The ignition and growth phase is the time-frame which people have to evacuate the enclosures in which the fire started. At a heat flux of about 4 kW/m², human skin experiences burn injuries, while pain sets in at heat fluxes as low as 1 kW/m² (Quintiere, 2006).

2.3.1.2   Flashover

Flashover is the rapid period of change between the growth stage and a fully-involved room fire (Quintiere, 1998). A heat flux of 20 kW/m² at floor level and/or a 500°C to 600°C smoke layer temperature, is often used to define flashover (Quintiere, 2006). When flashover occurs, the fire is characterised by a rapid lowering of the hot layer, flaming combustion overhead rolling along the ceiling, ghosting tongues of flame, the darkening of smoke to black escaping the openings, as well as flames emerging from the openings (NFCC, no date).

2.3.2   Fuel Controlled versus Ventilation Controlled Fires

During the burning of combustible materials in an enclosure, the fire can vary from fuel controlled to ventilation controlled. A fuel-controlled fire has sufficient oxygen to burn the fuel at a maximum rate which is only limited by the rate of pyrolysis. A ventilation controlled fire occurs when there are not sufficient oxygen levels to burn the fuel at a maximum rate, and the fuel is burnt at a rate determined by the oxygen supply. This is due to the enclosure being depleted of oxygen, and thus combustible gases cannot burn inside the enclosure, so the flames emerge from the windows where oxygen is available (Buchanan and Abu, 2017). When an additional vent is suddenly opened, or the glass of a window break during a ventilation controlled fire, a backdraft may result, as oxygen rapidly enters the enclosure and causes an almost explosive burning of gases leading to flashover (Karlsson and Quintiere, 1999).

2.3.3   Design Fire Estimation Methods

In order to predict the size of a fire, design fire estimation is required. There are several methods to estimate design fires. Some of the methods which could be applied to passenger train carriages in fire include the t^2 fire, summation method, Duggan's method and FDS, which will be discussed below (Darmody and Weaver, 2014).

Some historical passenger train fire incidents have been studied and the design fires estimated have been reported as shown in Table 2.1 (Darmody and Weaver, 2014).

Table 2.1: Historical design fires of passenger train fire incidents

Incident	Estimated Maximum HRR (MW)
Daegu train fire, Korea, 2003	20
Kaprun tunnel fire, Austria, 2000	15 to 50
Baku metro train fire, Azerbaijan, 1995	100
Montreal train fire, Canada, 1971	20.5
Montreal train fire, Canada, 1974	26.4

2.3.3.1 t^2 Pre-flashover Fires

A popular method of estimating the growth rate of a pre-flashover fire, is by using a parabolic curve in which the HRR is proportional to the time squared, as can be seen in Equation 2.1. The rate at which the increase occurs is dependent on the selected growth rate; slow, medium, fast or ultrafast, with corresponding growth constants (k) of 600, 300, 150 and 75. (Buchanan and Abu, 2017)

Equation 2.1: HRR of a t^2 fire

$$Q = \left(\frac{t}{k}\right)^2$$

In order to select an appropriate growth rate, the materials, geometry and ventilation in the train carriage need to be taken into account, but train fires usually involve a fast growth rate. This method can be useful for estimating the growth phase of passenger train fires up to a point where tenability conditions are exceeded. The usually predetermined maximum HRR used for t^2 curves, is often not the primary concern as the tenability conditions will be exceeded before the maximum HRR is reached. (Darmody and Weaver, 2014).

2.3.3.2   Summation Method

The summation method involves determining the total interior fire load and dividing it by the assumed burn time in order to obtain the HRR. In this method, the HRR is constant over the burn duration instead of a curve. The fuel load is taken from literature or by means of small-scale testing, but this method does not take ventilation conditions or material interaction into account and relies on an average value. (Darmody and Weaver, 2014)

2.3.3.3   Duggan's Method

Duggan's method builds on the summation method by summing the HRR curves of each exposed surface material in terms of HRR per unit area (HRRPUA) and multiplying each by the exposed surface area. This produces a HRR curve for the entire carriage interior. The heat flux levels assumed for each HRR curve are 50 kW/m^2 for horizontal materials such as ceilings, 35 kW/m^2 for vertical materials such as walls and 25 kW/m^2 for horizontal materials facing upward such as floors. This method assumes that all materials burn simultaneously, and does not take heat transfer, fire spread between materials, fire growth within the carriage or ventilation conditions into account. (Darmody and Weaver, 2014)

2.4   Standards for Passenger Trains

Internationally, relatively few passenger train fires have occurred in recent years, but the consequences of such an event are significant and may include a danger to lives, infrastructure damage, and may influence business continuity (Darmody and Weaver, 2014). For this reason, various standards and

guidelines exist with which passenger trains can be tested for compliance. Although some standards involve fire hazard assessment methods, the majority of standards follow a prescriptive approach, focussing on components within the train and not on the combination of items and materials which form the carriage and determine the safety of the train as a system. Standards are therefore ideal for compliance testing, but the data obtained from these tests needs to be processed further in order to determine the fire behaviour that could be expected during a real fire within a passenger train carriage. This will allow a performance-based approach to be followed, by assessing the safety of the train as a system.

In order to assess the performance of a passenger train in fire, a suitable design fire must be identified. The size of the design fire is dependent on the properties of the ignition source, the properties of the materials found in the train, as well as the geometrical properties of the carriage such as layout, size and ventilation (Darmody and Weaver, 2014). The ignition source plays an important role at this point as an accidental fire due to internal components overheating or a fire caused by an electrical fault will lead to a significantly smaller fire when compared to an arson attack where the ignition source involves accelerants and an intention to cause a significant amount of damage. Standards, however, do not account for arson attacks as these fires are generally scarce occurrences and thus not considered a standard risk and thus not treated conservatively (Coles *et al.*, 2009). It is also only in recent history that arson attacks on passenger trains have become a common occurrence in South Africa. The problem with the assumption of a smaller design fire is that small ignition sources, which are classified as a medium t^2 fire, do not lead to significant fire growth for trains adhering to NFPA 130 specifications, but large ignition sources, such as in the case of arson attacks, will likely lead to flashover when flammable liquids are used as accelerants, and these fires are closer to an ultrafast t^2 fire (Coles *et al.*, 2009).

In South Africa, there are no standards for fire related to passenger trains specifically. In order to assess passenger trains in fire, international standards are thus needed. Most passenger trains purchased for use in South Africa originate from other countries, in particular trains manufactured by Bombardier Transportation. These trains are thus originally designed according to international standards such as British Standards (BS), Europäische Norm (EN), which are European standards, American Society for Testing and Materials (ASTM) standards, National Fire Protection Association (NFPA) standards, or International Organization for Standardization (ISO) standards.

2.4.1   NFPA 130

NFPA 130 (NFPA, 2017) includes specifications for flammability, smoke emission, and fire performance of materials and assemblies, which apply to all operating environments. Tests are required according to several ASTM standards, as indicated in Table 2.2. These tests include small-scale tests, large-scale seat tests as well as fire resistance furnace tests.

Table 2.2: NFPA 130 - Fire test procedures and performance criteria for materials and assemblies (NFPA, 2017)

Category	Function of Material	Test Method	Performance Criteria
Cushioning	All individual flexible cushioning materials used in seat cushions, mattresses, mattress pads, armrests, crash pads, and grab rail padding [a–e]	ASTM D3675	$I_s = 25$
		ASTM E662	$D_s (1.5) = 100$
			$D_s (4.0) = 175$
Fabrics	Seat upholstery, mattress ticking and covers, curtains, draperies, window shades, and woven seat cushion suspensions[a–c, f–h]	14 CFR 25, Appendix F, Part I (vertical test)	Flame time = 10 sec
			Burn length = 6 in.
		ASTM E662	$D_s (4.0) = 200$
Other vehicle components	Seat and mattress frames, wall and ceiling lining and panels, seat and toilet shrouds, toilet seats, trays and other tables, partitions, shelves, opaque windscreens, combustible signage, end caps, roof housings, articulation bellows, exterior shells, nonmetallic skirts, battery case material, and component boxes and covers[a,b,i–k]	ASTM E162	$I_s = 35$
		ASTM E662	$D_s (1.5) = 100$
			$D_s (4.0) = 200$
	Thermal and acoustical insulation[a,b]	ASTM E162	$I_s = 25$
		ASTM E662	$D_s (4.0) = 100$
	HVAC ducting[a,b]	ASTM E162	$I_s = 25$
		ASTM E662	$D_s (4.0) = 100$
	Floor covering[b,k,l]	ASTM E648	CRF = 5 kW/m^2
		ASTM E662	$D_s (1.5) = 100$
			$D_s (4.0) = 200$
	Light diffusers, windows, and transparent plastic windscreens[b,i]	ASTM E162	$I_s = 100$
		ASTM E662	$D_s (1.5) = 100$
			$D_s (4.0) = 200$
	Adhesives and sealants[a,b,p]	ASTM E162	$I_s = 35$
		ASTM E662	$D_s (1.5) = 100 D_s$
			$(4.0) = 200$
Elastomers[a,b,i,j]	Window gaskets, door nosings, intercar diaphragms, seat cushion suspension diaphragms, and roof mats	ASTM C1166	Flame propagation = 100 mm (4 in.)
		ASTM E662	$D_s (1.5) = 100$
			$D_s (4.0) = 200$
Wire and cable	All	See 8.6.7.1.1.1 through 8.6.7.1.3.	See 8.6.7.1.1.1 through 8.6.7.1.3.
Structural components[m]	Flooring,[n] other[o]	ASTM E119	Pass

NFPA 130 also describes tenable environments in terms of hyperthermia, body surface burns and respiratory tract burns, where the heat exposure is a function of the exposure temperature and the radiant heat flux. Respiratory tract burns are said to occur when air above 60°C is inhaled, although skin burns would occur before that, starting at a radiant heat exposure of approximately 1.7 kW/m^2, with exposure time decreasing as the radiant heat flux increases as per Equation 2.2, where t refers to the time in minutes, and q refers to the radiant heat flux in kW/m^2. Exposure can be tolerated for several minutes at a radiant heat flux below 2.5 k/m^2. Where a hot layer has formed above the escape route, the radiant flux corresponds to a 200°C hot layer temperature. In terms of convective heat, Equation 2.3 is specified with T referring to temperature. Equation 2.4 is specified when considering the accumulated heat effects due to the radiant and convective heat a person is exposed to, thus the exposure temperature must be less than 60°C for 10 minutes. (NFPA, 2017)

Equation 2.2: Time to burning of skin due to radiant heat (NFPA, 2017, Equation B.3.3.2)

$$t_{Irad} = 1.33 \times q^{-1.35}$$

Equation 2.3: Time of exposure for convective heat (NFPA, 2017, Equation B.3.3.3a)

$$t_{Iconv} = (5 \times 10^7) \times T^{-3.4}$$

Equation 2.4: Maximum exposure time without incapacitation (NFPA, 2017, Equation B.3.3.3c)

$$t_{exp} = (1.125 \times 10^7) \times T^{-3.4}$$

2.4.2 EN 45545

EN 45545 (CEN, 2015) includes specifications which apply to specific operating environments, determined by whether the train frequently operates in tunnels, the availability of safe areas to exit the train, whether there are emergency trained staff on board, whether it includes double-decked carriages and whether it includes sleeping and couchette carriages. Each component within the train is subject to testing according to a requirement set which includes specifications on critical flux at extinguishment, maximum average rate of heat emission, peak HRR, flame spread and ignitability for each hazard level. Required tests include small scale cone calorimeter tests according to ISO 5660-1, flame spread tests according to ISO 5658-2 and ISO 9239-1, as well as furniture calorimeter tests according to ISO/TR 9705-2.

Hazard level 1 applies to operation category 1 – over-ground trains with no tunnels or elevated sections, where side evacuation is possible, and trains can stop with minimum delay, but is extended only to the design categories of standard vehicles, automatic vehicles without trained staff and double-decked vehicles. The requirement set R18 applies to seat assemblies and consists of two specifications, both related to furniture calorimeter testing. For hazard level 1, seats are required to have a peak heat release rate not exceeding 350 kW (which also applies to all other hazard levels), and have a Maximum Average Rate of Heat Emission (MARHE) not exceeding 75 kW/m^2. Additional requirements are also specified; the flame spread should not reach the edges of the seat surface or backrest, and the flame height should not exceed 1000 mm above the highest point of the seat surface during the test. A restriction is also included for safety; peak heat release rate values too high for test equipment safety, will result in a non-compliant product. These specifications, as well as the 350 kW limit, are used later to assess whether the Metrorail seats are compliant.

2.5 Experimental Research and Testing of Passenger Trains in Fire

For passenger trains, experimental work and testing has been done for many years, from small-scale material tests to large scale seat tests or experiments involving mock-ups of small sections of carriages, to full-scale carriages being ignited for experimental purposes, each with advantages and disadvantages. Small-scale material tests do not simulate real fire scenarios well but are the most affordable method of testing. Large-scale tests and experiments simulate localised fire behaviour, including ignition and early-stage fire growth but do not simulate fully developed fires well due to the reduced geometry and ventilation conditions that differ from those of real fire scenarios. Full-scale experiments are extremely costly, the direct measurement of HRR is difficult to achieve, and multiple fire scenarios cannot be tested due to typical budget limitations. (White, 2010)

Peacock and Braun concluded in 1984 that small-scale test results do not accurately predict large scale behaviour, and thus, full-scale tests are required (1984). Thereafter the USA National Institute of Standards and Technology (NIST) conducted a project involving an alternative approach which utilised HRR tests alongside fire modelling and fire hazard analysis, and involved cone calorimeter tests, large-scale and full-scale tests as well as zone models (Peacock and Braun, 1999; Peacock *et al.*, 2002, 2004). In 2001 Fire Standardisation Research of Railway Vehicles (FIRESTARR) proposed test

methods and conditions for the assessment of the fire performance of materials which was later used for the new European standard EN 45545 and included prescriptive requirements in terms of small-scale and large-scale tests (Briggs, Le Tallec, *et al.*, 2001; Briggs, Metral, *et al.*, 2001). Full-scale experiments were performed by Commonwealth Scientific and Industrial Research Organization (CSIRO), which led to important findings regarding fire behaviour; the important factors determining fire growth are the wall lining and combined design of the seat, HRR measurement is the focus of fire safety in assessing the fire performance of materials, and cone calorimeter test data provides useful data for fire modelling (White and Dowling, 2004).

Chiam (2005) and White (2010), however, were unsuccessful in predicting the HRR using material test data and FDS version 4, as the cone calorimeter test data were not suitable for use at lower heat fluxes. Hostikka and McGrattan attributed this to errors in the heat transfer solutions and thermal properties, and physical phenomena such as internal mass transfer and surface reactions being absent (2001).

Guillaume et al. (2014) used these past studies to predict fire growth for a complete design fire scenario (DFS), taking into account the limits of the numerical tools available. A multi-scale investigation was developed for scenarios identified by a fire risk analysis. The fire behaviour of the multilayer seats and inner wall panel were studied in detail using pyrolysis models, specifically FDS v5.5.3. The fire behaviour was studied from material to real scale. The design fire scenario includes the fire source, detection, ventilation systems, fire protection, evacuation strategy and train movement / stopping strategy.

For Metrorail trains, however, fire detection is manual and usually only occurs once the train reaches a station. There are also no systems in place for ventilation control, active or passive fire protection, or alerting the driver. Thus, in the Metrorail case, the worst-case fire design scenario is assumed, and it must be assumed that there will likely be no intervention before flashover has occurred.

The approach selected by Guillaume et al., shown in Figure 2.3, makes use of the multi-scale approach as the flame spread of the materials on-board trains is involved, which is challenging to model as it requires advanced knowledge of the materials and the thermo-chemical behaviour involved, which requires various scales to provide information on the fire behaviour. The small-scale testing involves studying fire behaviour and heat transfer in terms of materials, while the larger scales involve assemblies, configuration and mounting. After determining the decomposition chemical path and the kinetic constants associated, for each material, the cone calorimeter behaviour of the materials is modelled in FDS, measuring thermal transfer parameters where possible and obtaining others from literature. Thereafter heat transfer coefficients and mesh size are identified in order to model flame spread. The final step involves a validation case where a real-scale configuration is involved. (Guillaume, Camillo and Rogaume, 2014)

Guillaume et al. found that this multi-scale approach showed that the predictive method was capable of reproducing fire growth, HRR and temperatures, but the carbon monoxide and potentially other toxic species were not reproduced properly and could thus not be used to predict tenability conditions in this regard. The recommendation was to limit the assessment of tenability of passengers to thermal-related effects until further work has been done to improve the capability of combustion models. (Guillaume, Camillo and Rogaume, 2014)

A similar approach based on the burning of entire carriages is used for this thesis, but the validation of the full-scale numerical simulations was not possible.

Experiment part   **Numerical part**
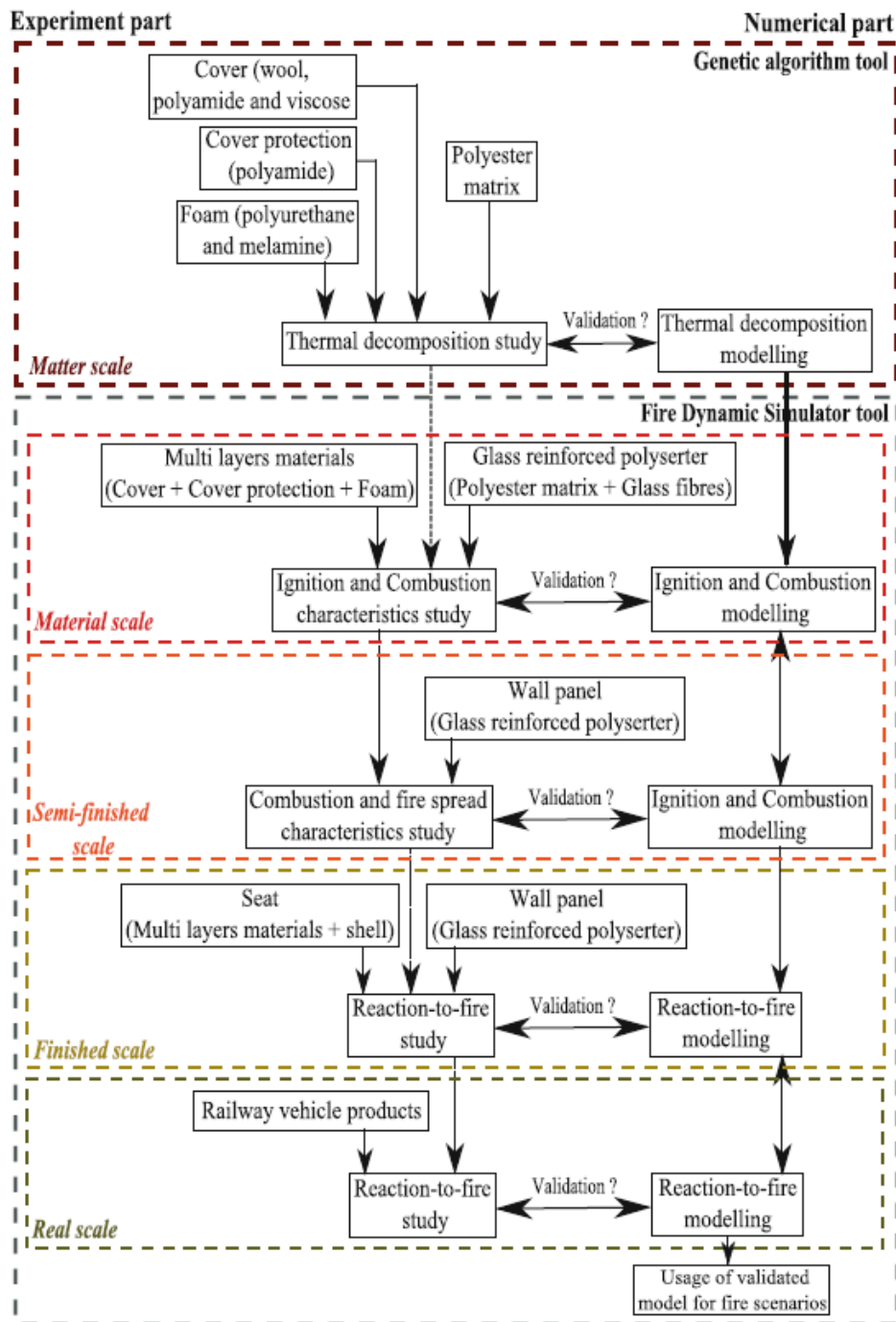
Figure 2.3: Multi-scale experimental-numerical approach (Guillaume, Camillo and Rogaume, 2014)

Fire does not scale well due to the complexity and interaction of the various parameters such as turbulence intensity, the thermal response of interior materials and radiation effects (Ingason, 2007). This makes large scale testing a requirement. If scaling were to be successful, each parameter would need to be scaled differently in order to obtain results which could compare with full-scale tests, which is not possible. With smaller fuel loads, temperatures are lower, which significantly affect the development phase leading to flashover. Composite materials, or items that consist of various materials, will not be represented well, as the interaction of materials also affects the resultant fire. These materials or items might need to be represented by equivalent materials or items depending on the scale which is used. Visually fire may be well represented, but data such as time, temperature, HRR etc., would not be well represented by a scale model.

2.6   Numerical Simulations

Testing and performing experiments on full-scale train carriages has not been done often, mainly due to the cost involved. A single test or experiment will also not provide a great amount of information, particularly in terms of studying the effect that different scenarios have on the fire behaviour that is observed. In order to study the fire behaviour in a train carriage, without performing multiple expensive tests, the fire scenarios can be replicated using numerical simulations in order to predict the behaviour that can be expected.

2.6.1   Types of Models

Plume models, zone models or computational fluid dynamics (CFD) models can be used to simulate pre-flashover fires (Buchanan and Abu, 2017).

2.6.1.1   Plume Models

Plume models describe axisymmetric fires by using simple empirical correlations (Buchanan and Abu, 2017).

2.6.1.2   Zone Models

Zone models, which are used for compartment fires, involve the compartment being divided into a hot upper layer and cooler lower layer, where mass and energy balances exist for each layer. The zones are allowed to interact with one another in order to determine the temperature of each zone. Zone models are physically and computationally relatively simple and are thus widely used for applications which do not require detailed spatial distributions of physical properties. (McGrattan *et al.*, 2015; Buchanan and Abu, 2017)

2.6.1.3   CFD Models

CFD models divide the domain in which a fire occurs into a grid of rectangular cells (McGrattan *et al.*, 2015). The temperature is determined for each cell by solving the fundamental equation of fluid flow (Buchanan and Abu, 2017). The process on which CFD is based, is outlined in Figure 2.4.

It makes use of Reynolds-averaged Navier-Stokes equations, which uses a time-averaged approximation of the conservation equations used in fluid dynamics. Large-eddy transport coefficients are used and return smoothed results, especially when large time-steps are used. (McGrattan *et al.*, 2015)
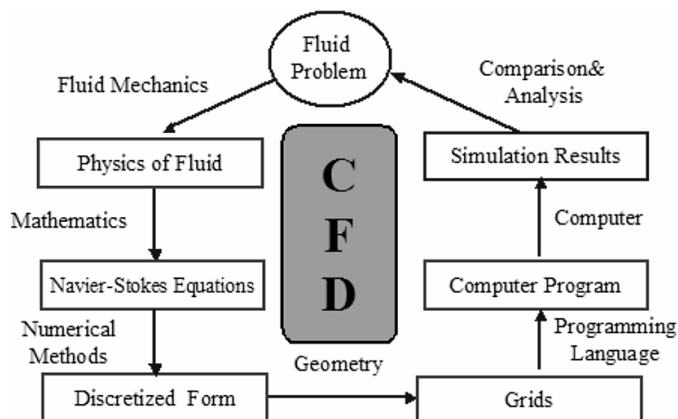
Figure 2.4: Computational Fluid Dynamics process (Zuo, 2005)

2.6.2 Fire Dynamics Simulator

The software used to perform numerical simulations in this study is known as Fire Dynamics Simulator (FDS) and was created by the National Institute of Standards and Technology (NIST). The graphical user interface known as PyroSim, which was created by Thunderhead Engineering, was used to prepare models for FDS simulations. Smokeview, also created by NIST, has been incorporated into PyroSim in order to visualise results.

FDS requires users to define a number of physical descriptions of the scenario and few numerical parameters. A rectilinear grid is applied to the domain, with dimensions specified by the user, in which the geometry under consideration is found. A uniform mesh is preferable for the large-eddy simulation aspect of FDS. The geometry is specified by the user as rectangular obstructions. If the obstructions do not align with the grid perfectly, due to a difference in dimensions or positions between the grid cells and the obstruction, the obstruction is snapped to the underlying grid using a simplification of the immersed boundary method (IBM). The domain can be divided into multiple meshes by the user in order to allow for faster, parallel processing using Message Passing Interface (MPI) processes. A staggered grid is used in which scalar values are applied to the centre of the cells while vectors are applied to the required cell faces. This allows for pressure cell velocity divergence to be represented naturally when pressure-velocity coupling is done.

FDS is based on Computational Fluid Dynamics (CFD), but removes the elements which are not relevant to fires. The basic features FDS makes use of is the low Mach large-eddy simulation, explicit second-order kinetic-energy-conserving numerics, a structured uniform staggered grid, a simple immersed boundary method for the treatment of flow obstructions, the generalised lumped species method, Deardorff eddy viscosity sub-grid closure, constant turbulent Schmidt and Prandtl numbers, the eddy dissipation concept for single-step reaction between the fuel and the oxidiser and grey gas radiation with finite volume solution to the radiation transport equation. (McGrattan *et al.*, 2015)

In FDS, an explicit second-order predictor/corrector scheme is used. A specific cell at a given time-step starts with values for density, lumped mass fractions, the velocity vector and the fluctuating stagnation energy per unit mass for that cell, as well as the background pressure. In order to determine the values for the next time-step, the predictor estimates the values of the cell at the next time step performing an explicit Euler step, calculating the temperature with the equation of state, calculating the divergence with estimated thermodynamic values, calculating the Poisson equation and confirming whether the values still conform to the Courant-Friedrichs-Lewy (CFL) stability condition. Thereafter the corrector corrects the density, lumped species mass fractions and background pressure for the time-step being calculated, uses the equation of state to calculate the temperature, performs time splitting for mass source terms, calculates the final temperature with the equation of state using the updated density and composition, calculates the divergence using the corrected thermodynamic properties, uses estimated values to calculate the pressure and corrects the velocity at the next time step. Thereafter the same procedure is applied to the following time-step. (McGrattan *et al.*, 2015)

2.6.2.1 Large-eddy Simulation (LES)

Large-eddy simulation (LES) is used to describe the turbulent mixing of volatiles and the products of combustion with the air around the fire. This defines the spread of smoke and hot gases and determines the burning rate of the fire. It makes use of equations determined by applying a low-pass filter to the transport equations for mass and momentum of a particular cell width, where kinetic-energy-conserving central difference schemes are used for the momentum, and physically-based closure is applied to the turbulent stress. (McGrattan *et al.*, 2015)

2.6.2.2 Mass and Species Transport

In order to simplify the simulations, FDS allows the user to specify a single fuel in terms of chemical reaction, which limits the number of fuel gases to keep track of over and above the oxygen, carbon

dioxide, carbon monoxide, nitrogen, water vapour and soot particles, which are present in all combustion processes. Using a single-step reaction, two transport equations are solved for the total mass; one for the fuel, as a single gas species, and one for the products, as a lumped species, which transport and react together. In order to use the lumped species, the mass fractions are defined for air (nitrogen, oxygen and trace amounts of water vapour and carbon dioxide), fuel and products, which is linearly related to the primitive species mass fractions, allowing matrix multiplication to be done in order to convert from the one to the other. When summing the transport equations over all species, the equation for the conservation of mass is confirmed. (McGrattan *et al.*, 2015)

2.6.2.3 Combustion and Radiation

FDS models aspects such as the turbulent combustion of fuels, in their gaseous form, and oxygen, the movement of thermal radiation through hot gases loaded with soot, thermal decomposition of real materials, and the movement of liquid fuel droplets and water. FDS generally applies a combustion model based on the mixing-limited, infinitely fast reaction of lumped species. The characteristic mixing time determines the rate at which reactant species within a cell are converted to products. Summing the lumped species mass production rates multiplied by their heats of formation determines the HRR per unit volume. Radiation is governed by the radiation transport equation (RTE) for non-scattering grey gas. Soot is responsible for the majority of thermal radiation emitted and absorbed, which is not significantly sensitive to wavelength, and thus the RTE only needs to be solved for a limited number of bands in the radiation spectrum, although this number can be increased by the user. To solve the radiation equation, the finite volume method (FVM) is used, similar to that of convective transport. (McGrattan *et al.*, 2015)

3 Background Information on Passenger Trains and Arson

3.1 Introduction

In this chapter, background information is discussed regarding passenger trains, specifically Metrorail trains, as well as the arson attacks experienced by the intra-urban trains in South Africa. This provides insight into the problems being experienced by Metrorail. The trains and materials discussed are tested in Chapter 5 and 6 and modelled in Chapter 7.

3.2 PRASA and Metrorail

PRASA (Passenger Rail Agency of South Africa) is a state-owned enterprise mandated to provide rail commuter services in South Africa. It is divided into four branches; commuter rail services in intra-urban areas are operated by Metrorail, while inter-urban commuter rail services are operated by Shosholoza Meyl, Autopax operates the coach services, and Intersite manages PRASA-owned property. (PRASA, 2015)

3.3 Reasons for Passenger Train Arson in South Africa

There is no clear answer as to why arson on passenger trains has become so frequent over the past few years, but most of the possibilities are linked to socio-economic problems. Some speculate that the taxi industry is responsible for the arson attacks as the passenger trains offer a cheaper alternative, and by removing the competitor, the taxis would have a monopoly on the low-cost commuter services industry. Others speculate that disgruntled commuters set the trains alight because the trains are not on time or are cancelled, which causes problems for people who need to be at work on time. Cancelled trains or delays are in turn caused by theft and vandalism of PRASA infrastructure.

The cost of a single arson attack on carriages in Cape Town station in November 2019, was R61 million (Isaacs, 2020). In 2018 and 2019, 45 carriages were damaged in fires, and from 2017 to 2019, the Metrorail fleet was halved as a result of arson (Daniel, 2019). Figure 3.1 to Figure 3.4 show examples of fire experienced on various Metrorail trains.

Figure 3.1: Carriages on fire at Cape Town station in June 2017 (Hendricks, 2017)

Figure 3.2: Carriages on fire at Cape Town station in July 2018 (Boshoff, 2018)

Figure 3.3: Carriage on fire pulling into Retreat station in July 2018 (Metrorail, 2018)

Figure 3.4: Burning train reigniting at Koeberg depot (City of Cape Town Fire, 2017)

3.4   Location of Arson Attacks

Most of the arson cases have occurred in the Western Cape on the intra-urban trains. There are some cases where disgruntled passengers have set trains alight in Gauteng due to the trains not being on time, or being stationary due to maintenance or infrastructure problems, preventing it from continuing on its journey. Many times the trains pull into stations with flames already protruding from the windows. In some cases, the trains have been set alight at Cape Town Station, which has a roof, unlike many of the other smaller stations. This has led to some platforms or the entire station being closed.

17

3.5 Carriages

3.5.1 Carriage Classes

Metrorail trains consist of three classes of carriages, Business, MetroPlus (first class) and Metro (third class). The carriage types most often targeted are the MetroPlus type. The Business class carriages depart from Paarl and stop only in Belville, and finally ends their journey at Cape Town station. The train only departs from Paarl in the morning and from Cape Town in the afternoon. Due to the higher ticket price and the limited stops, access to this train is limited, and ticketing officers are likely to be more strict. This limits the opportunities for arsonists to gain access to the train, and the long distances between stops also might act as a deterrent as arsonists usually set the seat in a carriage alight and disembark the train immediately. The Metro class carriages typically have fibreglass seats, as can be seen in Figure 3.5, which are placed along the sides of the trains, and thus there is not sufficient fuel to sustain the fire, and damage would be limited. Igniting a fibreglass seat would require an impractical amount of accelerants, and as the fire load would need to be brought onto the train in order to get a fire started in one of the Metro class carriages, this is a very unlikely carriage to be targeted by arsonists. This leaves the MetroPlus carriages as the likely target of arsonists. The seats are made of various materials, including foam for comfort, but access is not limited to these carriages as with the Business class carriages.

Figure 3.5: Metro fibreglass seats

3.5.2 Carriage Type

There are various types of carriages in use, each with different specifications and configurations of elements. All Metrorail carriages are either in the format of motor coaches or plain trailers, which only carry passengers. For simplicity, this study focusses on the plain trailers. The 5M and 10M ranges are used for the MetroPlus carriages, specifically the 5M2A, 10M3 and 10M5 with different seat types, but the arson attacks are directed specifically at carriages containing seats with fire properties, which make them vulnerable, such as the 5M2A carriages. Due to this fact, Metrorail is retrofitting seats with fewer combustibles found on the 10M5 and 10M3 carriage types in the 5M2A carriages, as shown in Figure 3.6.

Figure 3.6: Retrofitted seat in a 5M2A carriage

3.5.3   Condition of the Carriages

The Metro and MetroPlus carriages are not only subject to arson but also other forms of vandalism, such as graffiti, covering the interior wall lining with stickers and damage to the seats, doors and windows. For these reasons, windows are no longer made of glass or other materials which could easily be broken, but rather Perspex which is more durable. Even though the windows are more durable, the frames may still be kicked out, so the windows of the trains are likely to be open, either for ventilation, as there is no cooling system on board, or due to vandalism, as can be seen in Figure 3.8 and Figure 3.10. The doors may also be damaged, and it is common to see passengers standing in the doorway or hanging out while the train is moving as the doors are either forced open or are not able to close automatically when the train departs from a station (see Figure 3.7, Figure 3.9 and Figure 3.10). Many of the seats are also damaged by sharp objects so that the foam beneath the seat cover is exposed.

Figure 3.7: Doors and windows on moving MetroPlus carriage (African News Agency, 2019)

Figure 3.8: Windows on Metro carriages (Hendricks, 2020)

Figure 3.9: Windows and doors on overcrowded MetroPlus carriages (Mortlock, no date)

Figure 3.10: Overcrowded train (African News Agency, 2017)

Figure 3.11: Seat bottoms stripped from carriages in the Salt River depot workshop

Figure 3.12: Condition of seats in MetroPlus carriage (Mortlock, no date)

Generally, the vents in the ceiling are functioning correctly, and the fibreglass vent structures found on the outside of the carriage have even been replaced with more durable metal structures over time, as can be seen in Figure 3.13. The Bakelite wall and ceiling linings and the Marley floor linings seem to generally be in good condition and are reported to have been treated with a flame retardant.

Figure 3.13: Ceiling and ceiling vent components

3.6   Accelerants

The specific accelerants used by arsonists is not known and could also potentially vary. The accelerants used to ignite the fires are likely low cost and do not take up a large amount of space as the arsonists need to board the train undetected. Internationally, hydrocarbon liquids are commonly used accelerants in arson attacks (Beyler, 2004, p. 858). Occasionally, high-temperature accelerants such as thermite and substances similar to rocket propellants are used, which result in very high heat fluxes (250 kW/m^2 to 300 kW/m^2), heat release rates of around 10 kW/m^2, wood charring rates of up to 10 mm/min and melting of iron and steel (Beyler, 2004, p. 858). Due to the costs involved and the fires typically seen when Metrorail trains experience arson attacks, the accelerants used are not high-temperature accelerants. The fuel load inside the train, which gets ignited by the accelerants, however, may sometimes cause the melting of steel within the carriages after extended exposure.

Kerosene (referred to as paraffin in South Africa) is a product of petroleum distillation and contains mostly paraffins, but may also contain napthenes and aromatics, and has a peak heat flux of 2.9 kW/m^2, but its flashpoint is above room temperature in most countries (Beyler, 2004, p. 865). Petroleum is a blend of various types of hydrocarbons, with different vapour pressures, and additives, and high-octane automotive petroleum typically has an auto-ignition temperature of 440°C to 450°C (Beyler, 2004, p. 849). Propane burners have a peak heat flux of 34 kW/m^2 to 38 kW/m^2 with a HRR of 0.035 kW for needle flame and Kleinbrenner burners, while tube burners have heat release rates from 2.8 kW to 21 kW with similar heat flux values (Beyler, 2004, chap 11, Table 17).

3.7 Polymers

The majority of accidental or unwanted fires are fuelled by polymers such as paper, wood, fabrics, plastics and foams. Polymers are large molecules consisting of smaller parts covalently bonded together, known as monomers. (Hurley *et al.*, 1997, p. 167–168).

Polymers are found as natural, such as cellulose, semi-natural, such as cellulose acetate, bio-based, such as styrene-soya oil-divinyl benzene or synthetic (Hurley *et al.*, 1997, p. 167). Synthetic polymers are generally referred to as plastics (Hurley *et al.*, 1997, p. 168). Three classifications of synthetic polymers are thermoplastic polymers, thermosetting polymers and elastomers, which possess rubber-like properties (Drysdale, 2011, p. 5). Oil or coal are generally used as raw materials to produce synthetic polymers, and thus have the same flammability (Hurley *et al.*, 1997, p. 167).

Polymers vary in the degree of cross-linking, which determines the amount of volatiles produced during thermal decomposition. With a high degree of cross-linking, a significant amount of the material thermally decomposes into a carbonaceous char upon heating, which cannot form volatiles. An example of a polymer with a high degree of cross-linking is phenolic resins, which result in 60% char when the material is heated above 500°C. When heated, thermosetting polymers, such as phenolic resins, do not melt, but usually produce volatiles directly from their solid phase. Flexible foams such as polyurethane mostly have a very low degree of cross-linking, although increasing this significantly, will result in a more rigid foam. Although flexible polyurethane foams are also thermosetting polymers, when heated, they initially thermally decompose into molten products, which then decompose further to produce volatiles. (Drysdale, 2011, p. 5–7)

Thermoplastics do not have additional cross-linking covalent bonds, which thermosetting polymers do have (Hurley *et al.*, 1997, p. 168). Upon heating thermoplastics, they initially thermally decompose by softening and melting, which changes the material behaviour in fire. After melting, further thermal decompositions occurs, and the low molecular weight products evaporate. Polycarbonate and polyester are known as engineering thermoplastics (Hurley *et al.*, 1997, p. 174). Thermoplastic polymers, such as polyvinylchloride (PVC) and polymethylmethacrylate (PMMA), cause fire spread by falling droplets and may also turn into molten polymer pool fires, properties which are also shared with flexible polyurethane foams. (Drysdale, 2011, p. 5–7)

The melting point of polyester is reported to be 252°C to 292°C while PVC has a melting temperature of 100°C to 160°C (Beyler, 2004, Table 114). PMMA is reported as having a melting temperature of 160°C (Drysdale, 2011, Table 1.2).

3.8 Carriage Materials

The materials used in a passenger train carriage, can have a significant impact on the fire behaviour observed. The material which each component is made of can influence the growth and spread of the fire, for example, if the interior lining of the carriage is made of a material, which promotes fire spread, the carriage can quickly be engulfed in flames, especially if the material burns for long enough with a sufficient amount of heat being produced in order to ignite surrounding components such as seats, while materials that melt and drip or form pool fires, can spread the flames by dripping onto other components or forming pool fires next to seats.

3.8.1   Seats

The seats targeted by arsonists are formed by a separate back and bottom, which are fixed to a metal pipe frame with legs, which are fixed to the floor of the carriage, as can be seen in Figure 3.14. There is thus an open space below the seats. The seat backs are sloping, and thus, seats which are back-to-back are connected at the top but have a gap towards the bottom of the seat back. The back-to-back seats share a metal pipe frame. The seat bottom and back consist of an outer pleather layer and inner foam layers, which are glued to a wooden backing, as can be seen in Figure 3.15. The plywood backing of the seat bottom is not covered by the pleather layer on the bottom. The plywood backing of the seat back does not come in a consistent thickness, some are formed by thin plywood sheets supported by thicker spines, while others consist of a thicker wood of uniform thickness throughout. The foam layers are also not consistent from one seat to another and can be found in a few variations; a heavy honeycomb-like rubbery type foam with layers of standard polyurethane foam, rebonded foam consisting of small pieces of foam of various colours with layers of standard polyurethane foam, and layers of standard polyurethane foam with no other types of foam. All the variations of foam generally have a very light, low-density fibre lining layer between the pleather and the foam layers below.

Figure 3.14: Seats in carriage at Salt River depot workshop with seat bottoms already stripped

Figure 3.15: Material layers of seat back and seat bottom

Composite materials such as furniture, with a thin fabric layer on top of a thick polyurethane foam, could exhibit thermally thick, thermally thin or a unique trend (Beyler, 2004, p. 269). The Ignition Handbook describes a furniture composite sample, which consists of an acrylic fabric (546 g/m^2) on top of a high resilience polyurethane foam (36 kg/m^3). This specimen had a minimum heat flux of 7 kW/m^2, a critical heat flux of 6.3 kW/m^2 and an ignition temperature of 245°C (Beyler, 2004, chap 7, Table 8), similar values could be expected for the Metrorail seats which consist of similar materials. This sample fitted a

t^{-1} power ignitability plot, and generally, furniture composites do not fit well when attempting a thermally thick fit due to the cover fabric dominating ignition behaviour, as the foam with a much lower density, as its behaviour resembles thermal insulation during ignition (Beyler, 2004, p. 269)

3.8.1.1 Pleather

Pleather can consist of either polyvinyl chloride (PVC) or polyurethane (PU) sheets with either a cotton or a polyester backing (Sewport Support Team). It is not clear which material the pleather found on the seats consist of. The backing, also known as the scrim, also varies from seat to seat - some have a fine, dense threading and others have a thicker but more widely spread threading.

3.8.1.2 Lining Material

The white lining material between the pleather and polyurethane is of unknown nature, but it is visually similar to non-woven polyester fibre wadding, a material typically used as a lining between the cover fabric and the foam below. When the lining is compressed, as it would be in an intact seat, the lining is thinner, and thus more dense, than when it is removed from a seat. The older the seat, the thinner the lining becomes due to repeated pressure being applied and the lining not returning to its original thickness as the fibres become displaced and packed more densely.

3.8.1.3 Foam

The foam found in the seats can either be in the form of polyurethane, rebonded or a rubbery foam with a honeycomb structure, suspected to be latex foam. Rebonded foam is polyurethane foam, which has been shredded and bonded back together with adhesives, such as liquid polyurethane, while being compressed (*Rebond Foam Product Guide | OFS Maker's Mill*, no date). Polyurethane foam has a peak HRR of around 760 kW to 2630 kW with small or no room effect, or 138 kW/m^2 to 399 kW/m^2 at a radiant heat flux of 25 kW/m^2 (Hurley *et al.*, 1997, Table 26.15). Latex foam, on the other hand, has a peak HRR of 2720 kW or 479 kW/m^2 (Hurley *et al.*, 1997, Table 26.15), significantly higher than that of polyurethane foam. Smouldering can occur in polyurethane within 20 minutes at a critical radiation heat flux of 7 kW/m^2, while piloted flaming ignition occurs at 13 kW/m^2 and spontaneous flaming ignition occurs at 30 kW/m^2, within 1 minute of exposure (Hurley *et al.*, 1997, p. 586). When smouldering ignition is caused by heat transferred by conduction, the required heat flux is as low as 3 kW/m^2 when a large heated object is in direct contact with the polyurethane foam, but this is influenced by convection within a porous fuel such as polyurethane foam (Hurley *et al.*, 1997, p. 586).

3.8.1.4 Plywood

In South Africa, plywood is typically made of pine due to availability. Internationally, Douglas fir is also commonly used for plywood. Plywood and wood typically have similar thermal and ignition properties, although thermal conductivity in plywood is generally lower (Beyler, 2004, p. 964).

3.8.2 Windows

Due to vandalism, the windows are no longer made of glass and metal frames but rather a transparent sheet with a plastic frame. It is unclear which type of material the transparent sheet is made of and will need to be confirmed with testing. Transparent plastic sheets are generally made of polymethylmethacrylate (PMMA), also known as acrylic and sold under the trade names Perspex or Plexiglass, or polycarbonate, sold under the trade names Lexan or Makrolon.

3.8.2.1 Polymethylmethacrylate vs Polycarbonate

PMMA ignites faster than polycarbonate; 19 s compared to 37 s in a 50 kW/m^2 cone calorimeter, 92 s compared to 116 s with a needle flame, and PMMA even ignites at 850°C using glow wire ignition,

which polycarbonate does not (Beyler, 2004, Table 175). PMMA and polycarbonate can both resist impact better than glass, but PMMA can only resist impacting 17 times more than glass, while polycarbonate can resist 250 times more. Polycarbonate is more flexible than PMMA, which is prone to cracking under extreme impact due to its rigidity. Polycarbonate is, however, more expensive, and along with the high impact strength, it also has a good resistance to ignition. Polycarbonate will, however, turn yellow when continuously exposed to sunlight, but this can be reduced by UV-resistant products. PMMA performs much better outdoors though, with a guaranteed lifetime of 30 years, compared to the 10 years guaranteed for UV-resistant polycarbonate. Polycarbonate allows 89% of light through while PMMA allows 92% through. Polycarbonate scratches more easily than PMMA, although PMMA has the ability to be polished, which is not as easy to do with polycarbonate. (*Uses of Perspex® Acrylic Sheet vs Polycarbonate Sheet - Industrial Plastics*, no date)

3.8.2.2   Glass

If glass was still in use, cracks could be expected from 3 kW/m^2 to 5 kW/m^2 heat flux or 110°C to 200°C depending on the type and thickness of the glass, while breaking can be expected at 23 kW/m^2 or 150°C to 175°C, while the glass can be expected to fall out at 23 kW/m^2 to 43 kW/m^2 for various types of glass or 300°C for toughened 6 mm glass (Hurley *et al.*, 1997, Table 86.4).

3.8.3   Wall and Ceiling Lining – Bakelite

Phenol formaldehyde (phenolic) resin, also known as Bakelite, is used in high-pressure laminates, which consists of many layers of substrate with a thermosetting polymer, such as phenolic resin, in between, heat-cured at pressures over 7 atm (Beyler, 2004, p. 726). Laminates such as Bakelite are difficult to study thermally, as they delaminate explosively when exposed to heat (Beyler, 2004, p. 726). Phenolic resin starts to ignite when exposed to a radiant heat flux of 25 kW/m^2, taking 159 s to 296 s to ignite, while it ignites within 3 s to 13 s at a radiant heat flux of 50 kW/m^2 (Beyler, 2004, Table 183).

3.8.4   Floor – Marley (PVC)

The floor covering is made of Marley, the trade name of slip-resistant vinyl used for flooring (*Marley Dance Flooring - Studio Quality*, no date). In the 5M2A carriage, the polyvinyl chloride (PVC) covers a 20 mm thick plywood floor below, while in the 8M carriages, the floor is made of concrete.

3.8.5   Window Frame

The window frame is made of an unknown black plastic material which could be PVC, PMMA or polycarbonate. Previously the frames were metal, but due to vandalism, these have been replaced with plastic frames.

3.8.6   Partitions, Doors and Outer Body

The doors at the front and back end of the carriage are lined with Bakelite on the inside of the carriage. The side doors, however, are reported to be made of aluminium, and the outer body of the carriage is reported to be made of mild steel, the paint coating them is of unknown type. The partitions at either side of the side doors separate the train into three parts and are made of a metal, likely to be steel. Aluminium has a melting temperature of 660°C (Beyler, 2004, chap 4, Table 5), while steel has a melting temperature exceeding 1400°C (Buchanan and Abu, 2017, Table 2.2).

3.9   Material Properties

The properties of each material can have a significant influence on the fire behaviour within the carriage. The thermal inertia, for example, has a significant impact on the rate of increase of temperature on the

surface of a material, with a low thermal inertia resulting in a rapid rise of temperature at the surface (Drysdale, 2011, fig. 2.10).

3.9.1   Heat of Combustion

The heat of combustion (Δh_c), also known as the calorific value, describes the energy per unit mass contained within a material and is typically measured in kJ/kg. This is an important parameter in determining the amount of energy contained within the fuel, and is an input value required for FDS modelling, both as the reaction heat of combustion and the heat of combustion for each material in the material line. The heat of combustion has a significant influence on the value of the HRR as a higher heat of combustion will result in a higher HRR. Multiplying the heat of combustion by the density results in the energy per unit volume. The heat of combustion can either be described as the net heat of combustion, which is determined by burning a sample in a pure oxygen environment using a bomb calorimeter, or the effective heat of combustion, which describes the energy consumed in an environment, which does not allow for complete combustion. (Quintiere, 1998)

The references associated with each value in the ranges given in Table 3.1 are provided in Table A.2 and Table A.3 in Appendix A. Most fuels, whether they are gaseous, liquid or solid, have a heat of combustion between 15 MJ/kg and 50 MJ/kg (Buchanan and Abu, 2017).

Table 3.1: Literature ranges for material heat of combustion

Material	Heat of Combustion (kJ/kg)
Pleather	16430-19900
Seat lining	20300-32500
Rubbery foam	33900-40600
Polyurethane foam	23200-27200
Plywood	14200-19400
Bakelite	26700-31050
Window (PMMA)	24890-26200
Window (Polycarbonate)	29720
Marley floor	16430-19900

3.9.2   Density

Density (ρ) is defined as the mass per unit volume. This is an important parameter in determining the fire load as it determines the amount of fuel available and, thus, energy contained within a specific volume. It is an input value required for FDS modelling, both as the obstruction bulk density and the density of each material in the material line. The density of a material has a significant effect on early-stage fire development due to its impact on the available fire load. It can also influence the rate of fire spread, specifically in the flame spread across the surface of a material in FDS modelling, particularly as the thermal conductivity is approximately proportional to density (Drysdale, 2011). The density of a material can be determined simply based on its measured volume and by weighing the sample on a scale to determine the mass. In cases where a solid melts due to increased heat to become a liquid, such as with plastic, the density will vary with temperature. For simplicity, however, the density is assumed to be constant throughout in an FDS model. A similar approach was used by Hietaniemi et al. in their replication of upholstered furniture experiments (2004). The references associated with each value in the ranges given in Table 3.2 are provided in Table A.4 to Table A.6 in Appendix A.

Table 3.2: Literature ranges for material density

Material	Density (kg/m³)
Pleather	1100-1950
Seat lining	1230
Rubbery foam	68-85
Polyurethane foam	15-32
Plywood	420-630
Bakelite	1300-1750
Window (PMMA)	1150-1350
Window (Polycarbonate)	1120-1220
Marley floor	1200-1950
Aluminium	2707
Steel	8940

3.9.3 Specific Heat

The specific heat (c) is also known as the thermal capacity of a material and is measured in kJ/(kg.K). This value indicates the amount of heat or energy required to raise the temperature of 1 kg of material, by 1 K or 1 °C (Hurley *et al.*, 1997, p. 2, 140). The specific heat could either be at a constant pressure or at a constant volume, but for liquids and solids, these are more or less equal to one another (Hurley *et al.*, 1997, p. 2). In order to determine the specific heat curve of a substance, adiabatic calorimetry, differential scanning calorimetry, or a differential thermal analyser can be used (Hurley *et al.*, 1997, p. 287). FDS requires the user to specify the specific heat of each material on the material line. For simplicity, specific heat is typically assumed to be constant irrespective of temperature or pressure changes during numerical simulations. A similar approach was used by Hietaniemi et al. in their replication of upholstered furniture experiments (2004). The specific heat value has an influence on the flame temperature and, thus, is also linked to the spread as a lower flame temperature will cause the pre-heating zone to be ignited after a longer period of time (Hurley *et al.*, 1997, p. 141).

The references associated with each value in the ranges given in Table 3.3 are provided in Table A.7 in Appendix A.

Table 3.3: Literature ranges for material specific heat

Material	Specific Heat (kJ/(kg.K))
Pleather	1.05-1.76
Seat lining	1.03-1.3
Rubbery foam	1.76
Polyurethane foam	1.4-1.6
Plywood	2.3-2.85
Bakelite	1.42
Window (PMMA)	1.42-1.5
Window (Polycarbonate)	1.2-1.68
Marley floor	1.05-1.38
Aluminium	0.896
Steel	0.46

3.9.4 Thermal Conductivity

Thermal conductivity (k) is the measure of the movement of heat through a material by quantifying the amount of heat transferred through a unit thickness of material per unit of temperature difference, and

is measured in W/m.K (Buchanan and Abu, 2017). It varies with temperature and can also vary with orientation in anisotropic materials such as wood (Hurley *et al.*, 1997, p. 28). Together with density and specific heat, thermal conductivity influences the thermal inertia of a material, which governs the flame spread and ignition of the material in thermally thick solids (Hurley *et al.*, 1997, p. 211). When a material is transparent or porous, radiation and convection also contribute to the spread of heat within the material and not just conduction, as would be the case in a poreless, opaque material, and thus the temperature gradient plays a significant role in the thermal conductivity (Hurley *et al.*, 1997, p. 287). This means that thermal conductivity is temperature-dependent as both the temperature gradient, and changing of the structure of the material, influence the value. Thermal conductivity can be measured using various methods, including the guarded hot plate, heat-flow meter, hot wire, hot-disk or laser flash method (Yüksel, 2016). FDS requires the user to specify the thermal conductivity of each material on the material line, and for simplicity, this parameter is considered to be a constant. The references associated with each value in the ranges given in Table 3.4 are provided in Table A.8 in Appendix A.

Table 3.4: Literature ranges for material thermal conductivity

Material	Thermal Conductivity (W/m.K)
Pleather	0.14-0.26
Seat lining	0.05-0.17
Rubbery foam	0.19
Polyurethane foam	0.023-0.034
Plywood	0.107-0.22
Bakelite	0.25
Window (PMMA)	0.17-0.27
Window (Polycarbonate)	0.18-0.27
Marley floor	0.14-0.26
Aluminium	202-249
Steel	45.8

3.9.5   Emissivity

Emissivity (ε) is the thermal emission ability of a surface relative to that of a blackbody, which has an emissivity of 1 (Hurley *et al.*, 1997). This indicates the efficiency of the surface to act as a radiator (Drysdale, 2011). As this value is used to determine radiant heat flux, it will have an influence on the fire spread from one surface to another. The references associated with each value in the ranges given in Table 3.5 are provided in Table A.9 in Appendix A.

Table 3.5: Literature ranges for material emissivity

Material	Emissivity
Pleather	0.91-0.93
Seat lining	0.75-0.85
Rubbery foam	0.86
Polyurethane foam	0.17
Plywood	0.82-0.93
Bakelite	0.93
Window (PMMA)	0.25-0.26
Window (Polycarbonate)	0.88-0.89
Marley floor	0.91-0.93
Aluminium	0.035-0.05
Steel	0.07-0.88

3.9.6   Ignition Temperature

The ignition temperature (T_{ig}) determines at what point a material will ignite when exposed to a heat source. It refers to the surface temperature of the material at the point of ignition, either with the presence of a flame (piloted ignition), or ignition with no flame present (auto-ignition). The ignition temperature is one factor that determines the rate of flame spread as the material is heated ahead of the flame in the pre-heating zone, to a point where a sufficient amount of volatile gases are released for sustained flaming to take place. This is affected by the heat of gasification – the temperature at which the material evaporates into flammable gases. FDS requires the user to specify the ignition temperature of an obstruction on the surface line. (Beyler, 2004)

The references associated with each value in the ranges given in Table 3.6 are provided in Table A.10 to Table A.14 in Appendix A.

Table 3.6: Literature ranges for material ignition temperature

Material	Ignition Temperature (°C)
Pleather	189-600
Seat lining	372-508
Rubbery foam	310
Polyurethane foam	370-638
Plywood	203-446
Bakelite	367-614
Window (PMMA)	250-520
Window (Polycarbonate)	440-580
Marley floor	189-600

3.9.7   Critical Heat Flux

The critical heat flux (typically denoted as CHF or $Q"_{cr}$ in literature and consequently in this work) of a material describes the lowest heat flux at which a material will ignite after a period of exposure to the source of heat. Critical heat flux may provide a measure of the ignition temperature of a material and is typically determined using a cone calorimeter, although other techniques such as radiant panel tests, which are used in this work, can be employed. (Hurley *et al.*, 1997)

The references associated with each value in the ranges given in Table 3.7 are provided in Table A.15 and Table A.16 in Appendix A.

Table 3.7: Literature ranges for material critical heat flux

Material	Critical Heat Flux (kW/m^2)
Pleather	10-27.5
Seat lining	4.5-15
Rubbery foam	16-34.1
Polyurethane foam	16.4-20
Plywood	10.7-17.3
Bakelite	15-26
Window (PMMA)	3.33-18.6
Window (Polycarbonate)	11.5-26
Marley floor	10-27.5

3.9.8 Mass Loss Rate

The mass loss rate (typically denoted as MLR or ṁ in literature and consequently in this work) of a specific material is the amount of mass lost due to combustion over a specific period of time, measured in kg/s. This determines the growth rate and fire development in the combustion of a particular material. It can simply be measured by burning a sample while the sample is weighed on a scale and calculating the difference in mass over a specific period of time. In order to perform a numerical simulation in FDS, either the MLR or the HRR must be provided and must be linked to a time-dependent curve. Either a default, tan(h) or t^2 ramp-up time must be selected, or a custom curve must be input using data points (Thunderhead Engineering, 2021).

3.9.9 Heat Release Rate

Heat release rate (Q̇) is the most significant predictor of fire hazard (Babrauskas and Peacock, 1992). It is a measure of the amount of energy released per unit of time, measured in MW, and the value usually changes over time, resulting in a curve, which is used to characterise fire development (Karlsson and Quintiere, 1999). In order to determine the HRR of a material or object, the MLR and effective heat of combustion is required, as can be seen in Equation 3.1. The HRR can be determined with cone calorimeter or furniture calorimeter testing, during which the exhaust gases are analysed to determine the rate of combustion. Either the heat release rate per unit area (HRRPUA) or the MLR of an obstruction must be specified in order to perform a numerical simulation in FDS. The HRR must also be provided as a time-dependent curve which can either be the default ramp-up time or a user specified curve. The HRR is also provided as output data for the simulations.

Equation 3.1: HRR (Quintiere, 2006)

$$\dot{Q} = \dot{m}_F \times \Delta h_c$$

3.10 Fire Behaviour of Passenger Trains in Literature

The fire behaviour of various modes of public transport has been studied in literature. Railway cars from passenger trains showed a maximum HRR of 20 MW within 4750 s and 12.5 MW within 6750 s (Hurley *et al.*, 1997, fig. 26.95). A car was also tested with one half being steel and the other half being aluminium, resulting in a 44 MW maximum HRR within 3200 s, after the windows failed at 2400 s (Hurley *et al.*, 1997, fig. 26.95). The maximum HRR of subway cars has been reported by at 25 MW to 35 MW, reaching their maximum within 350 s to 700 s (Hurley *et al.*, 1997, fig. 26.96). The curve shows a sharp

increase to the maximum with a very short fully developed stage and an initially sharp decrease in HRR to around 1000 s, after which it flattens out. School buses have shown similar behaviour, with a rapid increase in HRR up to 500 s to 1000 s, to a maximum HRR of 28 MW to 34 MW, rapidly decreasing for 250 s to 500 s thereafter (Hurley *et al.*, 1997, fig. 26.97). Another study showed train seating, made of polyurethane with a 100% wool covering, reaching a maximum HRR of 2 MW within 1200 s and bus seating, made of polyurethane covered by a viscose, wool, polyester and polyamide blend, reaching a maximum of 1.3 MW within 350 s (Hurley *et al.*, 1997, fig. 26.98).

Upholstered furniture tested by NIST shows the same HRR curve, with the maximum HRR reaching, 0.7 MW (polyurethane and cotton chair), 2 MW (polyurethane and polyolefin chair) and 3.1 MW (polyurethane and polyolefin sofa), within 650 s, 280 s and 220 s respectively (Hurley *et al.*, 1997, fig. 26.114). This is to be expected as the majority of the fire load within trains are upholstered seats, thus the HRR curve of the train can be expected to show similar behaviour as that of single upholstered furniture items. Mattresses, which contained polyurethane foam with a polyester fibre pad below the PVC, materials similar to the seats found in Metrorail trains, showed a peak HRR of 335 kW (Hurley *et al.*, 1997, Table 26.16).

When the ignition position on an upholstered chair is considered, the chair back and chair bottom showed similar results with a peak HRR being reached within 900 s, but the chair seat resulting in a maximum HRR 0.3 MW lower (Hurley *et al.*, 1997, fig. 26.115). Having the ignition source at the side or the front of the chair, resulted in a delayed maximum HRR, delayed by 400 s and 1600 s respectively, but with the same maximum HRR as that of the chair back being exposed to the ignition source (Hurley *et al.*, 1997, fig. 26.115).

4 Test and Experimental Setup

4.1 Introduction

In this chapter, the tests and experiments used to obtain the parameters required for the Computational Fluid Dynamics (CFD) models that were developed in PyroSim / FDS, as discussed in Chapter 5, are presented. The small-scale tests include the determination of sample densities, bomb calorimeter tests to determine the heat of combustion and radiant panel tests to determine the ignition temperature, while the large-scale experiments involve the open-air burning of seats to determine the MLR of the seats. The results of the small-scale tests are provided and discussed in Chapter 5, while the large-scale experiment results are provided and discussed in Chapter 6. The values chosen for use for each of the parameters in FDS models are discussed in Chapter 7.

4.2 Material Properties

CFD software, such as FDS used in this work, requires a variety of thermal properties as input parameters. Some material properties are readily available in literature and can typically be specified as a constant value in FDS (as opposed to a temperature-dependent property), for example, specific heat, thermal conductivity and density. Other input parameters, such as HRR, are highly time, flux or temperature-dependent. These properties are typically obtained with standard tests, such as cone calorimeter testing to obtain HRR or effective heat of combustion. This Chapter discusses the testing conducted to obtain some of the FDS input parameters. Refer to the FDS users guide for more information regarding parameter specification (Thunderhead Engineering, 2021).

4.3 Overview of Tests and Experiments

To obtain the parameters listed above, the following list summarises the tests that have been done as part of this work. Specific details regarding the tests are discussed in the sections that follow.

1. Simple material characterisation tests to determine material density. This is not discussed below.

2. Bomb calorimeter tests to determine the calorific value of materials. The samples listed below have been tested.

    - 2 Bakelite samples

    - 2 window samples and 1 window frame sample

    - 2 pleather samples

    - 1 non-woven wadding sample

    - 3 polyurethane foam samples, 1 rebonded polyurethane foam sample and 1 rubbery foam sample

    - 1 plywood sample

3. Radiant panel tests to determine the time-to-ignition, ignition temperatures and/or critical heat fluxes of materials.

    - 4 marbled Bakelite samples and 3 plain Bakelite samples

    - 5 window samples and 1 window frame sample

    - 8 pleather samples

    - 4 blue pleather (with plywood backing) samples

- 2 polyurethane foam samples and 2 rubbery foam samples

4. Full-scale free burn experiments of seats from Metrorail carriages. MLR, flame height, radiant flux a distance from the sample and temperatures above the samples were measured.

- 4 experiments on different size passenger train seats.

4.4   Bomb Calorimeter Tests

In order to determine the net heat of combustion of the various materials, a bomb calorimeter test needed to be performed. First, the crucible in which the sample would be placed, had to be placed on the scale to zero the scale. Thereafter a small sample of material was taken, placed in the crucible and weighed. The foams were placed in the cup in single or multiple pieces as required, the wood was already cut into a suitable sample size, while the solid materials such as the Bakelite lining, window and window frame were grated into a powder as the materials could not be cut at the time or were too brittle to obtain a good sample by cutting or sawing, as can be seen in Figure 4.1. The mass of the sample was then noted. The samples needed to be smaller than 2 grams each to prevent the equipment from being damaged during testing by excessive heat being released, and also to ensure the sample fits inside the crucible to allow for accurate testing.

Figure 4.1: Sample preparation for bomb calorimeter testing

As the foam found in the train seats varied from seat to seat, depending on the supplier, and also depending on whether the correct material had been used by the supplier according to the requirements set by PRASA, each foam sample was only tested once. The value used for FDS cannot be accurately defined due to the significant variation in material properties, and an estimated, representative value will be determined. During testing, if any tests provided a net heat of combustion which did not seem to be appropriate, the test was repeated. The window material was tested twice as the material composition needed to be confirmed. PRASA described it as Perspex (PMMA) but the behaviour of PMMA compared to polycarbonate, varies significantly in a fire which could greatly influence the fire spread and growth due to potential melting behaviour as discussed in Section 3.7 and 3.8.2.1. The Bakelite lining collected had two different coverings, one plain and one marbled. Both were tested to determine whether the coverings were similar in terms of calorific value. The fabric covering of the seats which was collected, also differed when looking at the material structure of the scrim; one seemingly more dense than the other, and thus both were tested.

4.5 Radiant Panel Tests

In order to estimate ignition temperatures, critical heat fluxes and time-to-ignition radiant panel tests have been done. This was be done by exposing samples to heated radiant panels and measuring the heat flux during testing using a water-cooled heat flux gauge. Had a cone calorimeter been available at the time of testing, such equipment would have provided more accurate data regarding behaviour. Hence, this experimental setup provides estimates regarding material parameters, which should be refined in future research.

4.5.1 Experimental Setup

The Heat-transfer Rating Inducing System (H-TRIS), consisting of nine electrically powered radiant panels, mounted to a frame on wheels, was used. The system is based on the original work by Maluk et al. (2016), with further details of this specific system provided by Botha (2022). The HTRIS could be moved backwards and forwards, as required, on the set of rails, to achieve the desired heat flux. The radiant panel tests were performed in a room fitted with a hood and extraction fan, as can be seen in Figure 4.2.

From the critical heat flux, the ignition temperature can be calculated. When the surface temperature of samples could be measured during this test using a thermocouple, it gives an indication of the ignition temperature. Due to the behaviour of materials, not all parameters could be obtained from each material, and these tests were used to provide indicative ranges regarding material behaviour. Some materials melted rather than igniting, or distorted, meaning that front face temperatures were not accurately obtained. Hence, the data is used in conjunction with details in the literature in the following chapter.
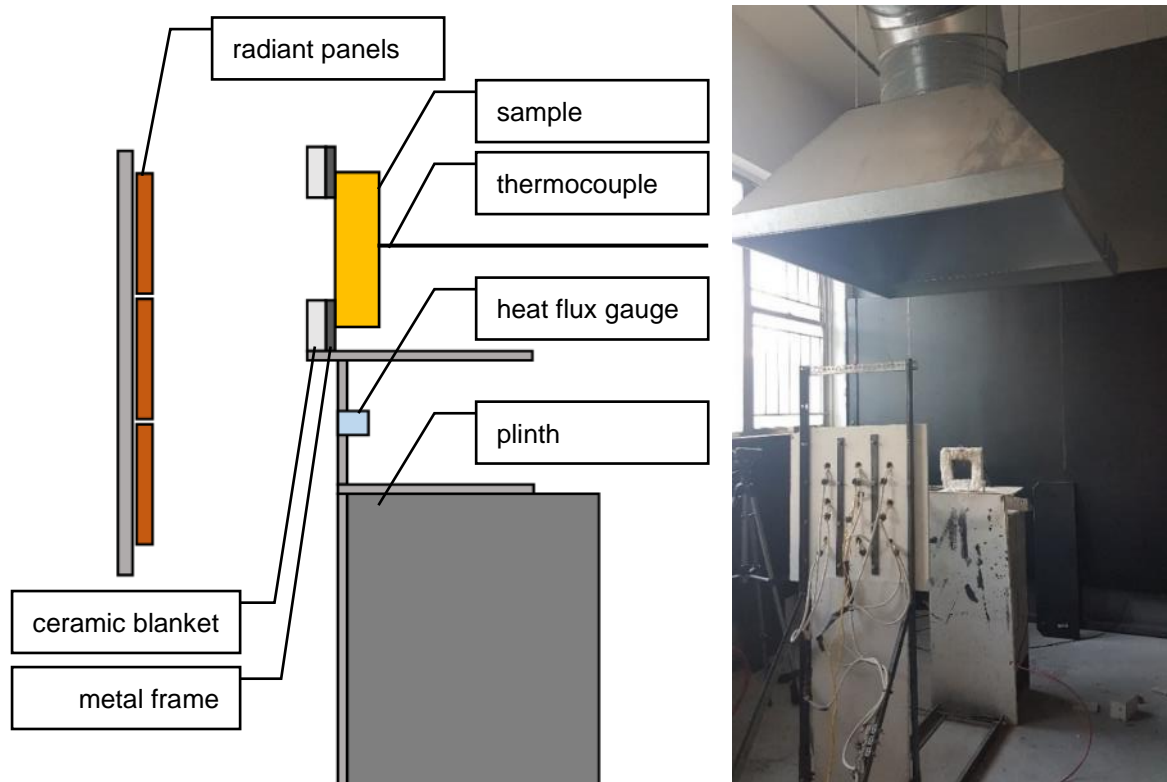
Figure 4.2: Radiant panel test setup showing an annotated diagram and a photo of the setup

Samples of around 130 mm x 130 mm, were cut from the various materials. In order to mount the material samples vertically, a metal frame was made with a 100 mm x 100 mm opening in the centre.

Supports were welded to the frame to allow it to stand upright. Ceramic blanket was used to cover the frame on the side exposed to the radiant panels, to prevent the heat from the metal frame from being conducted into the sample, as only radiant heat should be experienced by the sample for accurate results. The heat loss that each material would experience in a carriage fire was replicated by either insulating the back of samples with ceramic blanket or leaving the back exposed (such as for the window samples), in order to obtain a realistic ignition temperature. Details of the sample test insulation specification are provided in Chapter 5. The samples were all tested vertically as the majority of the materials are vertically orientated in carriages.

The samples were stuck to the metal frame with aluminium foil tape in such a way as to minimise gaps between the metal frame and the sample, which would lead to heat losses, without influencing the insulation conditions at the back of the sample, as can be seen in Figure 4.3.

Figure 4.3: Sample positioning and thermocouple placement

A water-cooled heat flux gauge was mounted in the position just below the sample, as shown in Figure 4.4, with its face in the same plane as the front surface of the sample, to allow for real-time heat flux data to allow for adjustments to be made to the position of the HTRIS as required. A gypsum board was placed in front of the sample until the HTRIS was heated up and in the approximate position to prevent large changes in heat flux, which would influence the time to ignition.

Figure 4.4: Positioning of water-cooled heat flux gauge

4.5.2   Material and Analysis Considerations

For the testing of the pleather, tests were completed with three different backing conditions; without insulation, with the materials that would usually be behind the pleather (foam etc.), as well as with ceramic blanket at the back, used to represent insulation that would usually be provided by these materials. Windows were tested without insulation at the back, and all other materials were tested with ceramic blanket providing insulation at the back.

In this test, the auto-ignition temperature was recorded or calculated, a value which can be expected to be much higher than the piloted ignition temperature, for which an ignition source would need to be present regularly to allow the pyrolysis gasses to ignite. When determining the auto-ignition temperature, the temperature of the surface on the exposed side of the sample must be recorded at the time at which ignition, in the form of a flame, is first noted (Hurley *et al.*, 1997, p. 648). As data was recorded regularly and time delays may occur when using thermocouples, it was necessary to use the maximum surface temperature prior to, and including, the moment of ignition as the auto-ignition temperature, which would reflect the actual auto-ignition temperature more accurately. Auto-ignition temperature is specific to the test conditions and can vary 150 °C or more for a particular material, especially in cases where orientation varies, or a change is made to the fluid mechanics or heat transfer (Hurley *et al.*, 1997, p. 648). This means that values found in literature are only an approximation and may differ significantly from the values measured during testing. This also has a significant influence on the calculation of the ignition temperature as the resultant ignition temperature will vary according to the heat transfer assumptions made and whether they reflect the actual conditions during testing. Surface temperatures are, however, more difficult to measure accurately than heat fluxes, and thus, the minimum or critical heat flux could be used to calculate the ignition temperature (Hurley *et al.*, 1997, p. 655). In the analysis conducted in Chapter 5, in order to obtain a good estimate of auto-ignition temperature, various heat loss conditions were considered, including ignoring heat losses as well as varying the convective heat transfer coefficient through the expected range of values.

The time to ignition was noted as the time at which sustained flaming was initiated spontaneously due to the radiant heat which each sample was exposed to, since the start of exposure when the heat flux had reached a stable level.

4.5.3 Uncertainties

The heat flux was determined by calculating the average of the heat flux measured by the water-cooled heat flux gauge. The heat flux experienced by the heat flux gauge was assumed to be the same as that experienced by the sample, although, in reality, this will differ slightly due to the angle of radiation from the centre of the radiant panels to the centre of the heat flux gauge and that of the centre of the sample not being exactly the same. When calculating the configuration factor of the sample and the heat flux gauge, the heat flux experienced by the sample will be around 85% of that experienced by the water-cooled heat flux gauge when the radiant panels are 10 cm from the sample, while it will be around 95% when the radiant panels are 1 m from the sample. There is, however, no way to mount the heat flux gauge in the centre of the sample while the sample is present, and a heat flux must be monitored throughout the test.

4.6 Large-scale Seat Experiment

Four free burn experiments on full-scale seats have been conducted on seats obtained from Metrorail carriages. The seats are somewhat damaged, with extensive wear. However, this provides a more representative scenario regarding actual conditions in trains. The experiments were done at the Ignis Testing facility, with walls on many sides, preventing wind from influencing experiments, and a free-standing roof, which allows smoke to be vented out.

As a large-scale furniture calorimeter is not currently available in South Africa to determine the HRR, the MLR was determined by burning a seat on a 1.2 m x 1.2 m scale and logging the mass throughout the experiment. Details of the experiment are provided in Figure 4.5. In order to validate results, thermocouples were placed above the seat, and a water-cooled heat flux gauge was placed at a specified distance from the seat. This was used in FDS modelling to confirm that the model replicates the fire behaviour that was observed during the experiment. Any material properties used from literature can thus be confirmed to be a good estimate of the actual property value.
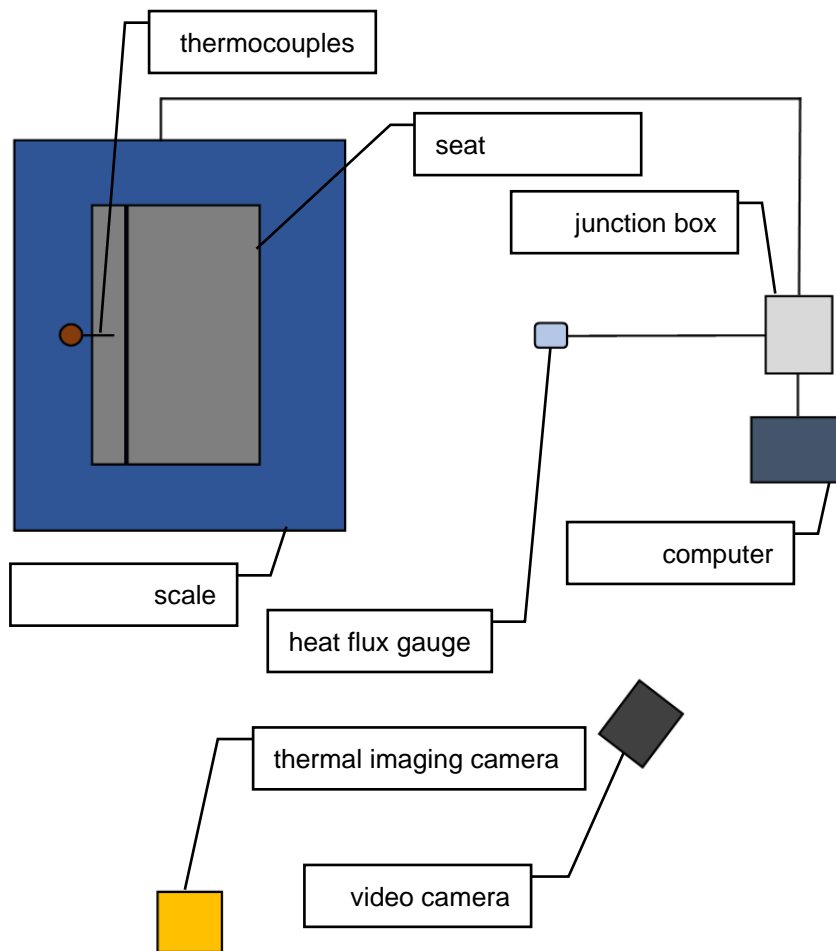
Figure 4.5: Plan view showing experimental setup for the free burn experiments

An inch value is used to describe the four seats tested as this is how they are described by PRASA, and represents the accurate length of each seat component. A conversion has been done in Table 4.1 from the inch values to the corresponding length in millimetres. The full-scale seat samples collected included one entire seat (see Figure 4.6), three loose seat backs (one 52 inch, one 36 inch and one 33 inch), three loose seat bottoms (one 52 inch, and two 36 inch) and a 52 inch back-to-back frame (see Figure 4.7). Other seat backs and bottoms that were collected were used for material samples for the bomb calorimeter and radiant panel tests, as discussed above.

The only preparation done with the seat samples was using a staple gun to fix the 52 inch seat bottom, which had come apart due to some screws being missing. This could have caused the premature ignition of the inner foam otherwise. Supports were welded to the frame at the back, as can be seen in Figure 4.6, thus they would have no influence on the burning of the seat. The seat was dried in front of a fan until completely dry to ensure moisture in the foam did not affect the results.

Table 4.1: Seat length conversion

Seat	Dimension (mm)
33 inch	838.2
36 inch	914.4
52 inch	1320.8
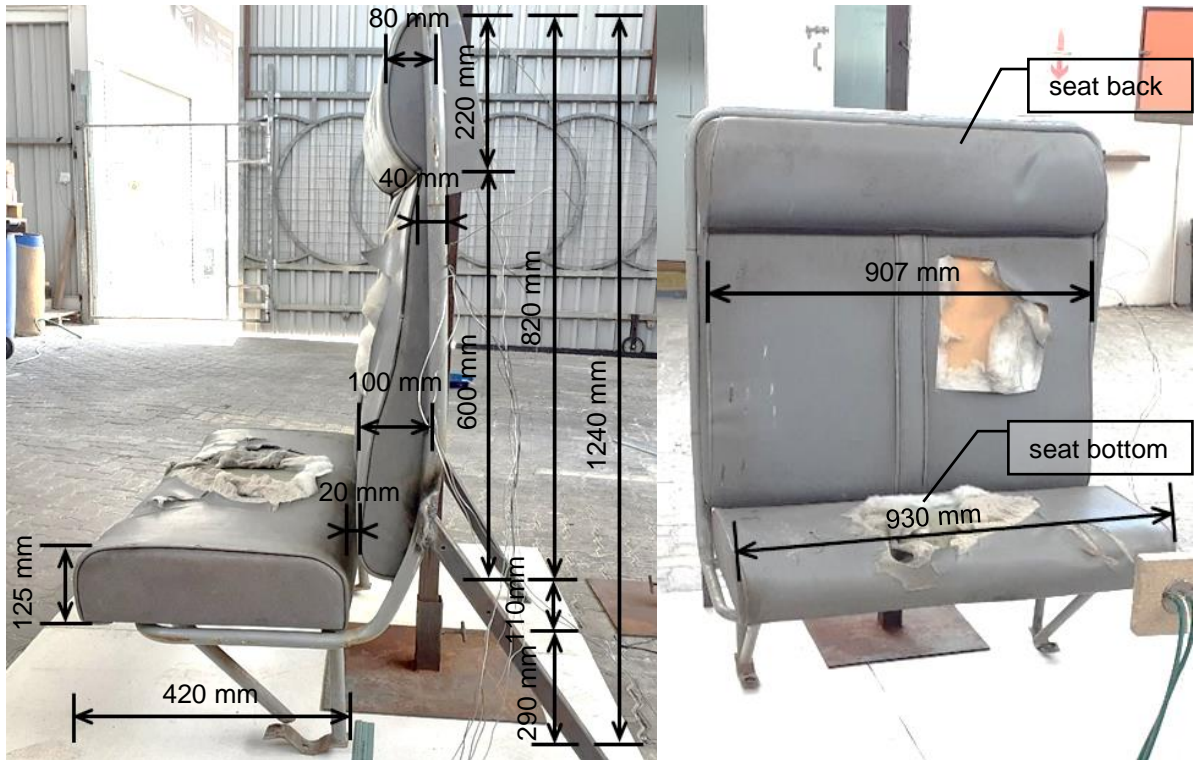
Figure 4.6: Dimensions of seat for Experiment 1

Figure 4.7: Dimensions of frame for Experiment 2, 3 and 4

In order to demonstrate the results from the FDS simulations of the experiments, 1.5 mm tip thermocouples were installed at various heights above the seat using a thermocouple tree stand, and a water-cooled heat flux gauge was placed 1 meter from the front of the seat, as shown in Figure 4.8. In order to protect the cables from the heat, they were wrapped in aluminium foil, as can be seen in Figure 4.9. The scale was connected to a logger, recording the mass every second, and the thermocouples and water-cooled heat flux gauge were also connected to a data logger via a junction box which also recorded measurements every second. The scale and water-cooled heat flux gauge had been calibrated and tested prior to the experiments being performed. The thermocouples were also checked using a handheld logger, and applying body heat to the tip. A Liquid Petroleum Gas (LPG) canister with a gas torch fitting, was used for ignition. In order to visually record the experiments, an infrared camera was set up to the side of the seat and a video camera at about a 45° angle.
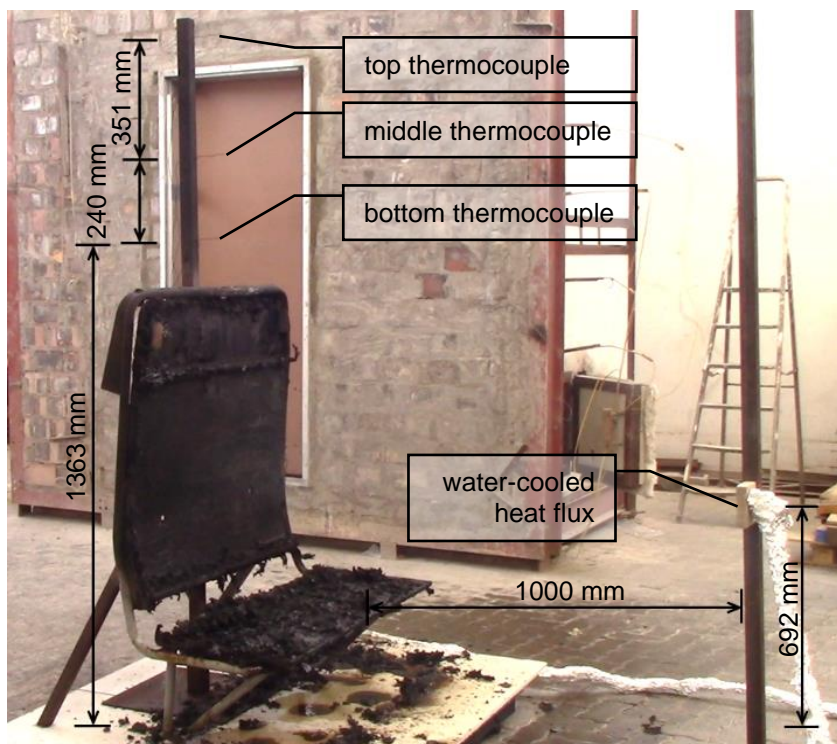
Figure 4.8: Positioning of thermocouples and water-cooled heat flux gauge

Figure 4.9: Experimental setup for full-scale seats showing the chairs soon after ignition

40

4.6.1 Experiment 1 – 36 Inch Seat

The first experiment was done using the 36 inch seat fixed to a slightly bent frame. Both the back and bottom of the seat were slightly vandalised. The seat was ignited using an LPG burner applied to the front of the seat bottom, in the centre, for 54 s. The experiment was allowed to run through all the stages of fire development, from growth to decay. Thereafter the fire was extinguished using water.

4.6.2 Experiment 2 – 36 Inch Seat Bottom and 33 Inch Seat Back

The second experiment was done using a 36 inch bottom with a 33 inch back, placed on the 52 inch frame. This frame was used due to the correct angle between the back and the bottom, and was reused for all subsequent experiments. The slope of the seat back could have an influence on the results as a more upright seat back could cause the fire to spread faster due to convection. The frame was not affected by the burning of the seats as it was made of steel and did not reach high enough temperatures to be damaged. Both the back and bottom of the seat were reasonably vandalised. The burner was applied to the front of the seat bottom, in the centre, for 31 s to ignite the seat. The experiment was allowed to run through all the stages of fire development, from growth to decay. Thereafter the fire was extinguished using water.

4.6.3 Experiment 3 – 36 Inch Seat on 52 Inch Frame

The third experiment was done using a 36 inch bottom with a 36 inch back, placed on the 52 inch frame. The back was not vandalised at all, while the bottom was reasonably vandalised. The ignition was applied to the back of the seat bottom, on the right, for 19 s. The fire was dampened toward the end, and thereafter, the experiment was ended early, once the maximum MLR had been suspected to have been reached. Due to the severe amount of smoke released, excessive heat and flames becoming dangerous, the fire was then extinguished using water.

4.6.4 Experiment 4 – 52 Inch Seat

The third experiment was done using a 52 inch bottom with a 52 inch back, placed on the 52 inch frame. Vandalism to the back was limited to a single cut while the bottom was intact. The burner was applied to the back of the seat bottom, in the centre, for 10 s. The experiment was ended early, once the maximum MLR had been suspected to have been reached. The fire once again started to become dangerous, so it was then extinguished using water.

4.7 Conclusions

This chapter has provided an overview of the experimental setups for small and large-scale experimental tests. In the following chapter, small-scale results and an analysis of material properties is provided. The subsequent chapter provides details regarding the full-scale experiments.

5 Small-scale Test Results

5.1 Introduction

In this chapter, the results of the small-scale material tests are discussed. First, the measurement and calculation of the material density is covered. Thereafter, the bomb calorimeter and radiant panel test results (of which the setup was covered in Chapter 4) are discussed. These results are then used for numerical simulations in FDS, which are discussed in Chapter 7.

5.2 Materials Tested

Samples were taken from the carriage interior lining, windows and seats of a passenger train carriage. Table 5.1 and Table 5.2 lists the samples considered in this study. Each material listed, has a description, a material ID, with the test indicated for which samples of the material were used. The material ID consists of a location, seat (S) or carriage (C), a material type, and, where required, a specific material, which is identified by physical properties or colour. Table 5.3 to Table 5.7 show the material samples as described in Table 5.1 and Table 5.2. As discussed previously, a range of materials have been installed within the seats meaning that there are a wide variety of types of material used for a single purpose (e.g. many different foams used in the seats), and these tests are not exhaustive of all the possible materials available.

Table 5.1: Materials considered for testing

Object	Material Type	Description	Material ID	Density	Bomb Calorimeter	Heat Flux
Wall & ceiling interior lining	Bakelite	Marbled	C_B_M	Measured	Yes	Yes
		Plain	C_B_P	Measured	Yes	Yes
Window	Window frame	Black plastic	C_WF	Measured	Yes	No
	Window	Transparent plastic	C_W	Measured	Yes	Yes
Seat (combined)	Pleather & plywood	Plywood with blue pleather	S_PIPW	Measured	No	Yes
	Pleather & polyurethane & rebonded foam & plywood	Pleather, yellow layer, rebonded foam (green / blue / yellow), plywood (seat bottom)	S_PIPURePW	N/A	No	Yes
	Rebonded & polyurethane	Yellow with rebonded green / blue / yellow	S_RePU	Measured	No	No
	Rubbery & polyurethane	Coarse honeycomb with yellow layer (seat back)	S_RuPU_C	Measured	No	No
		Fine honeycomb with yellow layer (seat bottom)	S_RuPU_F	Measured	No	No
		No honeycomb with yellow layer	S_RuPU_N	Measured	No	No

Table 5.2: Materials considered for testing continued

Object	Material Type	Description	Material ID	Density	Bomb Calorimeter	Heat Flux
Seat	Pleather	Backing with fine, dense threading	S_Pl_F	Measured	Yes	Yes
		Backing with thick, coarse threading	S_Pl_C	Measured	Yes	No
		Blue (on seat back plywood)	S_Pl_B	Calculated	No	Yes
	White lining	Non-woven lining	S_L	Measured	Yes	No
	Rubbery foam	Coarse honeycomb	S_Ru_C	Calculated	Yes	Yes
		Fine honeycomb	S_Ru_F	Calculated		No
		No honeycomb	S_Ru_N	Measured		No
	Rebonded foam	Grey / blue / white	S_Re_GBW	Measured	No	No
		Green / blue / yellow	S_Re_GBY	Calculated	Yes	No
	Polyurethane foam	Light blue	S_PU_B	Measured	No	Yes
		Grey & light blue layers	S_PU_GB	Measured	No	No
		Green	S_PU_Gn	N/A	Yes	No
		Grey	S_PU_Gy	Measured	No	No
		Orange	S_PU_O	Measured	No	No
		Yellow	S_PU_Y	N/A	Yes	No
		Yellow (dirty)	S_PU_YD	N/A	Yes	No
		Light & dark yellow layers	S_PU_YL	Measured	No	No
	Plywood	Seat back (9 mm, previously attached to fine honeycomb foam)	S_PW_Ba	Measured	Yes	No
		Seat bottom (15 mm)	S_PW_Bo	Measured		No
		Seat back (3.4 mm, attached to pleather)	S_PW_BaPl	N/A	No	No

Table 5.3: Material samples (carriage)
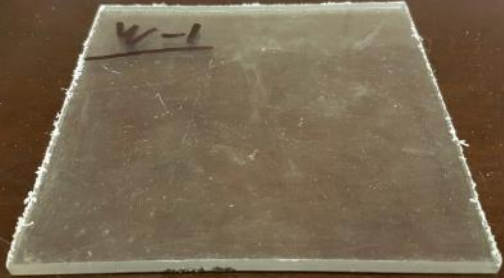
Material ID	Photo	
C_B_M		
C_B_P		
C_WF		
C_W		

44

Table 5.4: Material samples (seat, combined)

Material ID	Photo
S_PIPW	
S_PIPURePW	
S_RePU	
S_RuPU_C	
S_RuPU_F	

Table 5.5: Material samples (seat)
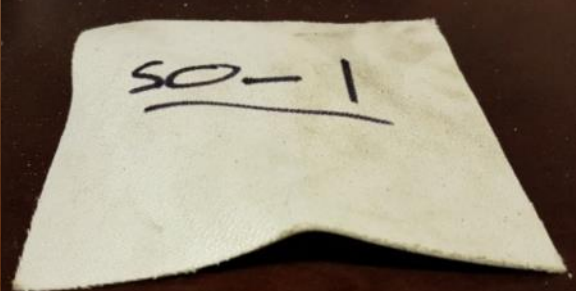
Material ID	Photo
S_PI_F	
S_PI_C	
S_L	
S_PU_B	
S_PU_GB	

Table 5.6: Material samples (seat) continued

Material ID	Photo
S_PU_Gn	
S_PU_Gy	
S_PU_O	
S_PU_Y	
S_PU_YD	
S_PU_YL	

Table 5.7: Material samples (seat) continued

Material ID	Photo	
S_Re_GBY		
S_Ru_N		
S_PW_Ba		
S_PW_Bo		

5.3   Material Density

In order to determine the density of the materials, dimensional measurements were taken, and each sample was weighed in order to obtain the mass thereof.

When modelling the fire behaviour of the seats and carriages, the density of materials is an important input parameter as it affects the amount of fuel available and the flame spread rate across the surface of a material in FDS (hence, affecting the early fire development). Hence, the discussions below provide details regarding obtaining a suitable and representative value for the materials tested. Due to the high variability associated with materials, data from the literature is also considered to provide a representative average value for models.

The density of materials can vary significantly between samples, especially for heavier samples or very thin samples (all the samples were cut to approximately the same length and width where possible). Two sets of measurements were taken, with the first set being less reliable due to potential equipment shortcomings, which was identified only after all measurements and analysis had been done. Due to this, the first set of measurements was used as a guide only. The measurements were redone, and the second measurement set is more reliable, meaning that typically in this work, the density determined from the second measurement was more heavily relied upon to determine the assumed density for each sample. The density determined by the first measurement was used to indicate a direction for rounding the values; whether the value should be rounded up or down. For larger density values, rounding was done to the nearest 5 or 10 kg/m^3, while smaller density values were rounded to the nearest 1 kg/m^3, as can be seen in Table 5.8 and Table 5.9.

Table 5.8: Measured material density

Material ID	Measured Thickness (mm)	Measured Density (kg/m^3)	Literature Density (kg/m^3)
C_B_M	4.5	1350	
C_B_P	4.5	1450	1300-1750
C_W	5.0	1270	1120-1350
C_WF	14.8	800	1120-1890
S_L	29.0	8	1230
S_Pl_C	1.0	625	
S_Pl_F	1.3	600	1100-1950
S_PIPW	4.5	695	420-1950
S_PU_B	20.0	13	
S_PU_GB	55.0	23	
S_PU_Gy	55.0	26	
S_PU_O	27.5	30	
S_PU_YL	20.0	51	15-32
S_PW_Ba	9.0	715	
S_PW_Bo	15.0	475	420-630
S_Re_GBW	51.0	95	
S_RePU	83.0	56	15-32
S_Ru_N	19.0	126	
S_RuPU_C	57.0	63	
S_RuPU_F	45.0	72	
S_RuPU_N	80.0	45	15-85

Table 5.9: Calculated material density

Material ID	Calculated Thickness (mm)	Calculated Density (kg/m^3)	Literature Density (kg/m^3)
S_Pl_B	1.1	635	1100-1950
S_Re_GBY	45.0	58	15-32
S_Ru_C	23.0	66	68-85
S_Ru_F	20.0	92	

The references to literature for the density values can be seen in Table A.4 to Table A.6 in Appendix A. When comparing the density values obtained from measurements to the range of values found in literature, most values were within range. The polyurethane foams in literature were generally around 15 kg/m^3 to 32 kg/m^3, while the samples (S_PU) were found to be 13 kg/m^3 to 51 kg/m^3 for the typical

foams. The rebonded foams (S_Re) had a slightly higher density of 56 kg/m^3 to 95 kg/m^3, but this is likely due to the adhesive material that holds the small pieces of foam together. The lining material (S_L), had a much lower density, of 8 kg/m^3, than the value given in literature, but this is likely due to the form in which the material's density was measured; non-woven compared to the solid form. The pleather can consist of either PVC or solid polyurethane, and the density of flexible PVC in literature ranges 1260 kg/m^3 to 1950 kg/m^3 (Hurley *et al.*, 1997, Table A.36). The density measured for the pleather samples are much lower at 600 kg/m^3 to 625 kg/m^3, but this includes the backing material, and the outer layer is more spongy than typical flexible PVC. The windows could either be PMMA or polycarbonate. In the literature, the densities of these materials fall within the same range; PMMA with a density of 1150 kg/m^3 to 1350 kg/m^3 and polycarbonate with a density of 1120 kg/m^3 to 1220 kg/m^3. The window has a density of 1270 kg/m^3, which compares well and may possibly be PMMA rather than polycarbonate when looking at the density, but the values are very close to one another, so no definite assumption can be made. The window frame could also be various types of plastic, but with a density of 800 kg/m^3, it is much lower than the density range of PVC, PMMA and polycarbonate, which is listed as 1120 kg/m^3 to 1890 kg/m^3 in the literature. This could be due to the method in which the window frame sample was measured as the window frame has hollow sections but was measured as a solid for practical reasons, while in literature the samples were typically solid materials.

As an average value is required for modelling purposes, the densities of like materials were averaged. In order to determine whether these averages are representative of the data used for the average, statistical parameters were considered. Only the Bakelite samples (C_B_M and C_B_M) and the pleather samples (S_Pl_C and S_Pl_F) gave representative averages when considering an acceptable coefficient of variation. The average value for Bakelite is 1400 kg/m^3, and for pleather, it is 612.5 kg/m^3. In order to determine a density of foam that is representative of the foam in the seat, a weighted average should rather be relied upon, thus using the density of specific foam layers in the seat. In order to determine the specific layers in a seat with no damage to the outer pleather layer and white lining, the remains of the seat must be studied after burning in order to make an informed estimation of the foam involved. For the plywood, the higher density value of 715 kg/m^3 was used as it was also closer to the density of the sample consisting of 1.3 mm pleather and 3.4 mm plywood.

A large variation in density can be seen, not only in foams that are not alike, but also for similar foams. Most foams are well represented by their density, but the honeycomb rubbery foam is not well represented due to the large honeycomb-like holes found in the structure, which were included in the sample dimensions for practical reasons. In the seats, these holes cause pockets with no density, which would typically be filled with air. This will lead to inaccuracies in modelling, but also affects the fire spread in experimental setups as the oxygen contained within these pockets, which can increase the size of the flames and the burning rate. The density, including the holes (S_Ru_C and S_Ru_F), was used for numerical simulation as it is not possible to account for the holes when using the density of S_Ru_N.

5.4   Bomb Calorimeter Tests

Table 5.10 shows the results obtained for the bomb calorimeter tests. Two bomb flasks were used for testing (number 16 and 36), alternating between the two to allow for sample preparation during the previous test. Each time a very high calorific value was obtained, the firing wire burnt through (a component of the equipment used for igniting the sample), as seen with sample 2 and sample 10, but not with sample 6, possibly due to the mass of the sample being just under three times lower than sample S_Ru and S_Re_GBY. The pleather material that covers the seats, produced severe corrosion in the bomb flasks and also left a hard substance that looked like wax in the crucible. The corrosion present in the bomb flask could possibly influence test results, but the result of S_PW, the only sample tested in a bomb flask that had been corroded by a previous test, is in the range of calorific values that can be expected for wood, and thus the result is considered valid. The aforementioned behaviour indicates that the combustion by-products of many of these materials are noxious, as would be expected.

Table 5.10: Bomb calorimeter test results

Sample ID	Preparation	Mass (g)	Bomb ID no.	Comment	Measured Heat of Combustion (MJ/kg)	Literature Heat of Combustion (MJ/kg)
C_B_M	grated	0.292	16		18.84	26.7-31.05
C_B_P	grated	0.2	36		18.36	
C_W_1	grated	0.236	36		23.32	24.89-29.72
C_W_2	grated	0.35	36		22.82	
C_WF	grated	0.18	16		34.46	16.43-29.72
S_L	N/A	0.199	16		20.24	20.3-32.5
S_Pl_C	N/A	0.326	36	Corrosion in bomb flask	18.97	16.43-19.9
S_Pl_F	N/A	0.38	36	Corrosion in bomb flask	23.08	
S_PU_Gn	N/A	0.217	36		29.17	23.2-27.2
S_PU_Y	N/A	0.214	36		27.32	
S_PU_YD	N/A	0.171	36		28.28	
S_Re_GBY	N/A	0.489	16	Firing wire burnt through and melted onto sleeve	34.49	23.2-27.2
S_Ru	N/A	0.467	16	Firing wire burnt through	43.38	33.9-40.6
S_PW	N/A	0.788	36	Cleaned corroded bomb flask used	18.19	14.2-19.4

The references of heat of combustion ranges from literature are shown in Table A.2 and Table A.3 in Appendix A. In the literature, polyurethane foam typically has a heat of combustion of 23.2 to 27.2 MJ/kg, while latex foam has a heat of combustion of 33.9 MJ/kg to 40.6 MJ/kg (Hurley *et al.*, 1997, Table A.32). The rebonded foam has a slightly higher heat of combustion of 34.5 MJ/kg than typical polyurethane foam, which could be attributed to the adhesive that binds the small pieces of foam to one another to form the composite. The rubbery foam has a much higher heat of combustion than typical polyurethane foams, which could be an indication that it is a latex foam rather than a polyurethane foam, but it also has a higher heat of combustion than even the latex foam. The foams found in the seats have higher than average heat of combustions than would typically be found in seats, which makes them a greater risk in fires. Accelerants such as propane, gasoline and heptane have a heat of combustion ranging from 44.6 MJ/kg to 46.9 MJ/kg, and thus the rubbery foam has a heat of combustion which is almost that of an accelerant, which is very dangerous as it is found in large quantities within South African train carriages.

In the literature, PVC is listed with a heat of combustion of around 16.4 MJ/kg to 19.9 MJ/kg. In the case that the pleather is made of PVC, it would compare well but is towards the higher end of the range and even exceeding these values. This may, however, be an indication that the pleather is rather a polyurethane-type pleather. PMMA has a heat of combustion of 24.9 MJ/kg to 26.2 MJ/kg in literature, while polycarbonate is listed as having a heat of combustion of 29.7 MJ/kg (Drysdale, 2011, Table 1.13). The window has a lower heat of combustion than the PMMA and thus is likely to be PMMA rather than polycarbonate. The frame has a much higher heat of combustion than even the polycarbonate found in literature, and thus, the frame is more likely made of polycarbonate than PMMA or PVC. Phenol formaldehyde in literature has a heat of combustion of 26.7 MJ/kg to 31.1 MJ/kg, which is much higher than the value measured for the Bakelite samples. The Bakelite samples have a heat of combustion closer to that of wood, which could indicate that the samples have a higher percentage of wood powder compared to resin than the typical phenol formaldehyde.

In order to determine the heat of combustion to be used for modelling, the calorific values of similar materials were compared to one another using statistical parameters, with the resulting values shown in Figure 5.1. The three polyurethane foam samples (S_PU_Y, S_PU_YD and S_PU_Gn) have an acceptable coefficient of variation, as well as the two window samples (C_W_1 and C_W_2) and the two Bakelite samples (C_B_M and C_B_P). All other groupings, such as groupings including polyurethane, rebounded, and rubbery foams, resulted in a coefficient of variation that was too high. A weighted average would thus also need to be used in order to determine the heat of combustion of the foams and of the seat. The pleather samples (S_Pl_C and S_Pl_F) do not correlate well, so using the average value thereof is not advisable, and thus, a conservative value (in terms of fire that would be the higher of the heat of combustion values) was chosen to be representative of the pleather.

Figure 5.1 shows the heat of combustion for all the materials after averaging had been done for the appropriate groups of materials. It should be noted that these are the heat of combustion values obtained from burning materials in a pure oxygen environment, while in reality, the materials would not burn as optimally, and thus, the heat of combustion will be reduced by an effectivity factor.

In order to determine an accurate value for the effective heat of combustion, the HRR would need to be measured in a cone calorimeter. The ratio of the HRR to the MLR at specific times during testing, would indicate the instantaneous effective heat of combustion, which would generally be constant for all materials except materials that char (Drysdale, 2011, p. 26). The bomb calorimeter tests give the net heat of combustion, but ideally, the effective heat of combustion should be obtained in future work. Combustion efficiency factors range from 1, for complete combustion in pure oxygen environments, to 0.4, which results in unstable combustion and the extinction of flames, and can be influenced by levels of carbon monoxide (Hurley *et al.*, 1997, p. 1182). The efficiency factor used to obtain the effective heat of combustion for FDS is discussed in Chapter 7.
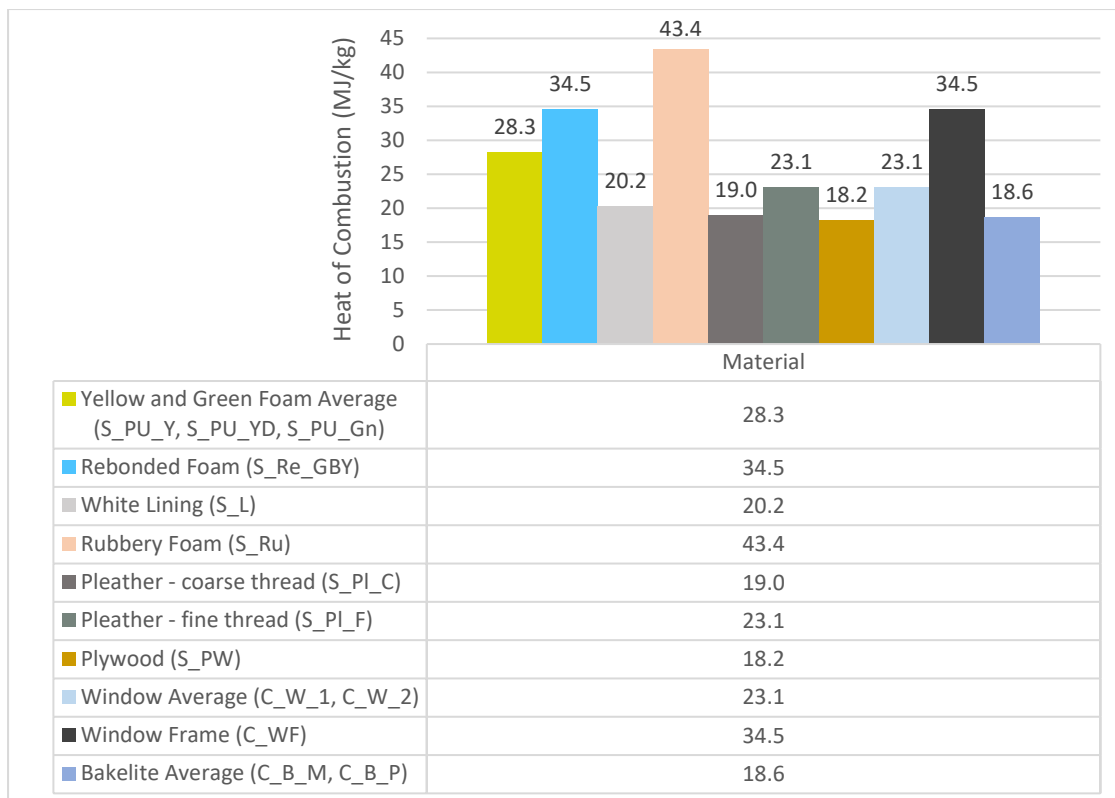
Figure 5.1: Calorific value of materials

5.5   Radiant Panel Tests

In order to determine the auto-ignition temperature of a specific material, radiant panel testing was done. For the solid materials, such as the Bakelite and window samples, a hole was drilled into the sample and stopped just before penetrating the front face. The thermocouple was placed in this hole to measure the surface temperature from behind, and pressure was applied to the thermocouple in order to ensure that it remains in place during testing. For thin, flexible materials, the thermocouple was pushed into the material as far as possible without penetrating the front face, and held in place using pressure. In these cases, temperature data was measured, but in other cases, this was not possible due to using ceramic blanket for insulation or samples not being suitable or not having holes drilled for thermocouples. In those cases, the ignition temperature was calculated.

The water-cooled heat flux gauge used is designed for use in an environment where the heat flux is dominated by radiation. Although it is also sensitive to convective heat flux, the contribution thereof is usually ignored. (Hukseflux, no date). An assumption is made that around critical heat flux, the heat losses are governed by radiation (Hurley *et al.*, 1997, p. 1150).

In cases where the H-TRIS was moved close to the sample, in other words, the heat flux was high, the boundary layer of the radiant panels could affect the heat flux experienced by the samples as it could include convective heat flux if the sample were to fall in the boundary layer. The ceramic blanket surrounding the frame might block off some of the convective heat flux and disturb the boundary layer as the surface of the ceramic blanket is not smooth. The convective heat flux being emitted by the sample may, however, become trapped below the ceramic blanket above the sample, which would cause additional heat to build up, influencing the ignition behaviour. It is, however, not possible to determine the effect of either boundary layer, as airflow parameters such as velocity would be required. This will not affect the measured ignition temperatures but will affect the calculated ignition temperatures as the radiant heat flux measured does not take the convective heat flux into account.

Figure 5.2 to Figure 5.6 show the various materials after radiant panel tests had been completed.

Figure 5.2: Bakelite (C_B_M and C_B_P) samples after radiant panel tests
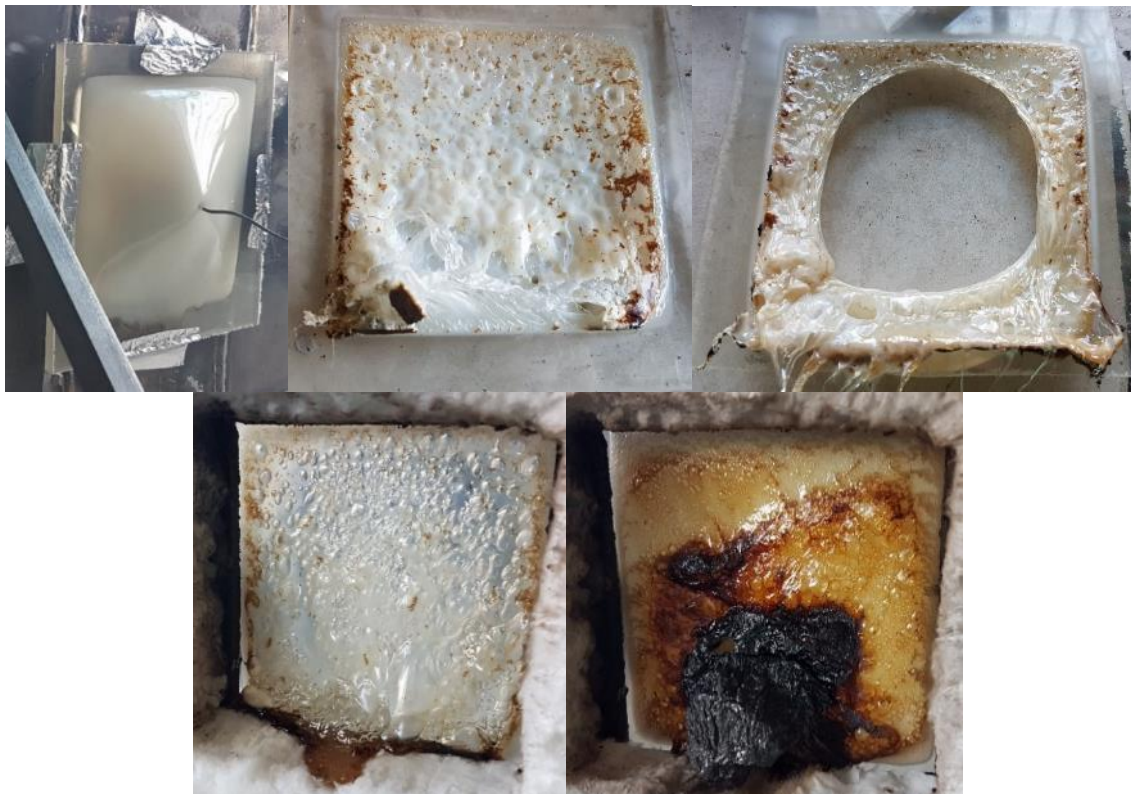
Figure 5.3: Window (C_W) samples after radiant panel tests

Figure 5.4: Blue pleather (S_PIPW) sample after radiant panel tests

Figure 5.5: Pleather (S_PI_F) samples after radiant panel tests

Figure 5.6: Rubbery foam (S_Ru_C) samples after radiant panel tests

In Table 5.11, the legend is shown for the following tables. "Test failed" refers to tests where the sample fell, a sample behaved in a way that would invalidate data or where the material behaviour would cause environmental changes which would influence ignition potential, such as the face of the material moving away from the radiant panels due to melting. "Ignition" refers to tests where the material ignited, while "No ignition" refers to tests where the material did not ignite after 15 minutes (ISO, 2019, p. 53) or did not have any more combustible material left. "HTRIS maximum temperature reached" refers to tests which had to be ended prematurely due to the equipment reaching the maximum safe operating temperature before ignition. "Data N/A" refers to calculated values, which are not applicable to the material due to the material not being thermally thick or thin as per the requirement for the equations for calculating time to ignition, as discussed below.

Table 5.11: Heat flux tables legend

Test Failed
Ignition
HTRIS maximum temperature reached
No ignition
Data N/A

In Table 5.12, all the samples tested are listed with their time-to-ignition values, the average heat flux recorded over the time of exposure of the sample to the radiant panels before ignition, and the maximum surface temperature before spontaneous ignition, with comments recorded during testing. In the comments, the timing refers to the duration of the sample's exposure to the radiant panels except where stated otherwise. The temperatures related to the ignition of Bakelite may be slightly lower than the surface temperature due to difficulties in accurately obtaining the front face temperature. Due to the opacity of the Bakelite material, it was not possible to judge the depth of the hole drilled into the solid material during drilling and thus the thickness of material between the surface and the thermocouple, or how deep the thermocouple is mounted. This coupled with the lower thermal conductivity of the Bakelite, may lead to inaccuracies in the temperature measured as these values may thus be lower than the actual surface temperature values. For this reason, the ignition temperature of 128°C of C_B_M_2 is disregarded in Table 5.16. In this case, the thermocouple was likely not close enough to the surface to detect the actual surface temperature. C_B_P_1 has no data as it was not possible to determine at what time the sample fell when considering the time at which the data was recorded, due to the video starting late and not allowing for correlation.

The surface temperature selected to represent Tig, is the maximum surface temperature up to the point of ignition, while the heat flux selected for $\dot{Q}"_R$ (radiative heat flux) is the average heat flux from the time of exposure to a particular range of heat flux (e.g. 30 kW/m^2 +/- 2.5 kW/m^2).

Table 5.12: Radiant panel test results and comments

Sample ID	t_{ig} (s)	Average Heat Flux (kW/m^2)	Maximum Temperature (°C)	Comment
		$\dot{Q}"_R$	T_{ig}	
C_B_M_1		44.5		HTRIS maximum temperature exceeded, no ignition in 1 min 48 s
C_B_M_2	74	45.7	128	No video
C_B_M_3	91	46.3	149	
C_B_M_4	97	46.0	221	
C_B_P_1				Video started late, 00:00:12 from start of video - pop, 00:03:41 from start of video - sample fell
C_B_P_2		46.5	252	HTRIS maximum temperature exceeded, no ignition in 2 min 42 s
C_B_P_3		45.6	240	Plain Bakelite with sticker, sticker turned to ash but didn't ignite, glowing, HTRIS maximum temperature exceeded, no ignition in 2 min 55 s
C_W_1		34.5	154	HTRIS maximum temperature exceeded, no ignition in 4 min 56 s
C_W_2	80	45.8		
C_W_3		41.3		Hole developed in sample around 2 minutes (window failed)
C_W_4		44.3		HTRIS maximum temperature exceeded, no ignition in 1 min 37 s, no hole in sample
C_W_5		49.7	160	HTRIS maximum temperature exceeded, no ignition in 1 min 45 s, no hole in sample
S_PI_F_1		21.9	273	Video started late, not insulated at back, sample "burnt" out, no ignition in 1 min 35 s
S_PI_F_2		45.1	249	Not insulated at back, sample shrivelled, sample fell 4 min 59 s
S_PI_F_3	41	37.3		
S_PI_F_4		21.0		Charring but no glowing or ignition after 15 minutes
S_PI_F_5		32.4		Glowing, HTRIS maximum temperature exceeded, no ignition in 11 min 47 s
S_PI_F_6		35.5		Glowing, HTRIS maximum temperature exceeded, no ignition in 3 min 20 s
S_PI_F_7	39	34.8		
S_PIPURePW	33	36.2		
S_PIPW_1	57	43.4		
S_PIPW_2	67	42.5		
S_PIPW_3	121	42.0		
S_PIPW_4	74	39.3		
S_PU_B_1	81	28.2	314	Glowing before ignition
S_PU_B_2		10.7	269	No ignition after 15 minutes at original heat flux, TC came loose at 15 min 21 s, ignition at 15 min 44 s from start, at higher heat flux +/- 30 kW/m^2 for +/- 35 s
S_Ru_C_1		20.6		No ignition after 5 minutes, sample melted and plane moved back, ignition at 5 min 36 s after increasing heat flux to +/- 35 kW/m^2 for +/- 10 s
S_Ru_C_2	35	40.0		

Table 5.13 indicates the material properties either measured or from literature. The sample thickness, τ, and density, ρ, has been measured as indicated in Table 5.8 and Table 5.9. For the blue pleather samples, the thickness, τ, refers to the thickness of the blue pleather only, as this is the material which will ignite. The specific heat, c, and the thermal conductivity, k, had to be obtained from literature (references are indicated in Table A.7 and Table A.8 in Appendix A) as testing was not practically possible.

Table 5.13: Radiant panel test material properties

Material ID	$\tau_{measured}$ (m)	$\rho_{measured}$ (kg/m³)	$c_{literature}$ (J/kg K)	$\tau\rho c$ (J/m²K)	$k_{literature}$ (W/m.K)	$k\rho c$ (W²s/m⁴K²)
C_B_M	0.0045	1350	1420	8627	0.250	479250
C_B_P	0.0045	1450	1420	9266	0.250	514750
C_W	0.0050	1270	1500	9525	0.200	381000
S_Pl_F	0.0013	600	1400	1092	0.200	168000
S_PIPURePW	0.0013	600	1400	1092	0.200	168000
S_PIPW	0.0011	635	1400	978	0.200	177800
S_PU_B	0.0180	13	1600	374	0.023	478
S_Ru_C	0.0570	90	1600	8208	0.023	3312

In order to determine whether a material sample is thermally thick or thin, the Biot number needed to be determined. This is, however, dependent on the convective heat transfer coefficient, but this can vary from 10 to 25 W/m²K. Convective heat transfer is related to the transfer of heat between the phases of the sample (gas, liquid or solid), thus the material properties, and is dependent on the airflow surrounding the sample, and is also dependent on the orientation and size of the sample (Drysdale, 2011, p. 35, 37, 52). This makes it difficult to determine an exact value of the convective heat transfer coefficient. The longer a sample is tested, the greater the influence of convective heat transfer on the surface temperature and ignition, as it can be considered a heat loss. To incorporate the variability of the convective heat transfer coefficient, three values were used in calculations in order to indicate the results at various levels of convective heat transfer. The lower range value of 10 W/m²K, as well as the upper range value of 25 W/m²K, was used, and also an average between the two of 17.5 W/m²K. Equation 5.1 was used to determine the Biot number of each sample, where τ is the thickness of the exposed material, and k is the thermal conductivity taken from literature as discussed previously.

Equation 5.1: Biot number (Drysdale, 2011, p. 54)

$$Bi = \frac{h \times \tau}{k}$$

A Biot number smaller than 0.1 indicates a material that is thermally thin (Drysdale, 2011, p. 252). The Biot numbers were calculated for each value of convective heat transfer coefficient, as well as whether the sample is thermally thick or thin.

For calculations including convective heat transfer, the transfer can either be on one side only or on both sides, depending on whether the sample is insulated. In the case where the material sample is insulated at the back, only the front will experience convective heat transfer. In this case, h will replace the 2h found in Equation 5.8. Table 5.14 shows which samples were insulated at the back and which were not, as well as whether h or 2h was used in Equation 5.8. The only case where the sample could

be considered as both insulated or not, are the blue pleather samples, which have a 3.4 mm plywood backing. As the backing is quite thin, the samples have been assumed not to be insulated at the back. S_Pl_F_3 was tested with the layers that would usually be found behind it, the foam layers and plywood, and this resulted in ignition and different behaviour to the pleather samples with nothing behind them, which indicated that these layers provide sufficient insulation so that these layers could be replaced with ceramic blanket for insulation. Table 5.14 also includes the absorptivity, an assumed constant, which was assumed to be 0.9 for all materials.

Table 5.14: Back insulation, convective heat transfer and absorptivity

Sample ID	Insulated	h or 2h	a
C_B_M_1	No	2	0.9
C_B_M_2	No	2	0.9
C_B_M_3	No	2	0.9
C_B_M_4	No	2	0.9
C_B_P_1	No	2	0.9
C_B_P_2	No	2	0.9
C_B_P_3	No	2	0.9
C_W_1	No	2	0.9
C_W_2	No	2	0.9
C_W_3	No	2	0.9
C_W_4	No	2	0.9
C_W_5	No	2	0.9
S_Pl_F_1	No	2	0.9
S_Pl_F_2	No	2	0.9
S_Pl_F_3	Yes	1	0.9
S_Pl_F_4	Yes	1	0.9
S_Pl_F_5	Yes	1	0.9
S_Pl_F_6	Yes	1	0.9
S_Pl_F_7	Yes	1	0.9
S_PIPURePW	Yes	1	0.9
S_PIPW_1	No	2	0.9
S_PIPW_2	No	2	0.9
S_PIPW_3	No	2	0.9
S_PIPW_4	No	2	0.9
S_PU_B_1	No	2	0.9
S_PU_B_2	No	2	0.9
S_Ru_C_1	No	2	0.9
S_Ru_C_2	No	2	0.9

In order to determine the specific heat, the thermal conductivity from literature was assumed for thermally thick materials, and calculations were done as per Equation 5.2 to Equation 5.5. A material was considered to be thermally thick or thin if it is classified as such at any of the considered convective heat transfer coefficients. This means that some materials were considered both thermally thick and thermally thin. The thermal conductivity does not vary widely, so this value is more likely to be in the range of the actual thermal conductivity of a material, compared to the specific heat. For thermally thin

materials, the measured values for τ and ρ were used in calculations, and thus, no assumptions were required, but none of these samples had temperature data. Table 5.15 shows the results of the calculated specific heat compared to the values found in literature, but none of the values are within range, and thus, it can be assumed that the losses do contribute or the temperatures measured are not reflective of the actual ignition temperature. There is, however, no simple equation that can be used to obtain specific heat values for thermally thick samples as the complementary error function of β, erfc(β), is required, which is dependent on either the specific heat or the depth of the heated layer, phenol, in turn, is dependent on the thermal diffusivity, α. These properties are, however, unknown. The specific heat values from literature should thus be relied upon.

Equation 5.2: Time to ignition for thermally thin materials, ignoring losses (Drysdale, 2011, p. 257, Equation 6.33)

$$t_{ig} = \rho \times c \times \tau \times \frac{T_{ig} - T_0}{\dot{Q}_R^{"}}$$

Equation 5.3: Time to ignition for thermally thick materials, ignoring losses (Drysdale, 2011, p. 257, Equation 6.32)

$$t_{ig} = \frac{\pi}{4} \times k \times \rho \times c \times \frac{\left(T_{ig} - T_0\right)^2}{\dot{Q}_R^{"}}$$

Equation 5.4: Time to ignition for thermally thick materials, ignoring losses, rearranged

$$k \times \rho \times c = \frac{t_{ig} \times \dot{Q}_R^{"~2}}{\frac{\pi}{4} \times \left(T_{ig} - T_0\right)^2}$$

Equation 5.5: Specific heat calculation using material properties k and ρ

$$c = \frac{k \times \rho \times c}{k \times \rho}$$

Table 5.15: Specific heat in literature vs calculated

Sample ID	$c_{literature}$ (J/kg K)	kρc (W^{2}s/m^{4}K^2)	Thick, ignore losses	
			kρc (calculated)	c (J/kg.K) (calculated)
			$(t_{ig}. \dot{Q}"_R{}^2)/((\pi/4).(T_{ig}\text{-}T_0)^2)$	
C_B_M_2	1420	479250	16730871	49573
C_B_M_3	1420	479250	15003212	44454
C_B_M_4	1420	479250	6433718	19063
S_PU_B_1	1600	478	949261	3174785

When including the losses due to convective heat transfer, all the samples which ignited and had ignition temperature data measured, were classified as thermally thick. There is no simple equation available to obtain specific heat values for thermally thick values as the complementary error function of β, erfc(β), is required, which is dependent on either the specific heat or the depth of the heated layer, which in turn is dependent on the thermal diffusivity, α.

Ignition temperatures were calculated using Equation 5.6 to Equation 5.8 and Equation 5.10 according to whether a material was thermally thick or thermally thin, while including and ignoring losses.

Equation 5.6: Ignition temperature for thermally thin materials, ignoring losses (Drysdale, 2011, p. 257, Equation 6.33)

$$T_{ig} = \frac{t_{ig} \times \dot{Q}_R^{"}}{\tau \times \rho \times c} + T_0$$

Equation 5.7: Ignition Temperature for Thermally Thick Materials, Ignoring Losses (Drysdale, 2011, p. 257, Equation 6.32)

$$T_{ig} = \sqrt{\frac{t_{ig} \times \dot{Q}_R^{" \, 2}}{\frac{\pi}{4} \times k \times \rho \times c}} + T_0$$

Equation 5.8: Ignition Temperature for Thermally Thin Materials, Including Losses (Drysdale, 2011: p. 252, Equation 6.25)

$$T_{ig} = \frac{a \times \dot{Q}_R^{"}}{2 \times h} \times \left(1 - \exp\left(\frac{-2 \times h \times t_{ig}}{\tau \times \rho \times c} \right) \right) + T_0$$

β is also calculated in order to calculate the ignition temperature of thermally thick samples. Equation 5.9 was used to calculate β, the cooling modulus, for each sample.

Equation 5.9: Cooling modulus (Drysdale, 2011, p. 253, Equation 6.26)

$$\beta = Bi \times Fo^2 = \frac{h \times t^{\frac{1}{2}}}{(k \times \rho \times c)^{\frac{1}{2}}}$$

Equation 5.10: Ignition Temperature for Thermally Thick Materials, Including Losses (Drysdale, 2011, p. 254, Equation 6.29)

$$T_{ig} = \frac{a \times \dot{Q}_R^{"}}{h} \times \left(1 - exp(\beta^2) \right) \times erfc(\beta) + T_0$$

In Table 5.16, the ignition temperatures are given for each material compared to the temperatures at which no ignition occurred, compared to a calculated ignition temperature. The ignition temperature, which is assumed when considering only the temperatures measured and calculated but not those found in literature are also given. In the case of the Bakelite samples, the temperatures at which no ignition occurred were higher than those at which ignition did occur. This could either be due to the outer layer differing (rough matt texture for marbled samples which ignited versus shiny and smooth texture for plain samples which did not ignite) or due to the lower heat flux experienced by the one sample and the heat source needing to be removed due to equipment safety protocols for both samples. In most cases, the calculated ignition temperatures were very high and, in cases with ignition temperatures to compare to, much higher than the measured ignition temperatures. This could be due to incorrect assumptions regarding material properties or the convective heat transfer coefficient, or the heat flux not being the actual critical heat flux and thus causing a higher ignition temperature to be

calculated. It must be noted that the equations provide only approximate values and are not to be considered to provide very accurate results. It must also be noted that the ignition temperatures are for spontaneous ignition, not for piloted ignition, as that is what was tested.

Table 5.16: Ignition temperature measured vs calculated and assumed ignition temperature

Material ID	Measured T_{ig} (°C)	Measured Temperature (no ignition) (°C)		Calculated (°C)	Literature T_{ig} (°C)	Assumed T_{ig} (°C)
C_B_M	149-221	240	252	662	367-614	225
C_W		154	160	779	250-580	250
S_Pl_F				632	189-600	200
S_Pl_B				897-1087	189-600	200
S_PU_B	314	269		159	370-638	315
S_Ru_C				136	310	310

The references for the ignition temperature ranges from literature are shown in Table A.10 to Table A.14 in Appendix A. In literature, PMMA has an ignition temperature of 250°C to 380°C and polycarbonate has an ignition temperature of 440°C to 580°C. This indicates that the window is likely made of PMMA as it has a lower ignition temperature. PVC has an ignition temperature of 311°C to 550°C in literature, and thus, the calculated value of pleather falls within range, but the calculated value for the blue pleather is much higher than in literature and thus unlikely to be correct. A polyurethane solid is listed as having a piloted ignition temperature of 271°C (Beyler, 2004, chap 15, Table 15). Polyurethane foam in literature has an ignition temperature of 370°C to 528°C. The light blue foam has a slightly lower ignition temperature and can be assumed to not have any fire-resistant treatment due to its low ignition temperature. Bakelite has an ignition temperature of 300°C to 614°C in literature, which is a very wide range. The Bakelite samples have a much lower ignition temperature and thus can be assumed to contain more wood powder as the paper reinforced phenol formaldehydes have ignition temperatures on the lower end of the range in literature. The calculated ignition temperature for Bakelite is higher than values found in literature. Latex foam is listed as having an ignition temperature of 310°C (Beyler, 2004, chap 15, Table 15), which is lower than that of typical polyurethane foam, making it very dangerous as it has a high density and high heat of combustion. The calculated temperature of rubbery foam is much lower than that of latex foam in literature and is thus unlikely to be accurate.

In the literature, materials such as plastic, which melt, have been found to be unlikely to ignite at all if they do not ignite within a short amount of time, due to the nature of the material decomposition and subsequent combustion. This would apply to the foam, window and pleather samples but not the Bakelite samples. The heat flux required to ignite samples may have been increased by the high velocity of the extraction system due to the expected toxic smoke that would be produced. Table 5.17 shows the approximate critical heat flux of the materials tested, which is calculated by finding the average between the highest heat flux at which no ignition took place and the lowest heat flux at which ignition did take place (ISO, 2019, p. 53). In ISO 5660, cases where the highest heat flux at which ignition does not occur, is higher than the lowest heat flux at which ignition occurs, triplicate tests are required, and the average of the results must be calculated. Due to time constraints, the two highest heat fluxes at which no ignition occurred and the two lowest heat fluxes at which ignition did occur, were averaged for the window and pleather. In the case of the window, only one sample ignited, and thus, this heat flux was taken into account twice with the two highest heat fluxes at which no ignition occurred. For the Bakelite, three values of each were used, as would be the case for triplicate tests.

Table 5.17: Critical heat flux of materials

Material ID	Measured Critical Heat Flux (kW/m^2)	Literature Critical Heat Flux (kW/m^2)
C_W	46.4	3.33-26
C_B_M	45.8	15-26
S_Pl_F	34.7	10-27.5
S_PU_B	>11, <28	16.4-20
S_Pl_B	<39	10-27.5
S_Ru_C	<39	16-34.1

The references for the critical heat flux ranges from literature can be found in Table A.15 and Table A.16 in Appendix A. In literature, polycarbonate has a critical heat flux of 11.5 kW/m^2 to 26 kW/m^2, while PMMA has a critical heat flux of 3.33 kW/m^2 to 18.6 kW/m^2. The window is thus more likely to be made of polycarbonate than PMMA when the comparative critical heat flux is considered. From literature, it can be seen that the materials with the highest critical heat flux are polycarbonate, PVC and phenolic formaldehyde, followed by polyurethane, while the materials with the lowest critical heat flux are PMMA, polyurethane foam and latex. This corresponds to the critical heat flux values obtained in spontaneous ignition conditions, with the window, Bakelite, and pleather having higher critical heat fluxes and the polyurethane foam having a much lower critical heat flux.

5.6   Summary of Sample Identification

The components in the carriage with unknown composition have been tested, and the results compared to possible matches in literature. In all the cases, the rubbery foam compared better to latex foam than to polyurethane foam, and thus it is very likely to be latex foam rather than typical polyurethane foam. The window was indicated to be more likely to be PMMA when considering the heat of combustion and the ignition temperature. The critical heat flux may have indicated that the window could be polycarbonate, but the values for both these materials do overlap significantly, so it cannot be definitively identified using this property. The window is thus very likely to be made of PMMA. The window frame compared well to polycarbonate when considering the heat of combustion but was not included in the radiant panel tests in order to confirm this identification. The window frame can be assumed to be polycarbonate, but there is a degree of uncertainty. The pleather was shown to be more likely to be a polyurethane-type pleather when considering the heat of combustion, but this could not be confirmed by the radiant panel tests as the ranges for each material were very close or not comparable due to differences in testing methods.

6 Large-scale Experimental Results

6.1 Introduction

In this chapter, the results of the experimental work are discussed. The large-scale experiments conducted as per Chapter 3 are covered. These results are then used for the FDS modelling, which is discussed in Chapter 7.

Various parameters were measured during the large-scale experiments performed on the seats. The experiments were recorded visually by video and by a thermal imaging camera which took photos at 7-second intervals. Data that was recorded included the MLR of the seat for the duration of the experiment measured by a scale, the temperature at three heights above the seat measured by thermocouples, and the heat flux at a point 1 m from the front edge of the seat bottom measured by a water-cooled heat flux gauge.

6.2 Visual Observations Made During Experiments

Table 6.2 shows the various occurrences and at what time from ignition they occurred for each experiment. Information regarding the condition and size of the seat samples are provided in Table 6.1. None of the seats were vandalised in a controlled manner as indicated in EN 45545 (CEN, 2015), but rather tested as received. Some of the seats were already vandalised, while others were in good condition.

Table 6.1: Conditions of experiments

	Experiment 1	Experiment 2	Experiment 3	Experiment 4
Condition of bottom	Slightly vandalised	Very vandalised	Very vandalised	No vandalism
Condition of back	Slightly vandalised	Very vandalised	No vandalism	One cut - limited
Back size	36 inch	33 inch	36 inch	52 inch
Bottom size	36 inch	36 inch	36 inch	52 inch
Ignition position	Front, centre	Front, centre	Right, back	Middle, back
Burnt through back	No	Yes	No, but possible if left longer	No

Table 6.2: Visual observations

Event	Time from Start of Experiment (min:s)			
	Experiment 1	Experiment 2	Experiment 3	Experiment 4
Ignition removed	00:54	00:31	00:19	00:10
Spread	01:16	00:39	00:35	00:45
Rapid spread	01:39	00:48	01:49	01:09
Black smoke	01:21	00:48	01:50	01:00
Severe black smoke	01:44	00:52	01:54	01:12
Visibility low	02:08	01:29	02:13	01:38
Spread to back	01:41	00:44	01:52	00:40
Melting / burning materials fall to floor	00:44	01:08	02:21	01:48
Flames recede	05:47	04:38	N/A	N/A
Dampened	N/A	N/A	03:19	N/A
Extinguished	10:51	05:26	03:54	03:13

6.2.1 Experiment 1 – 36 Inch Seat

The seat used for Experiment 1, had a bent back support frame, as can be seen in Figure 6.1, which had to be straightened, and supports had to be welded to the rusted and unstable frame to keep the seat upright, as can be seen in Figure 6.2. This seat is slightly more upright than would be found within the Metrorail trains, as further bending of the frame would have caused it to break. This should not affect the results very much except for spread to, and along the height of the back happening slightly faster than usual. On the left of Figure 6.2, the condition of the seat is also shown, with some vandalism. The seat was mostly covered in pleather, with some foam exposed and some of the white lining material hanging out.

On the right side of Figure 6.2, the seat is shown after the experiment, showing the entire back, excluding the plywood backing, having burnt away and only some foam and unburnt parts of pleather remaining on the wooden backing of the seat bottom, after the fire was extinguished. The plywood backing of the seat back is charred but remains intact. For this experiment, the plywood backing did not burn through, and the back of the seat was not burnt. This would prevent some heat from reaching the seat behind it, although the flames above the top of the seat are likely to still cause ignition of the seat behind it.

Figure 6.1: Seat for Experiment 1 prior to bending and adding supports

Figure 6.2: Condition of seat before and after Experiment 1

In Figure 6.3, the growth stage of Experiment 1 can be seen, with the first and last pictures taken within a period of 38 s from one another. This shows the rapid rate of spread and how quickly the fire reaches a fully developed stage. In all the pictures, fallen burning matter is visible with a sustained flame. In the case that the floor is made of a flammable material, this could lead to rapid spread along the floor and quickly engulf the entire carriage in flames.

Figure 6.3: Growth stage of Experiment 1

During the experiment, the fire was turbulent in nature, and the flames leaned forward or to the side, as can be seen in Figure 6.4. This may affect the temperatures measured by the thermocouples. Some burning particles landed on the calcium silicate boards at various points during the experiment and are visible towards the beginning of the experiment in Figure 6.4, as well as towards the end of the experiment in Figure 6.5. Most of the particles had flames that sustained for longer than 10 s. The

flames also exceed the maximum 1000 mm above the highest point of the seat, as can be seen in Figure 6.4, with the flames reaching the same height as the top of the thermocouple tree at the beginning of the experiment. The top thermocouple was 1 m above the top of the seat, but slightly below the top of the pole forming the thermocouple tree. The flames also reached the edges of both the seat bottom and seat back, failing two of the EN 45545-2 requirements for requirement set R18, which is specified for passenger seats (CEN, 2015). If the seat had been tested under a hood in a furniture calorimeter setup, the test would have to be ended as the equipment would have been in danger of being damaged. This is a third requirement that would have been failed.

Figure 6.4: Turbulent flames leaning forward (left), fully developed stage Experiment 1 (right)

Figure 6.5: Decay stage of Experiment 1

In Figure 6.6, the back of the seat can be seen to have little damage except for the melting of some of the pleather around the ventilation holes. Towards the bottom of the seat back, the wood has charred through, while the upper part of the seat back has no sign of exposure to fire. The seat bottom in Figure 6.7 has some soot towards the side of the seat, but the rest of the bottom of the plywood has no sign of exposure to fire. The sides of the seat bottom and seat back that were directly exposed to the fire are charred over the entire surface.

Figure 6.6: Seat back at end of Experiment 1

Figure 6.7: Seat bottom at end of Experiment 1

6.2.2   Experiment 2 – 36 Inch Seat Bottom and 33 Inch Seat Back

The seat used for Experiment 2 was severely vandalised, with a big portion of foam exposed on both the seat bottom and seat back, as can be seen on the left of Figure 6.8. A large piece of foam is also missing from the seat bottom. This seat has been placed on a frame that is usually used for seats that are back to back, and also, in this case, for a larger seat size, specifically the 52 inch seat. This should, however, not affect the results as the frame does not contribute to combustion and also does not block any heat from reaching any part of the seat. On the right of Figure 6.8, the seat can be seen after the fire was extinguished. The plywood backing has burnt away, with only the thicker support ribs and top panel remaining. This could cause the fire to spread quickly to the seat behind it. Only some foam remains on the wooden backing of the seat bottom, as can be seen in Figure 6.11.

Figure 6.8: Condition of seat before and after Experiment 2

68

Experiment 2 also had burning particles land on the calcium silicate boards at various times during the experiment, as can be seen in Figure 6.9 and Figure 6.10. Most of the particles also had sustained flaming for more than 10 s, and included large pieces of burning matter falling from the burning seat. Once again, the flames exceeded the maximum 1000 mm above the top of the seat, as can be seen in Figure 6.9, with the flames extending above the top of the thermocouple tree. Figure 6.10 also shows that the flames reach the edge of the seat back and seat bottom. Both the requirements for R18 have been failed. Again, had a furniture calorimeter been used, the experiment would have had to be ended due to equipment safety concerns, and thus, a third requirement would have been failed.

Figure 6.9: Fully developed stage Experiment 2

Figure 6.10: Decay stage of Experiment 2

Figure 6.11: Seat after Experiment 2

6.2.3   Experiment 3 – 36 Inch Seat on 52 Inch Frame

The seat bottom used for Experiment 3 was severely vandalised while the seat back had no damage at all, as can be seen on the left in Figure 6.12. Some of the foam is also missing from the seat bottom, and very little of the seat bottom is covered in pleather. Most of the foam on the seat back burnt out, but a significant amount of foam remained on the plywood backing of the seat bottom, as can be seen on the right of Figure 6.12, as the fire was extinguished early due to safety concerns. This seat also had a thinner plywood backing for the seat back, which could have burnt through had the fire been left to burn for longer.

Figure 6.12: Condition of seat before and after Experiment 3

Experiment 3 also had burning particles land on the calcium silicate boards at various points of time during the experiment, as can be seen in Figure 6.13. These particles also had flaming sustained for longer than 10 s. In this case, the flames also extended above the maximum 1000 mm above the highest point of the seat, and spread to the edges of the seat back and seat bottom, as can be seen in Figure 6.13. As the experiment had to be ended early due to safety concerns, three R18 requirements would have been failed.

Figure 6.13: Fully developed stage Experiment 3

On the left side of Figure 6.14, the damage to the backside of the seat can be seen. The vents towards the bottom of the seat back allowed flames to escape, and the pleather at the back started to burn. This would cause the seat behind it to ignite. On the right side of Figure 6.14, the remaining foam on the seat bottom can be seen. Most of the foam has burnt away in the middle of the seat, with the surrounding edges still having a significant amount of the thickness remaining. This could be due to the heat losses around the sides while the middle section is insulated by the foam around the edges, causing more

heat to build up. Some charring and melting of the top of the foam can be seen around the edges, while the middle is mostly only melted but not charred.

Figure 6.14: Seat after Experiment 3

6.2.4 Experiment 4 – 52 Inch Seat

The seat bottom used for Experiment 4 had no damage at all, while the seat back had a single cut in the pleather, but the foam was still covered, as can be seen on the left of Figure 6.15. There is still some foam remaining on the plywood backing of the seat back but not much foam remaining on the plywood backing of the seat bottom, as can be seen on the right of Figure 6.15. This seat also had a thinner plywood backing with thicker support ribs, which had the potential of burning through if left to burn for longer.

Figure 6.15: Condition of seat before and after Experiment 4

Figure 6.16 shows the ignition of the seat and the flames starting to spread along the seat back. The seat was ignited at the back of the seat bottom, in the corner formed by the seat back and seat bottom. The presence of the pleather on the seat back did not seem to reduce the spread compared to the experiments, which had significant vandalism with exposed foam.

Figure 6.16: Experiment 4 ignition of seat

Figure 6.17 shows the spread along the back towards the side, with the release of flammable vapours visible to the left of the flames, caused by the heating of the materials ahead of the flames.

Figure 6.17: Growth stage of Experiment 4

Experiment 4 had burning particles landing not only on the calcium silicate boards but also on the ground next to the scale, as can be seen on the left of Figure 6.18. These particles were again flaming for more than 10 s at various times during the experiment. On the right side of Figure 6.18, a large amount of black smoke can be seen, showing the smoke levels seen during these experiments. The flames exceeded the maximum height of 1000 mm above the top of the seat, and the flames reached the edges of both the seat bottom and seat back, as can be seen in Figure 6.18. As the experiment had to be ended due to safety concerns, three of the R18 requirements had again been failed.

Figure 6.18: Fully developed stage of Experiment 4

Figure 6.19 shows the remains of the seat after the fire had been extinguished. Some burnt pleather remained on the seat bottom with unrecognisable remnants of the foam. In Figure 6.20, there is clear evidence that the foam melts and drips as there are pieces of melted foam on the bottom of each hole of the honeycomb.

Figure 6.19: Seat after Experiment 4

Figure 6.20: Melted foam after Experiment 4

6.3   Mass Loss Rate

During the experiment, the mass measured by the scale was recorded every second. In order to determine the MLR, the ignition point and extinction point needed to be determined and then the mass at each point in time needed to be subtracted from the starting mass before ignition. In order to obtain the MLR curve, the change in mass was divided by the change in time at each point in time. A graph of the cumulative mass lost can be seen in Figure 6.21. Experiment 1 and Experiment 3 took longer for the growth stage to be reached, and thus mass loss was delayed. For this reason, the time of Experiment 2 and Experiment 4 were shifted by 60 s so that the growth and decay stages could be compared. Both experiments seemed to reach the growth stage around 60 s faster than in Experiment 1 and Experiment 3, which can clearly be seen in Figure 6.21, where the start of the growth stage lines up after shifting the time of Experiment 2 and Experiment 4.

Table 6.3: Initial scale reading and total mass lost per experiment

Experiment	Initial Scale Reading (kg)	Total Mass Lost (kg)
1	29.4	7.2
2	39.6	6.4
3	42.2	3.4
4	48.2	3.8

In Table 6.3, the starting mass of the seats is indicated, with Experiment 1 having a much lower mass due to the smaller metal frame that formed part of this seat. The same metal frame was used for Experiment 2, Experiment 3 and Experiment 4, with varying seat bottom and back sizes. Experiment 2 consisted of a 33 inch back, and a 36 inch bottom, the back and bottom of Experiment 3 were both 36 inches, and for Experiment 4 both the back and bottom were 52 inches. In Experiment 1, the back and bottom of the seat were both 36 inches, but the smaller metal frame was much lighter, causing it to have the mass to be lower than that of Experiment 2 with the smaller back. This justifies the starting masses for each experiment relative to one another.

In Figure 6.21, the total mass lost can be seen. Experiment 1 had a total loss of 7.2 kg, Experiment 2 had a total loss of 6.4 kg, and Experiment 3 and 4, which were only allowed to burn until the HRR had been reached, had a total mass loss of 3.4 kg and 3.8 kg respectively. The cumulative mass loss graphs compare very well between the experiments once the growth stage starts, with all the curves having roughly the same gradient at a given point in time.
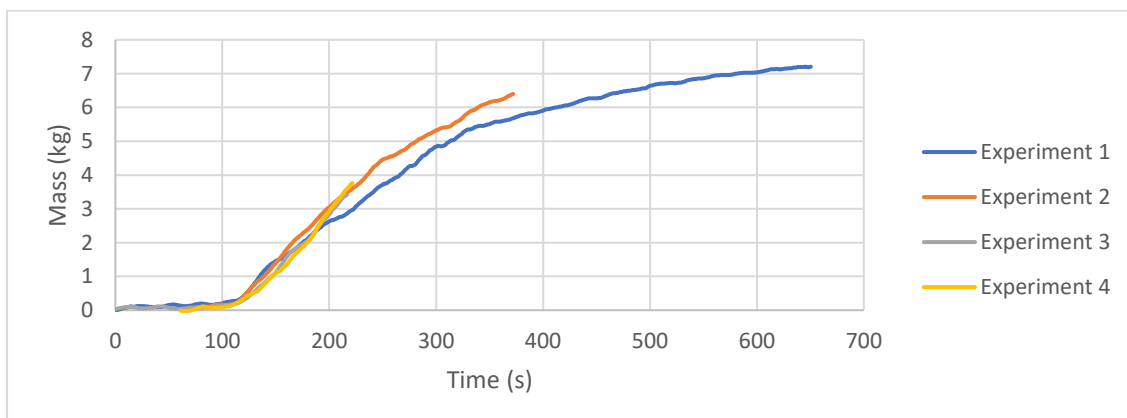
Figure 6.21: Cumulative mass loss

Figure 6.22 to Figure 6.25 have the seat mass plotted alongside the temperature at each thermocouple and the heat flux for each experiment, starting from ignition. The blue vertical line indicates the point at which the fire was extinguished. For Experiment 4, the data was cut off before the point at which the fire was extinguished, at "end data", as the data starts to behave as though water was sprayed over the fire at that point. Specifically, the increase in mass indicates this as well as the sharp decrease in heat flux. The data after the time at which the mass starts to increase has thus been disregarded and considered invalid. This does not influence the validity of the data before this point, and the curves all appear to be as expected.
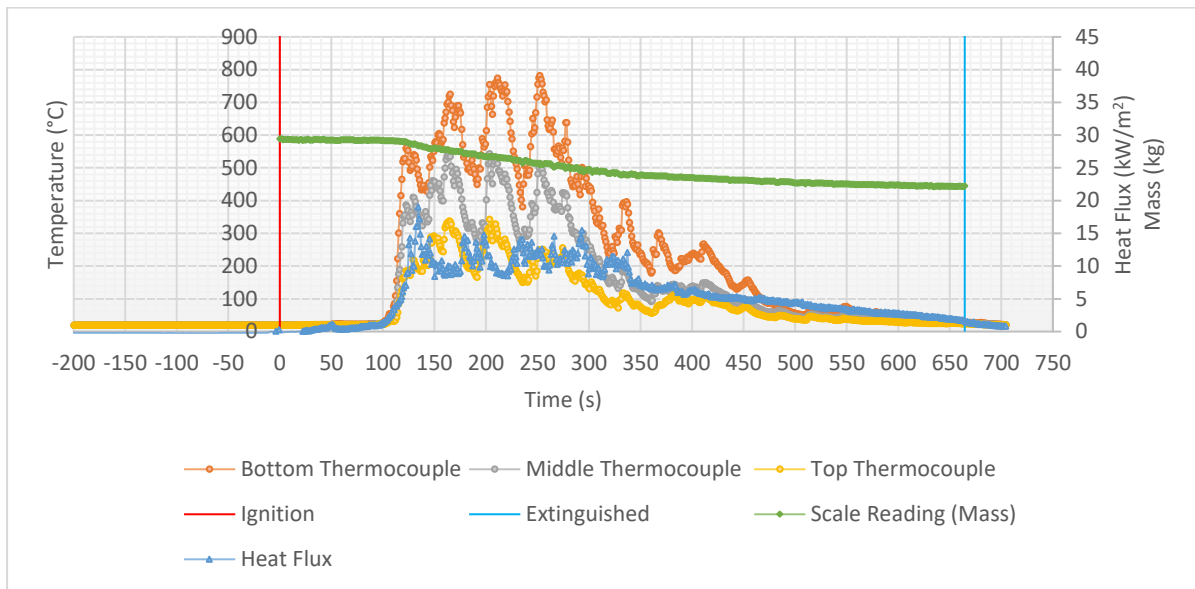
Figure 6.22: Experiment 1 - mass, temperature and heat flux
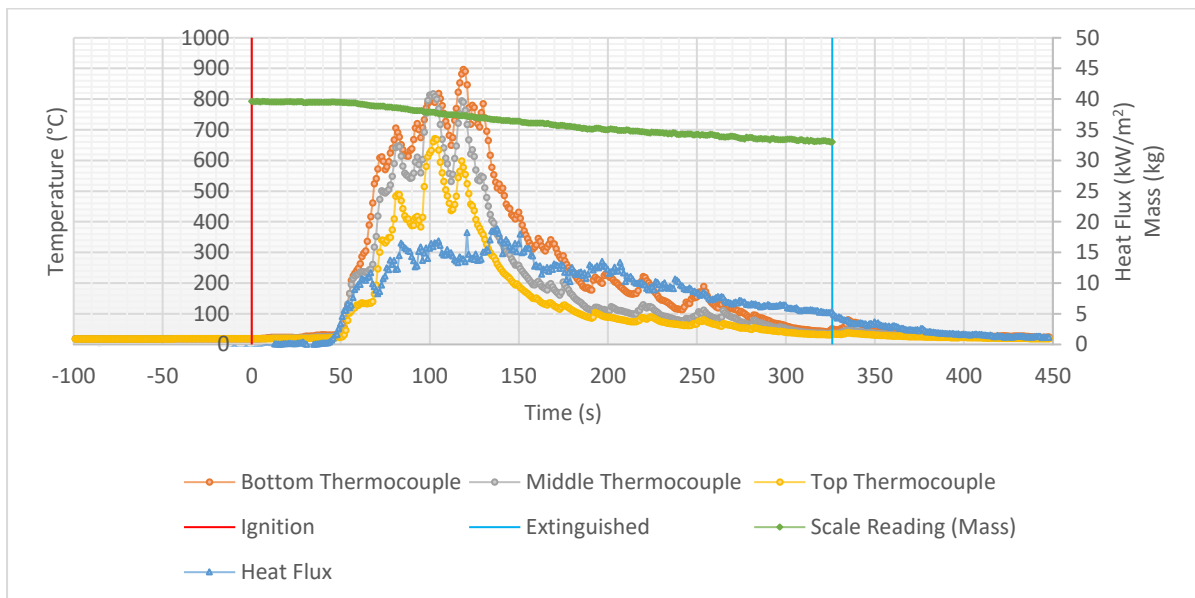
Figure 6.23: Experiment 2 - mass, temperature and heat flux
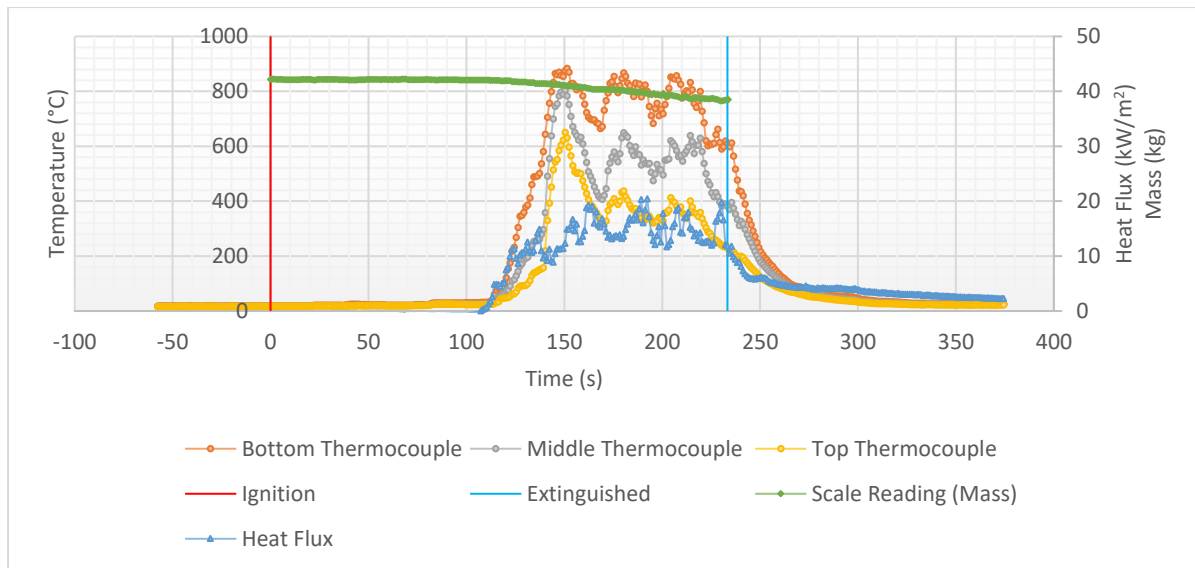
Figure 6.24: Experiment 3 - mass, temperature and heat flux
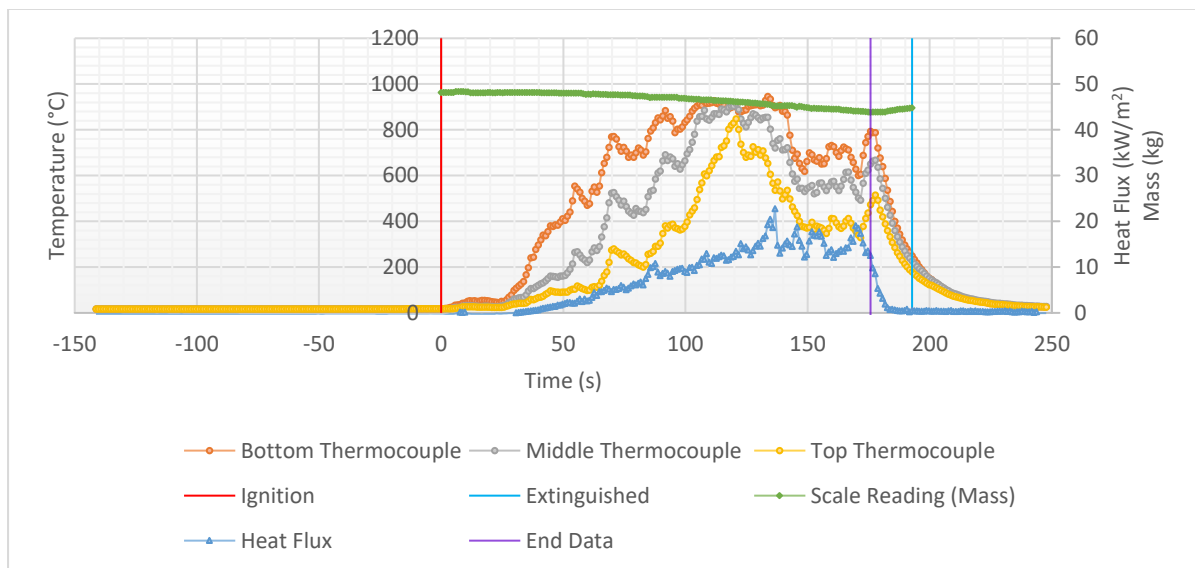
Figure 6.25: Experiment 4 - mass, temperature and heat flux

The raw MLR data for each experiment are shown in Appendix B. The MLR was calculated by dividing the change in mass by the change in time between adjacent recorded time steps.

As can be seen in these graphs, there is a lot of noise in the raw data. This is due to many factors, including environmental factors, the mass balance response during the experiment as the mass of the sample changes, as well as the manner in which a polymer burns (Staggs, 2005, p. 495). Gas bubbles through the molten polymer towards the surface and are then released, causing the mass to be lost bit by bit instead of in a continuous manner, and surface activity during the fire can also influence the results (Hasburgh *et al.*, 2004). In order to reduce the noise and obtain the MLR curve, the data needs to be processed first. The data was processed in 3 manners: Backward Difference, Central Difference and according to the method specified by ISO 5660. Once it was determined that these methods still did not return data that had been smoothed enough, the Savitzky-Golay data filter was applied as recommended by Staggs (2005). The details of this process are discussed in Appendix B.

The MLR curves for each experiment were plotted in Figure 6.26, after adjusting the time of Experiment 2 and Experiment 4, and after the MLR values below 0 were removed. These still remained after data smoothing and should be disregarded as the MLR cannot be negative at any point in time. A trend has emerged from the very noisy raw data seen before, with a rapid increase around 100 to 125 s and a peak MLR around 180 s. The curves of all the experiments compare very well, indicating a trend across all the experiments, showing that the results are reliable.
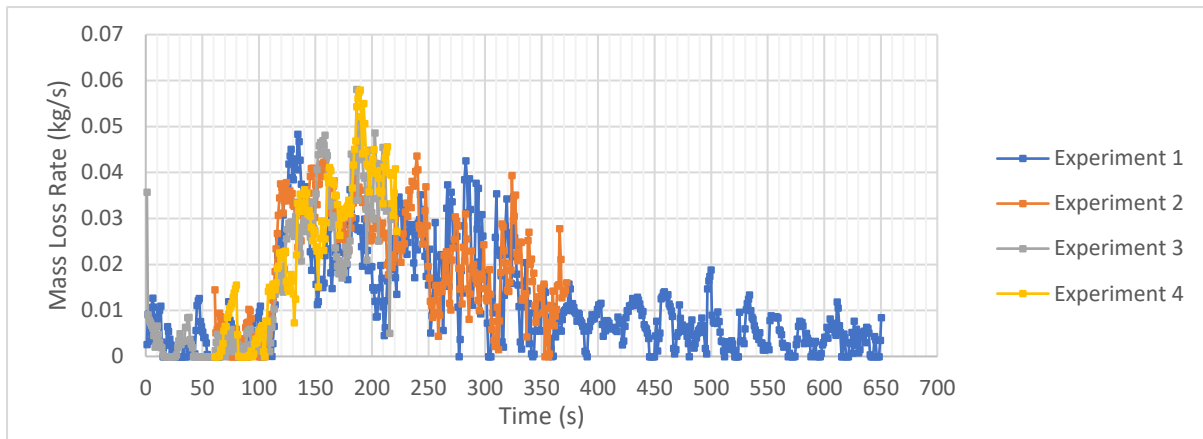
Figure 6.26: MLR

6.4   Heat Release Rate

In order to determine the estimated HRR curve, the MLR was multiplied by the estimated heat of combustion. The estimate can be taken from the heat of combustion of foam as this is the largest portion of volume in the seats and would thus have the biggest influence on the total heat of combustion. From Table 5.10, the heat of combustion for the yellow foam average at a minimum estimated efficiency factor of 0.75 is 20.9 MJ/kg, this can be considered to be the minimum heat of combustion for the seat. The maximum heat of combustion would be that of the rubbery foam at an efficiency factor of 1, with a heat of combustion of 43.4 MJ/kg. The minimum value is thus taken as 20 MJ/kg and the maximum value as 43.5 MJ/kg, resulting in the curves shown in Figure 6.27 and Figure 6.28, respectively. In Chapter 7, the actual heat of combustion is calculated, and an appropriate efficiency factor is applied.
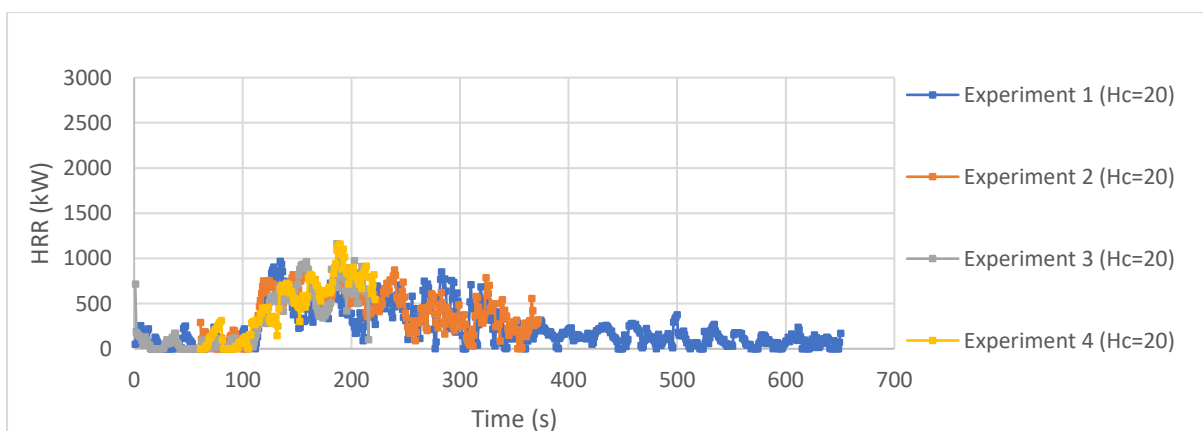
Figure 6.27: Minimum HRR curves
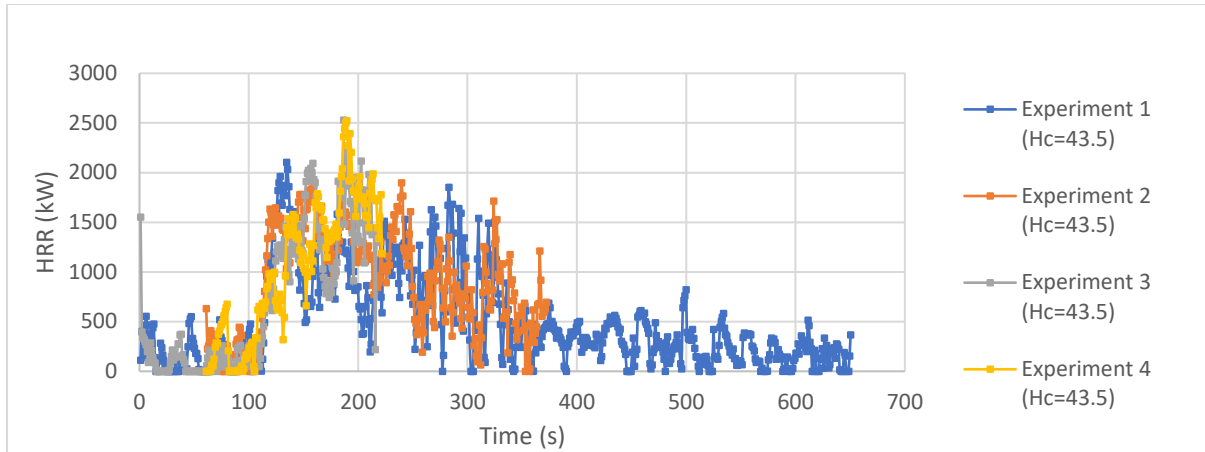
Figure 6.28: Maximum HRR curves

6.5 Temperatures and Heat Flux

In Figure 6.29, the heat flux curves are plotted, after being adjusted for time in the case of Experiment 2 and Experiment 4. This is the heat flux measured 1 m from the seat. The curves compare very well, with a rapid rise at around 100 to 125 s (the same time as the rapid rise seen in the MLR curves). The heat flux reaches a peak at around 200 s. The peak heat flux for Experiment 1 is 19 kW/m^2, for Experiment 2 it is 18.9 kW/m^2, for Experiment 3 it is 20.4 kW/m^2, and for Experiment 4 it is 22.8 kW/m^2. These peak heat fluxes could cause ignition for any of the materials found in the carriage in a piloted condition.
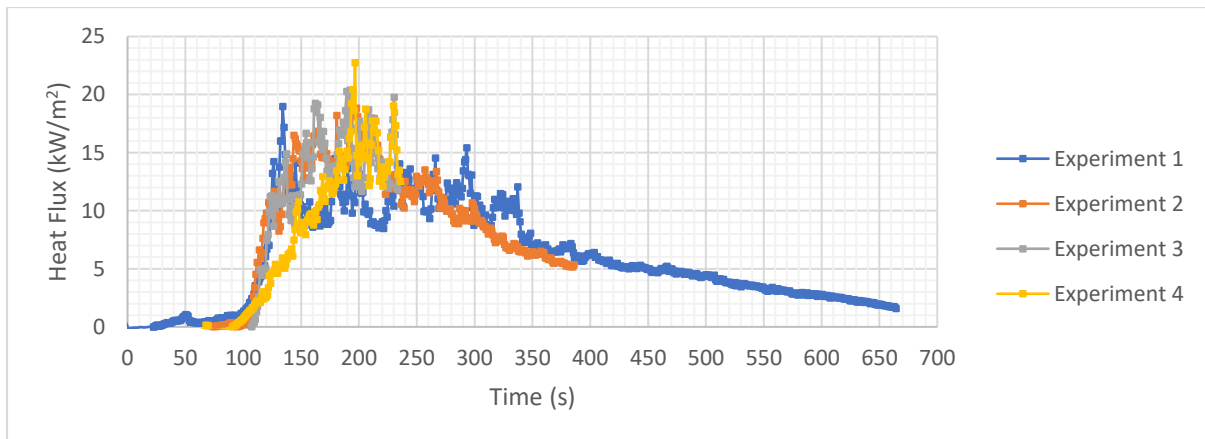
Figure 6.29: Heat flux

In order to see the correlation of the temperature and the MLR as well as the heat flux and the MLR, the thermocouple temperatures and heat flux was plotted alongside the MLR for each experiment. The graphs for Experiment 1 can be seen in Figure B.8 and Figure B.9, for Experiment 2 in Figure B.10 and Figure B.11, for Experiment 3 in Figure B.12 and Figure B.13, and for Experiment 4 in Figure B.14 and Figure B.15. In all cases, the curves compare very well with one another, with rapid rises and peaks overlapping well in general. The temperature curves of each experiment also correspond very well to one another, with mostly the amplitude differing along the height above the seat with very little differences otherwise. The bottom thermocouple maximum temperatures vary from around 780ºC to 940ºC, which is quite reasonable considering the fuel load differing significantly in some cases

78

(Experiment 2 vs Experiment 4). The MLR data is still noisy when compared to the smooth curves of the temperature and heat flux, as these do not experience the same factors causing noise as is the case with the scale measuring mass. Any further smoothing of the MLR may, however, cause a reduction in amplitude which may, in turn, affect the temperature and heat flux results in the numerical simulations.

The temperature curves and heat flux curves will be compared directly to the results obtained for heat flux and temperature in the same positions in the models. These will verify the validity of the models in predicting the behaviour seen in the experiments, and will also be an additional measure of how good the data smoothing of the MLR was at providing an estimate closer to the real MLR without noise.

7 Development and Results of Numerical Simulations

7.1 Introduction

In this chapter, the full-scale seat experiments are recreated in FDS version 6.7.6, using the material property results obtained in Chapter 5 and the MLR results obtained in Chapter 6. The results of the FDS simulations are then compared to the experimental results to benchmark the accuracy of the simulations. Thereafter, the single-seat numerical scenario is used in a full train carriage scenario. Various parametric fire scenarios are simulated, and the results thereof, are discussed.

The focus of the full train simulations is to understand and quantify tenability conditions and the amount of time passengers may have to escape from trains. The seat experiments and numerical models indicate that seats are not compliant with fire safety standards, meaning that full trains are not compliant. Hence, the work seeks to determine the likelihood of a fire disaster involving fatalities occurring based on evacuation considerations. Maximum HRR values are simply estimated based on data from single seats and ventilation conditions.

7.2 Single Seat Scenarios

In order to study the fire behaviour of a full train carriage FDS scenario, the seats needed to be recreated to obtain a simulation that is representative of the fire behaviour experienced during the experimental burning of the seats. The models were created using PyroSim, a graphical user interface for FDS. Simulations were performed for Experiment 1, 2, 3 and 4, and the numerical simulations are referred to as Scenario 1 to 4, respectively, which correspond to the experiment with the same number.

7.2.1 Geometry and Model Setup

The seat for each experiment was modelled according to the size of the seat used for the specific experiment. The seat was divided up into sections, as shown in Figure 7.1, in order to allow a single section to burn immediately, which represents the ignition of the seat, as well as to apply fewer material layers to areas where layers had been removed due to vandalism. The calcium silicate board on top of the scale was modelled as an inert mesh boundary and was taken to be the floor level at Z=0 m. The seat was modelled using approximated dimensions and position above the floor level, as shown in Figure 7.1. The dimensions not specified in Figure 7.1 due to variations between the models are shown in Table 7.1.

The heights of the devices above the floor level are given in Table 7.3. For Table 7.1 to Table 7.3, the actual dimensions from the experiments are also given for comparison. All the devices used in the experiments, namely the three thermocouples forming a thermocouple tree, as well as the heat flux gauge, were included in the model. The thermocouples, TC_Top, TC_Middle and TC_Bottom, were in line with the back of the seat back in the X-axis, and in the centre of the seat in the Y-axis. The heat flux gauge was also located in line with the centre of the seat in the Y-axis. In order to monitor flame height, a temporal statistic line was added at the front of the seat back in the centre with 133 points (every 0.05 m) from the top of the seat bottom to the top of the domain.

The number of solid radiation angles was set to 200 instead of the default value of 100 to achieve a smoother simulation of radiation, and thus, improving the accuracy of results. All other parameters were set to default, except where indicated otherwise.
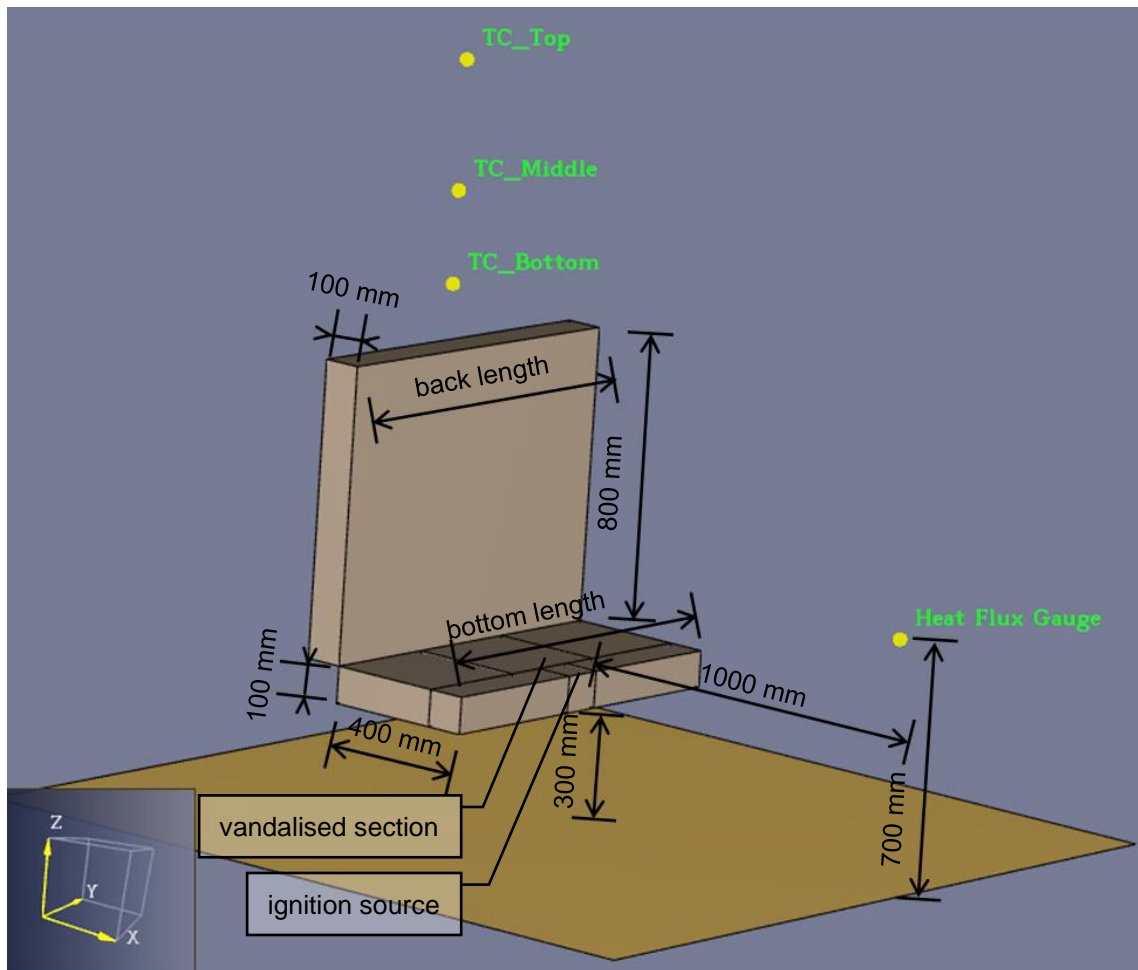
Figure 7.1: FDS model setup with dimensions

Table 7.1: Seat length

Scenario / Experiment	Seat Back			Seat Bottom		
	Seat Type	Actual Length (mm)	Model Length (mm)	Seat Type	Actual Length (mm)	Model Length (mm)
1	36 inch	907	900	36 inch	930	900
2	33 inch	831	850	36 inch	930	900
3	36 inch	907	900	36 inch	930	900
4	52 inch	1314	1300	52 inch	1335	1300

Table 7.2: Actual and model seat dimensions

		Actual	Model
Seat Bottom	Thickness (mm)	125	100
	Width (mm)	420	400
Seat Back	Thickness (mm)	71	100
	Height (mm)	820	800

Table 7.3: Device height from floor

Device	Actual Height from Floor (mm)	Model Height from Floor (mm)
Bottom Thermocouple	1363	1350
Middle Thermocouple	1603	1600
Top Thermocouple	1954	1950
Heat Flux Gauge	692	700

7.2.2   Domain and Cell Size

The cell and domain size directly affects how long a simulation will take to run, thus the smallest domain, which encompasses all flames, obstructions and devices, as well as the largest cell size that returns accurate results, is desired. In order to determine the size of cells within the domain, the D* value must be calculated. Cell sizes used by similar studies can also be considered to estimate an optimal starting cell size. Initial calculations are recommended to be done with a mesh cell size of D*/5 but must be verified to be suitable using a D*/10 and D*/20 mesh cell size (Thunderhead Engineering, 2021). In some cases, the cell sizes can be limited by obstruction sizes, as these must be similar to that of the object being simulated in order for accurate results to be obtained (Thunderhead Engineering, 2021).

Equation 7.1: Characteristic fire diameter (McGrattan *et al.*, 2017)

$$D^* = \left(\frac{\dot{Q}}{\rho_\infty \times c_p \times T_\infty \times \sqrt{g}} \right)^{\frac{2}{5}}$$

Using a density of 1.204 kg/m³, a specific heat of 1.005 kJ/kg.K), a temperature of 293 K and a gravitational acceleration of 9.81 m/s², as well as an assumed HRR of 1221 kW (the smallest maximum HRR between all experiments) , D* is calculated to be equal to 1.039 m. The cell size corresponding to each of these values is shown in Table 7.4. As the seat burnt in Experiment 2 require a 0.05 m cell size due to the size of the seat back, this is the cell size that was selected for the initial calculation even though D*/5 is much larger. This provides a fine mesh unlikely to influence numerical simulations.

Table 7.4: Mesh cell size according to characteristic fire diameter

D*/5	0.208 m
D*/10	0.104 m
D*/20	0.052 m

A 2 m x 2 m x 7 m domain was used for all seat types. The domain extended to 1 m in front of the seat, up to the water-cooled heat flux gauge, which was placed on the mesh boundary. The domain was split in two along the height, with the bottom mesh having cells of 0.05 m in size, up to a height of 3.4 m, and a coarser, 0.1 m cell size mesh was used from 3.4 m to the top of the domain, as can be seen in Figure 7.2. Open mesh boundaries were used on all sides except the bottom, to simulate the open-air burning conditions of the experiments. An inert surface was used for the bottom to represent the calcium silicate boards below the seat.
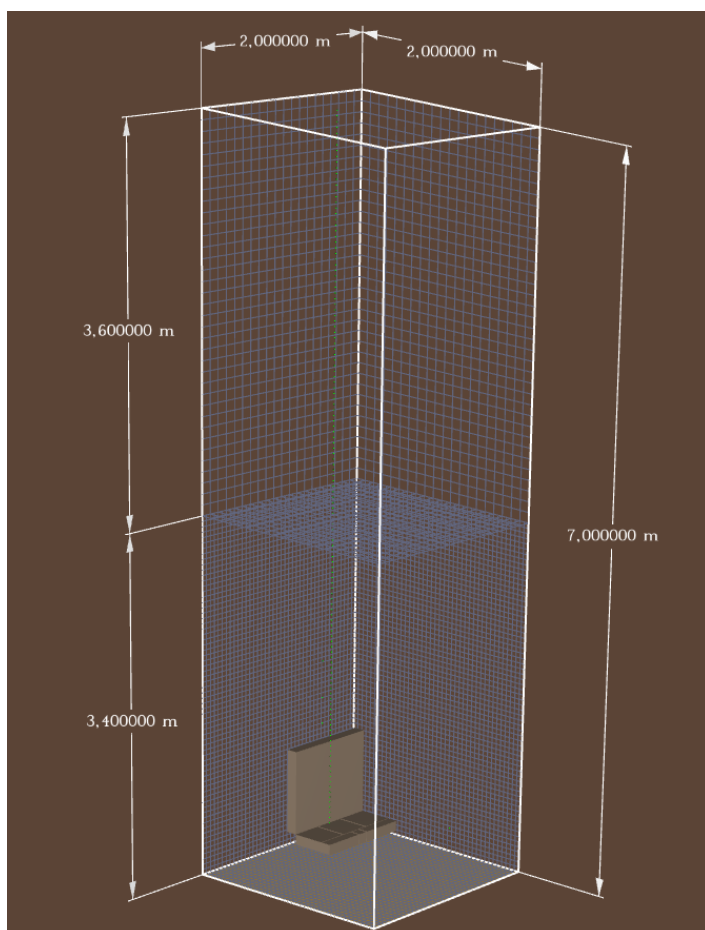
Figure 7.2: Single-seat model domain

A mesh sensitivity analysis was performed by using a bottom mesh cell size of 0.1 m and a top mesh cell size of 0.2 m. The results were compared, and the coarser, D*/10 mesh cell size provided similar heat flux and temperature results as the D*/20 mesh cell size, while the D*/20 results were closer to that of the experimental data, and thus the chosen mesh has been shown to provide results of sufficient accuracy. The comparisons of results are shown in Table 7.5, Figure 7.3 to Figure 7.5. There is good agreement between the general trends in the experimental and two numerical simulations. There are differences between the 0.05 D* and 0.1D* results locally. Hence, for further simulations, the finer mesh will be conservatively used.

Table 7.5: Comparison of fine and coarse mesh results

Result	D*/20, 0.05 m Mesh	D*/10, 0.1 m Mesh	Decrease (%)
Maximum Heat Release Rate (kW)	463.9	483.5	4.2
Maximum Heat Flux (kW/m^2)	13.1	15.5	18.1
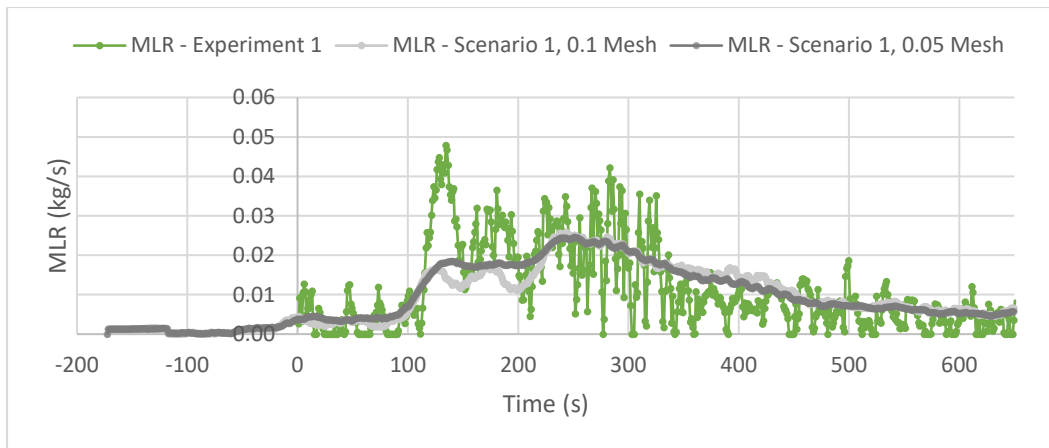
Figure 7.3: MLR comparison of coarser and finer mesh
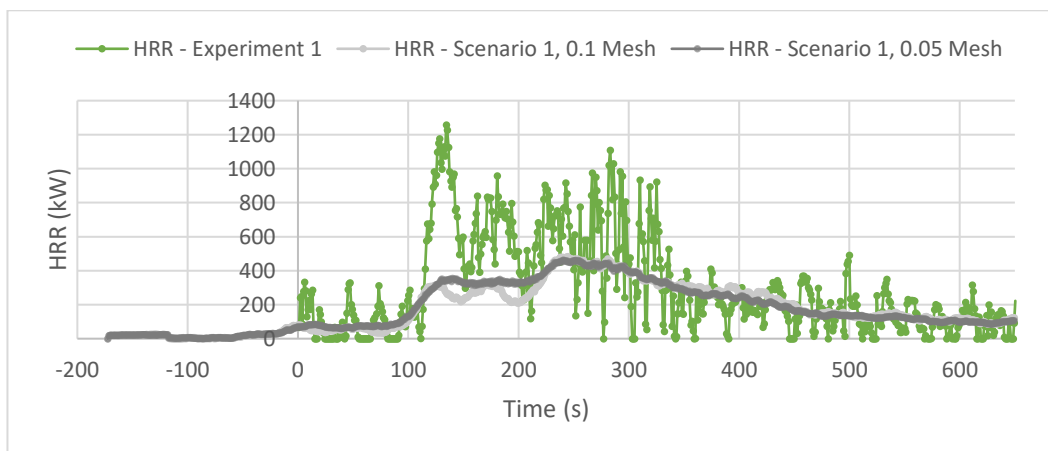
Figure 7.4: HRR comparison of coarser and finer mesh
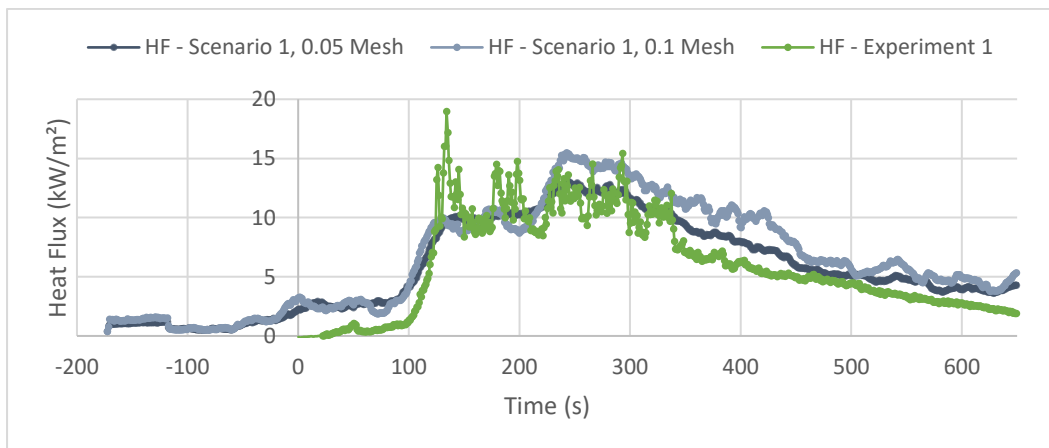
Figure 7.5: Heat flux comparison of coarser and finer mesh

7.2.3 Surface Material Properties

To obtain a seat model that accurately represents the experiments, the material properties obtained during testing as well as the MLR obtained from experiments are used. The material properties for each material layer are listed, as well as the ignition temperature and MLR, which represents the material layers as a whole. These properties determine the heat transfer within the seat.

7.2.3.1 Surface Backing Condition and Thickness

For both the seat back and seat bottom, the air gap backing condition was used. Multiple surfaces were applied to the obstruction instead of a single surface, the back of the obstruction with the material layers in reversed order, and all the other sides with the material layers in the normal order. This was done in order to ensure that the plywood, which is less flammable and has a reduced ability of surface flame spread compared to the pleather and foam, is on the correct side of the obstruction. Table 7.6 shows the thickness of each material found within the seat while the layers are shown visually in Figure 7.6 for the seat back of all scenarios, and in Figure 7.7 for the seat bottom of Scenario 1 and 2 and in Figure 7.8 for the seat bottoms of Scenario 3 and 4. The values for the thickness of the materials that cannot compress, such as pleather and plywood, were taken from measurements. The other materials, specifically the foams, have an estimated thickness which will allow the total thickness to add up to the actual thickness of the seat for the seat backs and the total thickness of the model seat for the seat bottoms.

Table 7.6: Thickness of individual seat materials

| | Thickness (m) | | | | | | | |
| | Scenario 1 | | Scenario 2 | | Scenario 3 | | Scenario 4 | |
Material	Back	Bottom	Back	Bottom	Back	Bottom	Back	Bottom
Pleather front	0.0012	0.0012	0.0012	0.0012	0.0012	0.0012	0.0012	0.0012
White lining	0.0100	0.0100	0.0100	0.0100	0.0100	0.0100	0.0100	0.0100
Polyurethane foam	0.0150	0.0738	0.0150	0.0738	0.0150	0.0200	0.0150	0.0200
Rubbery foam	0.0346	0.0000	0.0402	0.0000	0.0402	0.0538	0.0402	0.0538
Plywood	0.0090	0.0150	0.0034	0.0150	0.0034	0.0150	0.0034	0.0150
Pleather back	0.0012	0.0000	0.0012	0.0000	0.0012	0.0000	0.0012	0.0000
Total	0.0710	0.1000	0.0710	0.1000	0.0710	0.1000	0.0710	0.1000
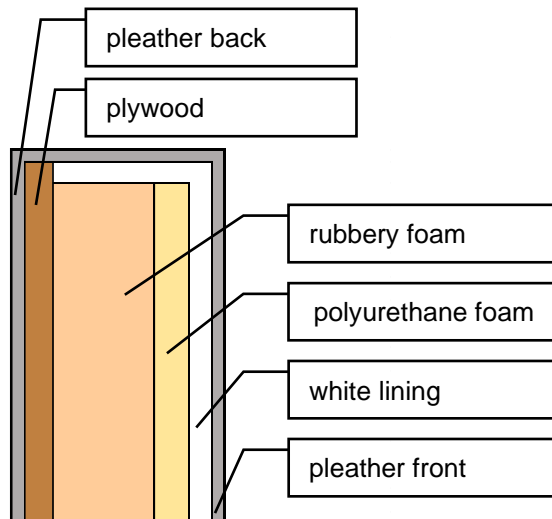
Figure 7.6: Individual seat materials - seat back
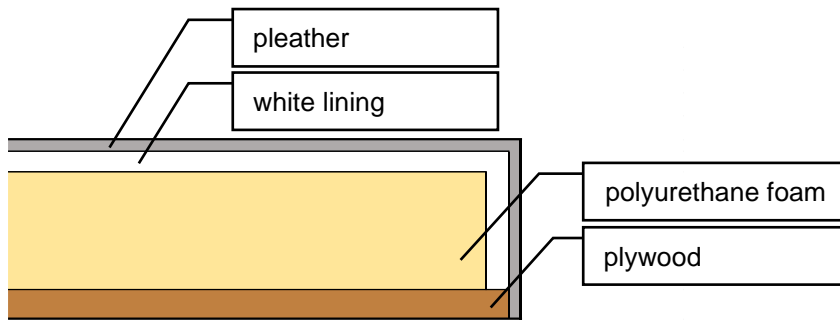
Figure 7.7: Individual seat materials - Scenario 1 and 2 seat bottom
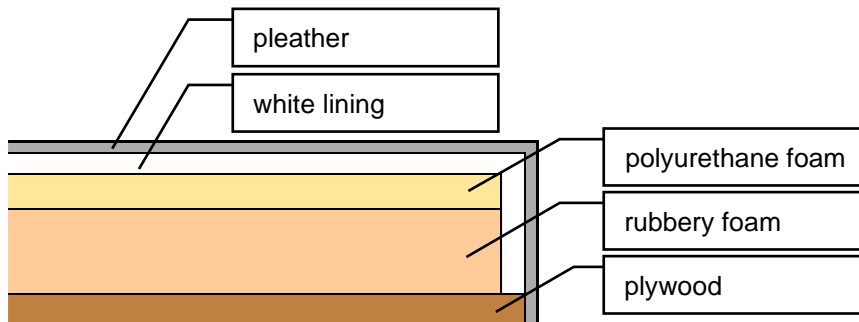
Figure 7.8: Individual seat materials - Scenario 3 and 4 seat bottom

The pleather and white lining layers were removed where vandalism had occurred in large areas of the seats. Figure 7.9 indicates the areas where the vandalism of the seats was included in the models. The seat backs and bottoms not shown did not have any or a significant area of vandalism, and thus no material layers were removed in modelling.
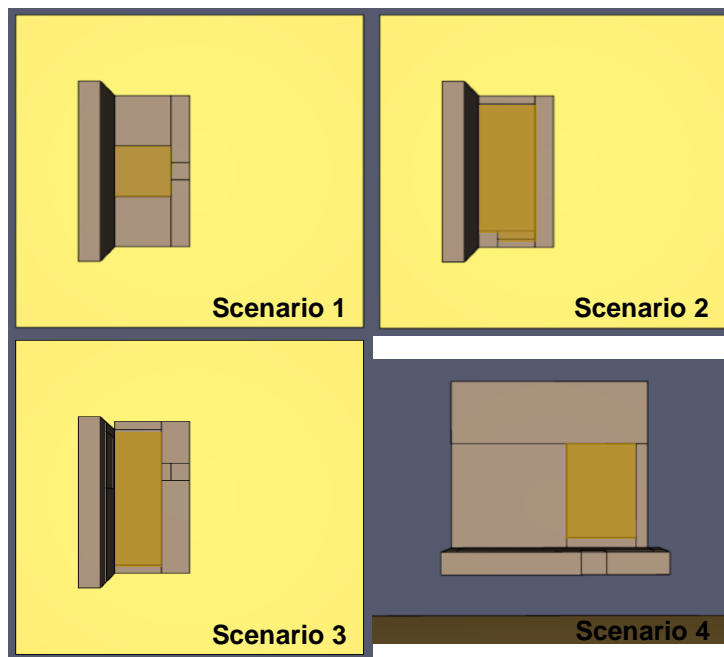
Figure 7.9: Vandalised areas of the seat backs and bottoms for each scenario

7.2.3.2 Summary of Material Density and Thermal Properties

Table 7.7 shows the heat of combustion of each material found within the seat as determined by testing in previous chapters. In order to calculate the effective heat of combustion, the heat of combustion was multiplied by an efficiency factor. An efficiency factor of 0.8 is suitable for mainly cellulosic materials (CEN, 2002, sec. E.3). These materials are both cellulosic (timber) and synthetic materials derived from oil (e.g. polyurethane and latex). However, based on the char observed in tests and soot produced, a factor of 0.8 was considered suitable for all materials. Large-scale calorimetry (not available in South Africa) would be required to confirm this.

Table 7.7: Heat of combustion of individual seat materials

Material	Heat of Combustion (kJ/kg)	Effective Heat of Combustion (kJ/kg)
Pleather	23100	18480
White lining	20200	16160
Polyurethane foam	28300	22640
Rubbery foam	43400	34720
Colourful foam	34500	27600
Plywood	18200	14560

The values used for material properties in FDS to simulate the heat transfer between the layers, to recreate the heat transfer that had occurred in experiments, have been summarised in Table 7.8. Table 3.1 to Table 3.7 show the ranges described in literature, while the specific values with references can be found in Table A.2 to Table A.16 in Appendix A.

Table 7.8: Individual seat material properties in FDS

Material	Pleather	White lining	Polyurethane foam	Colourful foam	Rubbery foam	Plywood
Density (kg/m^3)	600	23	51	58	66/92	715
Effective Heat of Combustion (kJ/kg)	18480	16160	22640	27600	34720	14560
Specific Heat (kJ/kg.K)	1.14	1.3	1.4	1.4	1.76	2.8
Thermal Conductivity (W/m.K)	0.26	0.14	0.034	0.034	0.19	0.14
Emissivity	0.92	0.8	0.17	0.17	0.86	0.87

The density of the white lining has been increased from 8 kg/m^3 to 23 kg/m^3 as the material is compressed from a thickness of 0.029 m to a thickness of 0.01 m in an intact seat. The rubbery foam has different densities depending on whether it is in the seat back or the seat bottom. The honeycomb-like holes found in the rubbery foam of the seat back are much smaller, and thus, the density of the material increases significantly, from 80 kg/m^3 to 140 kg/m^3. As no samples measured had only rubbery foam, a weighted average method was used to calculate the density of the rubbery foam after the polyurethane foam of known thickness and density, also found in the samples, had been subtracted from the total density.

The thermal conductivity that represents the rubbery foam is the thermal conductivity of polyurethane rubber (Hurley *et al.*, 1997, Table A.36), which may be higher than the thermal conductivity of the rubbery foam. The rubbery foam is, however, expected to have a higher thermal conductivity than the polyurethane foam due to its thicker matrix structure and larger but fewer pores.

7.2.3.3   Ignition Temperature

Table 7.9 shows the ignition temperatures of the materials that form part of the seat as described in literature. Table 3.6 shows the range described in literature, while the specific values with references can be found in Table A.10 to Table A.14 in Appendix A. The ignition temperature of the outer material is significant as it determines the initial fire spread and growth. As the fire develops, the ignition temperature of the seat becomes less significant as the temperature increases past the ignition temperature of any of the materials within the seat. The ignition temperature of the pleather is thus used to represent the seat as a whole. From literature, the ignition temperature of pleather can vary between 189°C and 600°C, although the lower end of this range are computed values for PVC flooring, while the piloted ignition temperature of flexible PVC starts at 182°C (Beyler, 2004, chap 14, Table 105), the piloted ignition temperature of solid polyurethane starts at 271°C (Beyler, 2004, chap 15, Table 15), the ignition temperature of flexible PVC starts at 318°C (Hurley *et al.*, 1997, Table A.36) and the auto-ignition temperature of semi-rigid PVC with plasticiser starts at 294°C (Beyler, 2004, chap 15, Table 15). The ignition temperature of the pleather was varied in the model of Experiment 1, and it was found that an ignition temperature of 200°C produced results that best represented the fire spread and HRR curve.

Table 7.9: Ignition temperature of individual seat materials selected for numerical simulations

Material	Ignition Temperature (°C)
Pleather	200
White lining	390
Rubbery foam	310
Colourful foam	370
Polyurethane foam	370
Plywood	250

7.2.3.4   Mass Loss Rate

The MLR curves were obtained from the experiments and were smoothed using the Savitzky-Golay data filter, as discussed in Chapter 5. The exact experimental MLR curves were used as the MLR input on the surface line for each numerical scenario. The data was not extrapolated to produce an estimated curve after the point at which the fires were extinguished, thus the simulations were terminated at the intervention point. To convert the MLR from kg/s, as recorded by the scale during the experiments and smoothed, to kg/m².s as required in FDS, the recorded MLR value at each time step was divided by the total burning area of the seat. From these values, the maximum MLR was obtained for each scenario, as required by FDS, and is listed in Table 7.10.

Table 7.10: Maximum MLR values for FDS modelling

Model	Maximum Mass Loss Rate (kg/s)	Burnt Area (m²)	Maximum Mass Loss Rate (kg/m².s)
Scenario 1 (Experiment 1)	0.048	1.134	0.042
Scenario 2 (Experiment 2)	0.044	1.072	0.041
Scenario 3 (Experiment 3)	0.058	1.134	0.051
Scenario 4 (Experiment 4)	0.058	1.638	0.035

Figure 7.10 depicts the ramp function used in FDS for each scenario, where the ramp function is the MLR curve as a fraction of the maximum MLR.
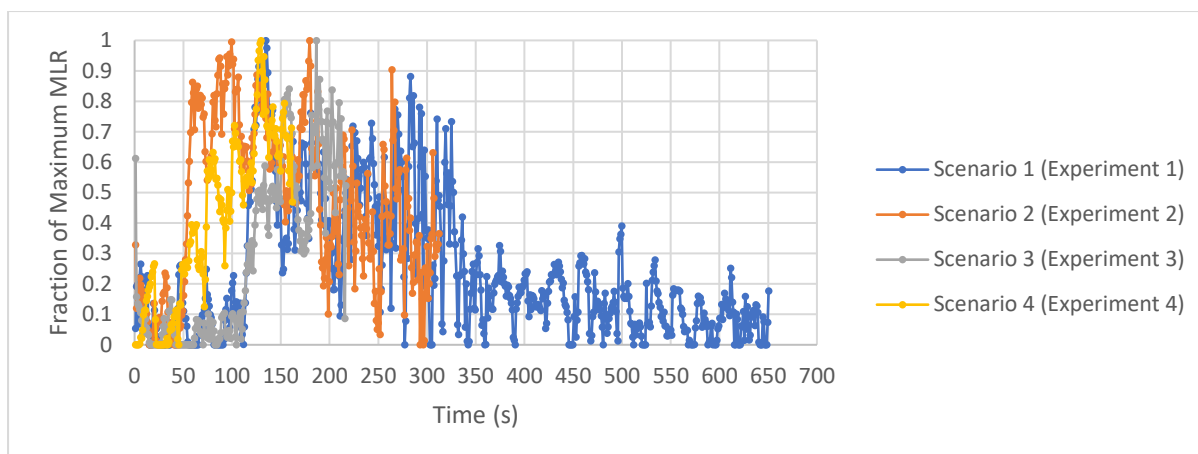
Figure 7.10: Mass loss rate curves as a fraction of the maximum MLR

7.2.4   Obstruction Material Properties

The combustion of an obstruction is defined by a reaction heat of combustion as well as a bulk density, which is representative of all the materials contained within the seat.

7.2.4.1   Reaction Heat of Combustion

In order to determine the heat of combustion of the seat as an obstruction, the weighted average method was used. The 36 inch seat bottom from Scenario 1, is shown as an example of the procedure that was applied to all the seat types listed in Table 7.1. The mass contribution of each individual material was used to calculate their contribution to the heat of combustion, as shown in Table 7.11. The experimental data, specifically the MLR, mainly consists of the combustion of the pleather, lining and foam, as the fire was extinguished prior to significant combustion of the plywood backing occurring. The plywood was thus excluded from the reaction heat of combustion, in order to determine a heat of combustion that would produce a HRR curve, which represents the materials that were burnt during the experiment.

Table 7.11: Seat heat of combustion according to weighted average of mass – 36 inch seat bottom

Material	Density (kg/m^3)	Mass (kg)	Percentage of Seat Excluding Plywood (%)	Heat of Combustion (kJ/kg)	Contribution to Seat Heat of Combustion Excluding Plywood (kJ/kg)
Pleather	600	0.524	20.1	23100	4637
White lining	8	0.090	3.4	20200	695
Polyurethane foam	51	1.654	63.4	28300	17929
Colourful foam	58	0.343	13.1	34500	4530
Plywood	715	4.154	0.0	18200	0
Total Including Plywood		6.766		Total	27791
Total Excluding Plywood		2.611			

As the effective heat of combustion is required for FDS modelling, an efficiency factor was applied to the net heat of combustion calculated for each scenario, as can be seen in Table 7.12. An efficiency factor of 0.8 has been applied, as discussed above.

Table 7.12: Seat effective heat of combustion for each scenario

Scenario / Experiment	Heat of Combustion (kJ/kg)			Effective Heat of Combustion (kJ/kg)
	Back	Bottom	Total	Efficiency Factor = 0.8
1	36339	27791	32877	26302
2	37088	27791	33289	26631
3	37107	37993	37159	29727
4	36608	37338	36931	29545

In order to confirm the heat of combustion of the seat, various values were used in the FDS model of Experiment 1, and the HRR curve obtained from the simulation was compared to the HRR curve that was obtained from experimental results. Using an efficiency factor of 0.8 in the simulation, produced a curve, which compared well with the experimental results.

7.2.4.2 Bulk Density

The bulk density, shown in Table 7.13, was first calculated by dividing the total mass calculated for each scenario by the obstruction volume for that specific scenario. To confirm these values, the total mass lost, for the experiments where most of the materials were combusted before being extinguished, was also divided by the obstruction volume to obtain a bulk density excluding plywood. For Experiment 2, the seat back plywood was, however, combusted. In order to include the plywood, the mass calculated for unburnt plywood and pleather back for each scenario, was added to the total mass lost and divided by the model volume. The values obtained from these calculations are shown in Table 7.14. The values in Table 7.13 and Table 7.14 compare relatively well, and thus the values calculated as shown in Table 7.13 can be used in FDS. The bulk density including the plywood was used; the values excluding plywood are for comparison purposes.

Table 7.13: Seat bulk densities

Scenario / Experiment	Density (kg/m^3)					
	Back		Bottom		Total	
	Including Plywood	Excluding Plywood	Including Plywood	Excluding Plywood	Including Plywood	Excluding Plywood
1	173	85	139	61	156	73
2	87	56	188	73	138	64
3	90	57	200	84	142	70
4	126	52	198	83	160	67

Table 7.14: Seat bulk density from total mass lost

Experiment	Total Mass Lost (kg)	Obstruction Volume (m^3)	Calculated Density (kg/m^3)	Plywood Mass (kg)	Total Mass Including Plywood (kg)	Calculated Density Including Plywood (kg/m^3)
1	7.20	0.102	70.9	9.46	16.66	164.0
2	6.40	0.097	65.8	4.15	10.56	108.6

7.2.5 Ignition of Model

The LPG burner used to ignite the seats during experiments, was simulated by dividing the obstruction into two sections and assigning an increased MLR to the ignition section, 0.1 m x 0.1 m x 0.1 m in size. The ignition obstruction was set to burn immediately in FDS and was placed in the position corresponding to that of the ignition during the experiments, as shown in red in Figure 7.12. For the length of time that the LPG burner was applied to the seat during experiments (see Table 7.15), the fraction of maximum MLR for the ignition section was increased to 1 for each corresponding numerical simulation scenario, in other words, 100% of the maximum MLR. Once this time had elapsed, the normal MLR curve was continued, as shown in Figure 7.11.

Table 7.15: Length of time ignition source was applied

Experiment	Time Exposed to Ignition Source (s)
1	54
2	31
3	19
4	10
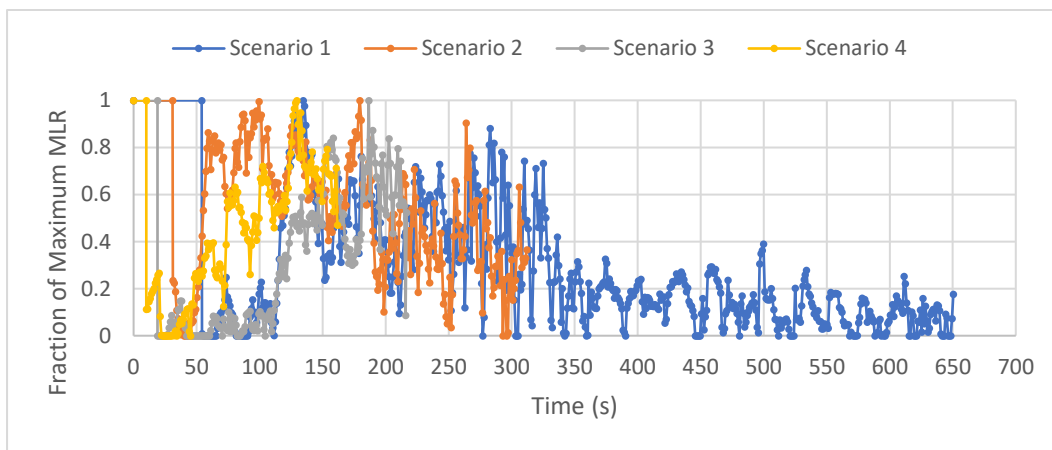
Figure 7.11: Mass loss rate curves as a fraction of the maximum MLR for ignition section
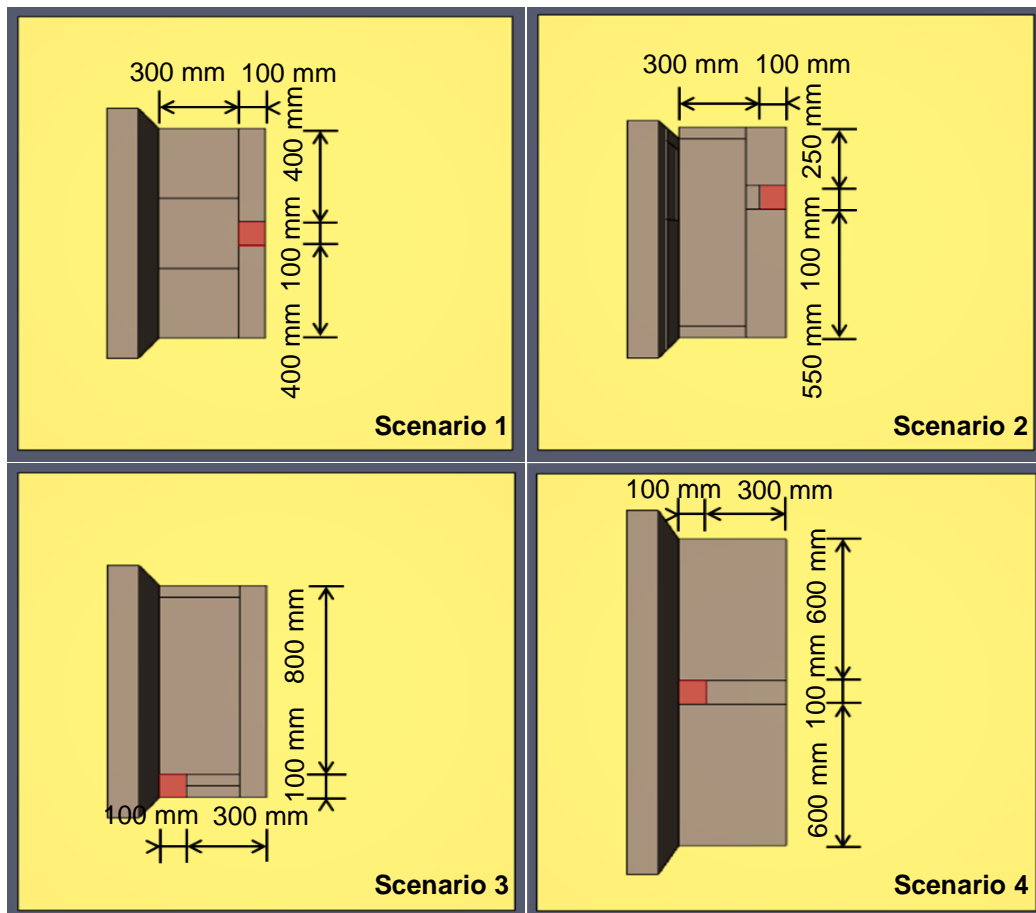
Figure 7.12: Position of ignition source in FDS models

7.2.6   Scenario 1 Results

To assess the accuracy of the FDS simulations, the simulations were benchmarked by comparing the simulation HRR and results produced by FDS to the experimental HRR and results. First, the HRR from the experiment was compared to the HRR from FDS. Thereafter the heat flux results were compared to one another. A water-cooled heat flux gauge device in FDS (Heat Flux Gauge) was positioned 1 m from the seat to measure the heat flux at that point, as shown in Figure 7.1. Thereafter the overall trend of the thermocouple readings was compared to the FDS temperature results, and each thermocouple (TC_Top, TC_Middle and TC_Bottom), used to measure temperature above the seat, was compared to the temperature results from FDS.

The size of the flame during ignition in the experiment and in the FDS simulation compare relatively well, as shown in Figure 7.13.
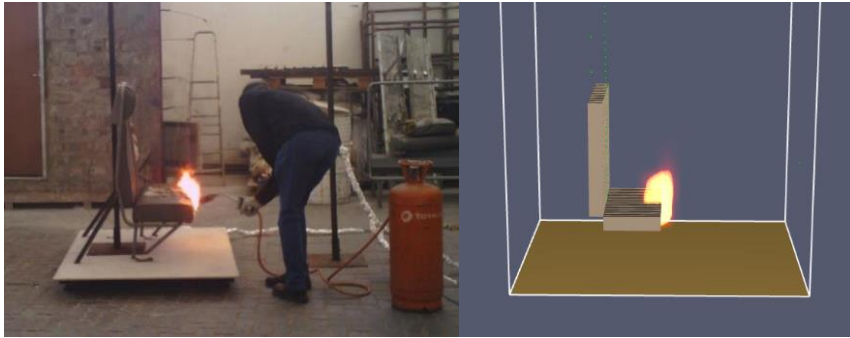
Figure 7.13: Ignition of Experiment 1 and Scenario 1

The flame spread is shown visually in Figure 7.14. In the experiment, the flame spread first occurred along the seat bottom (at 100 s), while in the simulation, the fire spread to the seat back (at 46 s from the start of the simulation, but 126.5 s before ignition when the offset is taken into account) before any significant spread occurred along the seat bottom. The spread along the seat bottom occurred at 173 s from the start of the simulation, but at the time of ignition when the offset is taken into account. In the FDS simulation, the vandalism to the seat back was also not modelled, and thus, the spread was onto a pleather covered section of the seat. Once significant spread had occurred on the seat bottom in the simulation, the fire was already of a significant size.

Figure 7.14: Flame spread in Experiment 1 and Scenario 1

Figure 7.15 shows the comparison between the experiment and the FDS simulation at the time of peak HRR. As can be seen, the flames were smaller in the simulation than those experienced during the experiment. For the experiment, the peak occurred at 134 s, while for the simulation, the initial peak seen in the experiment did not occur, and a peak was reached at 241 s.
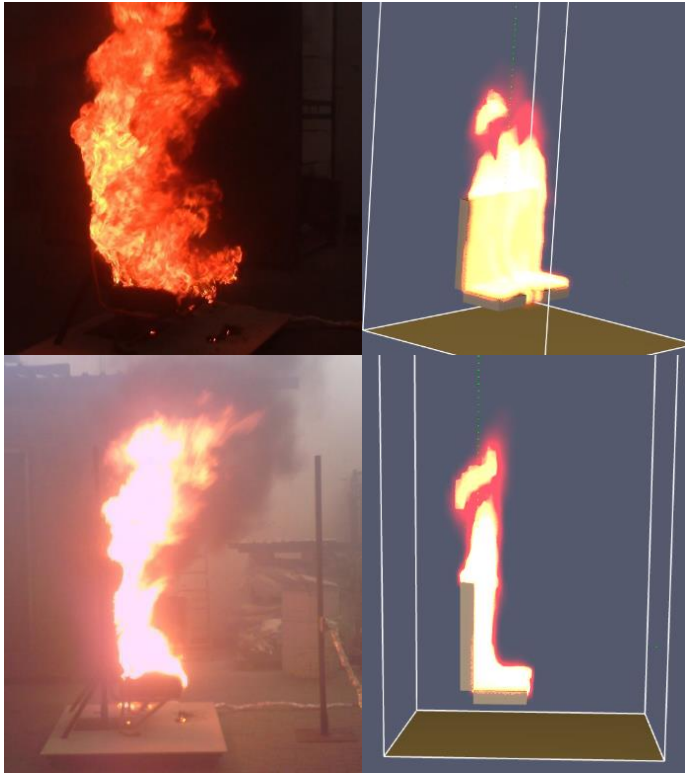
Figure 7.15: Peak HRR for Experiment 1 and Scenario 1

Just before the seat was extinguished in Experiment 1, most of the material had been combusted, and only small flames remained on the seat bottom, while the plywood had just been charred. In the simulation, however, the flames were still present on both the seat back and seat bottom, and the fuel of the first layer of cells had not burnt away completely yet. Figure 7.16 shows the comparison between the seats in the experiment and in the simulation at the end of the experiment.
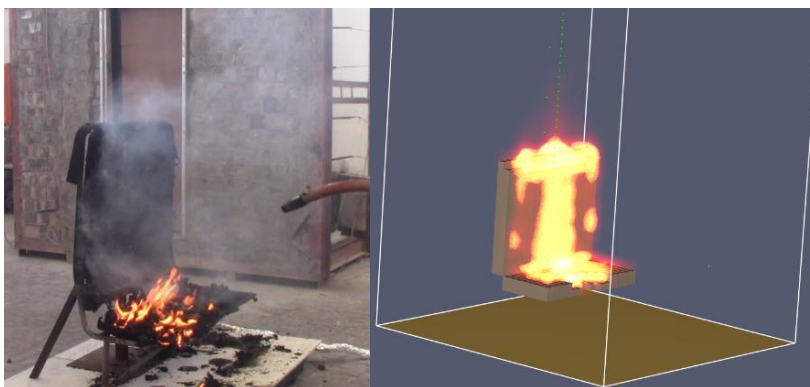
Figure 7.16: End of Experiment 1 and Scenario 1

The steady-state flame height reached around 1.91 m from the floor (1.51 m above the top of the seat bottom and 0.71 m above the top of the seat back) in FDS, which compares relatively well with the steady-state flame height of 2.25 m above the calcium silicate boards (i.e. the top of the scale platform, which serves as the floor), seen during the experiment.

7.2.6.1 Heat Release Rate

The HRR data from the experiment was compared to the HRR from the FDS simulation in Figure 7.17. The experiment lasted 650 s. Since the simulation takes longer to reach the growth stage, the curve was offset by 172.5 s for comparison reasons. The curve produced by the FDS simulation shows a good correlation to the experimental results, although it does result in a smoother curve, following the average of the data points, as would be expected due to the Reynolds-averaged Navier-Stokes (RANS) equations (McGrattan *et al.*, 2015). The maximum HRR reached in the FDS simulation is 464 kW, while the maximum HRR reached during the experiment is 1258 kW due to significant variations in localised behaviour.
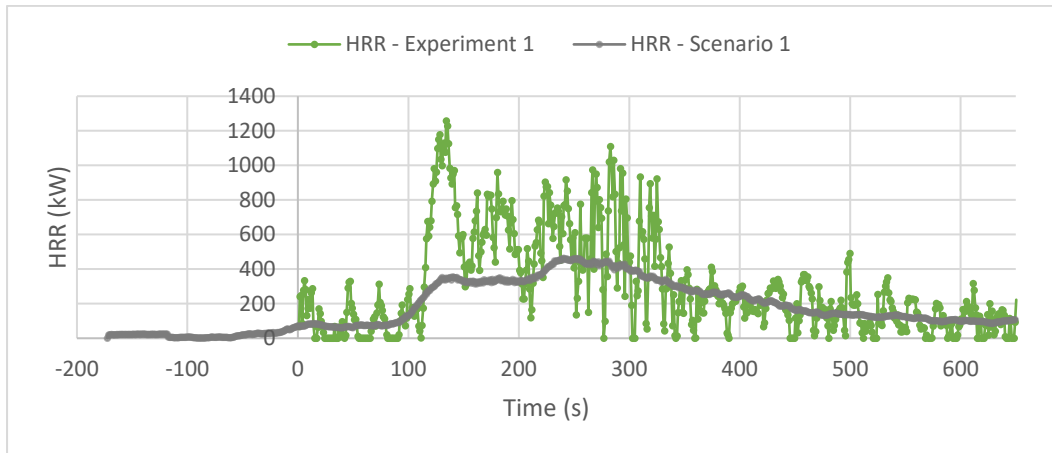
Figure 7.17: Comparison of Experiment 1 to Scenario 1 – HRR

7.2.6.2 Heat Flux Results

The overall trend of the heat flux curve obtained from the simulation compares relatively well with the experimental results, as shown in Figure 7.18. FDS does, however, over-predict the heat flux values at some points, while the peaks seen in the experimental results are not reached. The maximum heat flux predicted by the FDS simulation is 13.13 kW/m^2, which compares relatively well to the experimental maximum heat flux of 18.99 kW/m^2. This indicates that the smoothing of the data limits the accuracy of localised peaks, although general behaviour and trends are captured well.
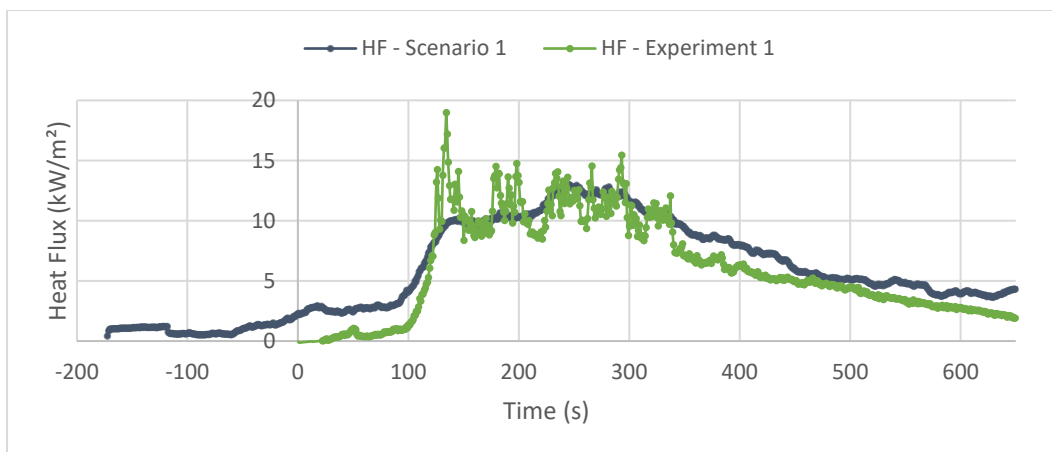
Figure 7.18: Comparison of Experiment 1 to Scenario 1 – heat flux

7.2.6.3   Temperature Results

The experimental and numerical temperatures are compared to one another in Figure 7.19. In general, the FDS simulation over-predicts the temperatures when compared to the thermocouple readings, but this is likely due to the more turbulent flames seen in the experiment, which moved away from the thermocouples at certain points in time. The temperatures of the bottom thermocouple in the simulation are also the lowest, compared to the top thermocouple, which shows the highest temperatures. This is the opposite of what happened during the experiment, and is likely due to the airflow where air entrainment resulted in lower thermocouples being less exposed to flames, and due to the general shape of the flames.
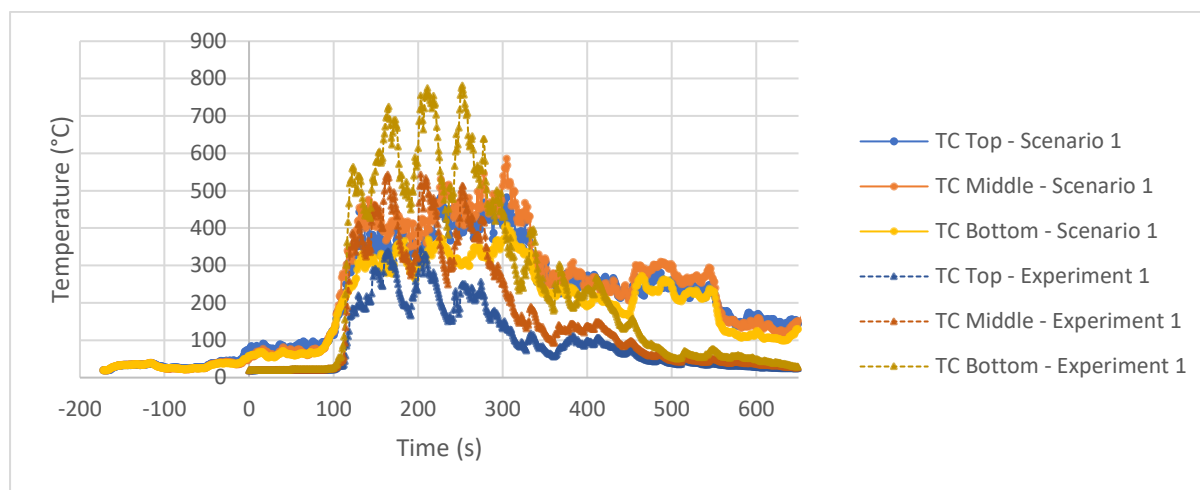
Figure 7.19: Comparison of Experiment 1 to Scenario 1 – thermocouple temperatures

The top thermocouple shows temperatures that were over-predicted by the FDS simulation for almost the entire duration of the experiment. The middle thermocouple shows a good correlation up to about 250 s, after which the simulation temperatures increase and continue over-predicting the temperatures when compared to the thermocouple readings obtained during the experiment. The bottom thermocouple shows the FDS model under-predicting the temperatures between about 125 s and 300 s, and over-predicting the temperatures from about 450 s.

7.2.7   Scenario 2 Results

In the experiment, the flame spread first occurred along the seat bottom (as soon as the ignition source was removed at 31 s), while in the simulation, the fire spread to the seat back (at 82 s from the start of the simulation, but 33 s before ignition when the offset is taken into account) before any significant spread occurred along the seat bottom. The spread along the seat bottom occurred at 146 s from the start of the simulation, but at 31 s after ignition when the offset is taken into account. Once significant spread had occurred on the seat bottom in the simulation, the fire was already of a significant size.

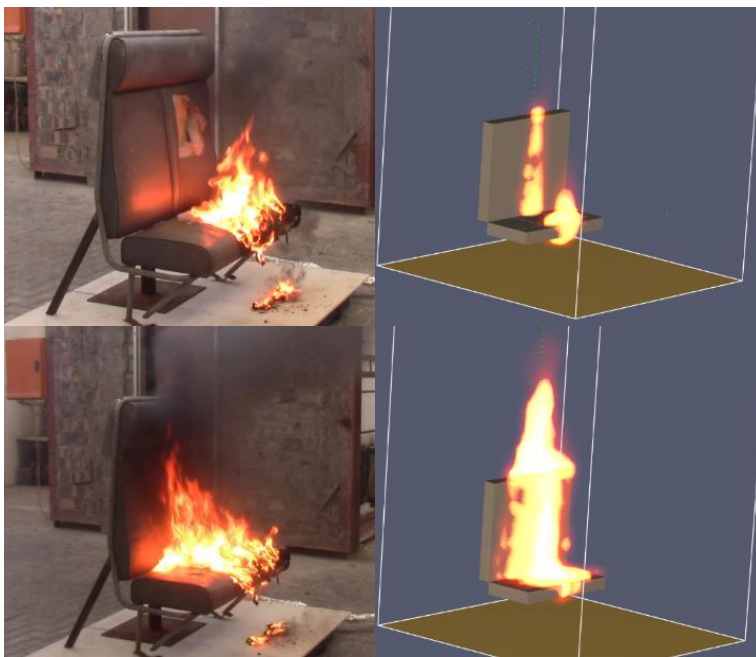The flames were slightly smaller in the simulation than those experienced during the experiment. For the experiment, the peak HRR occurred at 180 s, while for the simulation, the peak was reached at 160 s.

Just before the seat was extinguished in Experiment 2, a significant amount of the material had been combusted, and some flames remained on a section of the seat back and the majority of the seat bottom, while the plywood had burnt through completely. In the simulation, however, the significant flames were still present on both the seat back and seat bottom, and the fuel of the first layer of cells had not burnt away completely yet.

The steady-state flame height reached around 2.52 m from the floor (2.12 m above the top of the seat bottom and 1.32 m above the top of the seat back) in FDS, which compares well with the steady-state flame height of 2.25 m to 2.5 m above the calcium silicate boards, seen during the experiment.

7.2.7.1 Heat Release Rate

The HRR data from the experiment was compared to the HRR from the FDS simulation in Figure 7.20. The experiment lasted 312 s. Since the simulation takes longer to reach the growth stage, the curve was offset by 115 s for comparison reasons. The curve produced by the FDS simulation shows a good correlation to the experimental results, although it does result in a smoother curve as described in the results of Scenario 1. The maximum HRR reached in the FDS simulation is 684 kW, while the maximum HRR reached during the experiment is 1163 kW. Once again, general trends in HRR are captured well, but localised peaks in HRR are not matched.

Figure 7.20: Comparison of Experiment 2 to Scenario 2 – HRR

7.2.7.2 Heat Flux Results

The overall trend of the heat flux curve obtained from the simulation compares relatively well with the experimental results, as shown in Figure 7.21. FDS does, however, slightly over-predict the heat flux values after 150 s. The maximum heat flux predicted by the FDS simulation is 16.67 kW/m^2, which compares relatively well to the experimental maximum heat flux of 18.86 kW/m^2.

Figure 7.21: Comparison of Experiment 2 to Scenario 2 – heat flux

7.2.7.3 Temperature Results

There is a partial comparison in trends between the temperatures measured by the thermocouples during the experiment and the temperature results obtained from the FDS simulation. The temperatures are compared to one another in Figure 7.22. In general, the FDS simulation over-predicts the temperatures when compared to the thermocouple readings and also does not include the peaks seen in the experimental results. This is again by the shape of the predicted flame, with the FDS thermocouples being further into the flame zone.
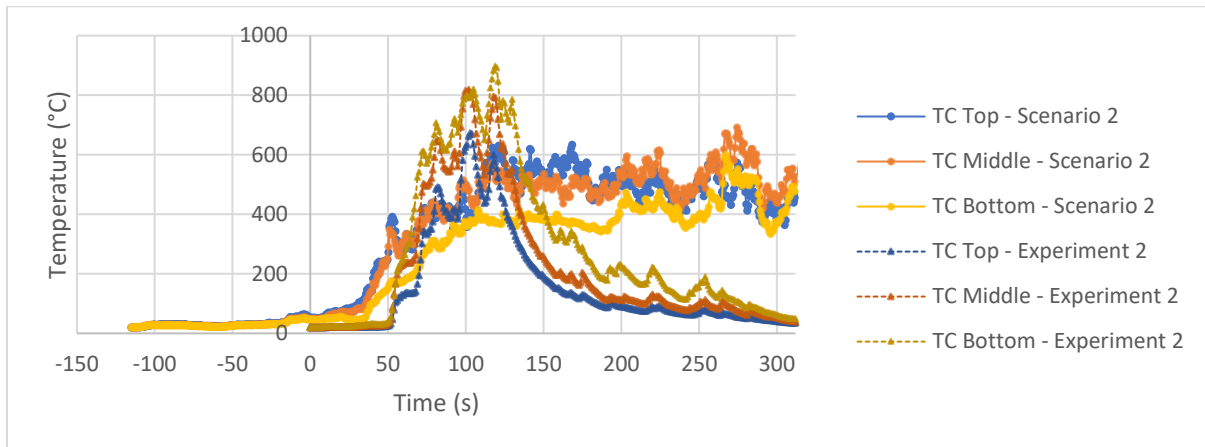
Figure 7.22: Comparison of Experiment 2 to Scenario 2 – thermocouple temperatures

7.2.8 Scenario 3 Results

In the experiment, the flame spread first occurred along the top of the seat bottom (as soon as the ignition source was removed at 19 s), while in the simulation, the fire spread along the underside of the seat back, as can be seen in Figure 7.23. This is likely due to the thickness of the obstruction compared to the thickness of the seat back at its underside. The back of the seat back also burnt before the flame spread along the seat bottom during the simulation, while in the experiment, the back of the seat back did not burn at all. The spread along the seat bottom occurred at 288.5 s from the start of the simulation, but at 130 s after ignition when the offset is taken into account. Once spread had occurred on the seat bottom in the simulation, the fire was already of a significant size.
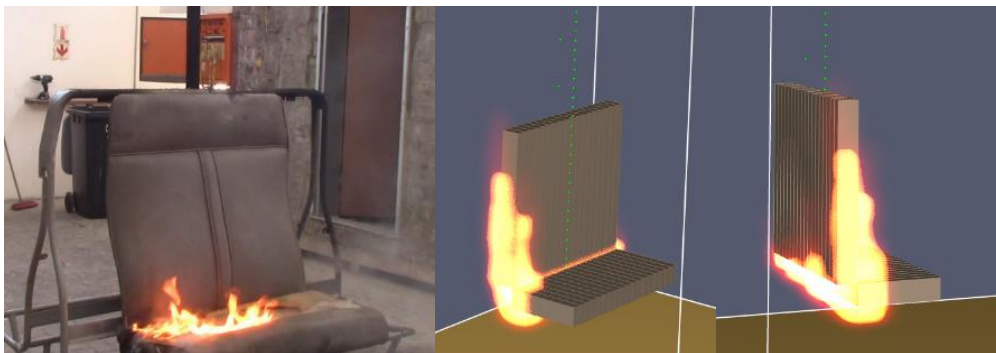
Figure 7.23: Flame spread in Experiment 3 and Scenario 3

The flames were visually significantly smaller in the simulation than those experienced during the experiment. For the experiment, the peak HRR occurred at 187 s, while for the simulation, the peak was reached at 164 s.

Just before the seat was extinguished in Experiment 3, the flames had spread over the entire seat back and seat bottom, while in the simulation, only a part of the seat back and seat bottom were involved.

The steady-state flame height reached around 3.37 m from the floor (2.97 m above the top of the seat bottom and 2.17 m above the top of the seat back) in FDS, which compares relatively well with the steady-state flame height of 2.25 m above the calcium silicate boards, seen during the experiment.

7.2.8.1 Heat Release Rate

The HRR data from the experiment was compared to the HRR from the FDS simulation in Figure 7.24. The experiment lasted 217 s. Since the simulation takes longer to reach the growth stage, the curve was offset by 157.5 s for comparison reasons. The curve produced by the FDS simulation shows a good correlation to the experimental results, although it does result in a smoother curve as described in the results of Scenario 1. The maximum HRR reached in the FDS simulation is 645 kW, while the maximum HRR reached during the experiment is 1715 kW.
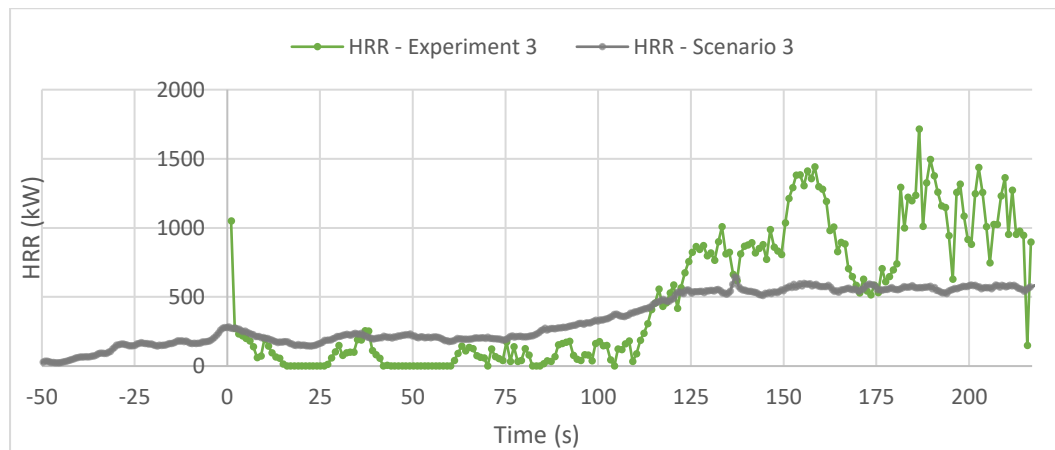
Figure 7.24: Comparison of Experiment 3 to Scenario 3 – HRR

7.2.8.2 Heat Flux Results

The overall trend of the heat flux curve obtained from the simulation compares relatively well with the experimental results, as shown in Figure 7.25. FDS does, however, under-predict the heat flux values after 120 s. The maximum heat flux predicted by the FDS simulation is 12.48 kW/m^2, whereas the experimental maximum heat flux is 20.4 kW/m^2.
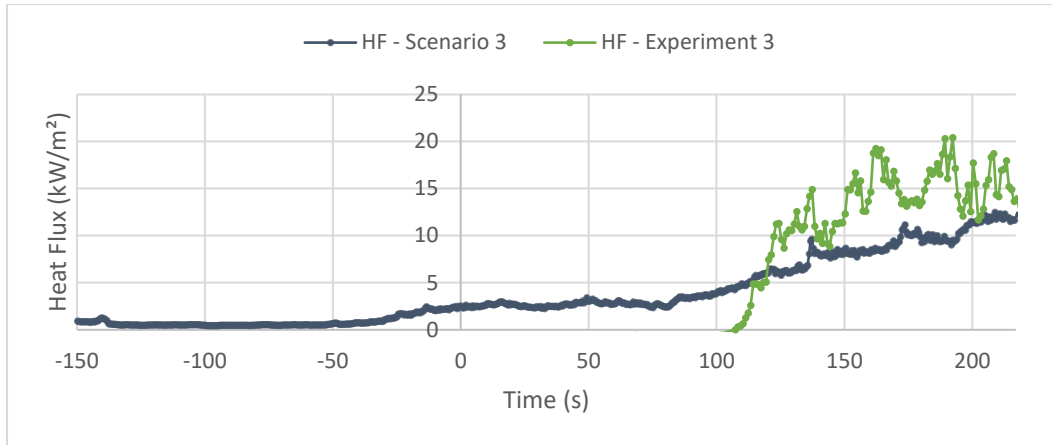
Figure 7.25: Comparison of Experiment 3 to Scenario 3 – heat flux

7.2.8.3 Temperature Results

The trends of the temperatures measured by the thermocouples during the experiment and the temperature results obtained from the FDS simulation compare relatively well. The temperatures are compared to one another in Figure 7.26. General trends and maximum temperatures are relatively similar in this case. This highlights that the simulated flame shape, and resultant position of thermocouples in the flame, is more comparable in this experiment.
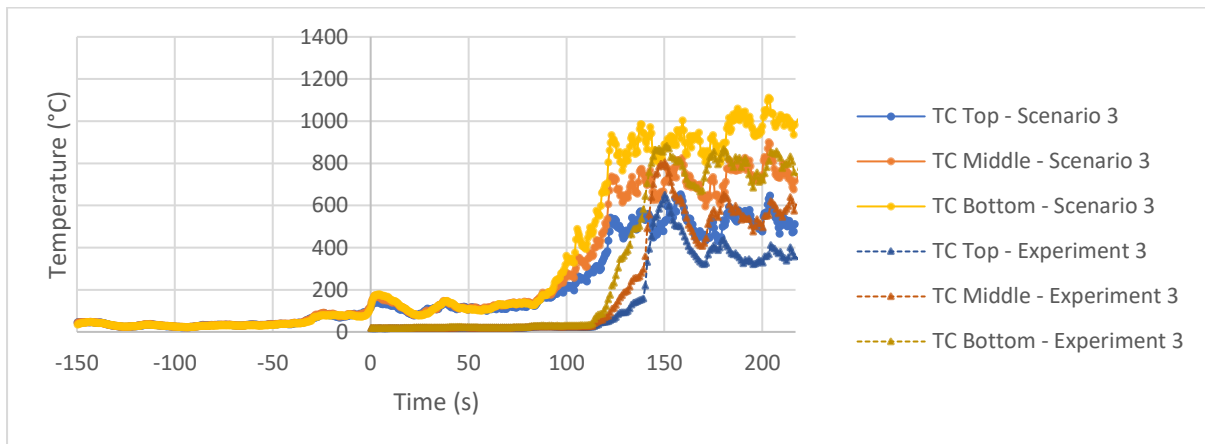
Figure 7.26: Comparison of Experiment 3 to Scenario 3 – thermocouple temperatures

7.2.9 Scenario 4 Results

The flame spread along the seat back was slower in the FDS simulation than in the experiment. Flames also moved up along the back of the seat back in the simulation, while in the experiment, the back of the seat back did not burn.

The flames were smaller in the simulation than those experienced during the experiment. For the experiment, the peak HRR occurred at 130 s, while for the simulation, the curve had not reached a peak by the end of the experiment.

The area of the seat involved at the end of the experiment is similar to that seen in the simulation, although in the experiment, the flames had moved closer to the edges of the seat.

The steady-state flame height reached around 3.42 m from the floor (3.02 m above the top of the seat bottom and 2.22 m above the top of the seat back) in FDS, compared to the steady-state flame height of 2.25 m above the calcium silicate boards, seen during the experiment.

7.2.9.1 Heat Release Rate

The HRR data from the experiment was compared to the HRR from the FDS simulation in Figure 7.27. The experiment lasted 162 s. Since the simulation takes longer to reach the growth stage, the curve was offset by 130 s for comparison reasons. The curve produced by the FDS simulation shows a good correlation to the experimental results, although it does result in a smoother curve as described in the results of Scenario 1. The maximum HRR reached in the FDS simulation is 729 kW, while the maximum HRR reached during the experiment is 1703 kW.
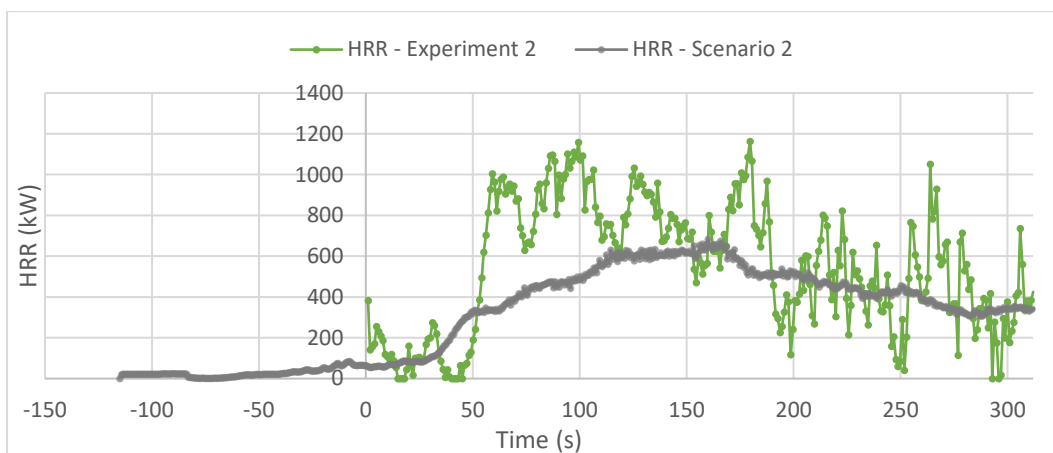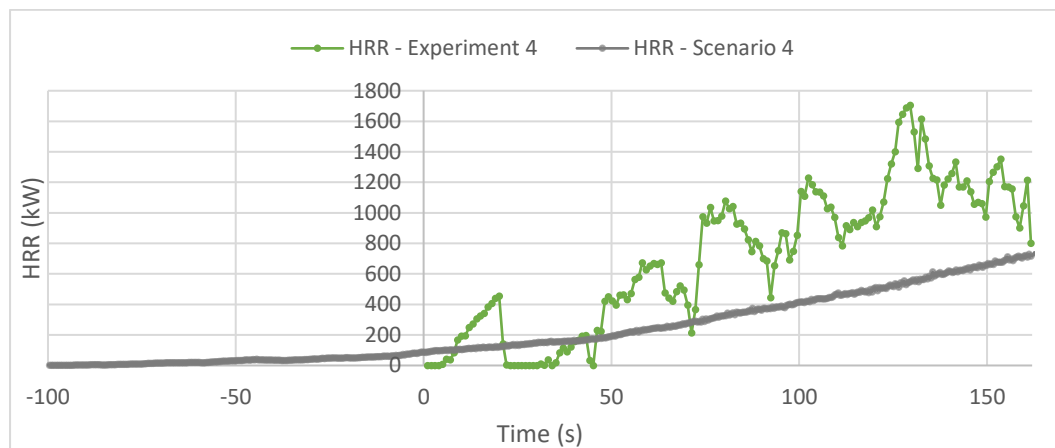

Figure 7.27: Comparison of Experiment 4 to Scenario 4 – HRR

7.2.9.2 Heat Flux Results

The overall trend of the heat flux curve obtained from the simulation compares relatively well with the experimental results, as shown in Figure 7.28. FDS does, however, over-predict the heat flux values after 150 s. The maximum heat flux predicted by the FDS simulation is 19.87 kW/m^2, which compares relatively well to the experimental maximum heat flux of 22.76 kW/m^2.
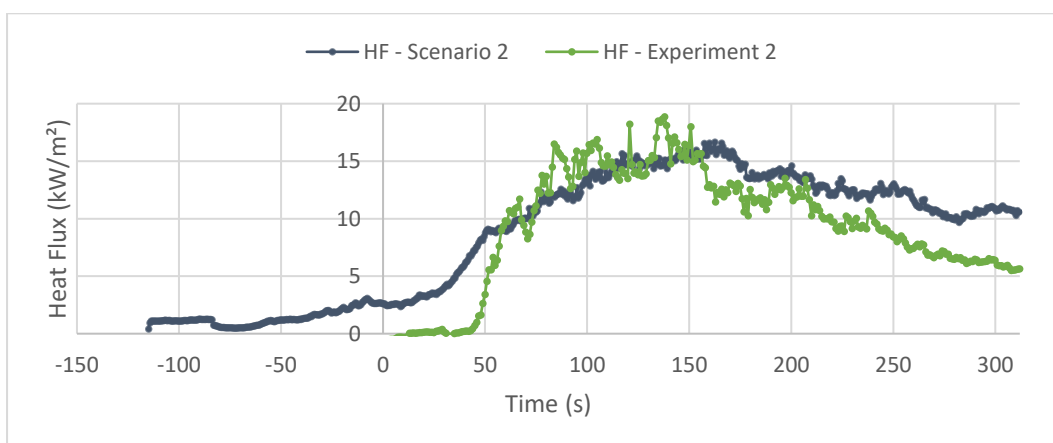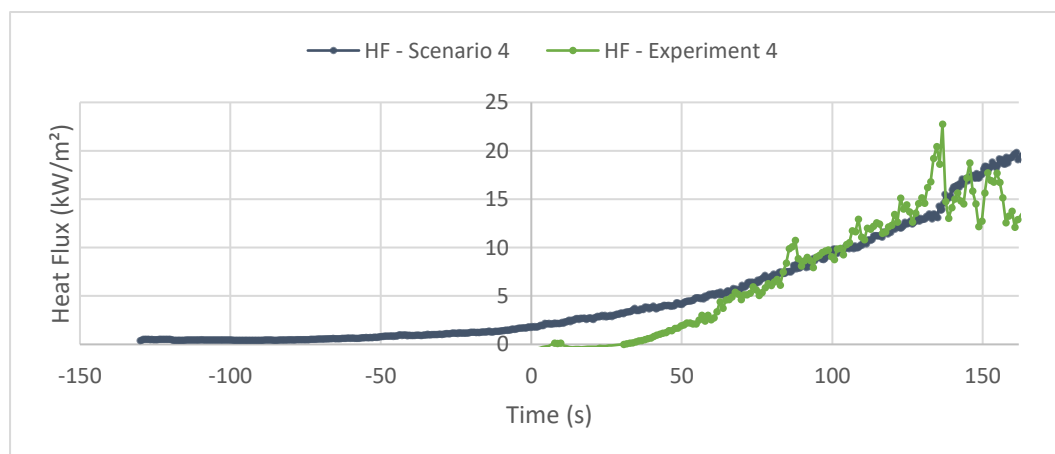

Figure 7.28: Comparison of Experiment 4 to Scenario 4 – heat flux

7.2.9.3   Temperature Results

The trends of the temperatures measured by the thermocouples during the experiment and the temperature results obtained from the FDS simulation compare relatively well. The temperatures are compared to one another in Figure 7.29.
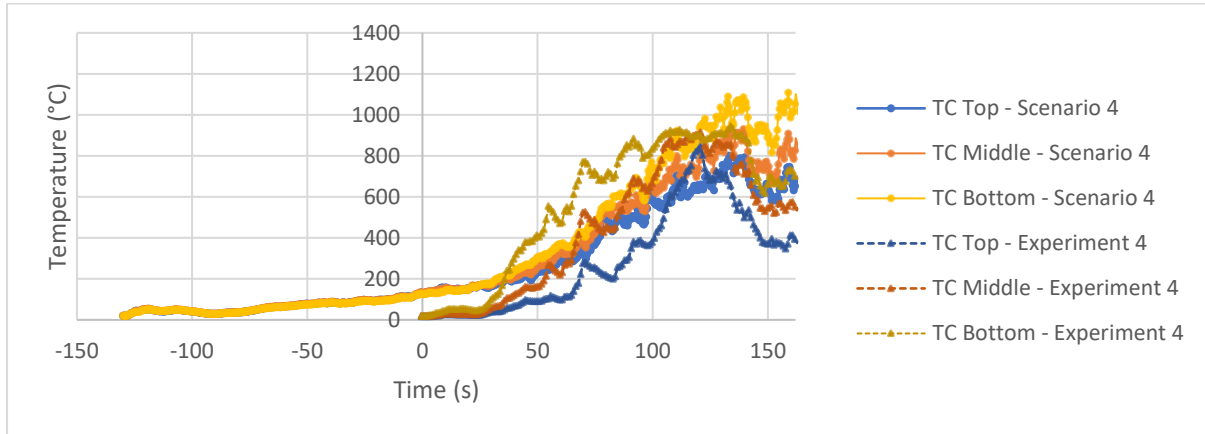
Figure 7.29: Comparison of Experiment 4 to Scenario 4 – thermocouple temperatures

7.2.10   Summary of Results from Numerical Simulations for Single Seat Experiments

Figure 7.30 and Figure 7.31 compare the results of the FDS simulations to one another to identify whether a trend exists. The heat release rates compare relatively well with one another, although the peak for Scenario 1 is slightly lower and the curve of Scenario 3 is not as smooth. During the experiments, the fires in Experiment 3 and 4 were also more intense than the fires in Experiment 1 and 2, but all experiments resulted in more intense fires than those seen in the numerical simulations. Although localised peak HRR and heat flux values are not accurately captured (due to the smoothing techniques and accuracy of equipment employed), the general trends compare relatively well. Hence, the simulations are not ideal for predicting localised behaviour and instantaneous maximum values. Nevertheless, they show consistent results that capture general behaviour meaning that they will be suitable for simulating full train behaviour where localised fluctuations are less important.
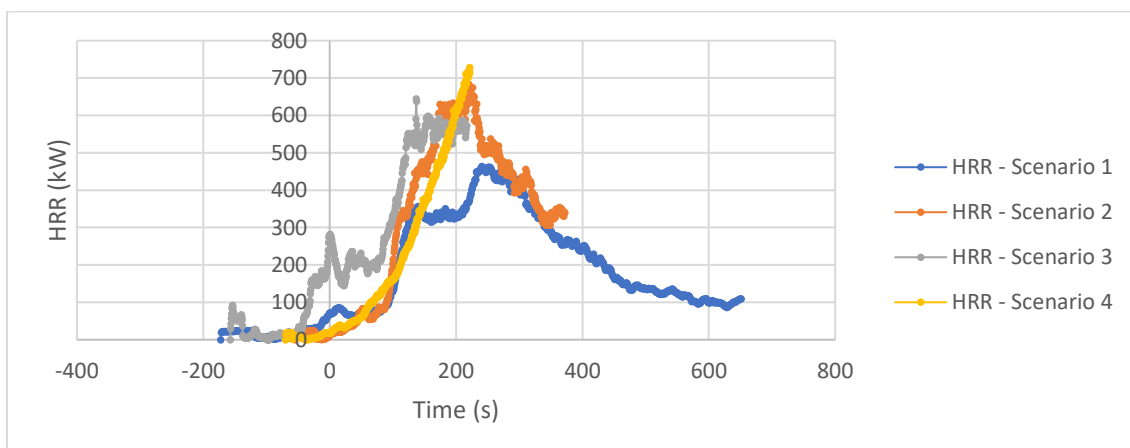
Figure 7.30: Comparison of HRR of FDS scenarios
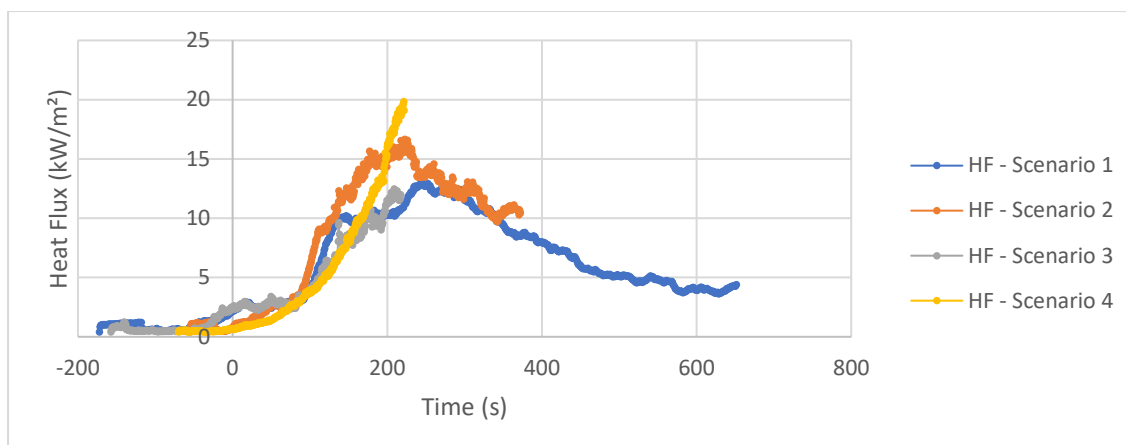
Figure 7.31: Comparison of heat flux of FDS scenarios

All of the experiments failed the maximum allowable peak HRR of 350 kW per seat stipulated by EN-45545-2 (CEN, 2015).

7.3 Full-scale Carriage Models

To study the fire behaviour in a passenger train carriage, the individual seat model was used within a model of the carriage. As Experiment 1 was the longest-running experiment and included the decay stage, as well as being a good representation of all the experiments, the material properties and dimensions from the Experiment 1 model were used except where indicated otherwise. However, it also had the lowest HRR, meaning that results predicted below are likely to be lower-bound estimates of behaviour that could potentially occur in real trains. If the properties and fire behaviour of Experiment 4 were applied in this section, the rate of flame spread and peak HRR would be significantly higher. As noted in the introduction of this chapter, the focus of this section is the tenability conditions and rate of fire development in the carriage. Peak HRR values are estimated based on simplified calculations below.

7.3.1 Geometry and Model Setup

Numerical simulation parameters applied were done as per the single-seat models presented above. The obstructions in the full carriage model include the seats, windows, doors, inner lining of the ceiling and walls, partitions, floor and the outer lining, which was represented as an inert material.

Figure 7.32 shows the layout of the windows, doors and partitions, including the actual dimensions and the dimensions used in the model, as well as the positions of the various seat types. The windows, doors and seats were given names to assist in identifying them. Figures showing windows, doors, partitions and vents with actual and modelled dimensions, as well as carriage layouts indicating seat and vent spacing with actual and modelled dimensions, are provided in Appendix C.
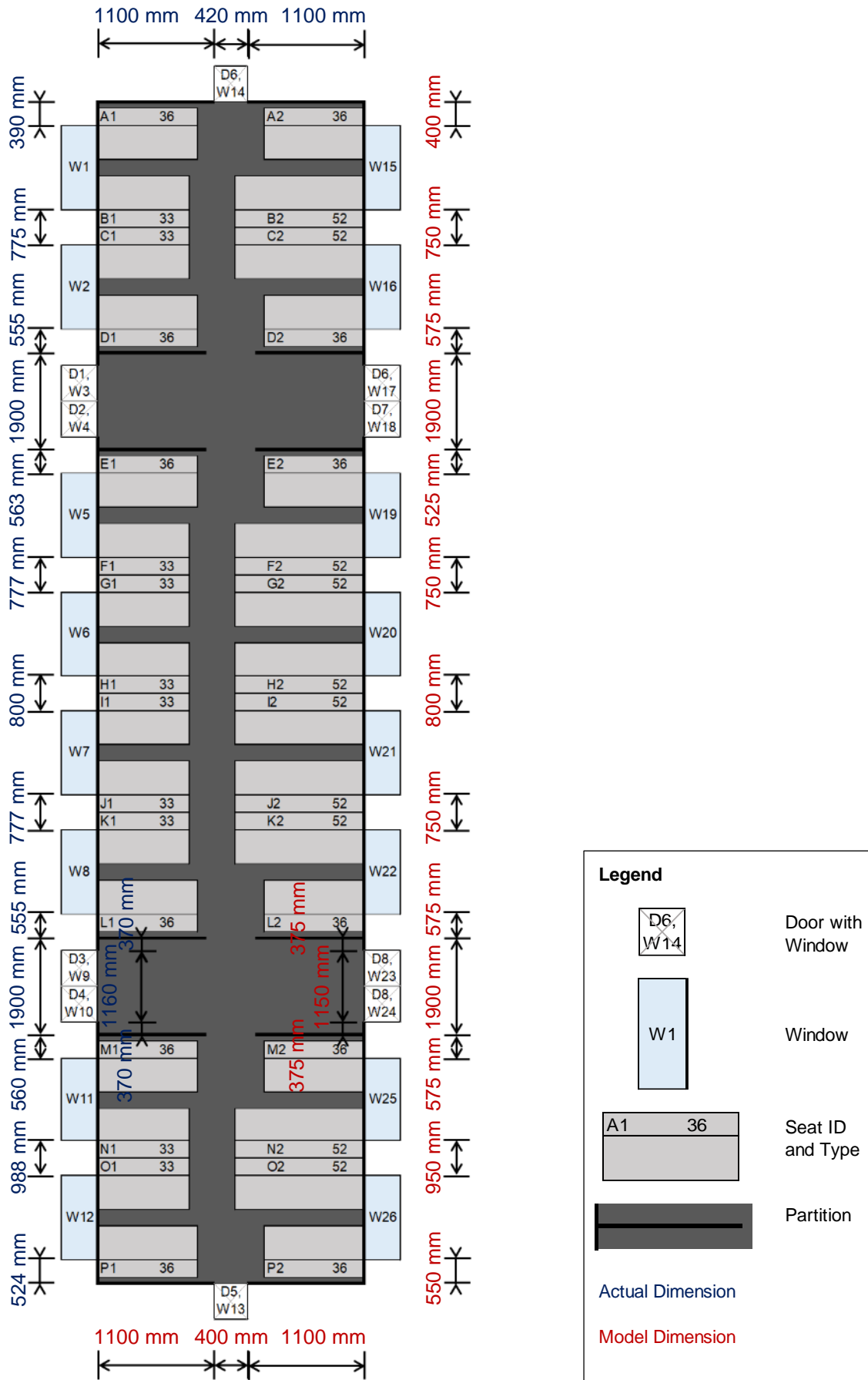
Figure 7.32: Layout of windows and doors in carriage

The windows can be opened by passengers in such a way that one quarter in the upper half can be shifted to the side, and the same can be done with one quarter in the lower half of the window. The windows, however, start melting at 160°C (Drysdale, 2011, Table 1.2), and an opening will start to form after a while. In order to replicate this behaviour, wall temperature devices were placed as close as possible to the centre of each quarter of the window, which allowed the obstruction to be set to disappear once the temperature reached 200°C, a temperature which accounts for the difference in the start of melting to an opening forming in the window. The windows which are found on the doors also had wall temperature devices in their centres to allow them to disappear. For the windows that were opened, the window, as well as the wall temperature device, was just shifted in front of the adjacent quarter to allow for the wall temperature of both to be measured, allowing them to disappear separately, as would be the case in reality.

For the cases where the carriage doors on the sides are open, the door obstruction was just removed from the model as it does not contribute to the fire load. The doors at the front and back of the carriage usually remain closed as these are not operated electronically and usually swing closed after being opened. The partitions are found on either side of the side doors, which separate the train into three sections.

The modelled vent cover reduces the velocity of the air moving through the vent. This is similar to the vent covers found on the train, but due to mesh cell size limitations, the modelled vent cover is much larger, but fulfils the same role as it would in reality. The vents have also been modelled with a minimum size as grates reduce the area of the vents in reality. The vents could not be measured as they were inaccessible, but they are estimated to be around 0.1 m to 0.15 m in diameter, while the modelled vents are 0.1 m x 0.1 m.

7.3.2 Fire Scenarios

In order to study the fire behaviour in a passenger train carriage and the effect of various conditions on the fire behaviour, fire scenarios need to be identified. To determine the worst case and likely case for fire behaviour, some variations in conditions were considered.

The first condition that was considered was the location of the ignition within the carriage. Arsonists will ignite a seat at a convenient location within the carriage, according to the situation they are faced at the time. Considerations they may have in selecting a seat to ignite may include avoiding detection of the fire so that they will not be caught, as well as escaping unharmed. The locations that have been identified as significant are a seat at either end of the carriage and a seat in the middle of the carriage. The end of the carriage is considered to be a likely scenario, while the middle of the carriage is estimated to be the worst-case scenario as the fire spread could move in both directions at the same time, reaching flashover much faster than fire spread in a single direction only.

The second condition that was considered was the ventilation conditions within the carriage. The windows, except those on the doors, can be opened by passengers and the doors are known to malfunction and remain open in some cases, while the ceiling vents are always open. Two cases to consider are thus minimum and maximum ventilation conditions given the available vents. In winter, many of the windows are likely to be closed due to the cold, but not all windows are likely to be closed. As there is a large fuel load within the carriage, some ventilation would still be required in order to allow the fire to grow and continue burning. The minimum ventilation condition was thus chosen to be half the windows open and all the ceiling vents open. The maximum ventilation condition would be all the windows, doors and ceiling vents open. This case would give an indication of whether the fire is fuel or ventilation controlled. The starting ventilation area for each case is shown in Table 7.16.

Table 7.16: Initial ventilation area

Ventilation	Maximum	Minimum
$A_{v,windows}$ (m^2)	5.04	2.52
$A_{v,doors}$ (m^2)	8.51	0
$A_{v,windows\ \&\ doors\ total}$ (m^2)	13.55	2.52
$A_{v,ceiling\ vents}$ (m^2)	0.12	0.12
$A_{v,total}$ (m^2)	13.67	2.64

The two cases of ignition location and the two cases of ventilation thus result in four fire scenarios, by combining the ignition location and ventilation. Table 7.17 shows the fire scenario assigned to each model. Scenario A, B, C and D represent the various fire scenarios considered. For all cases, the largest seat in a row was selected for ignition, as this is likely to represent the worst-case.

Table 7.17: Fire scenarios for FDS models

Scenario	Ignition Location	Ventilation
A	Seat A2 (front end)	Minimum
B	Seat I2 (middle)	Minimum
C	Seat A2 (front end)	Maximum
D	Seat I2 (middle)	Maximum

7.3.3 Mesh and Cell Size

The mesh was extended to at least 2 m around the sides of the carriage and to at least 3m above the top. The domain was not extended past the bottom of the train as the airflow and heat transfer behaviour below the train is not required. This resulted in a 22.5 m x 6.8 m x 5.6 m domain, as can be seen in Figure 7.33. Open mesh boundaries were used on all sides of the mesh to simulate open-air burning and unobstructed airflow.
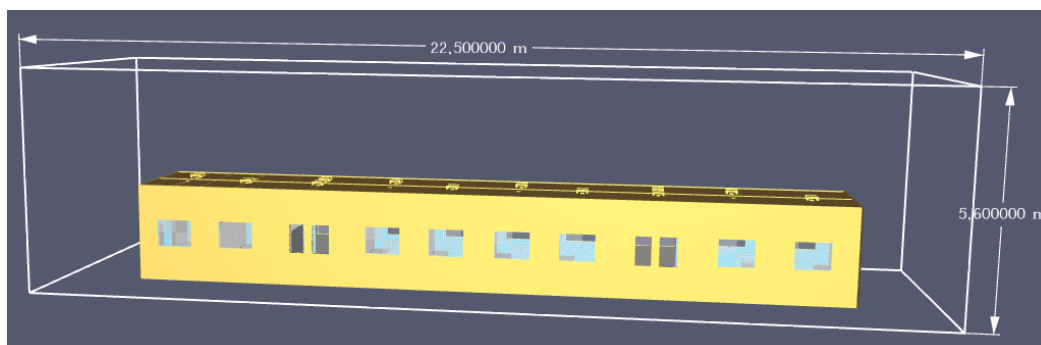
Figure 7.33: Full-scale carriage domain size

The mesh was split into two parts, as can be seen in Figure 7.34. The carriage and at least two cells around the carriage were modelled using the same mesh cell size as for the single seats, 0.05 m, due to obstruction size limitations. The positions of obstructions relative to one another and within the carriage were adjusted to fit this cell size, which did not require significant changes in distances between obstructions and vents. The area surrounding the carriage was modelled using larger mesh cells,

double the size of the carriage mesh cells, at 0.1 m. This was done to reduce the time it took to analyse the models and due to the much larger D* value, which does not require the mesh to be as fine as for the single-seat models. A mesh sensitivity analysis was completed for the single-seat scenarios, and this will also approximately be applicable to the full-scale carriage.
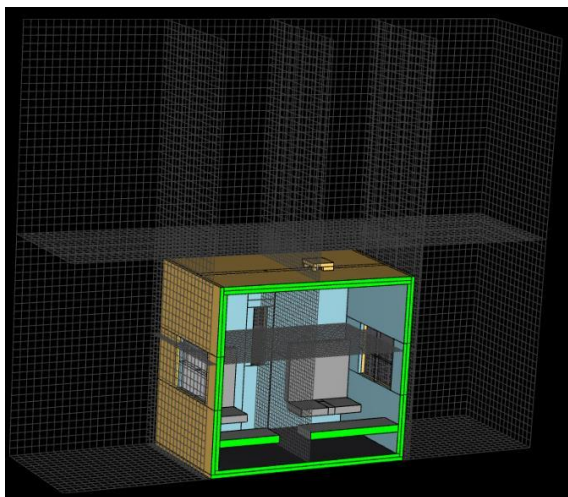
Figure 7.34: Full-scale carriage domain and mesh

7.3.4   Surface Material Properties

The surface material properties from the single-seat simulation were used for all the full-scale carriage scenarios. It was, however, noted after the full-scale simulations were completed that the rubbery foam layer had a density of 140 kg/m^2 instead of 92 kg/m^2 for the seat back and 80 kg/m^2 instead of 66 kg/m^2 for the seat bottom, which also affected the bulk density and the reaction heat of combustion calculations. In order to assess the effect on the simulation, both instances were repeated for the single-seat model and the results compared, as shown in Table 7.20 and Figure 7.38.

Material properties were selected for the other materials found in the carriage based on tests performed as described in Chapter 5, as well as values from literature where required. The other materials found in the carriage include the Bakelite wall and ceiling lining, the Marley (PVC) floor and the windows. The windows were assumed to be PMMA, as tests indicated that the windows were more likely to be PMMA than polycarbonate. As some components, such as the doors and partitions, are made of aluminium and steel respectively, the properties of steel and aluminium were also obtained from literature. As the metals would not combust, this was limited to the density, specific heat, thermal conductivity and emissivity, which could affect the flow of heat within and out of the carriage. Table 7.18 indicates the material properties as determined by testing discussed in Chapter 5, with some values not available being sourced from literature, while Table 7.19 indicates the material properties obtained from literature, except the ignition temperature of Bakelite which was determined through testing. Table 3.3 to Table 3.7 show the ranges described in literature, while the specific values with references can be found in Table A.2 to Table A.16 in Appendix A.

Table 7.18: Material properties of carriage materials determined by testing

Material	Thickness (m)	Density (kg/m³)	Heat of Combustion (kJ/kg)	Effective Heat of Combustion (kJ/kg)
Bakelite	0.0045	1400	18600	14880
Window	0.005	1270	23100	18480
Floor	0.002	1400*	19000*	15200
Steel	N/A	8940*	N/A	N/A
Aluminium	N/A	2707*	N/A	N/A
*literature				

Table 7.19: Material properties of carriage materials from literature

Material	Specific Heat (kJ/kg.K)	Thermal Conductivity (W/m.K)	Emissivity	Ignition Temperature (°C)
Bakelite	1.42	0.25	0.93	225*
Window (PMMA)	1.475	0.19	0.25	250
Window (Polycarbonate)	1.21	0.205	0.88	500
Floor	1.25	0.18	0.92	275
Steel	0.46	45.8	0.25	N/A
Aluminium	0.896	225	0.045	N/A
*measured				

7.3.4.1 Heat Release Rate

The HRR curves of the combustible materials found in the carriage were sourced from literature. The Bakelite is represented by a curve for phenolic resin, shown in Figure 7.35, which would be close to that of Bakelite (also known as phenol formaldehyde). The Bakelite found in the carriage is likely reinforced with paper or sawdust, which could influence the HRR, but a HRR curve more accurately representing the material, was not available.
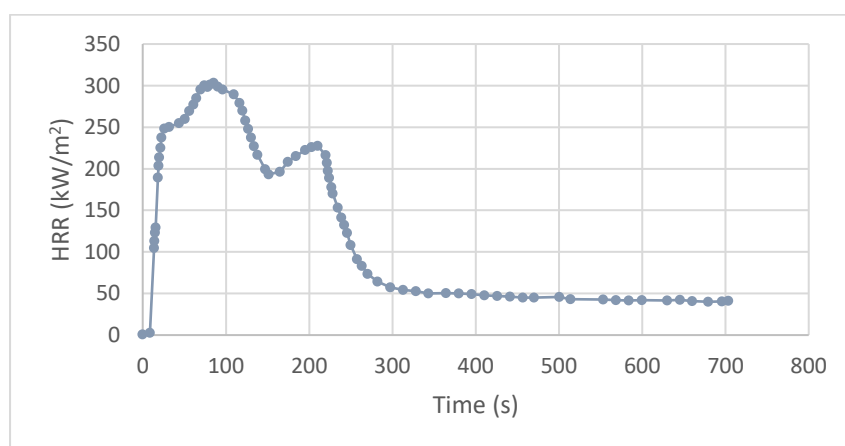
Figure 7.35: Heat release rate - phenolic resin (Zhou *et al.*, 2020)

The window was represented by a HRR curve, shown in Figure 7.36. The curve was obtained by Chow et al. (2006) in testing PMMA with a sample size of 2.4 m x 2.4 m, which is larger than the 0.89 m to 0.95 m wide, 0.685 m to 0.74 m high windows found in the carriages, which are generally also divided

into quarters and separated by frames. This could affect the HRR, but it is the best representation of the HRR of the windows that was available.
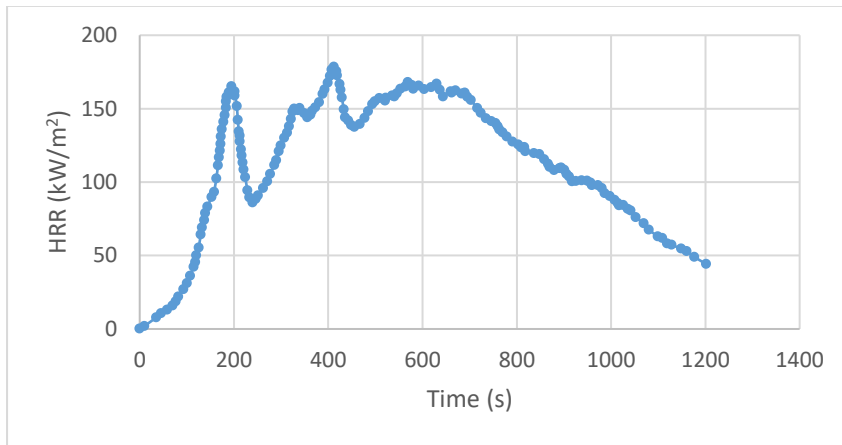
Figure 7.36: Heat release rate - PMMA (Chow *et al.*, 2006, fig. 2a)

The Marley floor is made of PVC and covers a plywood backing. Hence, a HRR curve of PVC was selected, as shown in Figure 7.37. The sample size used to obtain the curve was once again 2.4 m x 2.4 m, much smaller than the Marley floor found in the carriage. The Marley floor would burn before the plywood below it, and thus, the plywood was not included, especially as it would char and not necessarily contribute significantly to fire spread while covered by Marley.
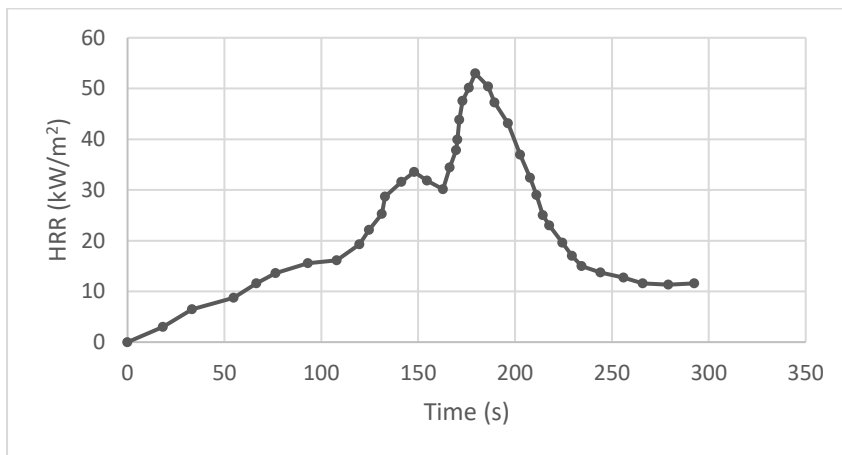
Figure 7.37: Heat release rate - PVC (Chow *et al.*, 2006, fig. 2a)

7.3.5   Obstruction Material Properties

The reaction heat of combustion, 27662 kJ/kg, originally calculated for the single-seat Scenario 1, was used for all the full-scale carriage scenarios, which differs from the reaction heat of combustion of single-seat Scenario 1 stated above. The single-seat reaction heat of combustion was used to represent the carriage, as this is the main fuel load within the carriage. The bulk density used for the seats in the full-scale carriage scenarios was 169 kg/m^2, a value originally calculated for single-seat Scenario 1. The new values used in the single-seat numerical simulation for Experiment 1 (Scenario 1), as stated above, was 26302 kJ/kg and 156 kg/m^2. In order to save computational time in rerunning the simulation, the

effect on the simulations was assessed by simulating both instances, original and new, for the single-seat numerical simulation, and comparing the results. No significant effect was found, with the original simulation compared to the new corrected surface material density, reaction heat of combustion and bulk density values used, as can be seen in Table 7.20 and Figure 7.38.

Table 7.20: Comparison of Scenario 1 single seat results new versus old

Result	Original	New	Increase (%)
Maximum Heat Release Rate (kW)	493.6	463.9	6.4
Maximum Heat Flux (kW/m^2)	14.1	13.1	7.1
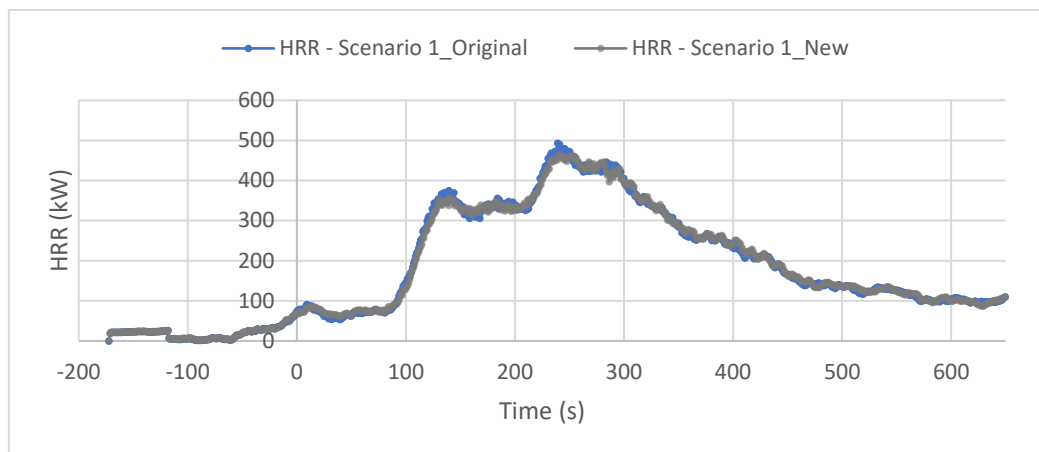
Figure 7.38: Comparison of Scenario 1 single-seat HRR original vs new

The ignition of the floor and wall and ceiling lining is uncertain, and the windows are set to disappear when the centre of each window reaches 200°C, and thus very little of the windows are likely to combust, if any at all, this further justifies the use of the seat reaction heat of combustion and bulk density.

7.3.6   FDS Simulation Results

As discussed above, the focus of the full train models is the estimation of time that passengers may have to evacuate trains based on tenability, rather than on post-flashover maximum heat release rates. It was shown by the simulations that all scenarios resulted in flashover and a ventilation controlled fire as the flames emerged from the windows, doors and ceiling vents, leaving the inside of the carriage starved of oxygen. This means that the carriages would be severely damaged in all the simulated scenarios, and passengers would need to disembark in order to survive the fire. As can be seen in Figure 7.39, the scenarios in which ignition was at the front end of the train, the growth stage started 50 s before that of the scenarios where ignition was in the middle of the carriage. Initially, the maximum ventilation scenarios had a lower HRR, due to the increased ventilation, but once sufficient heat had built up, and the vents did not allow enough cool air to enter, the HRR became higher than those of the minimum ventilation scenarios due to the increased oxygen availability caused by the larger ventilation area. The maximum HRR values for each scenario are given in Table 7.21, as well as the total time of the simulation. As can be seen in Figure 7.39, none of the scenarios reached the decay stage before the simulation had completed, and thus the maximum heat release rates are not necessarily the actual maximum if the scenarios had been allowed to be simulated for longer. Medium, fast and ultra-fast t^2 curves have also been indicated alongside the scenario HRR curves. Initially, the curves follow a medium to fast t^2 fire, but once the growth starts, even the slope of the ultra-fast t^2 curve is exceeded and by 225 s to 275 s, the fires result in fires larger than even ultra-fast t^2 fires. This indicates that the

fires resulting from these passenger train fires pose a significant risk. Future research should develop and calibrate the work to make it suitable for post-flashover and decay phases of the fire, especially if it needs to be investigated the potential damage that could result to train stations.

Table 7.21: Maximum HRR and total simulated time for each scenario

Scenario	Ignition Location	Ventilation	Maximum HRR (MW)	Simulation Time (s)
A	Front end	Minimum	35.59	336.50
B	Middle	Minimum	29.53	329.00
C	Front end	Maximum	36.42	310.50
D	Middle	Maximum	31.51	329.50
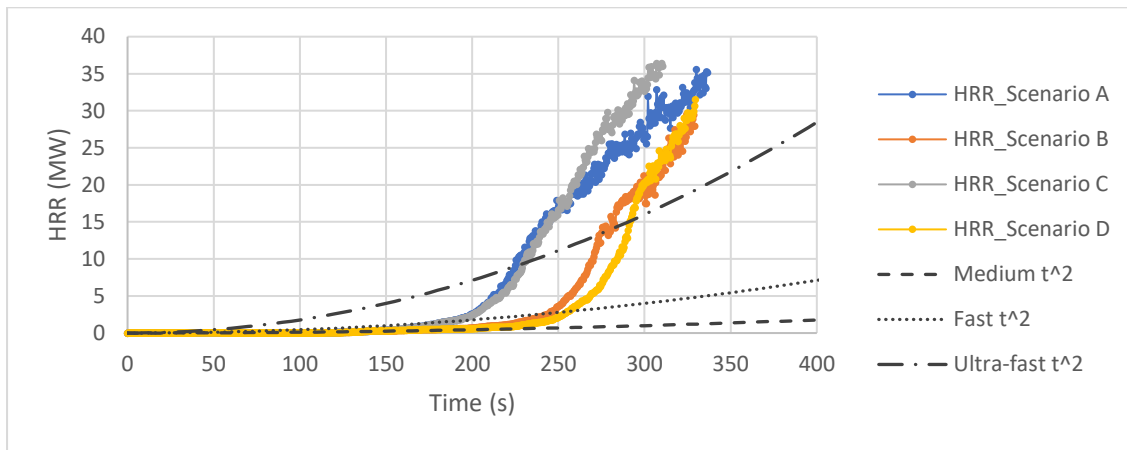
Figure 7.39: Heat release rate curves for each scenario

In order to determine the potential maximum HRR by assuming all the windows in each ventilation scenario had melted away, the ventilation areas were calculated, as can be seen in Table 7.22. This, along with the initial ventilation areas (ventilation area prior to any windows melting), calculated in Table 7.16, was used to determine the rate of burning. Thereafter, the ventilation controlled HRR was calculated based on ventilation conditions. Equation 7.2 and Equation 7.3 were used to determine the initial and maximum potential HRR for the carriage. H_v is the weighted average height of the wall vents by area, and A_v does not include the area of the ceiling vents. Table 7.23 shows the ventilation controlled HRR for the initial (before window melting) and potential maximum ventilation for the minimum and maximum ventilation scenarios.

Table 7.22: Potential ventilation area

Ventilation	Maximum	Minimum
$A_{v,windows}$ (m^2)	10.08	10.08
$A_{v,door\ windows}$ (m^2)	0.3	3
$A_{v,windows\ total}$ (m^2)	10.38	13.08
$A_{v,doors}$ (m^2)	8.51	0
$A_{v,windows\ \&\ doors\ total}$ (m^2)	18.89	13.08
$A_{v,ceiling\ vents}$ (m^2)	0.12	0.12
$A_{v,total}$ (m^2)	19.01	13.2

Equation 7.2: Ventilation controlled rate of burning (Buchanan and Abu, 2017)

$$\dot{m} = 0.092 \times A_v \times \sqrt{H_v}$$

Equation 7.3: Ventilation controlled HRR (Buchanan and Abu, 2017)

$$Q_{vent} = \dot{m} \times \Delta H_c$$

Table 7.23: Ventilation controlled HRR

	Ventilation	A_V (m^2)	H_V (m)	$\dot{m}$ (kg/s)	Q_{vent} (MW)
Initial	Maximum	13.55	1.29	1.42	37.27
	Minimum	2.52	0.35	0.14	3.61
Potential	Maximum	18.89	1.22	1.92	50.47
	Minimum	13.08	0.71	1.02	26.70

When compared to the results from the simulations, it can be seen that the ceiling vents contribute to increasing the maximum HRR beyond the ventilation controlled HRR calculated. This also confirms that all windows melt as the potential maximum HRR is exceeded for the minimum ventilation scenarios. This also indicates that the 50 MW fire calculated for the maximum ventilation scenarios could be reached if the simulations had continued.

The summation method, discussed in Section 2.3.3.2, was used to determine the total heat release rate for the carriage when considering the heat release rate of the individual seats, as shown in Table 7.24. A maximum HRR was assigned to each seat type according to the experiment and numerical simulation scenario, which best represented the dimensions of each seat type. A lower bound value is thus determined by using the maximum HRR obtained from the numerical simulations of the experiments, and an upper bound value was calculated using the HRR obtained from experiments. These values, however, do not include any other materials which may combust in the carriage.

Table 7.24: Estimated maximum HRR for a carriage based on the summation method

Seat Type	Number	Experiment HRR per Seat (MW)	Total FDS HRR (MW)	Total Experiment HRR (MW)	FDS HRR per Seat (MW)
33 inch	10	1.163	0.684	11.63	6.84
36 inch	12	1.258	0.464	15.10	5.57
52 inch	10	1.703	0.729	17.03	7.29
Total HRR for Carriage (MW)				43.8	19.7

The fully-developed fires, shown in Figure 7.40 and Figure 7.41, compares relatively well visually with the real fires that have been captured, as can be seen in Figure 3.3 and Figure 3.4. The flame heights obtained with the simulations are similar to those seen in real fires. It is also noticeable that at the end of the simulation, the flames are not yet emerging from the last window in Scenario A while the flames are emerging from all windows in Scenario C, while Scenario A has run for 26 s longer than Scenario C. This shows that the fire spread through the carriage is faster with increased ventilation. The same behaviour is seen with Scenario B compared to Scenario D, both of which have the ignition source starting in the middle of the carriage.
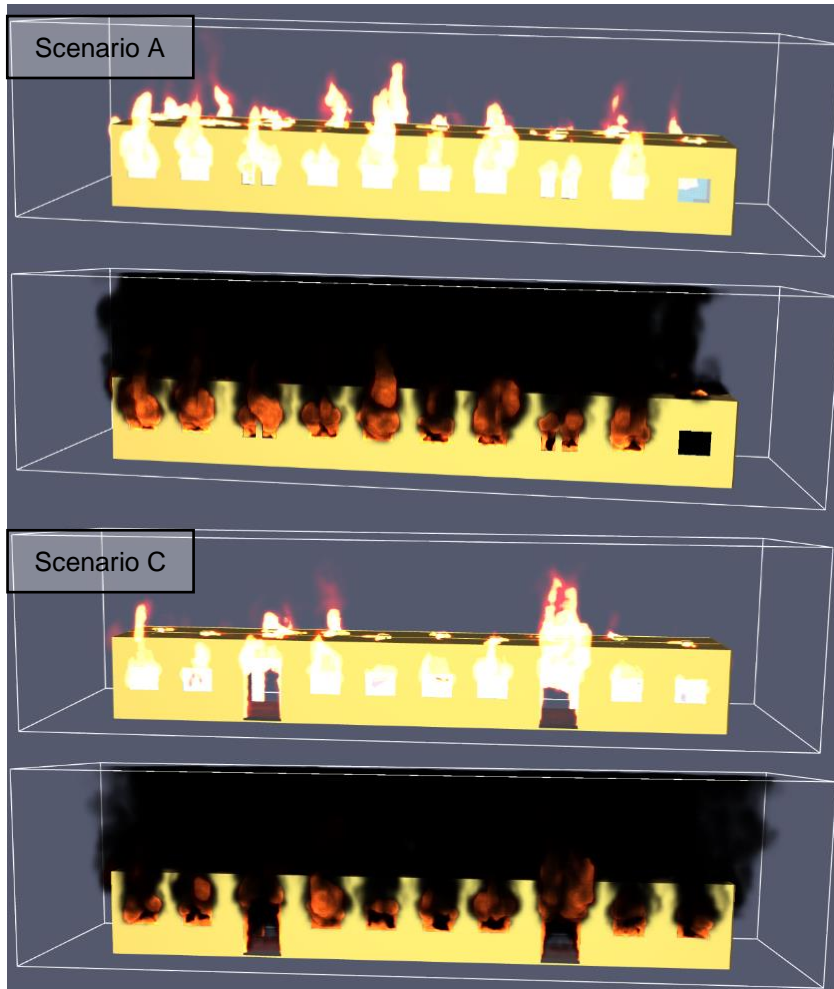
Figure 7.40: Fully-developed fire flames and smoke from carriage side for Scenario A and C
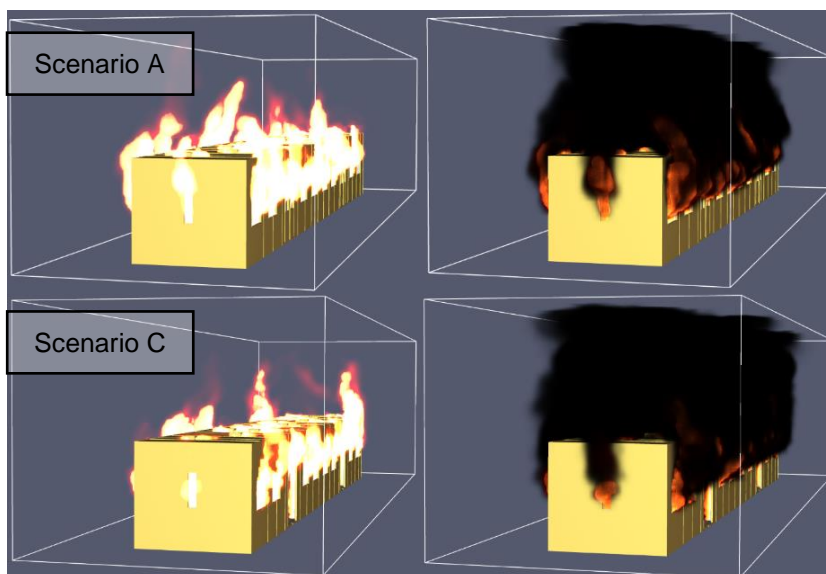
Figure 7.41: Fully-developed fire flames and smoke from carriage front for Scenario A and C

As can be seen in Table 7.25, the various timings of events are shown for each scenario. The times noted for all seat bottoms burning in Scenario A and B, marked with a *, indicate the level of flames reaching the seat bottoms, but due to limited ventilation, the seat bottoms at the carriage ends did not

ignite. Scenario A and C compare well to one another, while Scenario B and D also compare well to one another. The scenarios with maximum ventilation take longer to reach flashover, as would be expected.

Table 7.25: Timing of events during simulations (time in seconds)

Event	Scenario			
	A	B	C	D
Spread to seat behind	N/A	16	N/A	17
Spread to seat in front	157	173	158	176
Spread to seat at side	173	193	173	189
Flames reach ceiling	131	186	134	191
Flames roll along ceiling	148	199	149	211
Flames to seats at end	232	258	240	274
All seat bottoms burning	232*	267*	263	297
Flashover	232	267	260	294

7.3.6.1   Passenger Tenability Conditions

As per the specifications in NFPA 130 (NFPA, 2017) and the indicator of pain setting in at 1 kW/m^2 (Quintiere, 2006), some temperature and heat flux values were identified, and the times at which they occurred were noted in Table 7.26 and Table 7.27. Heat flux values which were selected were 1 kW/m^2, 1.7 kW/m^2, 2 kW/m^2 and 2.5 kW/m^2. Temperatures which were taken note of include 50°C, 60°C, 70°C and 80°C, although airways start burning at 60°C, but exposure at 60°C can be maintained for 10 minutes 7 seconds (607 s), but exposure at 70°C can be maintained for 5 minutes 59 seconds (359 s), and exposure at 80°C can be maintained for 3 minutes 48 seconds (228 s). The heat flux moves toward floor level at one set of seats before moving downward at the next set of seats for Scenario A and C, thus the exits may not be accessible while the conditions at the end of the carriage still fall within tenability limits. For Scenario B and D, the effect is not as significant. In terms of temperature, however, the area at the side doors has a lower temperature than the rest of the carriage for the maximum ventilation scenarios, and thus, the exits have a more tenable environment enabling escape as the passenger may still be able to breathe although they will sustain injuries to their skin.

Table 7.26: Incident heat flux timing in seconds

Incident Heat Flux (kW/m^2)	Location	Standing				Crawling			
		Scenario				Scenario			
		A	B	C	D	A	B	C	D
1	Middle	166	156	166	177	183	161	186	226
	End	173	170	174	200	203	224	209	249
1.7	Middle	178	190	180	206	198	205	200	240
	End	189	209	193	235	223	246	231	261
2	Middle	185	200	184	215	202	218	210	244
	End	196	215	202	243	230	252	240	265
2.5	Middle	191	206	188	226	205	228	212	250
	End	203	226	207	250	232	256	244	270

Table 7.27: Temperature timing in seconds

Temperature (°C)	Location	Standing				Crawling			
		Scenario				Scenario			
		A	B	C	D	A	B	C	D
48-52	Middle	133	144	149	148	213	211	224	253
	End	137	128	137	135	192	233	257	286
58-62	Middle	155	150	155	155	216	220	226	258
	End	141	135	144	144	200	244	263	292
68-72	Middle	161	155	161	168	218	228	227	260
	End	147	140	149	147	202	247	265	293
78-82	Middle	165	160	168	175	219	239	228	269
	End	150	144	155	150	203	249	267	296

From these timings, it is clear that the minimum ventilation scenarios allow for less time to escape untenable conditions, particularly Scenario A, where the ignition is at the front of the carriage. This does not include the opening of doors during escape, which may lead to backdraft or to a reduced HRR depending on which doors are opened and for how long. In order to escape with minimal injuries, passengers have around 130 s to 150 s to escape in an upright position, or 160 s to 250 s to escape if they resort to crawling. For escaping and likely surviving but having significant injury, passengers have around 140 s to 175 s to escape in an upright position, and for a crawling escape they have around 205 to 270 s. For the upright or standing escape, temperature is the governing tenability condition, while for crawling, the incident heat flux is the governing factor. These times are from the start of ignition and do not take the time required for detection, reaction and decision-making into account. With the narrow pathway in the centre of the carriage, these times may not be sufficient to allow passengers to escape, and will not allow all passengers to escape if the carriage is full of passengers.

7.3.7   Conclusion

The various scenarios compare relatively well with one another in terms of HRR. The simulations indicated that the minimum ventilation conditions lead to faster spreading fires, but all scenarios reached flashover within 300 s, and thus the ventilation provided by the maximum ventilation scenarios was not sufficient to prevent flashover from occurring. Maximum HRR values range up to around 50 MW showing that very extreme fires will occur, and will likely damage surrounding structures, such as train stations. This is consistent with recent incidents. These carriages present a significant fire hazard and are dangerous when passengers are involved as passengers cannot be guaranteed a safe escape and have very little chance of surviving when a carriage full of passengers ignites.

8 Conclusions and Recommendations

8.1 Overview

The work done in this study investigated the cause of the severe damage caused by arson attacks on Metrorail trains by studying the fire behaviour. A multi-scale approach was used to develop an understanding of the fire behaviour experienced in the passenger train carriages. Small-scale material tests were performed in order to determine the properties of the materials found within the carriages. Large-scale experiments were performed in order to study the fire behaviour of seat assemblies where various materials interact with one another. Data was also obtained from these tests and experiments to be used in numerical simulations. The large-scale experiments were simulated in FDS in order to get a better understanding of the capabilities of the software by comparing the results to those obtained in experiments. These large-scale numerical simulations were used to perform full-scale numerical simulations in order to study the fire behaviour in carriages under different fire scenarios and included a variation on ventilation conditions and ignition location within the carriage.

In Chapter 2, a literature study was performed in order to gain an understanding of fire behaviour and numerical simulations used to recreate this behaviour, and the principles involved, particularly in compartment fires, as well as fires in passenger trains. The testing and research that has been done in this regard and the standards used to test compliance were also discussed.

Chapter 3 provided background information on the problem of arson attacks on Metrorail trains in South Africa, as well as details regarding the targeted carriages and the materials found within them. Material properties were also covered, and literature values for material were provided.

Chapter 4 covered the setup of the small-scale material tests and the large-scale experiments. The small-scale tests involved density measurements, bomb calorimeter tests, and radiant panel tests, while the large-scale experiments involved burning seat assemblies in an open-air environment to obtain the MLR and heat flux and temperature values at various positions.

In Chapter 5, the results of the small-scale tests were discussed and further analysed in order to obtain data to be used in the numerical simulations.

Chapter 6 gave an overview of the large-scale experiment results and the steps taken to obtain a mass-loss rate curve for use in the numerical simulations.

In Chapter 7, the setup and results of the numerical simulations of the single-seat experiments and the full-scale carriages were discussed. Material properties were selected, and fire scenarios were identified for use in the numerical simulations. The results were further analysed, and the implications thereof discussed.

8.2 Summary of Findings

8.2.1 Small-scale Tests

From the various results obtained, the rubbery foam was identified as latex foam, while the windows are assumed to be PMMA. This informed the selection of material properties from literature where they were required. The most abundant materials found in the carriages, the latex foam and rebonded polyurethane foam, were found to have the highest heat of combustion. The heat of combustion of the latex foam was found to be close to that of accelerants such as propane, gasoline and heptane, which means that this material poses an extreme fire hazard in the Metrorail trains. The rebonded polyurethane foam and latex foam were also found to have significantly higher densities when compared to typical polyurethane foam, thus also posing a more severe hazard than seats containing only typical polyurethane foam, especially as the heat of combustion, which is measured per unit mass, is also significantly higher than that of typical polyurethane foam.

The radiant panel tests showed that all the tested materials would ignite at a radiant heat flux significantly lower than 50 kW/m², a radiant heat flux, which could be reached by carriages involved in fires. The stickers typically found on the interior wall panels in the trains were found to not have a greater ignition potential than the Bakelite without stickers. This indicated that all materials are likely to ignite when a Metrorail train carriage is involved in a fire. The windows samples melted to produce holes, which would mean that additional ventilation could become available during a fire, and thus, the windows would need to be modelled in such a way as to reproduce this behaviour as the ventilation in a carriage plays a significant role in the fire growth and behaviour.

8.2.2   Large-scale Experiments

The experiments performed on the seat assemblies resulted in very large fires, which would likely not be able to be done in furniture calorimeters or room fire tests, due to the severity of the fire, which would cause damage to equipment and lead to safety risks. Two of the four experiments were stopped before the decay stage as the acceptable safety risks had been exceeded and produced significant amounts of smoke, which likely had toxic components. All the seats failed at least three of the EN 45545-2 requirement set R18 criteria, which are that flames should not spread to the edges of the seat, or reach 1000 mm above the highest point of the seat surface, and that the maximum peak HRR of 350 kW should not be exceeded. The two experiments that were stopped early, failed a fourth criterion, which is that the fire should not reach a dangerous level during testing.

The maximum HRR observed during the experiments ranged between 1163 kW to 1715 kW. The maximum heat flux at 1 m from the seats ranged from 18.9 kW/m² to 22.8 kW/m², which is sufficient to ignite the next seat. The flame height ranged from 1.85 m to 2.1 m when measured from the top of the seat bottom.

8.2.3   Single Seat Numerical Simulations

The maximum heat release rates obtained from the simulations ranged from 464 kW to 729 kW, less than half of the maximum HRR values obtained in the experiments, but still exceeding the EN 45545-2 requirement of 350 kW. This is likely due to the significant smoothing caused firstly by the smoothing of the MLR data and the sensitivity of the equipment used, and secondly by the application of the Reynolds-averaged Navier-Stokes equations in FDS. The temperatures obtained at the positions of the thermocouples did not compare well with those measured during the experiments, except in the general trend, in other words, the time at which increases were seen, but the values did not compare well, and the bottom thermocouple was found to have the lowest temperatures in the simulation, while the opposite was true for the experiments. This is linked to the shape of the flame and the air entrainment patterns that occurred. The maximum heat flux ranged from 12.48 kW/m² to 19.87 kW/m², which compared relatively well to those measured during the experiments. The flame height from the simulations ranged between 1.51 m to 3.02 m, which also compares relatively well with those seen in the experiments. The various simulations also compared relatively well with one another, which meant that any of the simulations could conservatively be used in the full-scale numerical simulations. Scenario 1 was selected as it had the longest simulation time available and included the decay stage. Also, having the lowest HRR, it provides an upper bound estimate or tenability considerations, where data from other experiments would have provided predictions showing even less time to escape from trains.

8.2.4   Full-scale Numerical Simulations

Four fire scenarios were identified, varying ventilation between minimum and maximum, with maximum including all windows and doors open, and varying the ignition location between the front of the carriage and the middle of the carriage. The reaction heat of combustion and bulk density of the seats were used. All scenarios resulted in flashover before 300 s from ignition, and all were ventilation controlled fires. The fires were initially well represented by a medium to fast t² curve, but once fire growth had picked up, even an ultra-fast t² curve was exceeded, before flashover had occurred.

The scenarios where ignition was at the front of the carriage, showed the growth phase starting around 50 s sooner, and thus also had flashover occurring earlier than the scenarios where ignition was in the middle of the carriage. The worst case for ignition location was shown to be at either end of the carriage, likely due to the wall panel behind the seat and more heat building up in the section of the carriage with fewer vents. The minimum ventilation scenarios initially had a higher HRR, but once the fire growth had progressed, around the time of flashover, the maximum ventilation scenarios had a higher HRR, but flashover occurred sooner in the minimum ventilation scenarios. The worst-case scenario for the time of flashover is thus the minimum ventilation condition, but for ultimate peak HRR, the worst-case scenario is maximum ventilation. The passengers will, however, be affected more by the time at which tenability conditions are exceeded. For passengers, the worst-case scenario is thus ignition at either end of the carriage with minimum ventilation. For trains in stations and considering the damage caused to stations, however, the worst-case scenario would be ignition at either end of the carriage with maximum ventilation.

For the scenarios where ignition took place at the front of the carriage, the end of the carriage maintained tenable conditions after the side doors were no longer accessible due to tenability conditions being exceeded, thus passengers would need to exit through the back door. For maximum ventilation conditions, with side doors being open, the area at the doors remains within tenability conditions for longer than the rest of the carriage, allowing passengers to escape through the side doors.

Passengers have 130 s to 150 s to escape with minimal injuries, if any, while in an upright position, while they have 160 s to 250 s to escape when resorting to crawling. In order to possibly survive their escape, but potentially have severe injuries, passengers have around 140 s to 175 s when remaining upright, and 205 s to 270 s when resorting to crawling. These times include the time required to detect the fire, react and make decisions. Few passengers in a full carriage are thus likely to survive, and when the carriage is not full, survival is not guaranteed, especially considering the narrow passage in the centre of the train. These trains thus pose a significant fire hazard and are extremely dangerous when a fire occurs with passengers on board. Also, it should be remembered that predictions are based upon the lower bound FDS prediction of the seat HRR, rather than the upper bound Experiment 3 and 4 HRR measured. Hence, in reality, results may be even worse depending on how seats are ignited and the materials involved.

8.2.5 Summary of Recommendations to Improve Metrorail Train Safety in Fires

As a summary of behaviour: single seats fail fire safety recommendations based on European recommendations, which will typically be similar to requirements of other countries. Fire spread will occur rapidly, and entire trains can also not be considered compliant with fire regulations. Inhabitants have around 2-4 minutes to escape (and possibly less). For a train with a significant amount of passengers aboard, it is likely that fatalities will occur if people are not able to leave the trains extremely quickly. If a train full of people was (a) moving at the time of ignition, (b) had doors that failed to open, (c) had a number of mobility-impaired people on-board, or (d) if fires block exits, a disaster with many deaths could potentially result.

There are several aspects of the Metrorail trains which could be addressed in order to improve the safety of the trains for passengers, and reduce the damage caused when fires occur. Ultimately trains should comply with international regulations for fire safety which will address the majority of the safety issues. Recommendations that follow are based upon providing actions that could be considered in the immediate future while international specifications are being implemented. These do not constitute compliance with fire safety requirements.

The materials used for the seats need to be revised, and the latex foam and rebonded foam removed. Seat fabric covers with higher ignition temperatures could be implemented in order to increase the duration of the ignition and early growth phase. Fire-resistant linings could be used around the foam layers if foam is to be included in the seat. Foam layers should also be significantly reduced in thickness

in order to reduce the amount of material with a higher heat of combustion. PMMA windows could also be replaced with polycarbonate windows as polycarbonate performs better in fire.

The passage in the centre of the train could be widened, and the number of seats encroaching on the passage should be reduced in order to improve evacuation times. This will require smaller seats which would also reduce the amount of combustible material. Fire detection systems should be implemented, which could warn passengers as soon as smoke is detected, which will allow passengers to react sooner. A communication system should also be incorporated in order to alert the driver of the train. Once a carriage has been evacuated, the doors could be closed to reduce the peak HRR, and thus damage to the station. In order to do so, a system would need to be put in place which will identify when all passengers have disembarked. Furthermore, the improvement of security and training of officials may assist in reducing the number of arson events and improve response through staff members being able to attend to fires quickly.

8.3 Future Research and Recommendations

In order to improve the accuracy of the full-scale numerical simulations, it is recommended that materials are tested in a cone calorimeter in order to determine the ignition temperature and critical heat flux. Tests should also be done to determine other material thermal properties such as thermal conductivity, specific heat and emissivity. The seats should also be tested in a furniture calorimeter which will provide a HRR and indicate a more appropriate efficiency factor for the heat of combustion.

In order to improve the models of the single-seat numerical simulations, the slope of the seat back could be reproduced more accurately, and the honeycomb structure of the rubbery foam should be modelled accurately, which will influence fire spread and growth. A finer mesh could also be used in order to model the actual dimensions of the seats.

The fire scenarios used for the full-scale numerical simulations should be expanded to include scenarios where the train is moving, significant wind is blowing and with the train inside a station. This will provide a more comprehensive understanding of the fire behaviour. Scenarios with minimum ventilation should also be expanded to include the opening of doors as passengers escape, particularly the front and back doors at the ends of the carriage, which close if not held open.

Passenger evacuation behaviour should also be investigated in order to determine the time required for safe evacuation and the time required for all passengers to disembark when the carriage is full. To further study the effect of the tenability conditions, the toxicity of the smoke should also be investigated.

References

African News Agency (2017) *Train surfing puts lives at risk | eNCA*, *eNCA*. Available at: https://www.enca.com/south-africa/train-surfing-puts-lives-at-risk (Accessed: 26 November 2021).

African News Agency (2019) 'Burning tyres on tracks delay Cape Town trains — The Citizen', *The Citizen*. Available at: https://www.citizen.co.za/news/2172450/burning-tyres-on-tracks-delay-cape-town-trains/ (Accessed: 26 November 2021).

Babrauskas, V. and Peacock, R. (1992) 'Heat Release Rate: The Single Most Important Variable in Fire Hazard', *Fire Safety Journal*, 18, pp. 255–272. Available at: https://www.nist.gov/publications/heat-release-rate-single-most-important-variable-fire-hazard (Accessed: 13 January 2022).

Beyler, C. L. (2004) 'Ignition handbook, principles and applications to fire safety engineering, fire investigation, risk management, and forensic science', *Fire Safety Journal*, 40(3), pp. 295–296. doi: 10.1023/b:fire.0000026981.83829.a5.

Boshoff, R. (2018) 'Another train fire for Cape Town - but it's a drill', *Sunday Times*. Available at: https://www.timeslive.co.za/news/south-africa/2018-07-31-another-train-fire-for-cape-town-but-its-a-drill/ (Accessed: 26 November 2021).

Botha, A. D. (2022) *Behaviour of Recycled Construction Materials Subject to Fire Loading*. Stellenbosch University.

Briggs, P., Metral, S., *et al.* (2001) *FIRESTARR, final report*, *FIRESTARR Consortium, Contract SMT4-CT97-2164*.

Briggs, P., Le Tallec, Y., *et al.* (2001) 'The FIRE_STARR research project on the reaction-to-fire performance of products in European trainsle', in *9th International Interflam Conference, Edinburgh, Scotland*.

Buchanan, A. H. and Abu, A. K. (2017) *Structural Design for Fire Safety*. 2nd edn. John Wiley & Sons, Ltd. doi: 10.1002/9781118700402.

CEN (2002) *EN 1991-1-2:2002. Eurocode 1: Actions on structures - Part 1-2: General actions - Actions on structures exposed to fire*.

CEN (2015) 'BS EN 45545-2. Fire Testing of Materials and Components for Trains', *British-Adopted European Standard*.

Chiam, B. H. (2005) 'Numerical Simulation of a Metro Train Fire', *Fire Engineering*, pp. 1–340. Available at: http://www.civil.canterbury.ac.nz/fire/fe_resrch_reps.html.

Chow, W. K. *et al.* (2006) 'Full-scale burning tests on flame spread of plastic materials', *International Journal on Engineering Performance-based Fire Codes*, 8(3), pp. 99–111.

City of Cape Town Fire (2017) *Dieselfde trein brand Donderdag wéér | Maroela Media*, *Maroela Media*. Available at: https://maroelamedia.co.za/nuus/sa-nuus/dieselfde-trein-brand-donderdag-weer/ (Accessed: 26 November 2021).

Coles, A. *et al.* (2009) 'Predicting design fires in rail vehicles', *13th International Symposium on Aerodynamics and Ventilation of Vehicle Tunnels. 2. 819-833*. Available at: https://www.researchgate.net/publication/289046898_Predicting_design_fires_in_rail_vehicles (Accessed: 13 January 2022).

Daniel, L. (2019) 'Watch: Cape Town trains gutted by fire, MetroRail suspends services', *The South African*. Available at: https://www.thesouthafrican.com/news/metrorail-cape-town-train-fire-services-suspended-video/ (Accessed: 26 November 2021).

Darmody, M. and Weaver, S. (2014) 'Design Fires for Passenger Trains-How Do We Know We Have Them Right?', *Conference On Railway Excellence Adelaide*, (May), pp. 5–7.

Drysdale, D. (2011) *An Introduction to Fire Dynamics*. 3rd edn, *John Wiley & Sons, Ltd*. 3rd edn. doi: 10.1016/0010-2180(86)90037-4.

Emissivity Coefficient Materials (no date). Available at: https://www.engineeringtoolbox.com/emissivity-coefficients-d_447.html (Accessed: 29 October 2021).

Emissivity Table (no date). Available at: https://www.optotherm.com/emiss-table.htm (Accessed: 25 November 2021).

Guillaume, E., Camillo, A. and Rogaume, T. (2014) 'Application and Limitations of a Method Based on Pyrolysis Models to Simulate Railway Rolling Stock Fire Scenarios', *Fire Technology*, 50(2), pp. 317–348. doi: 10.1007/S10694-013-0379-9.

Hasburgh, L. E. *et al.* (2004) 'dComparison of the Heat Release Rate from the Mass Loss Calorimeter to the Cone Calorimeter for Wood-Based Materials', pp. 116–127.

Hendricks, A. (2017) *Commuters rebel as Metrorail fails | GroundUp*, *GroundUp*. Available at: https://www.groundup.org.za/article/commuters-rebel-metrorail-fails/ (Accessed: 26 November 2021).

Hendricks, A. (2020) *Lawyers dump PRASA after failure to pay R19 million | GroundUp*, *GroundUp*. Available at: https://www.groundup.org.za/article/lawyers-dump-prasa-after-failure-pay-r19-million/ (Accessed: 26 November 2021).

Hietaniemi, J., Hostikka, S. and Vaari, J. (2004) 'FDS simulation of fire spread – comparison of model results with experimental data', *VTT Building and Transport*, (January), p. 51.

Hostikka, S. and McGrattan, K. B. (2001) 'Large Eddy Simulation of Wood Combustion', *Interscience Communications Ltd*. NIST, pp. 755–762. Available at: https://www.nist.gov/publications/large-eddy-simulation-wood-combustion (Accessed: 18 January 2022).

Hukseflux (no date) *SBG01 heat flux meter | Hukseflux*. Available at: https://www.hukseflux.com/products/heat-flux-sensors/heat-flux-meters/sbg01-heat-flux-meter (Accessed: 11 January 2022).

Hurley, M. J. *et al.* (eds) (1997) *SFPE Handbook of Fire Protection Engineering*. 5th edn. Springer New York Heildelberg Dordrecht London. doi: 10.1016/s0379-7112(97)00022-2.

Hyman, B. (2019) 'Metrorail releases footage of train arson suspects, wants help finding them', *Sunday Times*. Available at: https://www.timeslive.co.za/news/south-africa/2019-12-09-watch-metrorail-releases-footage-of-train-arson-suspects-wants-help-finding-them/ (Accessed: 5 October 2021).

Imager, F. T. I. T. (1850) 'Emissivity Tables FTI 6 Thermal Imager Typical Emissivity Values', pp. 1–18. Available at: http://www.thermoview.ru/pdf/emis3.pdf.

Ingason, H. (2007) *Model Scale Railcar Fire Tests*, *Fire Safety Journal*. doi: 10.1016/j.firesaf.2006.11.004.

Isaacs, L. (2020) *Cape Town authorities probe Metrorail train fire*, *EWN*. Available at: https://ewn.co.za/2020/01/26/cape-town-authorities-probe-metrorail-train-fire (Accessed: 26 November 2021).

ISO (2019) *BS ISO 5660-1. Reaction-to-fire tests — Heat release, smoke production and mass loss rate*. BSI Standards Publication.

James, R. (no date) *Savitsky Golay Smoothing Coefficients - Google Drive*. Available at: https://docs.google.com/spreadsheets/d/1-2UF3jGQSGIFEt-T3QHliz9gIdcy73e3U5SR7b0qh-A/pubhtml# (Accessed: 15 September 2021).

Karlsson, B. and Quintiere, J. (1999) *Enclosure Fire Dynamics*, *Enclosure Fire Dynamics*. doi: 10.1201/9781420050219.

Lerch, V. *et al.* (2003) 'Thermomechanical properties of polycarbonate under dynamic loading', *Journal de Physique IV Proceedings*, 110. doi: 10.1051/jp4:20020687ï.

Maluk, C. *et al.* (2016) 'A Heat-Transfer Rate Inducing System (H-TRIS) Test Method', *Fire Safety Journal*. Available at: https://doi.org/10.1016/j.firesaf.2016.05.001.

Marley Dance Flooring - Studio Quality (no date). Available at: https://www.rubberflooringinc.com/dance-flooring/marley-dance-floor.html (Accessed: 26 November 2021).

McGrattan, K. *et al.* (2015) 'Sixth Edition Fire Dynamics Simulator Technical Reference Guide Volume

1 : Verification guide', 1, pp. 1–147.

McGrattan, K. *et al.* (2017) 'Fire Dynamics Simulator, Technical Reference Guide, Volume 3: Validation', *NIST Special Publication*, 3(6). doi: http://dx.doi.org/10.6028/NIST.SP.1018-3.

Metrorail (2007) *Metrorail*. Available at: http://www.metrorail.co.za/ (Accessed: 5 October 2021).

Metrorail (2018) *Another burning train pulls into Retreat Station | CapeTown ETC*, *Cape Town etc*. Available at: https://www.capetownetc.com/news/another-burning-train-pulls-into-retreat-station/ (Accessed: 26 November 2021).

Mortlock, M. (no date) *Lessons from London: How Cape Town could tackle its transport crisis*. Available at: https://thomsonfoundation.shorthandstories.com/LondonsHolyRail/index.html (Accessed: 26 November 2021).

NFCC (no date) *Understand signs and symptoms of flashover*. Available at: https://www.ukfrs.com/guidance/search/understand-signs-and-symptoms-flashover (Accessed: 23 January 2022).

NFPA (2017) 'NFPA 130 Standard for Fixed Guideway Transit and Passenger Rail Systems 2017 Edition'.

Noyed, D. (2017) *How is Latex Density Measured?*, *Sleep Foundation*. Available at: https://www.sleepfoundation.org/mattress-information/latex-density (Accessed: 5 September 2021).

Peacock, R. D. *et al.* (2002) 'Fire Safety of Passenger Trains, Phase 2: Application of Fire Hazard Analysis Techniques'. NIST. Available at: https://www.nist.gov/publications/fire-safety-passenger-trains-phase-ii-application-fire-hazard-analysis-techniques (Accessed: 18 January 2022).

Peacock, R. D. *et al.* (2004) 'Fire Safety of Passenger Trains; Phase 3: Evaluation of Fire Hazard Analysis Using Full-Scale Passenger Rail Car Tests (NISTIR 6563)'. NIST. Available at: https://www.nist.gov/publications/fire-safety-passenger-trains-phase-3-evaluation-fire-hazard-analysis-using-full-scale (Accessed: 18 January 2022).

Peacock, R. D. and Braun, E. (1984) 'Fire Tests of Amtrak Passenger Rail Vehicle Interiors. Final Report. 1978-1983 (NBS TN 1193)'. doi: 10.6028/NBS.TN.1193.

Peacock, R. D. and Braun, E. (1999) 'Fire Safety of Passenger Trains. Phase 1: Material Evaluation (Cone Calorimeter) (NISTIR 6132)'. doi: 10.6028/NIST.IR.6132.

PRASA (2015) *About Us | PRASA Corporate*. Available at: https://www.prasa.com/About.html (Accessed: 25 November 2021).

Quintiere, J. G. (1998) *Principles of fire behavior*. 2nd edn. CRC Press.

Quintiere, J. G. (2006) *Fundamentals of Fire Phenomena*. John Wiley & Sons Ltd.

Rebond Foam Product Guide | OFS Maker's Mill (no date). Available at: https://www.onlinefabricstore.com/makersmill/rebond-foam/ (Accessed: 18 November 2021).

Sewport Support Team *What is Faux Leather Fabric;Properties, How its Made and Where*. Available at: https://sewport.com/fabrics-directory/faux-leather-fabric (Accessed: 30 September 2021).

Staggs, J. E. J. (2005) 'Savitzky-Golay smoothing and numerical differentiation of cone calorimeter mass data', *Fire Safety Journal*, 40(6), pp. 493–505. doi: 10.1016/j.firesaf.2005.05.002.

'Thermal Properties of Polymers | Textile Study Center' (no date) *https://textilestudycenter.com/*. Available at: https://textilestudycenter.com/thermal-properties-polymers/ (Accessed: 25 November 2021).

ThermoWorks (no date) *Infrared Emissivity Table*. Available at: https://www.thermoworks.com/emissivity-table (Accessed: 29 October 2021).

Thunderhead Engineering (2021) *PyroSim User Manual*. Available at: https://support.thunderheadeng.com/docs/pyrosim/2021-3/user-manual/#_selecting_a_mesh (Accessed: 25 October 2021).

Uses of Perspex® Acrylic Sheet vs Polycarbonate Sheet - Industrial Plastics (no date). Available at: https://industrialplastics.com.au/perspex-sheet-vs-polycarbonate/ (Accessed: 10 July 2021).

White, N. (2010) *Fire Development in Passenger Trains*, *M.S. Thesis, Victoria University*. Available at:

https://citeseerx.ist.psu.edu/viewdoc/download?doi=10.1.1.667.7811&rep=rep1&type=pdf (Accessed: 22 November 2021).

White, N. and Dowling, V. P. (2004) 'Conducting a full-scale experiment on a rail passenger car'. Korean Institute of Fire Science and Engineering.

Yüksel, N. (2016) 'The Review of Some Commonly Used Methods and Techniques to Measure the Thermal Conductivity of Insulation Materials', *Insulation Materials in Context of Sustainability*. doi: 10.5772/64157.

Zhou, R. *et al.* (2020) 'Synergistic Effects of Aluminum Diethylphosphinate and Melamine on Improving the Flame Retardancy of Phenolic Resin', *Materials*, 13(1). doi: 10.3390/ma13010158.

Zuo, W. (2005) 'Introduction of Computational Fluid Dynamics'. FAU Erlangen-Nürnberg.

Appendix A

Table A.1 shows the abbreviations and associated reference used for Table A.2 to Table A.16.

Table A.1: References for material property tables

Abbreviation	Reference
D	(Drysdale, 2011)
DL	(Lerch *et al.*, 2003)
ET	(*Emissivity Coefficient Materials*, no date)
IH	(Beyler, 2004)
OT	(*Emissivity Table*, no date)
SF	(Noyed, 2017)
SFPE	(Hurley *et al.*, 1997)
TSC	('Thermal Properties of Polymers | Textile Study Center', no date)
TV	(Imager, 1850)
TW	(ThermoWorks, no date)

Table A.2: Material heat of combustion

Material Type	Material	Heat of Combustion (kJ/kg)		Reference
Accelerant	Gasoline	Gross	46900	IH, Ch. 10 Tbl. 5
Accelerant	Heptane	Net	44600	SFPE, Tbl. 26.21
Accelerant	Heptane	Unspecified	45000	SFPE, Tbl. 18.2
Accelerant	Heptane	Net	44560	IH, Ch. 15 Tbl. 1A
Accelerant	Newspaper	Gross	19700	SFPE, Tbl. A.32
Accelerant	Propane	Net	46000	SFPE, Tbl. A.38
Accelerant	Propane	Net	46450	D, Tbl. 1.13
Accelerant	Propane	Net	46330	IH, Ch. 15 Tbl. 1A
Foam	Polyurethane (flexible) foam GM21	Net	26200	SFPE, Tbl. A.39
Foam	Polyurethane (flexible) foam GM23	Net	27200	SFPE, Tbl. A.39
Foam	Polyurethane (flexible) foam GM25	Net	24600	SFPE, Tbl. A.39
Foam	Polyurethane (flexible) foam GM27	Net	23200	SFPE, Tbl. A.39
Foam	Polyurethane foams	Unspecified	24400	D, Tbl. 1.2
Interior lining	Phenol	Net	31050	SFPE, Tbl. A.30
Interior lining	Phenol formaldehyde	Net	26700-30400	SFPE, Tbl. A.31
Latex foam	Latex foam	Gross	33900-40600	SFPE, Tbl. A.32
Pleather	Polyester	Net	32500	SFPE, Tbl. A.38
Pleather / Floor / Window frame	PVC	Net	16430	D, Tbl. 1.13
Pleather / Floor / Window frame	PVC	Unspecified	19900	D, Tbl. 1.2
Plywood backing	Plywood	Unspecified	14200-18800	SFPE, Tbl. 26.33
Plywood backing	White pine	Net	17800	SFPE, Tbl. A.32

Table A.3: Material heat of combustion continued

Material Type	Material	Heat of Combustion (kJ/kg)		Reference
Plywood backing	Wood	Unspecified	18500	IH, Ch. 7 Tbl. 6
Plywood backing	Wood	Gross	19500	IH, Ch. 10 Tbl. 5
Plywood backing	Wood (pine)	Net	17900	SFPE, Tbl. A.39
Plywood backing	Wood (Ponderosa pine)	Net	19400	SFPE, Tbl. 5.3
Seat lining	Polyester	Net	23800	SFPE, Tbl. 5.3
Seat lining	Polyester	Net	20300-28500	SFPE, Tbl. A.31
Seat lining	Polyester	Net	32500	SFPE, Tbl. A.38
Window / Window frame	PMMA	Net	25200	SFPE, Tbl. A.39
Window / Window frame	PMMA	Unspecified	26200	D, Tbl. 1.2
Window / Window frame	PMMA	Net	24890	D, Tbl. 1.13
Window / Window frame	PMMA	Unspecified	24900	IH, Ch. 7 Tbl. 6
Window / Window frame	Polycarbonate	Net	29720	D, Tbl. 1.13

Table A.4: Material density

Material Type	Material	Density (kg/m^3)	Reference
Aluminium	Aluminium: pure	2707	SFPE, Tbl. A.27
Accelerant	Gasoline	740	D, Tbl. 5.2
Accelerant	Heptane	675	SFPE, Tbl. 26.21
Accelerant	Heptane	675	D, Tbl. 5.2
Accelerant	Heptane	684	D, Tbl. 1.1
Accelerant	Kerosene	820	D, Tbl. 5.2
Accelerant	Liquid propane	585	D, Tbl. 5.2
Accelerant	Propane	585	D, Tbl. 1.1
Foam	Polyurethane	15	D, Tbl. 7.3
Foam	Polyurethane	22	D, Tbl. 7.3
Foam	Polyurethane	32	D, Tbl. 7.3
Foam	Polyurethane foams	20	D, Tbl. 2.1
Interior lining	Phenol formaldehyde	1300	SFPE, Tbl. A.36
Interior lining	Phenol formaldehyde (phenolic, Bakelite), 13.7 mm	1368	IH, Ch. 15 Tbl. 17
Interior lining	Phenolic, FR	1750	IH, Ch. 14 Tbl. 23
Latex foam	Latex	68-85	SF
Pleather	Polyurethane C32	270	IH, Ch. 14 Tbl. 185
Pleather	Polyurethane C42	300	IH, Ch. 14 Tbl. 185
Pleather	Polyurethane elastomer, 14.2 mm	1200	IH, Ch. 14 Tbl. 185
Pleather	Polyurethane F32	340	IH, Ch. 14 Tbl. 185
Pleather	Polyurethane F42	320	IH, Ch. 14 Tbl. 185
Pleather	Polyurethane G32	290	IH, Ch. 14 Tbl. 185
Pleather	Polyurethane G42	290	IH, Ch. 14 Tbl. 185
Pleather	Polyurethane H32	340	IH, Ch. 14 Tbl. 185
Pleather	Polyurethane H42	360	IH, Ch. 15 Tbl. 17
Pleather	Polyurethane rubber	1100	SFPE, Tbl. A.36
Pleather / Floor	Polyvinylchloride (PVC, flexible)	1260-1950	SFPE, Tbl. A.36

Table A.5: Material density continued

Material Type	Material	Density (kg/m^3)	Reference
Pleather / Floor / Window frame	PVC	1400	D, Tbl. 1.2
Pleather / Floor / Window frame	PVC minivan panel cover	1200	SFPE, Tbl. A.37
Pleather / Floor / Window frame	PVC non FR	1480	IH, Ch. 14 Tbl. 72
Pleather / Floor / Window frame	PVC siding	1890	IH, Ch. 15 Tbl. 19
Pleather / Floor / Window frame	PVC, clear, 13.2 mm	1478	IH, Ch. 15 Tbl. 17
Pleather / Floor / Window frame	PVC, clear, 3.1 mm	1384	IH, Ch. 15 Tbl. 17
Pleather / Floor / Window frame	PVC, FR	1505	IH, Ch. 15 Tbl. 19
Pleather / Floor / Window frame	PVC, FR A (reduced acid emission formulation)	1580	IH, Ch. 14 Tbl. 72
Pleather / Floor / Window frame	PVC, FR B (reduced acid emission formulation)	1560	IH, Ch. 14 Tbl. 72
Pleather / Floor / Window frame	PVC, FR C	1560	IH, Ch. 14 Tbl. 72
Pleather / Floor / Window frame	PVC, FR D (reduced acid emission formulation)	1510	IH, Ch. 14 Tbl. 72
Pleather / Floor / Window frame	PVC, grey, 13.2 mm	1433	IH, Ch. 15 Tbl. 17
Plywood backing	Eastern pine	64	IH, Ch. 14-137
Plywood backing	FR plywood	590	IH, Ch. 14 Tbl. 224
Plywood backing	Hoop pine, FR (4 mm)	580	IH, Ch. 14 Tbl. 223
Plywood backing	Japanese red pine	253	IH, Ch. 14-225
Plywood backing	Plywood	528	IH, Ch. 7 Tbl. 13
Plywood backing	Plywood	583	IH, Ch. 7 Tbl. 13
Plywood backing	Plywood	470	IH, Ch. 14 Tbl. 224
Plywood backing	Plywood	440	IH, Ch. 15 Tbl. 19
Plywood backing	Plywood (12 mm)	550	IH, Ch. 14 Tbl. 223
Plywood backing	Plywood (13 mm)	630	IH, Ch. 7 Tbl. 36
Plywood backing	Plywood (15 mm)	440	IH, Ch. 14 Tbl. 223
Plywood backing	Plywood (18 mm)	520	IH, Ch. 14 Tbl. 223
Plywood backing	Plywood (5.5 mm)	600	IH, Ch. 14 Tbl. 223
Plywood backing	Plywood (9 mm)	450	IH, Ch. 14 Tbl. 223
Plywood backing	Plywood (9.4 mm)	630	IH, Ch. 14 Tbl. 223
Plywood backing	Plywood, FR	460	IH, Ch. 15 Tbl. 19
Plywood backing	Plywood, FR (11.5 mm)	600	IH, Ch. 14 Tbl. 223
Plywood backing	Plywood, FR (15 mm)	460	IH, Ch. 14 Tbl. 223
Plywood backing	Plywood, FR (9 mm)	620	IH, Ch. 14 Tbl. 223
Plywood backing	Plywood: D. fir (ASTM; 5 plies)	541	IH, Ch. 15 Tbl. 19
Plywood backing	Plywood: D. fir (MB; 3 plies)	513	IH, Ch. 15 Tbl. 19
Plywood backing	Plywood: D. fir 9% MC	525	IH, Ch. 15 Tbl. 19
Plywood backing	Plywood: D. fir FR (ASTM; 5 plies)	558	IH, Ch. 15 Tbl. 19
Plywood backing	Plywood: oak veneer (Forintek; 5 plies)	479	IH, Ch. 15 Tbl. 19
Plywood backing	Plywood: Southern pine FRT (5 plies)	599	IH, Ch. 15 Tbl. 19

Table A.6: Material density continued

Material Type	Material	Density (kg/m^3)	Reference
Plywood backing	Plywood: Southern yellow pine 9% MC	600	IH, Ch. 15 Tbl. 19
Plywood backing	Plywood: Southern yellow pine FR 9% MC	580	IH, Ch. 15 Tbl. 19
Plywood backing	White pine	360	IH, Ch. 7 Tbl. 4
Plywood backing	White pine (30 degrees)	430	SFPE, Tbl. A.28
Plywood backing	Wood: Monterey pine 0% MC	460	IH, Ch. 15 Tbl. 19
Plywood backing	Wood: ponderosa pine 2% MC, rough surface	420	IH, Ch. 15 Tbl. 19
Plywood backing	Wood: ponderosa pine 9.3% MC, rough surface	420	IH, Ch. 15 Tbl. 19
Plywood backing	Wood: Southern pine 9.7% MC	508	IH, Ch. 15 Tbl. 19
Plywood backing	Yellow pine	640	D, Tbl. 2.1
Plywood backing	Yellow pine (23 degrees)	640	SFPE, Tbl. A.28
Seat lining	Unsaturated polyester	1230	SFPE, Tbl. A.36
Steel	Steel (mild)	8940	D, Tbl. 2.1
Window	Glass (plate)	2700	D, Tbl. 2.1
Window	Glass, window (20 degrees)	2700	SFPE, Tbl. A.28
Window / Window frame	PMMA	1190	SFPE, Tbl. A.36
Window / Window frame	PMMA	1190	D, Tbl. 1.2
Window / Window frame	PMMA (FIN)	1190	IH, Ch. 7 Tbl. 9
Window / Window frame	PMMA (PX)	1180	IH, Ch. 7 Tbl. 9
Window / Window frame	PMMA, black, 10 mm thick	1200	IH, Ch. 7 Tbl. 8
Window / Window frame	PMMA, black, 12.7 mm	1290	IH, Ch. 15 Tbl. 17
Window / Window frame	PMMA, black, 6.4 mm	1264	IH, Ch. 15 Tbl. 17
Window / Window frame	PMMA, clear, 12.7 mm	1187	IH, Ch. 15 Tbl. 17
Window / Window frame	PMMA, clear, 6.4 mm	1173	IH, Ch. 15 Tbl. 17
Window / Window frame	PMMA: clear glazing	1150	IH, Ch. 15 Tbl. 19
Window / Window frame	PMMA: clear glazing	1350	IH, Ch. 15 Tbl. 19
Window / Window frame	Polycarbonate	1200	SFPE, Tbl. A.36
Window / Window frame	Polycarbonate	1220	IH, Ch. 15 Tbl. 19
Window / Window frame	Polycarbonate (Lexan), 13 mm	1193	IH, Ch. 15 Tbl. 17
Window / Window frame	Polycarbonate minivan panel structure	1120	SFPE, Tbl. A.37
Window / Window frame	Polycarbonate minivan shelf, main panel	1180	SFPE, Tbl. A.37
Window / Window frame	Polycarbonate, FR, hollow inside	1200	IH, Ch. 15 Tbl. 19

Table A.7: Material specific heat

Material Type	Material	Specific Heat (kJ/(kg.K))	Reference
Aluminium	Aluminium: pure	0.896	SFPE, Tbl. A.27
Foam	Polyurethane foams	1.4	D, Tbl. 1.2
Interior lining	Phenol formaldehyde	1.42	SFPE, Tbl. A.36
Pleather / Floor	Polyvinylchloride (PVC, flexible)	1.14-1.38	SFPE, Tbl. A.36
Pleather / Floor / Window Frame	PVC	1.05	D, Tbl. 1.2
Pleather / Floor / Window Frame	PVC minivan panel cover	1.37	SFPE, Tbl. A.37
Pleather / Foam	Polyurethane C32	1.6	IH, Ch. 14 Tbl. 185
Pleather / Foam	Polyurethane C42	1.6	IH, Ch. 14 Tbl. 185
Pleather / Foam	Polyurethane F32	1.6	IH, Ch. 14 Tbl. 185
Pleather / Foam	Polyurethane F42	1.6	IH, Ch. 14 Tbl. 185
Pleather / Foam	Polyurethane G32	1.6	IH, Ch. 14 Tbl. 185
Pleather / Foam	Polyurethane G42	1.6	IH, Ch. 14 Tbl. 185
Pleather / Foam	Polyurethane H32	1.6	IH, Ch. 14 Tbl. 185
Pleather / Foam	Polyurethane H42	1.6	IH, Ch. 14 Tbl. 185
Pleather / Latex Foam	Polyurethane rubber	1.76	SFPE, Tbl. A.36
Plywood backing	FR plywood	2.3	IH, Ch. 14 Tbl. 224
Plywood backing	Plywood	2.3	IH, Ch. 14 Tbl. 224
Plywood backing	Yellow pine	2.85	D, Tbl. 2.1
Plywood backing	Yellow pine (23 degrees)	2.8	SFPE, Tbl. A.28
Seat lining	Unsaturated polyester	1.3	SFPE, Tbl. A.36
Seat lining	PET	1.03	ET
Steel	Steel (mild)	0.46	D, Tbl. 2.1
Window	Glass (plate)	0.84	D, Tbl. 2.1
Window	Glass, window (20 degrees)	0.84	SFPE, Tbl. A.28
Window / Window frame	PMMA	2.09	SFPE, Tbl. A.36
Window / Window frame	PMMA	1.42	D, Tbl. 1.2
Window / Window frame	PMMA (FIN)	1.46	IH, Ch. 7 Tbl. 9
Window / Window frame	PMMA (PX)	1.5	IH, Ch. 7 Tbl. 9
Window / Window frame	PMMA: Polycast	4.12	IH, Ch. 15 Tbl. 19
Window / Window frame	Polycarbonate	1.2-1.22	SFPE, Tbl. A.36
Window / Window frame	Polycarbonate minivan panel structure	1.68	SFPE, Tbl. A.37
Window / Window frame	Polycarbonate minivan shelf, main panel	1.51	SFPE, Tbl. A.37

Table A.8: Material thermal conductivity

Material Type	Material	Thermal Conductivity (W/m.K)	Reference
Aluminium	Aluminium: pure	202-249	SFPE, Tbl. A.27
Foam	Polyurethane foams	0.034	D, Tbl. 2.1
Interior lining	Phenol formaldehyde	0.25	SFPE, Tbl. A.36
Pleather / Floor	Polyvinylchloride (PVC, flexible)	0.17-0.26	SFPE, Tbl. A.36
Pleather / Floor / Window frame	PVC	0.16	D, Tbl. 1.2
Pleather / Floor / Window frame	PVC minivan panel cover	0.14	SFPE, Tbl. A.37
Pleather / Foam	Polyurethane C32	0.023	IH, Ch. 14 Tbl. 185
Pleather / Foam	Polyurethane C42	0.023	IH, Ch. 14 Tbl. 185
Pleather / Foam	Polyurethane F32	0.023	IH, Ch. 14 Tbl. 185
Pleather / Foam	Polyurethane F42	0.023	IH, Ch. 14 Tbl. 185
Pleather / Foam	Polyurethane G32	0.023	IH, Ch. 14 Tbl. 185
Pleather / Foam	Polyurethane G42	0.023	IH, Ch. 14 Tbl. 185
Pleather / Foam	Polyurethane H32	0.023	IH, Ch. 14 Tbl. 185
Pleather / Foam	Polyurethane H42	0.023	IH, Ch. 14 Tbl. 185
Pleather / Latex foam	Polyurethane rubber	0.19	SFPE, Tbl. A.36
Plywood backing	FR plywood	0.107	IH, Ch. 14 Tbl. 224
Plywood backing	Plywood	0.107	IH, Ch. 14 Tbl. 224
Plywood backing	Plywood: D. fir 9% MC	0.421	IH, Ch. 15 Tbl. 19
Plywood backing	Plywood: Southern yellow pine FR 9% MC	0.22	IH, Ch. 15 Tbl. 19
Plywood backing	White pine (30 degrees)	0.112	SFPE, Tbl. A.28
Plywood backing	Wood: ponderosa pine 2% MC, rough surface	0.158	IH, Ch. 15 Tbl. 19
Plywood backing	Wood: ponderosa pine 9.3% MC, rough surface	0.183	IH, Ch. 15 Tbl. 19
Plywood backing	Yellow pine	0.14	D, Tbl. 2.1
Plywood backing	Yellow pine (23 degrees)	0.147	SFPE, Tbl. A.28
Seat lining	Unsaturated polyester	0.17	SFPE, Tbl. A.36
Seat lining	Polyester (PET)	0.14	TSC
Seat lining	Polyester	0.05	ET
Steel	Steel (mild)	45.8	D, Tbl. 2.1
Window	Glass (plate)	0.76	D, Tbl. 2.1
Window	Glass, window (20 degrees)	0.78	SFPE, Tbl. A.28
Window / Window frame	PMMA	0.27	SFPE, Tbl. A.36
Window / Window frame	PMMA	0.19	D, Tbl. 1.2
Window / Window frame	PMMA (FIN)	0.21	IH, Ch. 7 Tbl. 9
Window / Window frame	PMMA (PX)	0.17	IH, Ch. 7 Tbl. 9
Window / Window frame	PMMA: Polycast	0.432	IH, Ch. 15 Tbl. 19
Window / Window frame	Polycarbonate	0.2-0.21	SFPE, Tbl. A.36
Window / Window frame	Polycarbonate minivan panel structure	0.18	SFPE, Tbl. A.37
Window / Window frame	Polycarbonate minivan shelf, main panel	0.27	SFPE, Tbl. A.37

Table A.9: Material emissivity

Material Type	Material	Emissivity	Reference
Accelerant	Kerosene	0.37	D, Tbl. 5.4
Accelerant	Petrol	0.36	D, Tbl. 5.4
Aluminium	Aluminium: Ordinarily rolled (100°C)	0.035	SFPE, Tbl. 4.2
Aluminium	Aluminium: Ordinarily rolled (500°C)	0.05	SFPE, Tbl. 4.2
Aluminium	Aluminium: Highly polished (1°C)	0.04-0.05	SFPE, Tbl. 4.2
Foam	Polyurethane foams	0.17	D, Tbl. 5.11
Interior lining	Lacquer: Bakelite	0.93	TW
Latex foam	Rubber (soft, grey)	0.86	SFPE, Tbl. 4.3
Pleather / Floor / Window frame	PVC	0.91-0.93	TW
Plywood backing	Plywood	0.83-0.98	TW
Plywood backing	Plywood: commercial, smooth finish, dry	0.82	TW
Seat lining	Polyester	0.75-0.85	OT
Steel	Mild steel (polished)	0.1	TV
Steel	Mild steel (smooth)	0.12	TV
Steel	Polished sheet: 260°C	0.1	TV
Steel	Polished sheet: 38°C	0.07	TV
Steel	Polished sheet: 538°C	0.14	TV
Steel	Steel Galvanised Old	0.88	ET
Steel	Steel: galvanised	0.28	TW
Window	Glass (fused quartz)	0.75-0.8	SFPE, Tbl. 4.3
Window	Glass Nonex	0.82-0.78	SFPE, Tbl. 4.3
Window	Glass Smooth	0.92-0.95	SFPE, Tbl. 4.3
Window	Plexiglass: Perspex	0.86	TW
Window	Pyrex	0.8-0.9	SFPE, Tbl. 4.3
Window / Window frame	PMMA	0.25	D, Tbl. 5.11
Window / Window frame	PMMA	0.26	D, Tbl. 2.11
Window / Window frame	Polycarbonate (40-60°C)	0.88-0.89	DL

Table A.10: Material ignition temperature

Material Type	Material	Ignition Temperature (°C)		Reference
Accelerant	Diesel	Auto-ignition	225-256	IH, Ch. 15 Tbl. 2
Accelerant	Gasoline	Auto-ignition	300-350	IH, Ch. 15 Tbl. 2
Accelerant	Gasoline, 100 octane	Auto-ignition	429	IH, Ch. 15 Tbl. 2
Accelerant	Gasoline, 65 octane	Auto-ignition	248	IH, Ch. 15 Tbl. 2
Accelerant	Gasoline, 75 octane	Auto-ignition	258	IH, Ch. 15 Tbl. 2
Accelerant	Gasoline, 92 octane	Auto-ignition	390	IH, Ch. 15 Tbl. 2
Accelerant	Gasoline, 87 octane	Auto-ignition	412	IH, Ch. 15 Tbl. 2
Accelerant	Heptane	Auto-ignition	223-255	D, Tbl. 6.2
Accelerant	Heptane	Auto-ignition	223	IH, Ch. 15 Tbl. 1B
Accelerant	Heptane	Auto-ignition	215	SFPE, Tbl. 17.1
Accelerant	Heptane	Auto-ignition	223	SFPE, Tbl. 18.2
Accelerant	Heptane	Spontaneous	247.2	SFPE, Tbl. A.29
Accelerant	Heptane	Auto-ignition	222.8	SFPE, Tbl. A.34
Accelerant	Kerosene	Auto-ignition	210-283	D, Tbl. 6.2
Accelerant	Kerosene	Auto-ignition	227	IH, Ch. 15 Tbl. 2
Accelerant	Mineral spirits, incl. some lighter fluids and charcoal lighters	Auto-ignition	242	IH, Ch. 15 Tbl. 2

Table A.11: Material ignition temperature continued

Material Type	Material	Ignition Temperature (°C)		Reference
Accelerant	Newspaper	Piloted & Auto-ignition	229	IH, Ch. 15 Tbl. 15
Accelerant	Paraffin wax	Auto-ignition	245	IH, Ch. 15 Tbl. 2
Accelerant	Propane	Auto-ignition	500	IH, Ch. 15 Tbl. 1B
Accelerant	Turpentine	Auto-ignition	252	IH, Ch. 15 Tbl. 2
Floor	PVC 4 flooring	Computed	119	IH, Ch. 14 Tbl. 129
Floor	Rubber flooring (rubber tile)	Computed	183	IH, Ch. 14 Tbl. 129
Floor	PVC 5 flooring	Computed	189	IH, Ch. 14 Tbl. 129
Floor	PVC 3 flooring (soft PVC)	Computed	222	IH, Ch. 14 Tbl. 129
Floor	PVC 2 flooring (PVC tile)	Computed	373	IH, Ch. 14 Tbl. 129
Floor	PVC 1 flooring (PVC tile)	Computed	395	IH, Ch. 14 Tbl. 129
Floor / Window frame	PVC, rigid, FR	Auto-ignition	571	IH, Ch. 15 Tbl. 15
Floor / Window frame	PVC, rigid	Auto-ignition	480-550	IH, Ch. 15 Tbl. 15
Foam	Polyurethane foam, flexible	Auto-ignition	370-378	IH, Ch. 14 Tbl. 173
Foam	Polyurethane foam, flexible	Piloted & Auto-ignition	335	IH, Ch. 15 Tbl. 15
Foam	Polyurethane foam, flexible	Auto-ignition	370-378	IH, Ch. 15 Tbl. 15
Foam	Polyurethane, foam	Auto-ignition	528	IH, Ch. 15 Tbl. 15
Foam	Polyurethane, FR foam 10% P	Auto-ignition	638	IH, Ch. 15 Tbl. 15
Foam	Polyurethane, FR foam 5% P 50% Cl	Auto-ignition	554	IH, Ch. 15 Tbl. 15
Foam	Polyurethane, FR foam 50% Cl	Auto-ignition	528	IH, Ch. 15 Tbl. 15
Interior lining	Phenol formaldehyde	Auto-ignition	482-614	IH, Ch. 15 Tbl. 15
Interior lining	Phenol formaldehyde	Unspecified	429	SFPE, Tbl. A.36
Interior lining	Phenol formaldehyde with paper reinforcement	Auto-ignition	367-430	IH, Ch. 15 Tbl. 15
Interior lining	Phenol formaldehyde with paper reinforcement	Piloted	300-311	IH, Ch. 15 Tbl. 15
Interior lining	Phenol formaldehyde with paper reinforcement	Auto-ignition	399	IH, Ch. 7 Tbl. 20
Interior lining	Phenol formaldehyde, solid	Auto-ignition	482	IH, Ch. 14 Tbl. 173
Interior lining	Phenolic, FR	Unspecified	450	IH, Ch. 14 Tbl. 23
Latex foam	Latex foam (natural rubber)	Auto-ignition	310	IH, Ch. 15 Tbl. 15
Pleather	Polyurethane solid (not foam)	Piloted	271	IH, Ch. 15 Tbl. 15
Pleather	PVC foam, flexible	Piloted & Auto-ignition	441	IH, Ch. 15 Tbl. 15
Pleather / Floor	PVC, semi-rigid, with 40 phr dioctyl phthalate plasticiser	Auto-ignition	294	IH, Ch. 15 Tbl. 15
Pleather / Floor	PVC, semi-rigid, with 50 phr dioctyl phthalate plasticiser	Auto-ignition	311	IH, Ch. 15 Tbl. 15
Pleather / Floor	PVC, flexible	Auto-ignition	424	IH, Ch. 15 Tbl. 15
Pleather / Floor	PVC, flexible	Auto-ignition	441	IH, Ch. 15 Tbl. 15
Pleather / Floor	Polyvinylchloride (PVC, flexible)	Unspecified	318-374	SFPE, Tbl. A.36
Pleather / Floor	PVC, film	Auto-ignition	438-454	IH, Ch. 14 Tbl. 173
Pleather / Floor	PVC, film	Auto-ignition	438-454	IH, Ch. 15 Tbl. 15

Table A.12: Material ignition temperature continued

Material Type	Material	Ignition Temperature (°C)		Reference
Pleather / Floor / Window frame	PVC minivan panel cover	Unspecified	357	SFPE, Tbl. A.37
Pleather / Floor / Window frame	PVC/acrylic (Kydex)	Computed	376	IH, Ch. 15 Tbl. 19
Pleather / Floor / Window frame	PVC, FR	Computed	415	IH, Ch. 15 Tbl. 19
Pleather / Floor / Window frame	PVC siding	Computed	427	IH, Ch. 15 Tbl. 19
Pleather / Floor / Window frame	PVC, unspecified grade	Auto-ignition	454	IH, Ch. 15 Tbl. 15
Pleather / Floor / Window frame	PVC	Auto-ignition	455	IH, Ch. 14 Tbl. 105
Pleather / Floor / Window frame	PVC, unplasticised	Auto-ignition	474	IH, Ch. 14 Tbl. 173
Pleather / Floor / Window frame	PVC FR	Unspecified	500	IH, Ch. 14 Tbl. 104
Pleather / Floor / Window frame	PVC, pure without plasticiser	Auto-ignition	474-600	IH, Ch. 15 Tbl. 15
Pleather / Foam	Polyurethane	Auto-ignition	415	IH, Ch. 14 Tbl. 105
Pleather / Foam	Polyurethane, flexible, high resilience	Auto-ignition	413-429	IH, Ch. 14 Tbl. 182
Pleather / Foam	Polyurethane, flexible	Auto-ignition	426-445	IH, Ch. 14 Tbl. 182
Pleather / Foam	Polyurethane, flexible, FR	Auto-ignition	430-450	IH, Ch. 14 Tbl. 182
Pleather / Foam	Polyurethane, high resilience, FR	Auto-ignition	431-453	IH, Ch. 14 Tbl. 182
Pleather / Latex foam	Polyurethane rubber	Unspecified	356	SFPE, Tbl. A.36
Plywood backing	Georgia pine	Auto-ignition	203	IH, Ch. 7 Tbl. 2
Plywood backing	Pine-heartwood	Auto-ignition	238-300	IH, Ch. 14 Tbl. 215
Plywood backing	Pine-sapwood	Auto-ignition	239	IH, Ch. 14 Tbl. 215
Plywood backing	Plywood	Computed	386	IH, Ch. 15 Tbl. 19
Plywood backing	Plywood	Computed	390	IH, Ch. 15 Tbl. 19
Plywood backing	Plywood	Computed	290	IH, Ch. 15 Tbl. 19
Plywood backing	Plywood	Computed	620	IH, Ch. 15 Tbl. 19
Plywood backing	Plywood	Computed	373	IH, Ch. 15 Tbl. 19
Plywood backing	Plywood	Unspecified	390	SFPE, Tbl. 21.3
Plywood backing	Plywood (13 mm)	Auto-ignition	254	IH, Ch. 7 Tbl. 36
Plywood backing	Plywood FR (12.7mm)	Unspecified	620	SFPE, Tbl. 23.1
Plywood backing	Plywood, FR	Computed	480	IH, Ch. 15 Tbl. 19
Plywood backing	Plywood: D. fir -- FR	Computed	362	IH, Ch. 15 Tbl. 19
Plywood backing	Plywood: D. fir -- FR	Computed	387	IH, Ch. 15 Tbl. 19
Plywood backing	Plywood: D. fir (ASTM)	Computed	336	IH, Ch. 15 Tbl. 19
Plywood backing	Plywood: D. fir (ASTM; 5 plies)	Computed	355	IH, Ch. 15 Tbl. 19
Plywood backing	Plywood: D. fir (MB)	Computed	326	IH, Ch. 15 Tbl. 19
Plywood backing	Plywood: D. fir (MB; 3 plies)	Computed	369	IH, Ch. 15 Tbl. 19
Plywood backing	Plywood: D. fir 9% MC	Unspecified	368	IH, Ch. 15 Tbl. 19
Plywood backing	Plywood: D. fir FR (ASTM; 5 plies)	Computed	362	IH, Ch. 15 Tbl. 19

Table A.13: Material ignition temperature continued

Material Type	Material	Ignition Temperature (°C)		Reference
Plywood backing	Plywood: oak veneer	Computed	357	IH, Ch. 15 Tbl. 19
Plywood backing	Plywood: oak veneer (Forintek; 5 plies)	Computed	280	IH, Ch. 15 Tbl. 19
Plywood backing	Plywood: Southern pine	Computed	323	IH, Ch. 15 Tbl. 19
Plywood backing	Plywood: Southern pine FRT (5 plies)	Computed	403	IH, Ch. 15 Tbl. 19
Plywood backing	Plywood: Southern yellow pine 9% MC	Unspecified	368	IH, Ch. 15 Tbl. 19
Plywood backing	White pine	Piloted	375-446	IH, Ch. 7 Tbl. 4
Plywood backing	Wood: Monterey pine 0% MC	Unspecified	349	IH, Ch. 15 Tbl. 19
Plywood backing	Wood: Monterey pine 11% MC	Unspecified	340	IH, Ch. 15 Tbl. 19
Plywood backing	Wood: ponderosa pine 2% MC, rough surface	Computed	288	IH, Ch. 15 Tbl. 19
Plywood backing	Wood: ponderosa pine 9.3% MC, rough surface	Computed	367	IH, Ch. 15 Tbl. 19
Plywood backing	Wood: Southern pine 9.7% MC	Computed	320	IH, Ch. 15 Tbl. 19
Plywood backing	Wood: Southern pine 95 Cone 0.27 1.60×10-7 0.88 367	Computed	367	IH, Ch. 15 Tbl. 19
Seat lining	Unsaturated polyester	Unspecified	380	SFPE, Tbl. A.36
Seat lining	Polyester	Auto-ignition	485-508	IH, Ch. 14 Tbl. 105
Seat lining	Polyester	Piloted	372-390	IH, Ch. 14 Tbl. 105
Seat lining	Polyester	Piloted	379	IH, Ch. 14 Tbl. 108
Seat lining	Polyester, unsaturated	Auto-ignition	420-500	IH, Ch. 14 Tbl. 108
Window / Window frame	PMMA	Piloted	310	D, Tbl. 6.8
Window / Window frame	PMMA	Auto-ignition	392-520	IH, Ch. 15 Tbl. 15
Window / Window frame	PMMA	Auto-ignition	456	IH, Ch. 7 Tbl. 20
Window / Window frame	PMMA	Unspecified	380	SFPE, Tbl. 21.3
Window / Window frame	PMMA	Unspecified	378-383	SFPE, Tbl. A.36
Window / Window frame	PMMA (FIN)	Unspecified	311	IH, Ch. 7 Tbl. 10
Window / Window frame	PMMA (PX)	Unspecified	311	IH, Ch. 7 Tbl. 10
Window / Window frame	PMMA with halogenated FR agents	Unspecified	370-376	IH, Ch. 7 Tbl. 34
Window / Window frame	PMMA without FR	Unspecified	306-312	IH, Ch. 7 Tbl. 34
Window / Window frame	PMMA, black, 10 mm thick	Unspecified	266	IH, Ch. 7 Tbl. 8
Window / Window frame	PMMA: black, Polycast	Unspecified	250-355	IH, Ch. 15 Tbl. 19
Window / Window frame	PMMA: clear glazing	Computed	195	IH, Ch. 15 Tbl. 19
Window / Window frame	PMMA: clear glazing	Computed	289	IH, Ch. 15 Tbl. 19
Window / Window frame	PMMA: Polycast	Computed	278	IH, Ch. 15 Tbl. 19
Window / Window frame	PMMA: Type G	Computed	378	IH, Ch. 15 Tbl. 19
Window / Window frame	PMMA: unspecified	Unspecified	345	IH, Ch. 15 Tbl. 19

Table A.14: Material ignition temperature continued

Material Type	Material	Ignition Temperature (°C)		Reference
Window / Window frame	Polycarbonate	Auto-ignition	516-580	IH, Ch. 15 Tbl. 15
Window / Window frame	Polycarbonate	Computed	528	IH, Ch. 15 Tbl. 19
Window / Window frame	Polycarbonate	Computed	561	IH, Ch. 15 Tbl. 19
Window / Window frame	Polycarbonate	Computed	455-464	IH, Ch. 15 Tbl. 19
Window / Window frame	Polycarbonate	Unspecified	500-580	SFPE, Tbl. A.36
Window / Window frame	Polycarbonate (Lexan 9034)	Computed	485	IH, Ch. 15 Tbl. 19
Window / Window frame	Polycarbonate minivan shelf, main panel	Unspecified	497	SFPE, Tbl. A.37
Window / Window frame	Polycarbonate, FR, hollow inside	Computed	495	IH, Ch. 15 Tbl. 19
Window / Window frame	Polycarbonate/ polyetherimide	Computed	518	IH, Ch. 15 Tbl. 19
Window / Window frame	Polycarbonate/ABS	Unspecified	440	IH, Ch. 15 Tbl. 19
Window / Window frame	Polycarbonate/ABS, FR	Unspecified	440	IH, Ch. 15 Tbl. 19

Table A.15: Material critical heat flux

Material Type	Material	Critical Heat Flux (kW/m^2)	Reference
Accelerant	Newspaper	10	SFPE, Tbl. A.35
Floor	PVC 1 flooring (PVC tile)	16.78	IH, Ch. 14 Tbl. 129
Floor	PVC 2 flooring (PVC tile)	14	IH, Ch. 14 Tbl. 129
Floor	PVC 3 flooring (soft PVC)	93	IH, Ch. 14 Tbl. 129
Floor	PVC 4 flooring	6.13	IH, Ch. 14 Tbl. 129
Floor	PVC 5 flooring	2.42	IH, Ch. 14 Tbl. 129
Floor	Rubber flooring (rubber tile)	4.74	IH, Ch. 14 Tbl. 129
Foam	Polyurethane foams (flexible)	53 (radiative)	SFPE, Tbl. 36.16
Interior lining	Phenol	15-26	SFPE, Tbl. A.35
Interior lining	Phenol formaldehyde	20	SFPE, Tbl. A.35
Interior lining	Phenol formaldehyde (phenolic, Bakelite), 13.7 mm	26	IH, Ch. 15 Tbl. 17
Latex foam	Latex	16	SFPE, Tbl. A.35
Latex foam	Rubber, natural, 12.7 mm	17.1	IH, Ch. 15 Tbl. 17
Latex foam	Silicone rubber, 12.2 mm	34.1	IH, Ch. 15 Tbl. 17
Pleather	Polyurethane elastomer, 14.2 mm	22.5	IH, Ch. 15 Tbl. 17
Pleather	PVC fabric (ASTM E2058 FPA)	26	SFPE, Tbl. A.35
Pleather / Floor	PVC sheets (ASTM E2058 FPA)	15	SFPE, Tbl. A.35
Pleather / Floor	PVC, flexible (ASTM E1354 Cone)	21	SFPE, Tbl. A.35
Pleather / Floor	PVC, flexible (ASTM E2058 FPA)	10	SFPE, Tbl. A.35
Pleather / Floor / Window frame	PVC, clear, 13.2 mm	20.5	IH, Ch. 15 Tbl. 17
Pleather / Floor / Window frame	PVC, clear, 3.1 mm	52.8	IH, Ch. 15 Tbl. 17
Pleather / Floor / Window frame	PVC, grey, 13.2 mm	27.5	IH, Ch. 15 Tbl. 17
Pleather / Foam	Polyurethane, flexible	16.4	IH, Ch. 14 Tbl. 182
Pleather / Foam	Polyurethane, flexible, FR	20	IH, Ch. 14 Tbl. 182
Plywood backing	Plywood	10.7	IH, Ch. 15 Tbl. 19
Plywood backing	Plywood: D. fir -- FR	14	IH, Ch. 15 Tbl. 19
Plywood backing	Plywood: D. fir (ASTM; 5 plies)	13.6	IH, Ch. 15 Tbl. 19

Table A.16: Material critical heat flux continued

Material Type	Material	Critical Heat Flux (kW/m²)	Reference
Plywood backing	Plywood: D. fir (MB; 3 plies)	15.2	IH, Ch. 15 Tbl. 19
Plywood backing	Plywood: D. fir FR (ASTM; 5 plies)	14	IH, Ch. 15 Tbl. 19
Plywood backing	Plywood: oak veneer (Forintek; 5 plies)	8.9	IH, Ch. 15 Tbl. 19
Plywood backing	Plywood: Southern pine FRT (5 plies)	17.3	IH, Ch. 15 Tbl. 19
Plywood backing	White pine	4.51	IH, Ch. 14-129
Plywood backing	Wood: Monterey pine 0% MC	13.1	IH, Ch. 15 Tbl. 19
Plywood backing	Wood: Monterey pine 11% MC	10.8	IH, Ch. 15 Tbl. 19
Plywood backing	Wood: Southern pine 9.7% MC	10.7	IH, Ch. 15 Tbl. 19
Seat lining	Polyester	10-15	SFPE, Tbl. A.35
Seat lining	Polyester	4.5	IH, Ch. 14 Tbl. 131
Window / Window frame	PC panel (ASTM E2058 FPA)	16	SFPE, Tbl. A.35
Window / Window frame	PMMA	3.33	IH, Ch. 7 Tbl. 7
Window / Window frame	PMMA (FIN)	4.7	IH, Ch. 7 Tbl. 7
Window / Window frame	PMMA (PX)	4.3	IH, Ch. 7 Tbl. 7
Window / Window frame	PMMA, black, 10 mm thick	3.33	IH, Ch. 7 Tbl. 8
Window / Window frame	PMMA, black, 12.7 mm	18.6	IH, Ch. 15 Tbl. 17
Window / Window frame	PMMA, black, 6.4 mm	7.2	IH, Ch. 15 Tbl. 17
Window / Window frame	PMMA, clear, 12.7 mm	7.1	IH, Ch. 15 Tbl. 17
Window / Window frame	PMMA, clear, 6.4 mm	5.7	IH, Ch. 15 Tbl. 17
Window / Window frame	PMMA: clear glazing	4	IH, Ch. 15 Tbl. 19
Window / Window frame	Polycarbonate	23	IH, Ch. 15 Tbl. 19
Window / Window frame	Polycarbonate (ASTM E1354 Cone)	15-20	SFPE, Tbl. A.35
Window / Window frame	Polycarbonate (ASTM E2058 FPA)	15	SFPE, Tbl. A.35
Window / Window frame	Polycarbonate (Lexan 9034)	26	IH, Ch. 15 Tbl. 19
Window / Window frame	Polycarbonate (Lexan), 13 mm	11.5	IH, Ch. 15 Tbl. 17

Appendix B

Mass Loss Rate Data

Figure B.1 to Figure B.4 show the MLR for each experiment. The MLR was calculated by dividing the change in mass by the change in time between adjacent recorded time steps.
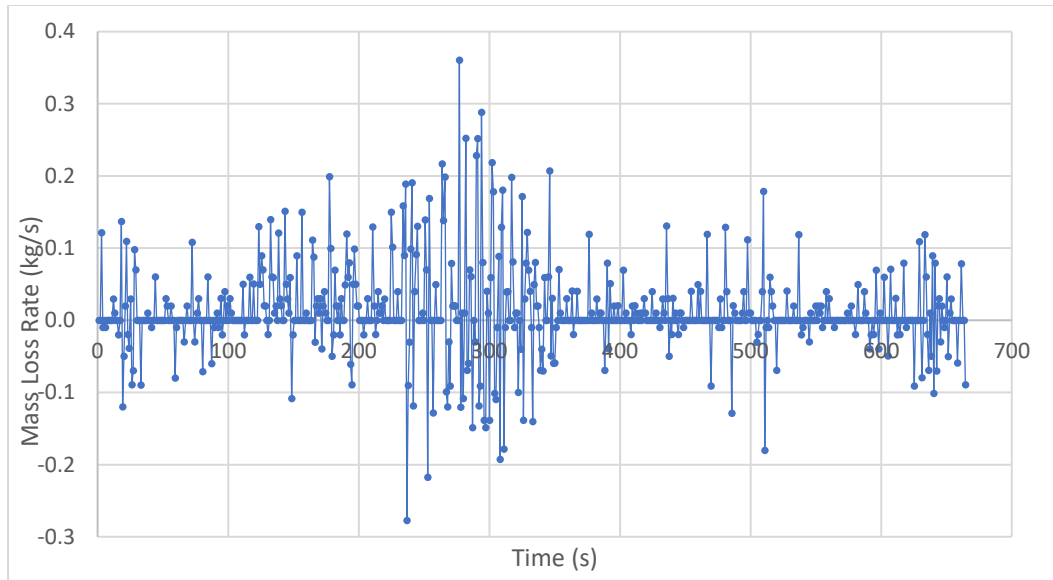
Figure B.1: Experiment 1 - MLR
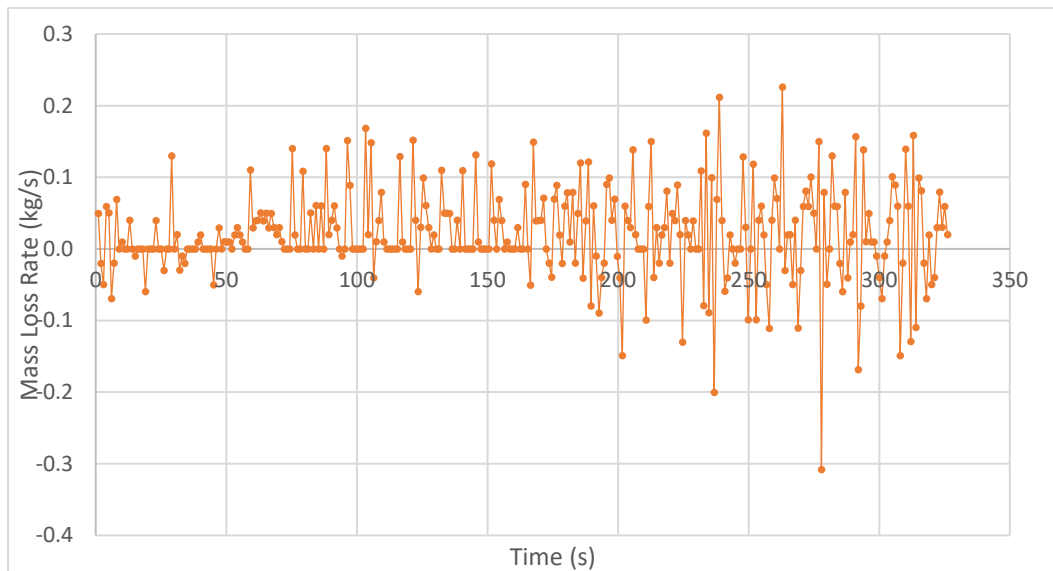
Figure B.2: Experiment 2 - MLR
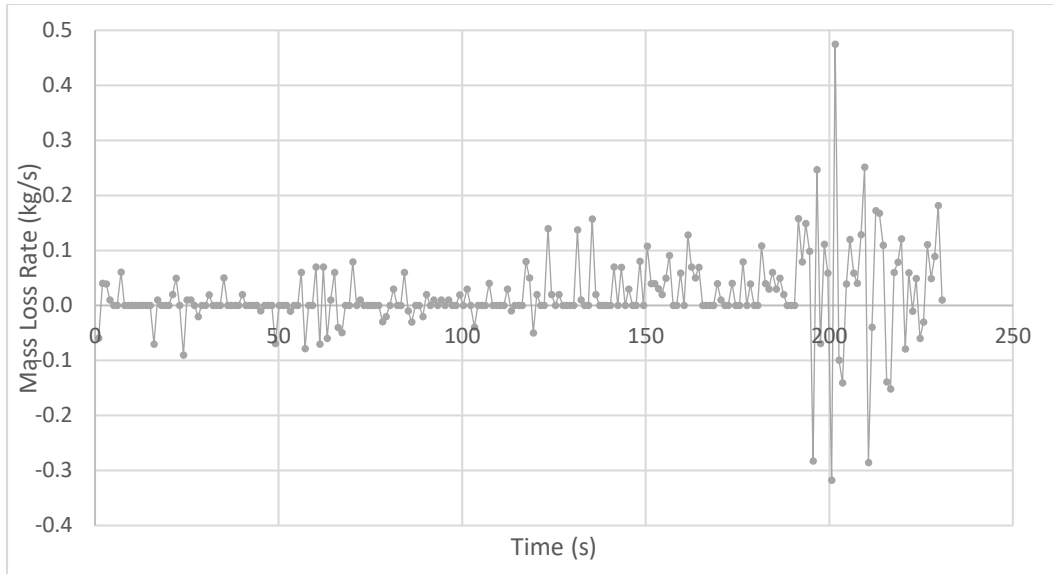
Figure B.3: Experiment 3 - MLR
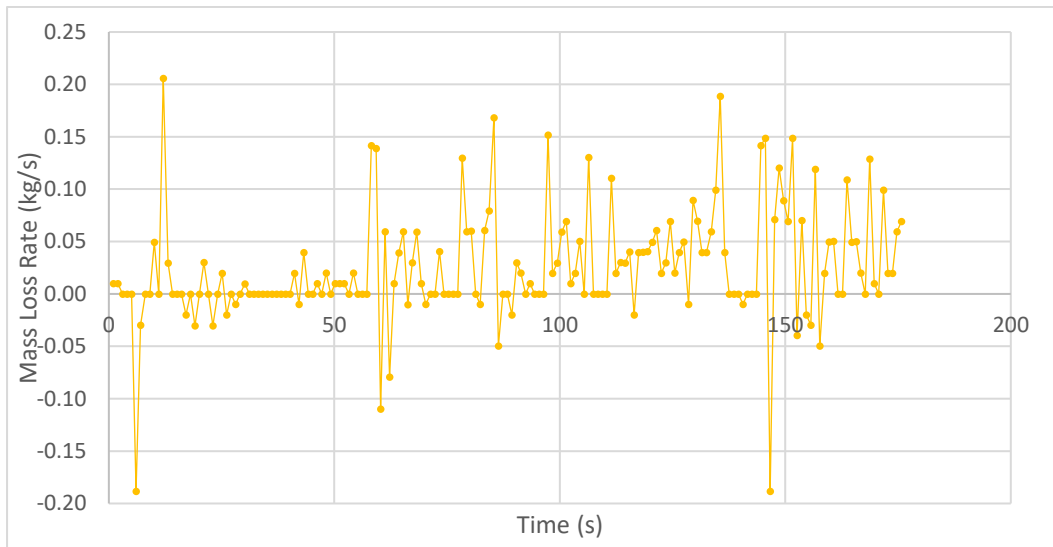
Figure B.4: Experiment 4 - MLR

Backward Difference Method

Equation B.1 is the standard method of differentiation between two data points and calculates the change in mass over the change in time between two adjacent data points which were recorded during the experiment.

Equation B.1: MLR - backward difference method

$$\frac{dm_i}{dt_i} = \frac{m_{i-1} - m_i}{t_i - t_{i-1}}$$

Central Difference Method

For this method, also used by Staggs (2005), the differentiation is done by considering the data point before and after the data point under consideration to determine an average mass loss which is then divided by the change in time between two adjacent data points recorded during the experiment, as per Equation B.2. Staggs recommends this method over the ISO 5660 method due to the comparatively lower variance in the noise.

Equation B.2: MLR - central difference method

$$\frac{dm_i}{dt_i} = \frac{\frac{m_{i-1} - m_{i+1}}{2}}{t_i - t_{i-1}}$$

As this method was recommended by Staggs (2005), it was expanded to span over more data points, between the original 3 and 15 data points. It was also expanded to further smooth the data by averaging the MLR obtained over between 3 and 21 resultant MLR values, spaced centrally over the MLR value under consideration. Due to the inclusion of data points over a range of up to 15 data points, the MLR may remove the peaks and troughs of the curve, the standard central difference method was considered to be most representative. The smoothed MLR curve, averaging over a number of MLR values, gave the best results when using 11, 13 and 15 MLR values for averaging, as can be seen in Figure B.5 and Figure B.6. Averaging over 15 MLR values gave the smoothest data for the central difference method, as can be seen in Figure B.7.

ISO 5660 Method

The method given in ISO 5660 to calculate the MLR from recorded scale data makes use of five-point numerical differentiation. Formulae (Equation B.4 to Equation B.7) are specified for the first two and last two data points where there are not enough data points before or after the data point being considered to be able to use the generic formula (Equation B.3).

Equation B.3: MLR - ISO 5660 method – ith data point

$$\frac{dm_i}{dt_i} = \frac{m_{i-2} - m_{i+2} - 8(m_{i-1} - m_{i+1})}{12(t_i - t_{i-1})}$$

Equation B.4: MLR - ISO 5660 method - first data point

$$\frac{dm_0}{dt_0} = \frac{-25m_0 + 48m_1 - 36m_2 + 16m_3 - 3m_4}{12(t_0 - t_{-1})}$$

Equation B.5: MLR - ISO 5660 method - second data point

$$\frac{dm_1}{dt_1} = \frac{-3m_0 - 10m_1 + 18m_2 - 6m_3 + m_4}{12(t_1 - t_0)}$$

Equation B.6: MLR - ISO 5660 method - second last data point

$$\frac{dm_{n-1}}{dt_{n-1}} = \frac{3m_n + 10m_{n-1} - 18m_{n-2} + 6m_{n-3} - m_{n-4}}{12(t_{n-1} - t_{n-2})}$$

Equation B.7: MLR - ISO 5660 method - last data point

$$\frac{dm_0}{dt_0} = \frac{25m_n - 48m_{n-1} + 36m_{n-2} - 16m_{n-3} + 3m_{n-4}}{12(t_n - t_{-1})}$$

Staggs found that this method produced a lower truncation error but a higher variance in the noise than the central difference method (2005).

Savitzky-Golay Data Filter

The Savitzky-Golay filter works well for smoothing data as it is a low-pass filter. Staggs found that this filter greatly improved noisy MLR curves, using a polynomial of order 2 and 11 symmetrical points (2005). As the data obtained from the scale was extremely noisy, 15, 17, 21 and 29 data points were considered. The best results were obtained using 29 data points, 14 on each side of the mass value under consideration. The mass value calculated for each point in time was determined by applying Equation B.8. Where there were fewer points before the mass value under consideration, the same mass value was used as m_0 as the mass remains constant before ignition takes place. The data was cut off at a point where the data points after the mass value under consideration, would no longer be enough, as there is no way to extend the mass data past the point of extinguishment. In the case of 29 data points, the smoothed mass data was cut off at 14 s before the fire was extinguished.

Equation B.8: Savitzky-Golay method (order: 2, data points: 29)

$$m_i' = \frac{\sum_{j=i-14}^{j=i+14} k_j m_j}{8091}$$

With k being the corresponding coefficient of data point m_j in Table B.1.

Table B.1: Savitzky-Golay coefficients (order: 2, data points: 29) (James, no date)

Data Point	Coefficient
i	629
i±1	624
i±2	609
i±3	584
i±4	549
i±5	504
i±6	449
i±7	384
i±8	309
i±9	224
i±10	129
i±11	24
i±12	-91
i±13	-216
i±14	-351

After applying the smoothing filter, Equation B.1 is applied as normal to obtain the mass loss data. In Figure B.5 and Figure B.6, the methods are compared to one another, and the averaged data from the central difference method and Savitzky-Golay filter method clearly show a great improvement compared to the backward difference and ISO 5660 methods.
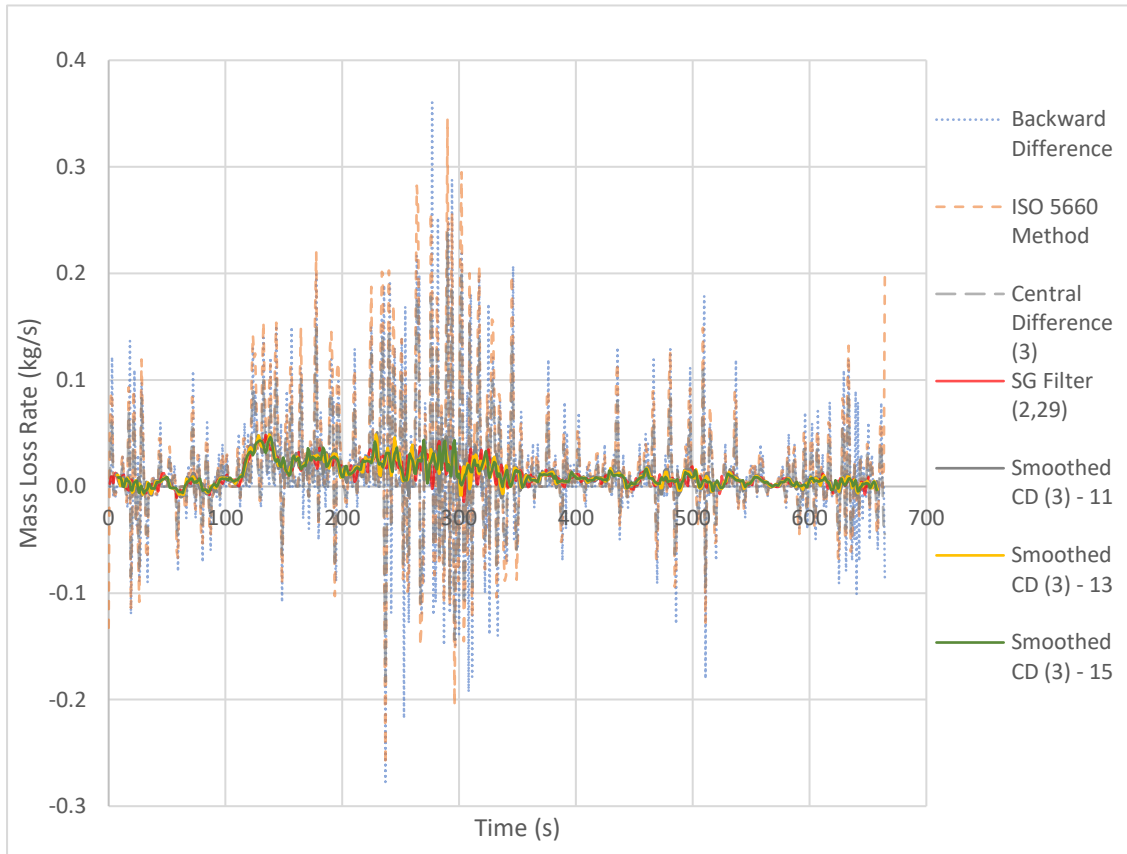
Figure B.5: Experiment 1 MLR data smoothing
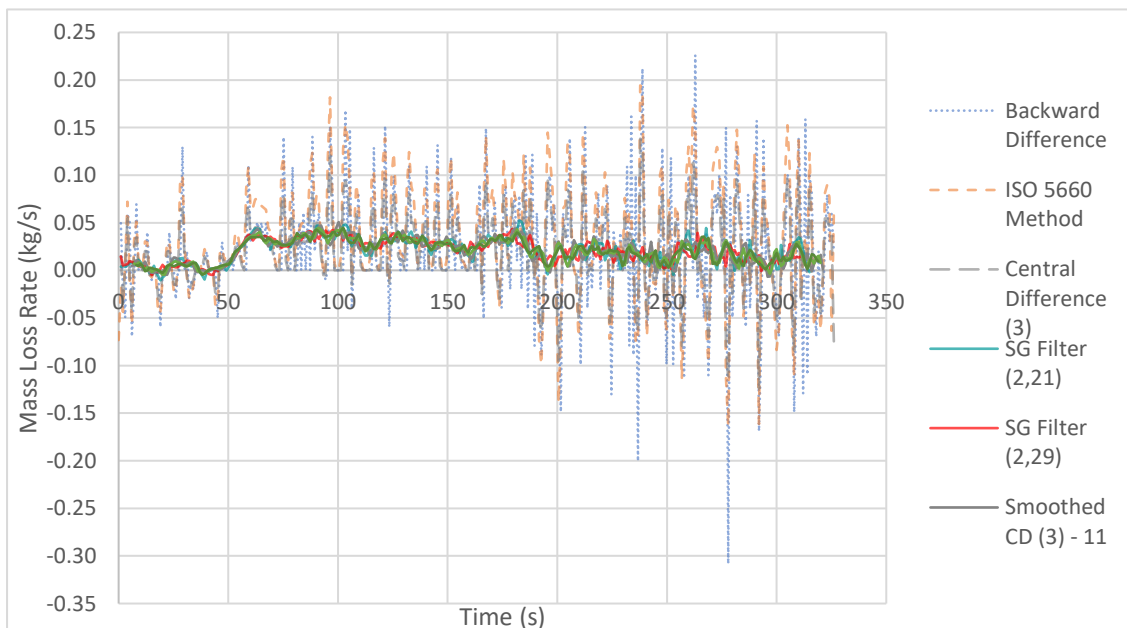
Figure B.6: Experiment 2 MLR data smoothing

When considering only the case where the central difference method data is averaged over 15 data points, and the Savitzky-Golay method of order 2 over 29 data points, as in Figure B.7, the Savitzky-Golay filter clearly has a much smoother curve. The Savitzky-Golay filter of order 2 over 29 data points was thus used to create a curve which was used in the modelling of each experiment.
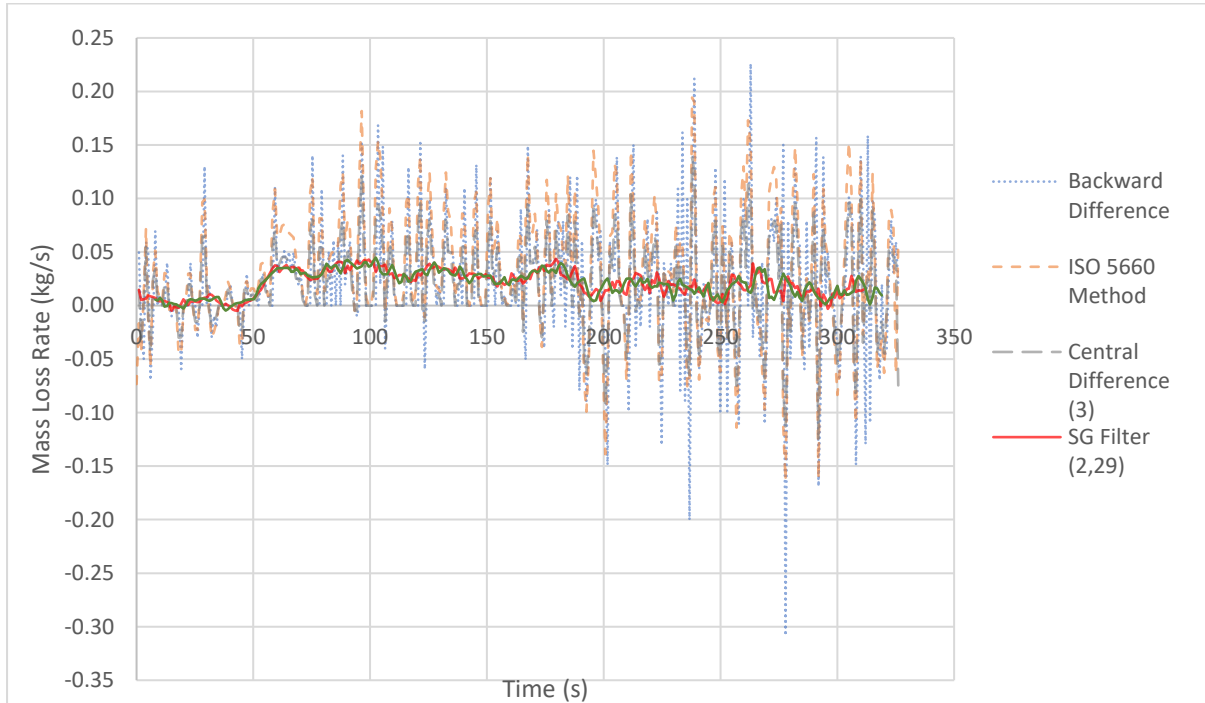
Figure B.7: Experiment 2 MLR data smoothing – Savitzky-Golay vs smoothed central difference

Temperature and Heat Flux
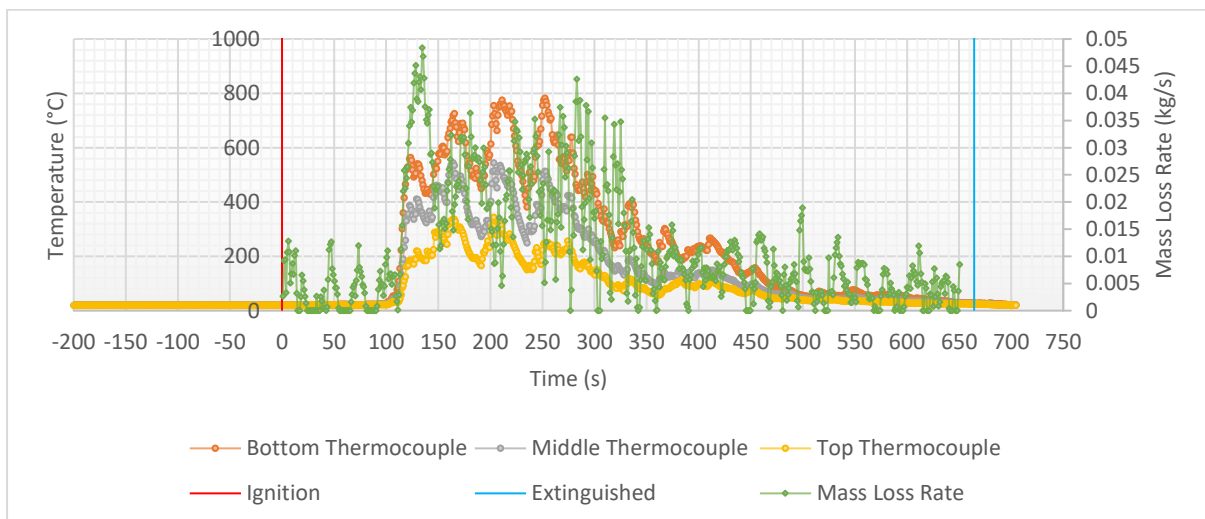
Figure B.8: Experiment 1 - MLR and temperature
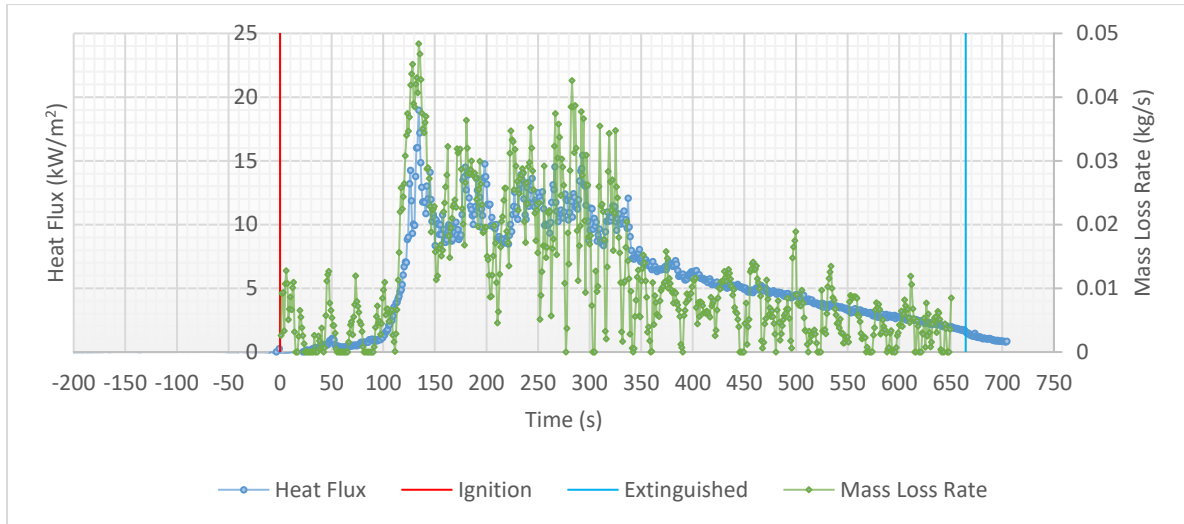
Figure B.9: Experiment 1 - MLR and heat flux
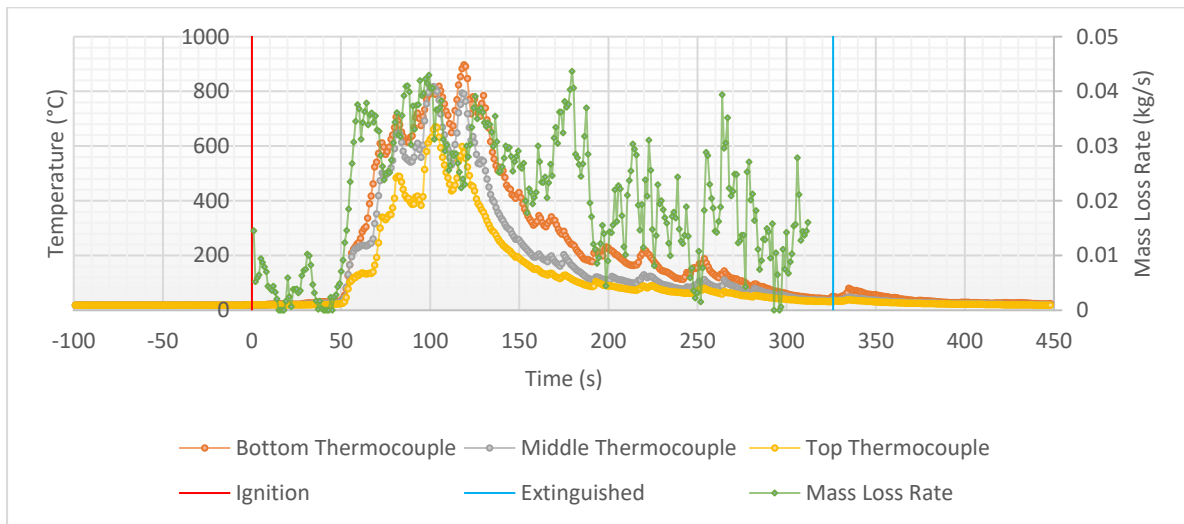
Figure B.10: Experiment 2 - MLR and temperature
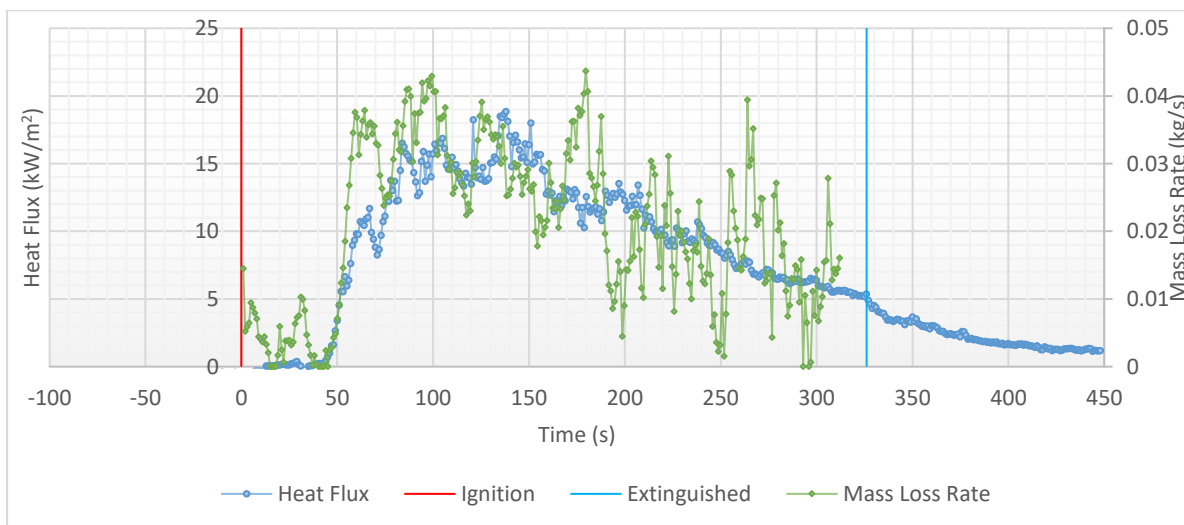
Figure B.11: Experiment 2 - MLR and heat flux
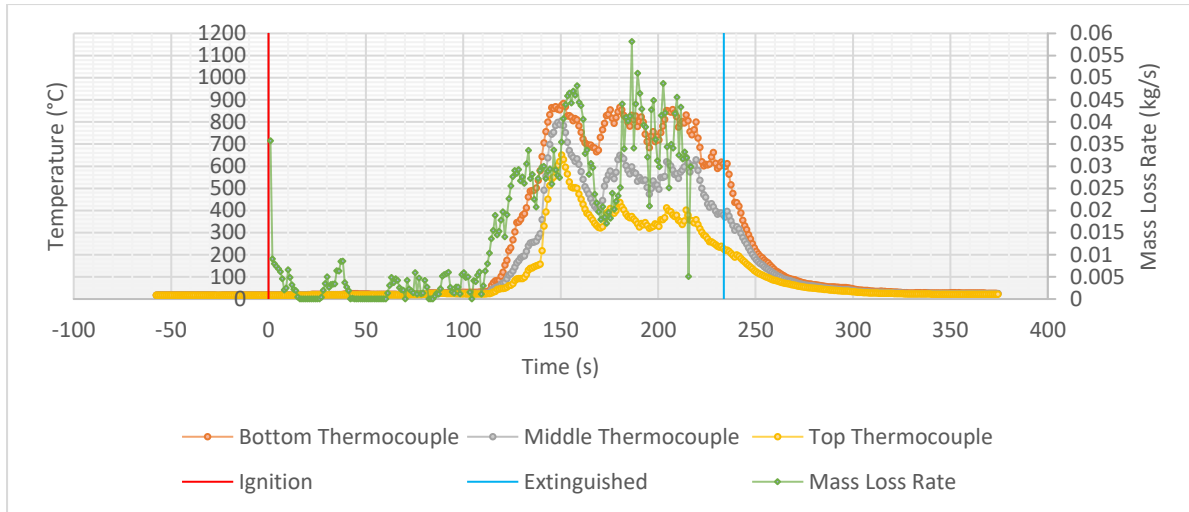
Figure B.12: Experiment 3 - MLR and temperature
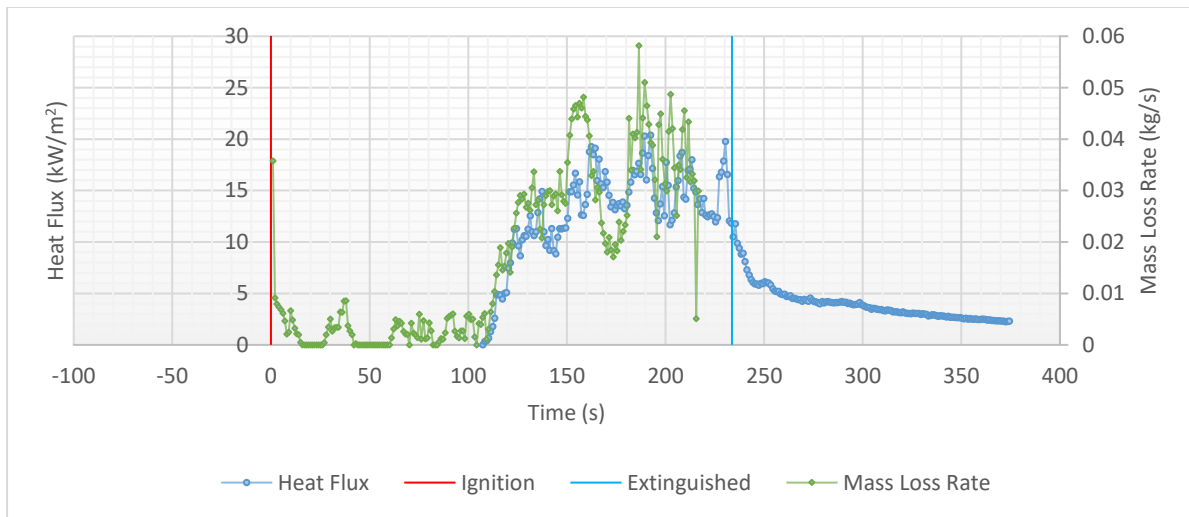
Figure B.13: Experiment 3 - MLR and heat flux
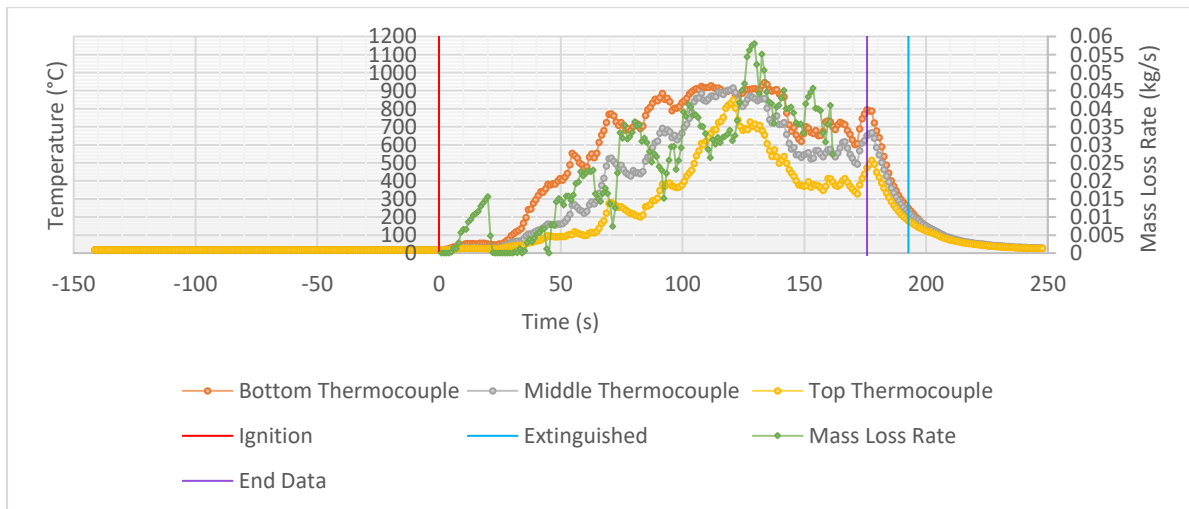
Figure B.14: Experiment 4 - MLR and temperature

143
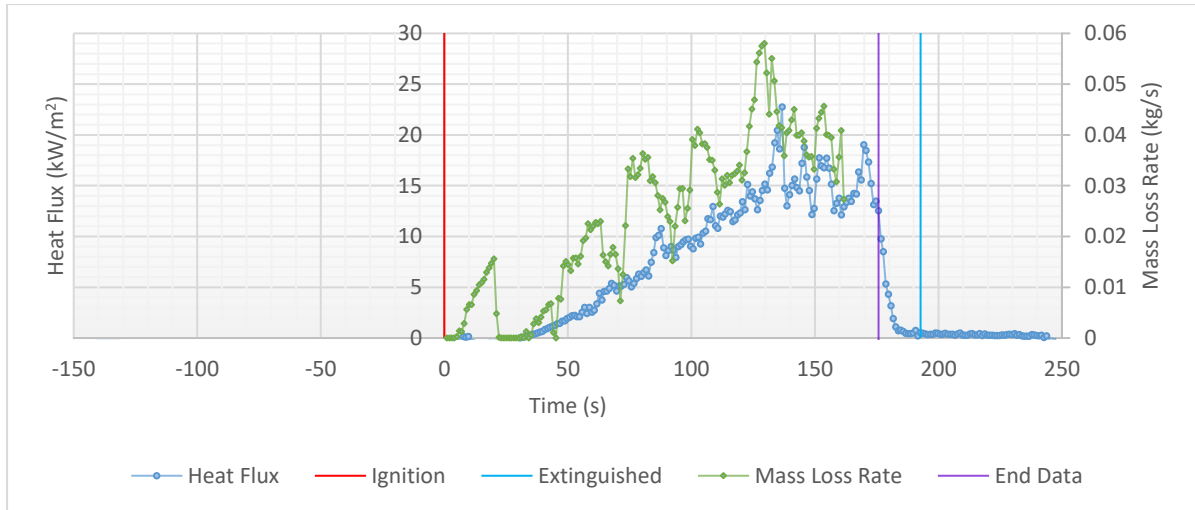
Figure B.15: Experiment 4 - MLR and heat flux

Appendix C

The dimensions of the windows are shown in Figure C.1, including the actual dimensions and dimensions used in the model.
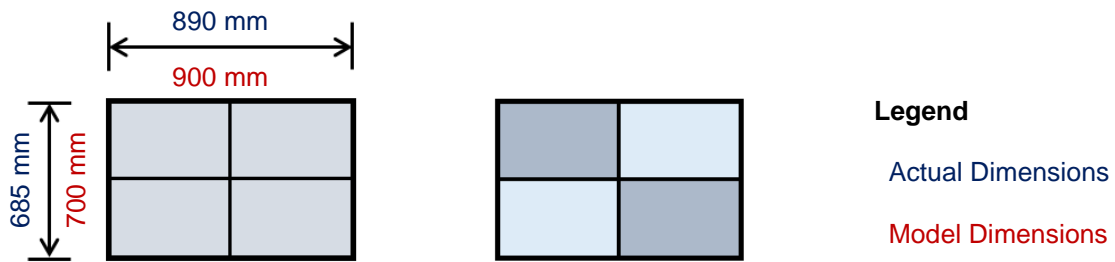
Figure C.1: Window closed and open

The dimensions of the doors are shown in Figure C.2 and Figure C.3, including the actual dimensions and dimensions used in the model.
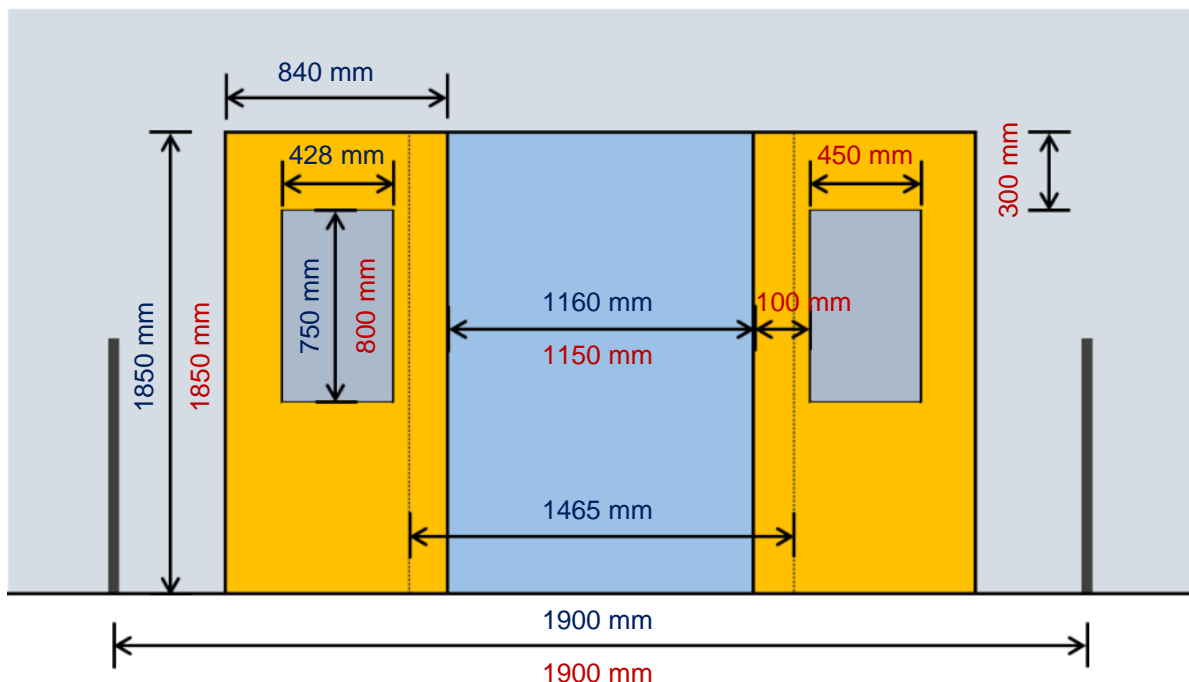
Figure C.2: Carriage side doorway

145
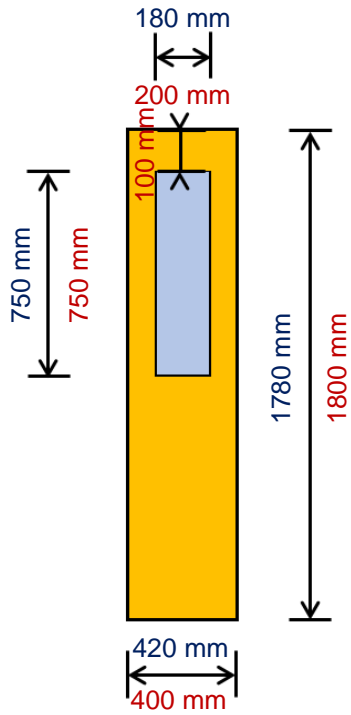
Figure C.3: Carriage end door

Figure C.4 shows the actual and modelled dimensions of the partitions.
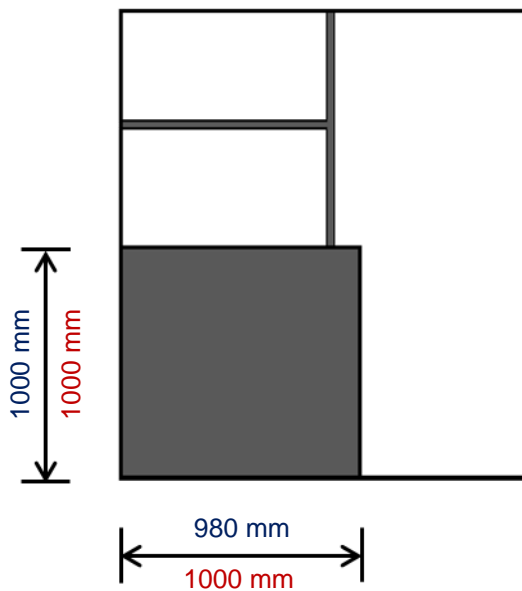
Figure C.4: Carriage partition

Figure C.5 shows the actual and modelled dimensions of the seats, while Figure C.6 shows the actual and modelled layout of the seats and partitions.
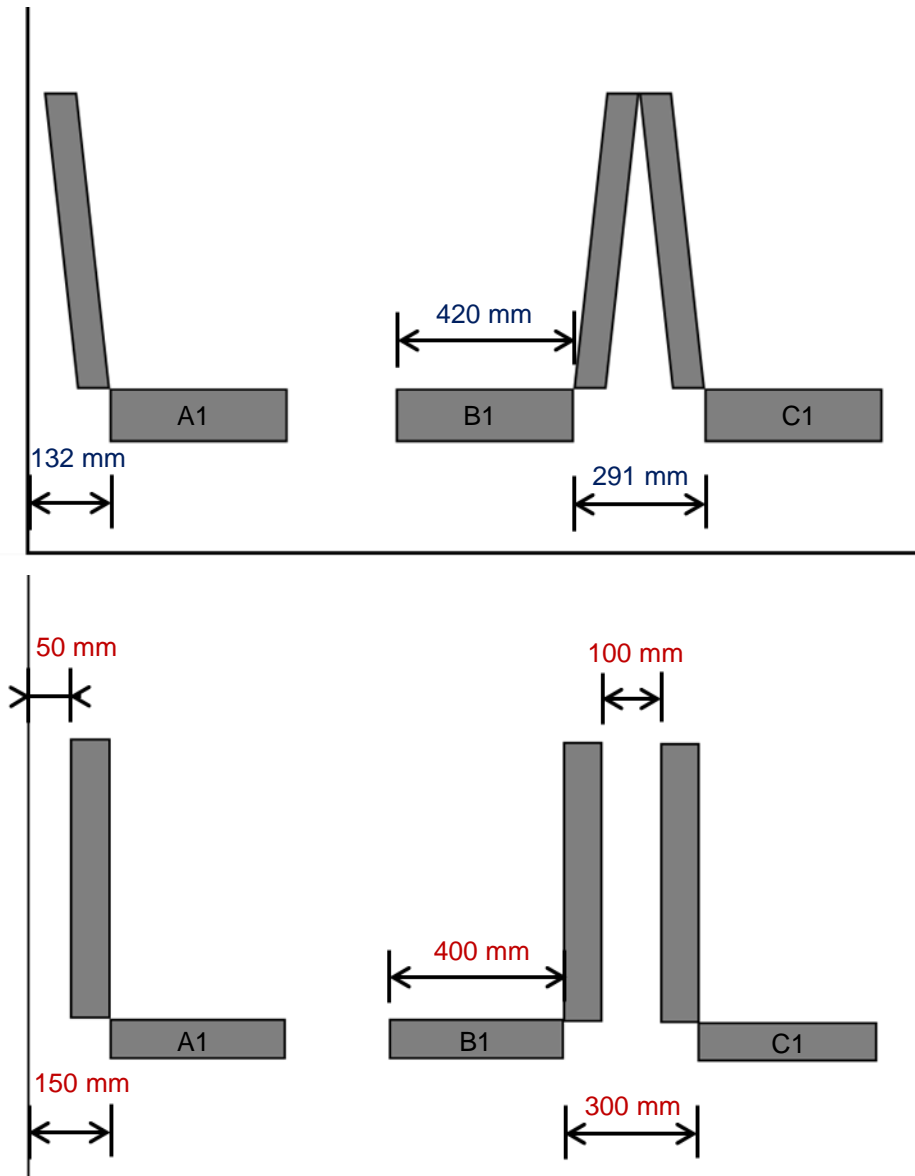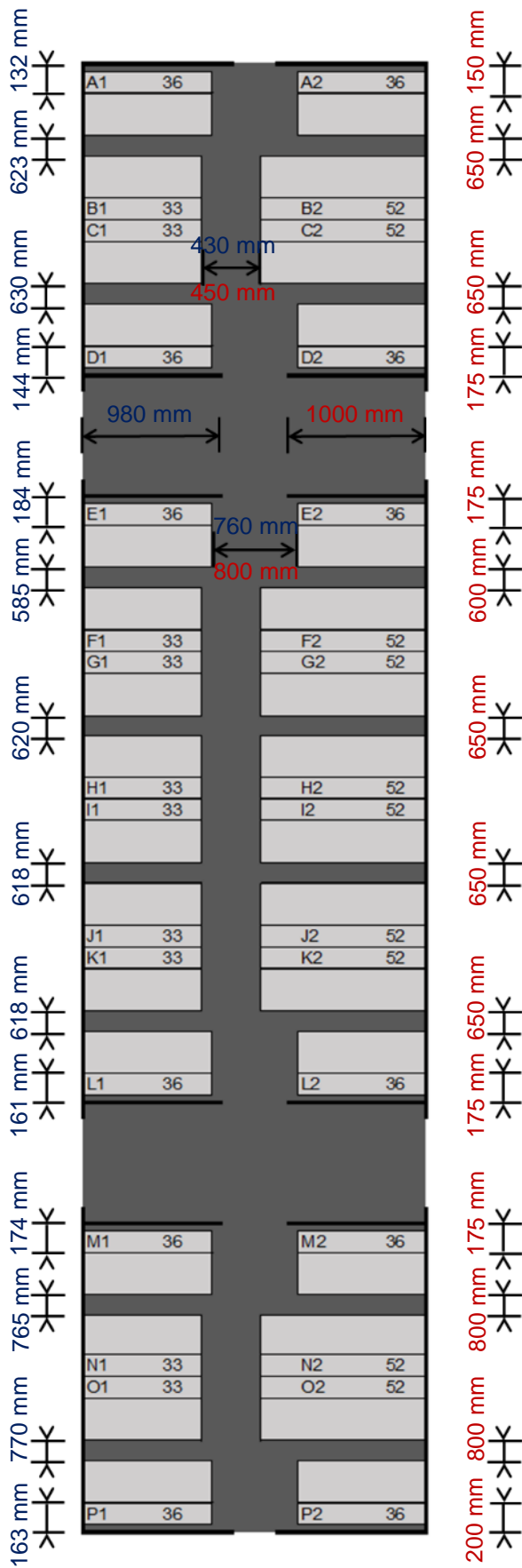
146

Figure C.5: Actual vs modelled seats

Figure C.6: Layout of seats and partitions in carriage

Figure C.7 shows the dimensions of the modelled vent cove, while Figure C.8 shows the layout of the ceiling vents with actual and modelled dimensions.
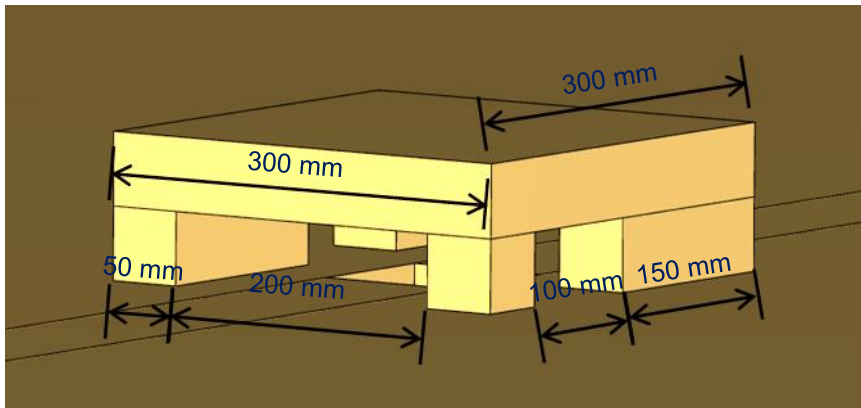

Figure C.7: Modelled ceiling vent cover

Figure C.8: Layout of carriage ceiling vents